Miscibility Variations in Compositionally Grading Petroleum Reservoirs

by

Lars Høier

A Dissertation for the Partial Fulfillment
of Requirements for the
Degree of Doktor Ingeniør

Division of Petroleum Engineering
and Applied Geophysics

Norwegian University of Science and Technology

August, 1997

Acknowledgement

I wish to express my sincere gratitude to my supervisor Professor Curtis H. Whitson who has been an excellent advisor and a good friend through the last four years. Curtis introduced me to a number of challenging problems connected to compositional modelling and simulations, and the cooperation with him has made the work with this thesis very interesting.

Senior Researcher Erik Lindeberg, IKU, has been my other advisor, and I will like to thank him for all help and many fruitful discussions on compositional gradients in general and thermal diffusion in particular. Both Erik, and Dr. Kim Knudsen, DTU, has been very helpful in the discussion of different theories for thermal diffusion and have pointed out several weaknesses in existing theories.

The main parts of the work on miscibility variations with depth and injection gas composition had not been possible without the supervision from Dr. Aaron Zick. Aaron gave us permission to use his unpublished MMP algorithm, and during the work he had several important suggestions for interesting topics to look into.

I would also like to thank my father and Curtis for helping me with the language part of the thesis.

Sincere thanks to Knut Uleberg, Andreas Haldoupis, Øyvind Fevang, Vidar Haugse, and other colleagues at the institute, for cooperation and many long and interesting discussions.

The opportunity to undertake this study has been possible with financial support provided by the Norwegian Research Council, Phillips Petroleum Company, and the RESERVE program.

Finally, I wish to express my deepest gratitude to my mother and father for all support and encouragement. I am also indebted to my wife Bente, and Even for understanding, patience and support during the work with this thesis.

Trondheim, August 1997
Lars Høier

Summary

Vertical Compositional Gradients

Numerous examples of petroleum reservoirs with considerable compositional variation with depth have been found in different parts of the world. It is important to be able to model and quantify these gradients for calculation of initial hydrocarbons in place and gas-oil contact, design of surface production requirements, and design of immiscible gas and water injection processes.

The main governing equations for static one-dimensional modelling of vertical compositional gradients are given. Solution techniques these equations are discussed, both in the case of isothermal chemical/gravity calculations and when including thermal gradients. Based on these equations it has been shown that compositional variations with depth can be large in near-critical systems. As a direct result of the compositional variations, other physical properties will vary as a function of depth, e.g. saturation pressure, reservoir fluid density, mixture molecular weight, and producing gas-oil ratio. Isothermal gravity/chemical equilibrium (GCE) calculations are performed in different reservoir fluid systems to quantify the effects of the compositional gradients. It has been shown that the largest variations with depth are found in saturated and near-saturated near-critical fluid systems.

Accurate determination of the gas-oil contact (GOC) is important for practical production strategy and determination of hydrocarbons-in-place. An improved GOC algorithm is suggested which is 1.5 - 4 times faster than an ordinary interval-halving method. GOC calculations are based on the isothermal GCE method, and the new algorithm calculates both saturated and undersaturated GOCs.

A considerable uncertainty exists in the precise determination of reference composition, depth, pressure, and temperature. The sensitivity of isothermal GCE calculation results with changes in reference conditions has been analysed. We find the modelling results to be particularly sensitive to errors in reference depth and saturation pressure. A method is proposed to estimate the effect of an error in saturation pressure alone, and it is shown that this potential error can significantly change the predicted position of the GOC.

Three approaches for calculations of initial hydrocarbons in place for a reservoir with significant compositional variations have been analysed. Simplified methods can lead to significant errors in the results. We recommend that a rigoreous reservoir fluid variation with depth be used when calculating in-place volumes.

Natural geothermal gradients and thermal diffusion are normally neglected in calculations of vertical compositional distributions. Only the Belery-da Silva (1990) extension of Dougherty and Drickamer's (1955) model for thermal diffusion in multicomponent mixtures has so far been applied to quantify this effect. Additional theories for thermal diffusion are discussed (Haase, 1969 and Kempers, 1989). The models have been implemented for one-dimensional stationary state calculations in several fluid systems to *quantify* differences in these thermal diffusion models.

Limited measurements on thermal diffusion exist complicating the evaluation of different thermal models. However, comparisons with an extensive experimental study of thermal diffusion factor in a binary system show that neither the model of Kempers nor the model of Dougherty and Drickamer shows qualitative agreement with measurements in the entire investigated pressure and temperature-region.

Based on our calculation results when thermal-, chemical-, and gravity forces have been included in static 1D systems the following conclusions have been made:
(1) the Haase and Kempers models predict a thermal diffusion effect that opposes gravity in almost all systems investigated, (2) at near-critical conditions the Belery-da Silva model predicts thermal effects that are opposite and considerably larger than the gravity effect, often generating non-physical (mechanically unstable) solutions, and (3) far rom critical conditions the Belery-da Silva model typically predicts thermal effects that oppose gravity in gases and enhances the compositional gradients in oils.

Our study demonstrates that the three thermal diffusion models are only internally consistent for thermal diffusion ratio in the case of *lean gases* .For a given (p,T,z_i) condition in *oils* the models do not provide internally consistent results with respect to the *sign* and the *magnitude* of the thermal diffusion factor.

Based on the conclusions above it is recommended that additional experiments on thermal diffusion in binary and multicomponent systems be performed to study (1) the sign, and (2) the magnitude of the thermal diffusion ratio. Measurements should be performed at *liquid conditions*, where large inconsistencies exist between the models. The theories should be tested against existing and new measurements. If necessary, a new model for thermal diffusion should be developed.

Developed Miscible Gas Injection

A key parameter in the evaluation of a miscible gas-related EOR process is the minimum miscibility pressure (MMP), or alternatively the minimum miscibility enrichment (MME). Simulation methods and calculation algorithms for determining miscibility are discussed, and consequences of variation in pressure, temperature, injection gas composition and reservoir fluid composition have been analysed. It is shown that relative permeability and capillary pressure have *no impact* on 1D slimtube simulation MMPs. Slimtube simulations, with correct elimination of numerical dispersion, are recognized to yield reliable results for minimum miscibility conditions. However, interpretation of slimtube simulation results are somewhat dependent to a subjective evaluation. A procedure has been proposed to quantify the potential extrapolation uncertainty in several methods for elimination of numerical dispersion. It has been shown that there exists a significant case-dependent uncertainty in MMP determination by slimtube simulations.

Single cell (VGD and CGD) calculated MMP algorithms have been found to highly overpredict MMP of enriched injection gases. These algorithms are based on the assumption that miscibility develops either at leading-edge front (VGD) or at the point of injection (CGD). This assumption will only hold in the case of dry/lean injection gases where the VGD MMP can equal the true MMP. It has been shown that the CGD MMP can be lower than the saturation pressure. The VGD MMP will *always* be larger than or equal to the saturation pressure, independent of the injection gas composition.

Zick (1986) has shown that the development of a miscible process most often is a combination of a condensing and vaporizing (C/V) mechanism, where components are transported in both directions between the phases and the intermediate component transfer is a key mechanism. The Zick multi-cell algorithm takes this component transfer into account, and we have found this algorithm to predict MMP within the extrapolation uncertainty of slimtube result for a series of different fluid systems. The algorithm is computationally efficient and we have applied it for large ranges in compositions.

MMP as a function of injection gas has been studied. The VGD, CGD and C/V MMPs have been calculated and compared with slimtube simulations. It has been shown that the true MMP decreases with increasing enrichment level of the injection gas by a solvent, above a threshold enrichment level, E*, (where the C/V mechanism exists). MMP is not sensitive to solvent enrichments at enrichments less than E*

(where the VGD mechansim exist). At E > E* the developed miscible process is a combined C/V mechanism, and the true MMP decreases abruptly. Consequently, applying single cell methods for MMP determination at these conditions can incorrectly lead to the conclusion that a miscible gas injection is not economic or technically feasible. Based on our studies we recommend that E* always be determined when miscible gas injection is evaluated as a potential EOR candidate.

The effect of isothermal compositional gradients on miscibility conditions has been investigated with the Zick multicell algorithm and slimtube simulations. The variation in MMP with depth (MMP(h)) can be directly related to the compositional variation with depth. It has been demonstrated that the MMP(h) variation in a slightly volatile oil reservoir is negligible, while relatively large variations in MMP(h) were found in saturated or near-saturated near-critical oils.

Miscibility conditions in gas condensates are given particular attention. We find that the VGD MMP equals the dewpoint pressure in gas condensate systems. The C/V mechanism can yield MMPs that are significantly lower than the dewpoint pressure if an enriched gas is injected into a gas condensate system. We find the slimtube simulations in gas condensates to suffer severly from grid effects. The grid effect is particularly pronounced when the injection gas enrichment level is slightly higher than E*. "Snapshots" of slimtube simulations show the buildup of an oil bank at the condensing edge of the miscible front. Large compositional variations take place over small distances, and detailed grid refinement is needed to capture the C/V mechanism. If to few grids are used then an erroneous VGD MMP can be predicted.

The calculations of MMP in gas condensate systems below the dewpoint suggest that the retrograde condensate properties dominate the MMP. Miscibility conditions below the dewpoint in a gas condensate system contradicts the traditional way of thinking, and has to our knowledge not been reported previously. The calculations, both with the Zick multicell algorithm and slimtube simulations, show a potential for improved economics in gas cycling processes using a slightly enriched injection gas.

The temperature effect on MMP(E) and MMP(h) has been investigated. When injecting an enriched gas it has been shown that the main effect of a decrease in temperature is similar to an increase in pressure. It has been demonstrated how the inclusion of thermal models in the calculation of vertical compositional variations may have a large impact on the MMP(h) results. The MMP(h) variations are typically decreased in gases and oils when Kempers or Haase's models are used, while MMP(h) typically increases in oils if the Belery-da Silva model are used.

Contents

Chapter 1

Introduction

1.1 Objective

One of several important topics related to practical reservoir engineering is precise knowledge about the fluid properties in a reservoir. Variation in physical properties with depth can potentially have a significant impact on dynamic properties such as the flow behaviour in the reservoir, and static properties like initial hydrocarbons in-place. At an early stage in the production life of a petroleum reservoir, limited knowledge about vertical variations in physical properties may exist. Consequently, calculation algorithms often are applied to estimate such variations.

If gas injection is considered for a reservoir then miscible displacement may be a feasible process. Reliable and robust calculation methods are needed to determine the minimum miscibility pressure (MMP) for a given injection gas, or minimum miscibility enrichment (MME) at a given reservoir pressure.

The main objective of this work has been to investigate and apply calculation methods and algorithms for modelling (a) compositional variations with depth, and (b) developed miscibility conditions.

One important aspect of this study has been to perform investigations for a wide range of reservoir fluid systems. To do this, vertical fluid communication over large depth intervals has been assumed to (1) study physical property variations with depth predicted by the isothermal gravity/chemical equilibrium model, (2) quantify and investigate the Soret effect for systems with vertical temperature gradient, and (3) evaluate miscibility conditions for a large compositional space (i.e. for reservoir fluids and injection gases). In the study of isothermal gradient calculations an efficient gas-oil contact algorithm was developed for saturated and undersaturated gas-oil contacts.

An important feature of developed miscibility and compositional variations with

depth is the potentially large compositional space resulting from these phenomena. In both cases the composition may go through a critical transition from gas to oil. This places stringent requirements to the accuracy of the equation of state used in the calculations.

Fluid samples and existing EOS characterizations from several North Sea reservoirs form the basis for this work. In the miscibility study the effect of mixtures of available North Sea hydrocarbon separator gases was emphasized.

We were given permission to use an unpublished multicell algorithm by A. Zick, to calculate minimum miscibility pressure. The algorithm is computationally efficient, and opens the possibility for "mapping" MMP variations with composition and temperature. A major task was to critically quantify and test the algorithm for accuracy compared with single cell calculation algorithms and slimtube simulations.

Miscibility variations with depth in compositionally graded reservoirs were subsequently investigated by applying the Zick multicell algorithm on a number of different fluid systems. The two main topics of this thesis are thus linked through our study of minimum miscibility conditions in compositionally grading reservoirs.

Parts of the work on miscibility variations with depth were presented in a lecture by C. Whitson at the 7th Abu Dhabi International Petroleum Exhibition and Conference. The title of the presentation was "EOS Fluid Characterization for Miscible Displacement Processes", October 13-17, 1996.

The work on MMP in compositionally grading reservoir and particularly in gas condensate reservoirs was presented in a lecture by Whitson at the SPE meeting in Hannover, March 20, 1997, with the title "Minimum Miscibility Conditions in Gas Condensate and Compositionally Grading Reservoirs".

1.2 Organization

As outlined in Section 1.1 the thesis has been divided into two main parts:
(1) compositional variations with depth, and (2) development of miscibility though gas injection. The two following chapters discuss these topics in detail. Conclusions and recommendations for further work, nomenclature and reference lists are given at the end of each chapter.

Consequently, it should be possible to read the chapters separately. However, a number of the studies on MMP and MME variations in compositionally grading reservoirs (Chapter 3) are based on results in Chapter 2. Also, the fluid systems and EOS characterizations presented in Chapter 2 form the basis for further analyses in Chapter 3.

Complete EOS characterizations, predicted compositional variations in a GOC search, slimtube MMP determination results, and grid sensitivity analyses of the Zick multicell algorithm are given in Appendices at the end of the thesis.

Chapter 2

Vertical Compositional Gradients

In this chapter we investigate modeling procedures for calculating vertical compositional gradients in petroleum reservoirs. Isothermal algorithms assuming chemical-gravity equilibrium are applied to reservoirs ranging from low-GOR oils to lean gas condensates. An improved algorithm for precise determination of gas-oil contact is suggested . Implementation of thermal diffusion in modelling compositional gradients is considered and its effect on the results at stationary state is quantified and compared with isothermal results. Also, the inclusion of vertical compositional gradients in defining hydrocarbons in place is addressed.

2.1 Introduction

Petroleum reservoir modeling has traditionally been based on the assumption that the initial state of each hydrocarbon phase can be described by a vertically uniform composition. This assumption may have severe limitations, as will be demonstrated in this chapter.

Numerous examples of petroleum reservoirs with significant compositional gradients can be found in the literature , e.g. Schulte (1980), Bath et al. (1983), and Creek and Schrader (1985). Most examples report decreasing methane content and solution gas-oil ratio with increasing depth (i.e. when we consider the variation downwards in the reservoir); the amount of heptane and heavier components (C_{7+}) increase with depth. The variation in composition with depth generates a variation in other reservoir fluid properties, such as density, molecular weight, and saturation pressure. Compositional gradients are particularly important for thick reservoirs or reservoirs with large structural relief.

Reservoirs initially at pressure and temperature near critical conditions of the in situ fluids show larger compositional variations with depth than highly undersaturated reservoir fluids. Thus, the magnitude of the initial compositional gradients can, in a

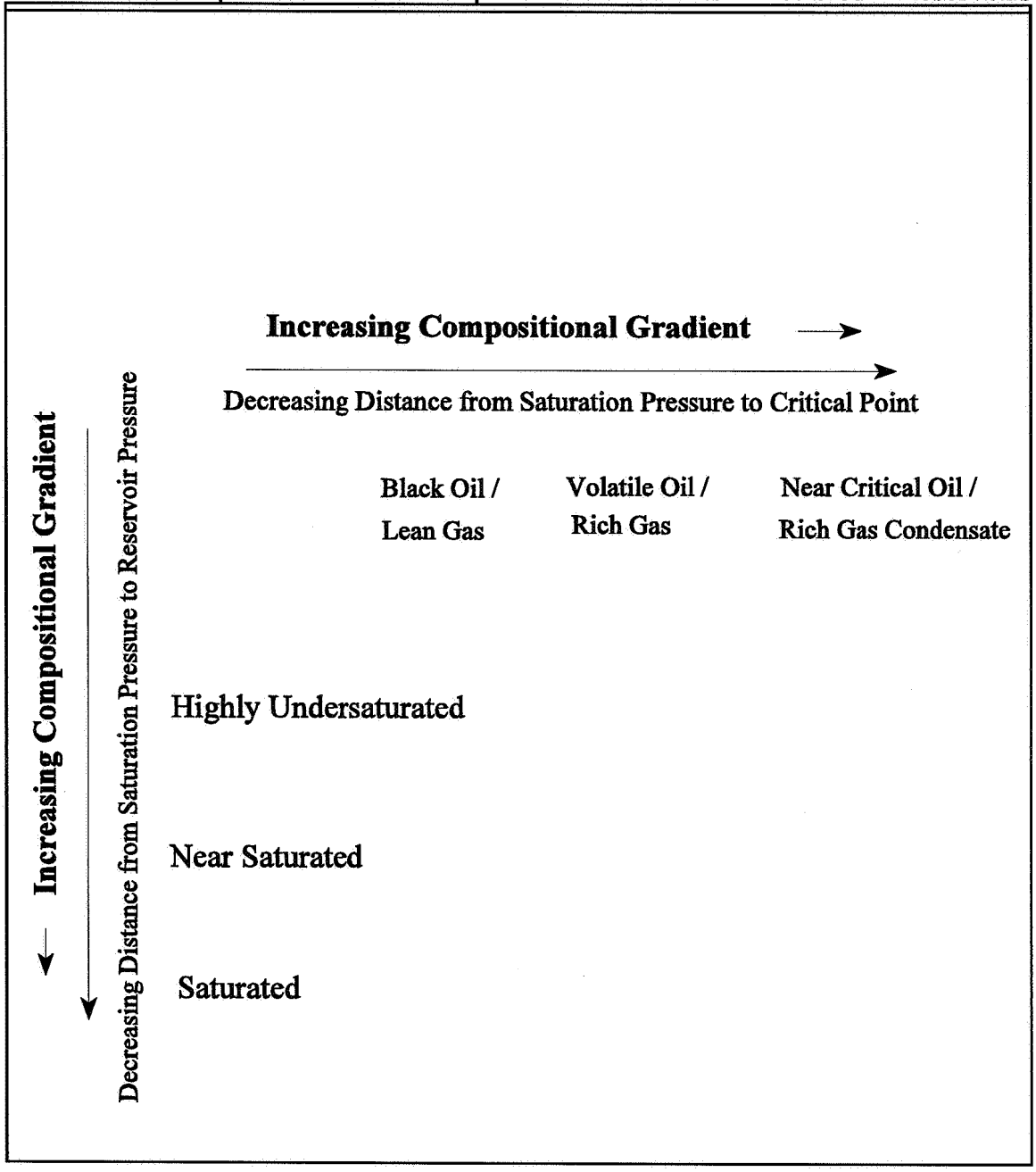

Fig. 2.1 Schematic illustration of different classes of reservoirs and degree of compositional gradients.

static one-dimensional situation, be directly related to how close the initial reservoir conditions are to the critical condition. As illustrated in Fig. 2.1 the vicinity to the critical condition can schematically be divided into two parts: (a) the distance from reservoir pressure to saturation pressure at the reservoir temperature, and (b) the distance between the critical point and saturation pressure at the reservoir temperature.

Consequently, a highly undersaturated low-GOR oil or a lean gas system will normally have little compositional variation with depth, while a near-saturated or

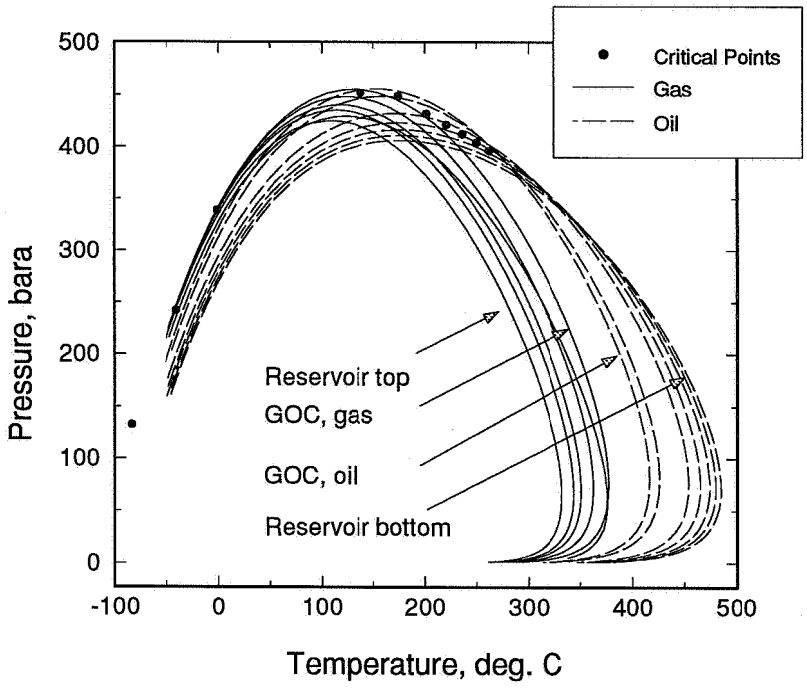

Fig. 2.2 Phase envelope calculations for composition at different depths in a near-critical reservoir.

saturated volatile oil or rich gas condensate system will show significant variation.

Fig. 2.2 shows phase envelopes calculated for a series of different depths in a near critical reservoir with a saturated gas-oil contact (GOC)[1], i.e. a reservoir fluid with significant compositional gradients. The composition at each depth in the reservoir has a different phase envelope and critical point, as shown in the figure.

In near-saturated near-critical systems the reservoir fluid may yield a continuous transition from gas to oil with depth, without a saturated GOC. There exists an "undersaturated" gas-oil contact where the distance between the saturation pressure and the reservoir pressure is at a minimum. This situation will occur if the following three criteria are fulfilled: (1) reservoir pressure is larger than the saturation pressure over the entire reservoir thickness, (2) reservoir temperature at the top of the reservoir

[1] The gas-oil contact (GOC) is defined as a transition from bubblepoint-to-dewpoint mixtures at a specific depth.

is larger than the critical temperature for the mixture at that depth, and (3) reservoir temperature at the bottom is smaller than the critical temperature for the mixture at that depth.

In the North Sea, reservoirs exhibiting the different compositional gradient behaviour discussed above can be found.

Quantifying compositional gradients may be important for the following engineering calculations :

- Calculations of initial hydrocarbons in place (stock-tank oil and surface gas).
- Prediction of gas-oil contact.
- Design of surface production requirements.
- Design of immiscible gas and water injection processes (variation in mobility ratio with depth).
- Design of developed miscible gas injection processes (variation in miscibility conditions with depth).

These factors can have a significant economic impact on field development, and they form the basis for the further discussion in this chapter. Miscibility variation with depth in oil and gas condensate reservoirs is discussed separately in Chapter 3.

Limited information about the geology and reservoir fluid properties exists in the early development of a reservoir. Before production starts only a few reservoir fluid samples may exist. Consequently, it is important to be able to estimate the compositional variation with depth to gain knowledge about possible scenarios of the fluid state at other depths. A question that typically exists is whether vertical fluid communication exists between different geological units (layers or fault blocks) in the reservoir. Compositional gradient modelling result can potentially be used in this analysis. As more information becomes available, measured compositional variations can be compared to predictions and the existing model can be modefied or replaced to give a more consistent variation with depth.

In recent years oil companies have started including vertical compositional variation in reservoir fluid models. Several commercial phase behaviour programs (PVTSIM,

PVT, PVTx)[2] now provide isothermal calculations algorithms for determination of initial vertical gradients in petroleum reservoirs based on cubic equations of state. The majority of commercial PVT packages use isothermal methods to determine the compositional variation with depth, considering gravity alone as the source for the compositional variation. Most reservoir simulators (ECL300 and MORE-EOS) can be initialized with vertical compositional variations, based on isothermal models.

In this chapter we focus entirely on fluid properties. Geological considerations can be important in the application of these results, but we have chosen to focus on fluid calculation procedures. The effect of capillary pressure has been neglected. Also, we consider "static" situations only, i.e. with no bulk convective movement.

In part two of this chapter we discuss criteria for thermal convection and give the main governing equations for static one-dimensional modelling of vertical compositional variations. Both thermal and isothermal derivations are considered. Also, solution strategy of the equations is discussed. These equations and solution techniques form the basis for further analyses in this chapter.

In part three we quantify and analyse the effects of compositional gradients based on the equations derived in part two. It is shown how the magnitude of compositional variations in different cases can be understood directly from the main governing equations. Typical variations with depth for reservoirs fluid systems varying from gases to oils are calculated and discussed. Also, a discussion of algorithms for precise determination of the gas-oil contact is given, and an improved GOC algorithm is proposed.

As fluid samples are normally taken from depth intervals, uncertainty exists in the definition of the reference conditions of depth, temperature and pressure. In the last part of section three we discuss this uncertainty in the determination of composition with depth and analyse the sensitivity of isothermal calculation results with changes in reference conditions. Finally, an example of the impact on hydrocarbon in place estimates as a function of compositional variation with depth is given.

Natural geothermal gradients will be present in petroleum reservoirs and this effect alone can generate compositional gradients in the fluid through thermal diffusion. Implementation of thermal diffusion and gravity *simultaneously* for modelling

---

[2] PVTSIM distributed by Calsep and Dewpoint; PVT distributed by Schlumberger GeoQuest; and PVTx distributed by PERA.

vertical compositional gradients has been proposed by Belery and da Silva (1990) among others. Several theories for thermal diffusion exist. The most referenced are the theories of Dougherty and Drickamer (1955), Haase (1969), and Kempers (1989). Apparently, the quantitative influence of these theories on compositional variations with depth in multicomponent mixtures has not been quantified and compared earlier. This is discussed in part four of the chapter. The results are compared and analysed, and the main effects on the resulting fluid state are discussed.

In part five of the chapter we summarize the main conclusions and suggest further work on selected topics.

2.2 Main Governing Equations and Solution Techniques

In this section we derive the main equations describing compositional gradients in a one-dimensional system with no bulk movement. Criteria for thermal convection in a horizontal layer heated from below are also given. Algorithms and solution techniques for the three cases of isothermal calculations, passive thermal and thermal diffusion calculations in a gravity field are discussed separately.

2.2.1 General Derivation

Petroleum reservoirs are three-dimensional heterogeneous system with dynamic aquifers, geological changes, spatial variable reservoir geology, local temperature variations and mechanically unstable fluid conditions potentially influencing the fluid distribution. The inherent complexity of such a system under the influence of chemical, gravity, and thermal forces makes the accurate prediction of fluid distributions extremely difficult, if not impossible. Simplefying assumptions are necessary, and in this subsection we derive the equations for one-dimensional (1D) "static" calculations of compositional gradients. A short discussion of the probability for thermal convection is given prior to the derivation for a static system.

Criteria for thermal convection

Natural geothermal gradients can induce mechanically unstable conditions in a reservoir, provided the main effects from the thermal gradients are larger than the effect of gravity. In a saturated porous medium heated from below this can be the case, as discussed by Horton and Rogers (1945). If certain conditions are fulfilled, slow well-organized fluid flow patterns will occur with descending cold fluid regions and ascending varm fluid regions.

There exists a well established mathematical theory for calculating the onset of thermal convection in saturated porous media. Lapwood (1948) and Palm (1960) describes the phenomena by use of a set of non-linear equations which have their origin in the laws of conservation of mass, momentum and energy. Through combination of these equations a dimensionless number is found to be the fundamental parameter describing the onset of convection. This number, the Rayleigh number, is in a horizontal porous medium given as

$$Ra = \frac{k\, g\, \beta\, \Delta T\, \Delta h}{\kappa_m\, \nu} \qquad (2.1)$$

where

k	=	permeability
g	=	gravitational acceleration
β	=	coefficient of thermal expansion
Δh	=	vertical dimension of the horizontal porous medium
ΔT	=	the thermal difference over Δh
κ_m	=	thermal diffusivity of the total porous medium
ν	=	fluid kinematic viscosity

Notice that the thermal diffusivity equals the thermal conductivity divided by the product of density and specific heat. Kinematic viscosity equals the viscosity divided by density.

For simple boundary conditions Palm (1960) shows that stable convective movements are established if the reservoir conditions are such that the Rayleigh number exceeds a critical value $4\pi^2$. This criterion is valid for a porous medium of infinite extent. Thus, the conditions for mechanical instability for a fluid in a porous medium is given by the Rayleigh number. The theory presented above is valid for a one-component system. Several authors have applied the criterion in studies of petroleum reservoirs, as described below.

Rabinowicz et al. (1985) studied the possibility for thermal convection in the Ekofisk Field and concluded that thermal convection can have existed in the past. However, the authors concluded that at the present geological time the Rayleigh number is lower than the critical value, and hence convection is no longer active.

Montel et al. (1989) presented a 2-dimensional dynamic segregation model to predict compositional variations including convection and thermal diffusion. Several configurations with dipped layers were simulated and compared with isothermal static predictions. The fluid considered was a pseudoized three component mixture. Under conditions where convection was caused by the temperature gradient, the convective flow patterns were found to vanish after a period. This was found to be caused by component segregation. As a result the fluid became mechanically stable. Consequently, the transient state was found to induce compositions significantly different from the static model, but *the final state was found to be the same as the one*

predicted by the isothermal static model . This is an interesting observation because in most cases we only are interested in the "final" state to characterize a petroleum reservoir.

Jaqumin (1990) stated that vertical temperature gradients usually are insufficient to generate stable convective currents in petroleum reservoirs. However, Jaqumin showed that small *horizontal* temperature gradients may induce convection, and the author derived the equations describing this phenomena for a multicomponent system. Calculations were given for a two component system with idealized boundary conditions. The results showed how convection in this case would lead to mixing.

Bedrekovitsky (1993) discussed the mechanically unstable solutions due vertical temperature gradients in a petroleum reservoir. The author found that the Rayleigh number exceeded the critical number only in the fractured parts of the reservoir where effective permeability is high.

Notice also that heterogenities in a porous medium will influence convective currents (Høier, 1993) and thus make predictions of the effects difficult. For an extensive discussion of thermal convection in heterogeneous media, see Bjørlykke et al. (1988).

The following derivations are based on the assumption that thermal convection is not present.

1D Compositional Gradients Calculations in Multicomponent Systems

In the absence of convection, mass transport on a molecular scale can lead to a distribution of components as a function of depth. This transport can be described by irreversible thermodynamics, provided the reservoir conditions are at a near equilibrium situation. The flux equations describing mass flux, J_i, and heat flux, J_q, in a near equilibrium state can be assumed to be linear homogeneous functions of the independent forces in the system.

To assume and apply linear transport processes is normally a good approximation in the limit of a near equilibrium state (Førland et al., 1988). Consequently, the normal procedure for applying irreversible thermodynamics in a multicomponent system is as follows; (1) identify the independent forces in the system, (2) chose a reference frame, e.g. one component, where all changes refer to this reference frame, (3) set up the equations for mass and heat flux, and (4) identify the coupling coefficients

connecting forces and fluxes.

When both gravity and thermal gradients act on a multicomponent mixture, we identify the independent driving forces X_k and X_n as

$$X_k = g - \frac{\nabla_T \mu_k}{M_k} \quad \text{and} \quad X_u = - \frac{\nabla T}{T} \tag{2.2}$$

where

$\nabla_T \mu_k =$ gradient in chemical potential, component k, at constant temperature
M_k = molecular weight for component k
T = temperature
g = gravity

Here, the chemical potential is given as

$$\mu_k = \left(\frac{\partial G}{\partial n_k}\right)_{p,T,n_{k \neq i}} \tag{2.3}$$

where

G = Gibbs free energy for the system
n_k = moles of component k .

The gradient in chemical potential for component k is given as

$$\begin{aligned} \nabla \mu_k &= \nabla_T \mu_k - S_k \nabla T \\ &= V_k \nabla p + \sum_{i-1}^{n-1} \left(\frac{\partial \mu_k}{\partial x_i}\right)_{p,T,i \neq k} \nabla x_i - S_k \nabla T \end{aligned} \tag{2.4}$$

where

S_k = partial molar entropy
V_k = partial molar volume
p = pressure

n = the total number of components in the mixture.

The **stationary state** is defined as the state the multicomponent system will reach after a transient period where the mass fluxes for each component k equal zero. In the following we will consider this state and derive the main equations describing it. Several approaches exist for deriving the equations for stationary state in a static multicomponent fluid. The following derivation mainly follows the work of Faissat et al. (1994).

In the following derivation the choice of the centre of mass (barycentre) of the mixture is chosen as our reference. The mass flux of component k is given relative to the barycentre so that

$$J_k = \rho_k (v_k - v) \tag{2.5}$$

where

ρ_k = density of component k
v_k = velocity of component k
v = barycentre velocity

As shown by Faissat et al. the mass flux in a multicomponent system with an induced temperature gradient over the system is given as

$$J_i = \sum_{k=1}^{n-1} L_{ik} (X_k - X_n) + L_{iu} X_u \tag{2.6}$$

and the heat flux is given as

$$J_q = \sum_{k=1}^{n-1} L_{uk} (X_k - X_n) + L_{uu} X_u \tag{2.7}$$

where L_{ik} and L_{iu} are the phenomenological coefficients connecting forces and fluxes. Onsager (1931a, 1931b) has shown that these coefficient matrixes are symmetric, such that $L_{ik} = L_{ki}$ and $L_{iu} = L_{ui}$.

For convenience, Faissat et al. introduce a new coupling coefficient, Q_k^*, the "energy of transport" such that

$$L_{iu} = \sum_{k=1}^{n-1} L_{ik} Q_k^* \qquad i=1,..,n-1 \tag{2.8}$$

and further

$$Q^* = \sum_{i=1}^{n} \frac{m_k}{m} Q_k^* \tag{2.9}$$

where

m_k, m = the mass of component k and the total mass, respectively
Q^* = specific heat of transport for the mixture

Introducing these parameters in the expression for mass flux leads to

$$J_i = \sum_{k=1}^{n-1} L_{ik} (X_k - X_n + Q_k^* X_u) \qquad i=1,..,n-1 \tag{2.10}$$

As the stationary state is characterized by zero mass flux, we obtain

$$X_k - X_n + Q_k^* X_u = 0 \qquad k=1,..,n-1 \tag{2.11}$$

We now want to derive an expression for X_n to simplify the equation above. Consider the expression for X_k (Eq. 2.2), which when applying Eq. 2.4 can be written :

$$\begin{aligned} \sum_k m_k X_k &= \sum_k m_k g - \sum_k m_k \frac{\nabla_T \mu_k}{M_k} \\ &= m g - \sum_k n_k \nabla \mu_k - S \nabla T \end{aligned} \tag{2.12}$$

where we have multiplied all terms with m_k and summed over all components k.

The Gibbs-Duhems equation states that

$$\sum_k n_k \nabla \mu_k + S \nabla T - V \nabla p = 0 \qquad (2.13)$$

If this expression is introduced in Eq. 2.12, we get $\sum_i^n X_k \cdot m_k = 0$, when hydrostatic equilibrium is assumed, i.e. $V \nabla p = V \rho g = m g$. We now apply this result on Eq. 2.11 to obtain an expression for X_n in terms of Q^* , and get

$$X_n = (\sum_{k-1}^{n} Q_k^* \frac{m_k}{m}) X_u = - Q^* \frac{\nabla T}{T} \qquad (2.14)$$

Consequently, Eq. 2.11 can be written

$$X_k = (Q_k^* - Q^*) \frac{\nabla T}{T} \qquad k=1,..,n \qquad (2.15)$$

Inserting the expression for X_k given by Eq. 2.2 and the terms for $\nabla_T \mu_k$ given by Eq. 2.4 we obtain the main governing equation in Faissat et al.'s paper:

$$\sum_{i-1}^{n-1} (\frac{\partial \mu_k}{\partial x_i})_{p,T,x_{k \neq i}} \nabla x_i = (M_k - \rho V_k) g + M_k (Q^* - Q_k^*) \frac{\nabla T}{T} \quad k=1,..,n \qquad (2.16)$$

This equation is valid for cases that have a barycentre reference frame.

Montel and Gouel (1985) derive a corresponding expression for the main governing equation, in the form

$$\sum_{i=1}^{n-1} \left(\frac{\partial \mu_k}{\partial x_i}\right)_{p,T,x_{k\neq i}} \nabla x_i = (M_k - \rho V_k)\, g - F_k^T \frac{\nabla T}{T}$$
$$= F_k^G - F_k^T \frac{\nabla T}{T} \qquad k=1,..,n \tag{2.17}$$

where F_k^T is a model-dependent expression involving the thermal diffusion for each component k.

These derivations show that the problem involves one gravity term and one temperature dependent term. If a valid model for thermal diffusion can be found such that the term F_k^T can be calculated, all other terms in Eqs. 2.16 and 2.17 can be found analytically from an equation of state. This is discussed in the following sections.

Consequently, if Eqs. 2.16 or 2.17 can be solved numerically, the 1D compositional variation with depth in a reservoir can be calculated, provided that (1) a valid EOS characterization exists, (2) a model for thermal diffusion exists, and (3) precise knowledge about reservoir fluid composition, pressure and temperature *at one depth* exists.

2.2.2 Isothermal Calculations

Already in the late 19th century Gibbs showed that by including gravity, the balance of forces in an *isothermal* equilibrium situation leads to the expression

$$\nabla_T \mu_k - M_k g = 0 \qquad k=1,..,n \tag{2.18}$$

for each component k in a multicomponent mixture. The net effect of the graviational force is that light components move upwards while heavy components will move downwards. The effect of the gradient in the chemical potential is elimination of any spatial compositional difference. Consequently, the equation can be seen as a result of Newton's second law, where the forces balance each other for each component in the equilibrium state. In this equilibrium situation the Gibbs free energy is minimized.

Eq. 2.18 can be rewritten by writing the gradient in the chemical potential at constant temperature to obtain

$$\nabla_T \mu_k - M_k g = V_k \nabla p + \sum_{i=1}^{n-1} \left(\frac{\partial \mu_k}{\partial x_i}\right)_{p,T,x_{i\neq k}} \nabla x_i - M_k g = 0 \qquad k=1,..,n \quad (2.19)$$

and by rearranging we hence get

$$\sum_{i=1}^{n-1} \left(\frac{\partial \mu_k}{\partial x_i}\right)_{p,T,x_{i\neq k}} \nabla x_i = (M_k - V_k \rho)\, g \qquad k=1,..,n \quad (2.20)$$

This is the main equation for compositional gradient calculations at isothermal gravity chemical equilibrium (GCE). We recognize that the Gibbs equation is consistent with the expressions derived through irreversible thermodynamics by letting the thermal gradient equal zero in Eq. 2.16. Eq. 2.20 can be solved efficiently by introducing the fugacity, as discussed below.

Solution Technique

We introduce the fugacity, f_k , where $\mu_k = R\,T \ln f_k + constant$ such that

$$\nabla_T \mu_k = R\,T\, \nabla_T (\ln f_k) = M_k\, g \qquad k=1,..,n \quad (2.21)$$

In the isothermal 1D situation considered we let $\nabla_T \rightarrow \frac{d}{dh}$. Let h^0 be the reference depth, $f_i(h^0)$ the fugacity at that depth, and $f_i(h)$ the fugacity at any depth h. In terms of these variables Eq. 2.21 yields

$$f_k(h) = f_k(h^0)\, \exp\left(-\frac{M_k\, g\, (h - h^0)}{R\,T}\right) \qquad k=1,..,n \quad (2.22)$$

Fugacity can be calculated by an equation of state. Eq. 2.22 plus the constraint that

the sum of the mole fractions for each depth h must equal one, forms the set of equations to solve the isothermal compositional variation with depth. Thus, by specifying a new depth, h, the pressure and composition at this depth can be determined from the equations above.

Michelsen (1985) has proposed highly efficient methods to calculate saturation pressures. Whitson and Belery (1994)[3] noticed the similarity between the set of the equations applied in isothermal GCE calculations and the ones used in saturation pressure calculations, and applied similar methods as Michelsen's in the solution of Eq. 2.22, introducing the function

$$R(p,z) = 1 - \sum_{k=1}^{n} \left[z_k \left(\frac{1}{f_k(p,z)} \right) \left(f_k\,(p^0,z^0)\, \exp\left(-M_k g (h - h^0)\right) \right) \right] \qquad (2.23)$$

where

$f_k(p^0, z^0)$ = fugacity for component k at reference conditions
$f_k(p, z)$ = fugacity for component k at depth h

For each specified depth the function $R(p,z)$ is forced to zero through (a) Newton-Raphson update of pressure and (b) successive substitution update of composition, accelerated with the general dominant eigenvalue method (GDEM). Both points above are similar to the solution technique in Michelsen's saturation pressure algorithm. As stressed by Whitson and Belery, the method of volume translation (Peneloux et al., 1982) must be included in the fugacity calculation,

$$f_k = f_k^* \exp\left[c_k \left(\frac{p}{R\,T} \right) \right] \qquad (2.24)$$

where

f_k^* = fugacity of component k, *without* any volume shift
c_k = volume shift parameter of component k
R = the universal gas constant.

---

[3] Michelsen, in a personal communication to Whitson in 1993, revealed the similarity to the saturation pressure calculation by noting that the sum of the mole fraction = 1 was the constraint equation for the isothermal gradient calculation.

Whitson and Belery (1994) showed the effect of neglecting volume translation in Eq. 2.23 to be significant in a near critical oil example. In an ordinary equilibrium calculation (for example a flash calculation) where ratios of fugacities are used, the volume shift term cancel. However, the fugacities in Eq. 2.23 are determined at different pressures and the effect of volume shift can not be neglected.

In the isothermal compositional gradient calculations in this thesis we apply Whitson and Belery's solution technique for Eq. 2.23.

A typical calculation procedure in the isothermal GCE calculations is as follows:

1. Input data are reservoir fluid composition, pressure and temperature for a specific reference depth, a valid EOS-characterization, and top and bottom depths of the reservoir.

2. The reservoir pressure and composition in the reservoir are found at each depth by solving Eq. 2.23. Volume shift is included in the calculation of fugacities and fugacity derivatives.

3. At each depth the converged solution is tested as to whether it is thermodynamically stable (Michelsen, 1982). If unstable, the gradient calculation at that depth is reinitialized with the unstable test phase composition from the stability test.

4. The stable solution for pressure and composition at one depth is used to initialize the search for the solution at a new depth (to speed up the calculations).

5. When all isothermal GCE calculations have been completed, the saturation pressure at each depth is calculated. The converged solution for saturation pressure and K-values are used to initialize the calculations at a new depth, again to optimize calculation speed.

6. A GOC search may optionally be performed. The algorithm for GOC determination is given in Section 2.3.3. If a saturated GOC is detected then the compositional variation with depth is discontinuous across the GOC. The incipient phase composition from a saturation pressure calculation *at the GOC* may be used to initialize the calculations in step 5 after passing the GOC.

Other important variables such as density, viscosity, gas-oil ratio and mixture molecular weight can subsequently be calculated as a function of depth.

2.2.3 Passive Thermal Diffusion

Faissat et al. (1994) use the expression "passive thermal gradient" for a hypothetical situation where a thermal gradient exists but thermal diffusion is neglected. Although this is a theoretical situation, it could be applied to gain information about the influence of temperature on parameters like density and saturation pressure for a given compositional variation with depth.

Solution Technique

Eq. 2.17 can be solved numerically, setting the term that involves thermal diffusion, F_k^T, to zero, but including the temperature dependency of all other parameters. This equation can be solved through successive substitution of pressure and composition for each depth. As outlined by Belery and da Silva (1990), all terms in Eq. 2.20 can be found analytically from an equation of state, i.e. density, partial molar volume and the derivative of chemical potential with respect to mole fraction. In terms of the fugacity coefficient, $\phi_k = f_k/(x_k p)$, this derivative is found by

$$\begin{aligned}\left(\frac{\partial \mu_k}{\partial x_i}\right)_{p,T,x_{i\neq k}} &= RT\left(\frac{\partial}{\partial x_i}\left[\ln\phi_k - \ln x_k - \ln p\right]\right)_{p,T,x_{i\neq k}} \\ &= RT\left(\frac{\partial \ln\phi_k}{\partial x_i} - \frac{\delta_{ik}}{x_k}\right)_{p,T,x_{i\neq k}} \qquad k=1,..,n\end{aligned} \tag{2.25}$$

The derivative of the fugacity coefficient can be calculated analytically from a cubic equation of state with respect to moles or mole fraction of component k. (Michelsen and Mollerup, 1986).

The temperature at a given depth is found from $T(h) = T^0 + \nabla T(h^0 - h)$, where T^0 is the temperature at reference conditions. If unstable solutions are detected, a saturation pressure calculation is performed to test if a phase change has occurred when going from depth h to a new depth $(h+\Delta h)$. If a phase change has occurred within this interval, interval halving can be used to detect the GOC more accurately,

before continuing the calculation procedure further. Consequently, if a GOC is present it will be detected during the calculation procedure.

With the exception of the points discussed above and the numerical solution techniques, the main strategy for calculating compositional gradients is the same as in the isothermal case.

Whitson and Belery (1994) calculated the effect of "passive thermal diffusion" on a near critical reservoir. They found the effect to be small when compared with ordinary isothermal GCE calculations. The inclusion of a thermal gradient with no thermal diffusion is also found to have small effects in calculation examples presented in Section 2.4.

2.2.4 Including Thermal Diffusion

As shown above the 1D stationary state for a multicomponent mixture can be found from Eq. 2.17, when gravity and temperature gradients act on the system. To provide accurate estimates of compositional variations with depth a valid model including thermal diffusion thus has to be available. Several theories for thermal diffusion exist. The most well known are the theories of Haase (1969), Kempers (1989) and the Belery-da Silva (1990) extension of Dougherty and Drickamers (1955) theory. Only the Belery-da Silva model has been used (in Eq.2.17) to quantify the effect of thermal diffusion on compositional gradients in multicomponent systems. As will be discussed in Section 2.4, the theories above are solved numerically using Eq. 2.17.

Solution Technique

The solution technique including thermal diffusion mainly follows the strategy outlined in Section 2.2.3. As will be shown in Section 2.4, the thermal term in Eq. 2.17 can be found from correlations and a cubic equation of state. Thus, we are able to calculate all terms in the governing equations of each depth. Eq. 2.17 is solved numerically with successive substitutions, accelerated with GDEM for composition, and successive substitution for pressure. Gaussian elimination is applied in the inversion process to calculate ∇x_i, and hence the compositional variation with depth. These calculations show that thermal diffusion can have a significant effect on compositional variations with depth. The methods described here has been applied to a series of different fluid systems in Section 2.4.

2.3 Application of the Isothermal Equations

In this section we solve the main equations for isothermal compositional gradient calculations for a number of realistic petroleum fluid systems. Typical features for the results are given based on calculations with a cubic equation of state. An improved algorithm for GOC determination is suggested and tested against traditional methods. We discuss the main source of errors in sampling and its effect on gradient calculations. It is shown that the uncertainty in reference conditions can have a significant effect. Implementation of compositional gradients in calculations of hydrocarbon in place are performed. When a near critical reservoir fluid is considered the in place results differs significantly from results with uniform composition.

2.3.1 Typical Compositional Variations with Depth

Section 2.2 established that the main equations for isothermal gradient calculations can be derived from basic thermodynamically principles, and efficiently solved with an iterative method. Several authors have discussed the phenomenon of compositional variation with depth and applied Gibb's equation for 1D *isothermal* equilibrium calculations.

Muskat (1930) addressed compositional variation with depth in petroleum reservoirs, and solved Eq. 2.18 for the simplified cases of (1) ideal solutions and (2) cases where all component molar volumes are equal. Two binary mixtures were treated in detail, and Muskat's results lead to the conclusion that compositional variations with depth due to gravity are negligible.

Sage and Lacey (1938) came to the opposite conclusion when modelling composition with depth for a binary hydrocarbon liquid phase and a binary hydrocarbon gas (C_1-nC_4). They noted that variations with depth of gas-oil-ratio and specific gravity had been observed in several hydrocarbon reservoir. The authors found the compositional variations with depth to be significant in their binary example. Calculations were based on solving the Gibb equation by assuming ideal solutions to evaluate the chemical potential, and using correlations to calculate partial volumes. Sage and Lacey made the important observation that the magnitude of the gravitational effect is large in the vicinity of a critical point. Interestingly, they also commented that they suspected that the effects estimated in the isothermal case would be *enhanced* if a temperature effect was included in the calculations.

From Sage and Lacey's important work, and until 1980 there have been several papers where reservoirs with compositional gradients are mentioned. Schulte (1980) extended the application of the isothermal gradient calculation, by replacing the ideal solution behaviour assumed in Sage and Lacey's work and instead using a cubic equation of state (Soave and Peng-Robinson EOS). Schulte addressed the importance of using a valid EOS characterization, by demonstrating the relatively large effect of binary interaction coefficients (BIPS) on the calculations. The author gave examples with saturated and undersaturated GOC in the Brent and the Statfjord formations of the Brent field, respectively. The observed saturation pressure gradients in the Brent Field was found to be three too five times larger than predicted by Schulte's approach.

In the 1985 technical SPE Conference, several papers reported compositional gradients in petroleum reservoirs. Metcalfe et al. (1985) reported compositional gradients in the Anschutz Ranch East Field, and correlated the compositional variations as linear functions of depth. Creek and Schrader (1985) presented observed compositional gradients and isothermal GCE calculations in the East Painter Reservoirs, containing both gas condensate and volatile oil.

Riemens et al. (1988) reported compositional variations in the Birba Field, with a saturated GOC and with an liquid/solid transition resulting in a tar mat in the lower part of the reservoir. The reported isothermal GCE calculations showed a significant compositional variation with depth.

It is seen directly from Eq. 2.20 that the composition gradients can be expected to be large if

1. the term $(\frac{\partial \mu_k}{\partial x_i})_{p,T,x_{i \neq k}}$ is small, e.g. close to critical conditions.

and / or

2. the term $(M_k - V_k \rho)\, g$ is large.

Hirschberg (1988) focused on the $(M_k - V_k \rho)\, g$ term and stated that heavy oils at conditions far away from critical conditions can have significant compositional gradients if large molecules are present with a density significantly different from the reservoir mixture density. This could be the case if asphalthenes are present in substantial amounts in the oil. The author discussed the role of asphalthenes in

compositional grading by applying a two-component molecular model to calculate viscosity variations with depth in a North African oil field. The theory was applied to heavy oils with specific gravity $\gamma_o = 0.88 - 0.93$. This type of oil is uncommon in the North Sea.

Lee (1989) presented calculation methods for predicting compositional gradients when including transition zones caused by capillary forces. By combining input values of rock properties and fluid properties, examples are given that show the predictions of capillary zones. However, comparison between the calculations and actual reservoirs was not presented.

Numerous reservoirs in the North Sea have been found to have significant compositional variations with depth in the period 1970-1997. Whitson and Belery (1994) give an extensive discussion of references on compositional variation with depth. Also, the authors present compositional gradient calculations for several reservoir fluids from four different fields in the North Sea: (1) a black oil (BO) reservoir with gas cap, (2) a slightly volatile oil (SVO) reservoir with gas cap, (3) a volatile oil reservoir (VOA) and (4) a near critical highly volatile oil reservoir with gas cap.

The authors key observations from the isothermal gradient calculations in the near critical reservoir are as follows:

- For most systems the compositional gradients are inversely proportional with the degree of undersaturation.

- The effect on C_{7+} split is small, if selection of components is performed in an appropriate way. Isothermal calculations with 25 pseudocomponents and 5 pseudocomponents did not show any significant difference.

The latter observation could be questionable as a general rule following Hirschberg's argumentation, as Whitson and Belery's example was a relative near critical light oil where asphalthenes play no role in the predicted segregation. In calculation examples with heavy oils the effect discussed by Hirschberg can be lost if the heaviest components are lumped into one pseudo component.

We have used the fluid systems given by Whitson and Belery (1994) as the basis for most of our studies of compositional gradients.

Table 2.1 Reference conditions for four fluid system.

Component	BO system	SVO system	VOA system	NCO system
CO2	0.262	0.265	0.930	0.550
N2	0.367	0.785	0.210	1.250
C1	35.193	45.622	58.770	66.450
C2	3.751	6.092	7.570	7.850
C3	0.755	4.429	4.090	4.250
IC4	0.978	0.865	0.910	0.900
C4	0.313	2.260	2.090	2.150
IC5	0.657	0.957	0.770	0.900
C5	0.152	1.406	1.150	1.150
C6	1.346	2.097	1.750	1.450
F1	4.779	4.902	5.381	4.885
F2	4.374	9.274	5.866	3.200
F3	4.003	9.880	5.003	2.300
F4	10.084	7.362	3.519	1.663
F5	7.728	3.804	1.992	1.052
F6	5.922			
F7	4.538			
F8	4.445			
F9	3.117			
F10	3.020			
F11	2.527			
F12	1.689			
Total	100.000	100.000	100.000	100.000
C_{7+}	56.226	35.222	21.760	13.100
M_{7+}	243.000	225.000	228.000	220.000
h^0 (m)	1550	2695	3160	3049
T^0 (deg.C)	68	95	130	132
p^0 (bara)	160	267	492	469

As these fluid systems range from black oil/dry gas to near critical oils and gas condensates, they should represent typical reservoir fluid systems in the North Sea (and elsewhere). The complete EOS characterization for these systems are given in Appendix A. Reference conditions of depth , composition, temperature and pressure, are given in Table 2.1. The BO and the SVO examples represent reservoirs at

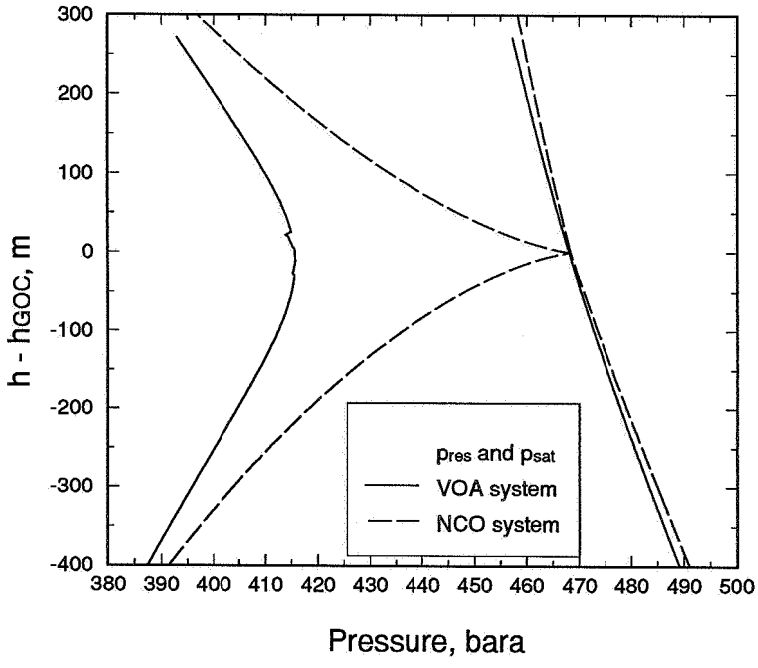

Fig. 2.3 Reservoir pressure and saturation pressure in VOA and NCO reservoirs. Isothermal GCE calculations.

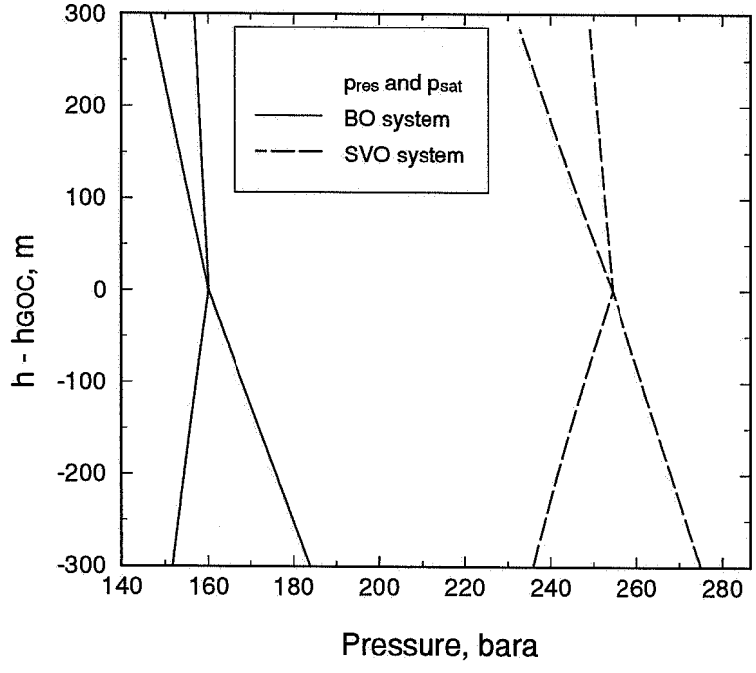

Fig. 2.4 Reservoir pressure and saturation pressure in a BO and a SVO reservoir. Isothermal GCE calculations.

conditions far from critical conditions, see Fig. 2.3. The VOA system represents a system with continuous change from a gas condensate to a volatile oil, while the NCO system has a saturated gas-oil contact, as seen in Fig. 2.4.

We apply the isothermal GCE procedure presented in Section 2.2.2 on the four fluid systems. Figs. 2.5 and 2.6 show results for the derivative of compositional variation with depth for C_1 and C_{7+}, plotted relative to the GOC.

Our results clearly demonstrates how the compositional variation with depth is largest in the vicinity of the critical conditions, as discussed earlier in this section. The maximum compositional variation is found at the gas-oil contact in the near critical oil case. The example with the second largest variation is the VOA system, with its largest variation at the undersaturated GOC. This depth represents the minimum distance between the initial reservoir pressure and the saturation pressure (see Fig. 2.4.). This distance is thus significantly larger than the zero distance between saturation pressure and reservoir pressure at the gas oil contact in the NCO case. Hence, the compositional variations at this point is larger in the NCO case than in the VOA case.

The slightly volatile oil case and the black oil example both show smaller compositional gradients than the VOA example, and with a distinct discontinuity at the saturated GOC. The black oil is far from critical conditions and shows the smallest compositional variation with depth. The same main behaviour is found when studying the gradient in saturation pressure for these fluid systems. Consider Fig. 2.7, which is taken from Whitson and Belery's paper. The typical trends in saturation pressure follow directly from the variations in composition. The gradients in saturation pressure for the different fluid systems were found to be in the range from 0.025 bara/m for the black oil example to 1 bara/m in the vicinity of the GOC for the near critical oil example.

EOS-Characterization

When applying a cubic equation of state in isothermal GCE calculations to predict property variations with depth, it is important to have a valid EOS-characterization. "Valid" in this context is an EOS that predicts absolute component fugacities and phase densities accurately. As seen directly from Eq. 2.23, the governing terms in isothermal GCE calculations include molecular weight, volume translation and fugacity. Fugacity can be directly related to vapour-liquid equilibrium (VLE) data. This suggests that VLE data should be the key laboratory data required to tune the

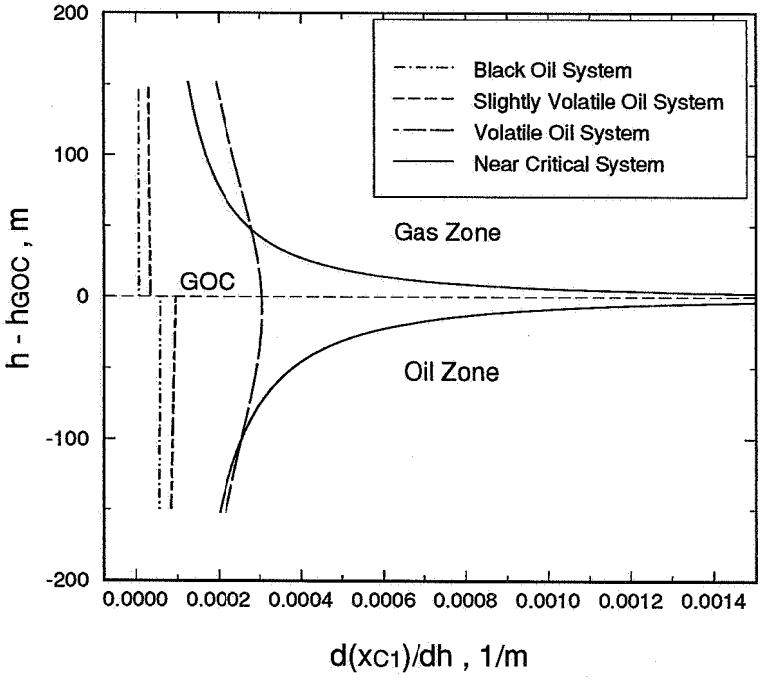

Fig. 2.5 Calculated gradients in methane mole fraction.

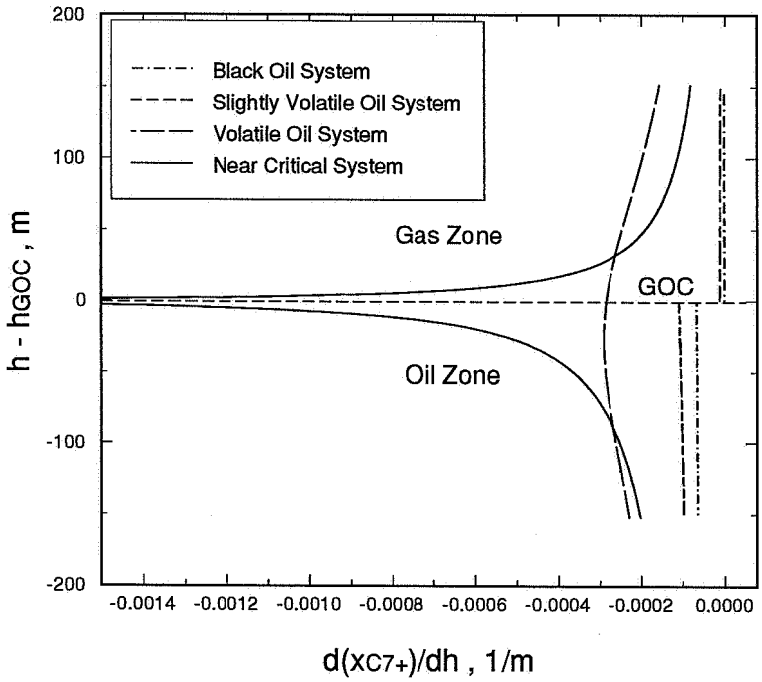

Fig. 2.6 Calculated gradients in C_{7+} mole fraction.

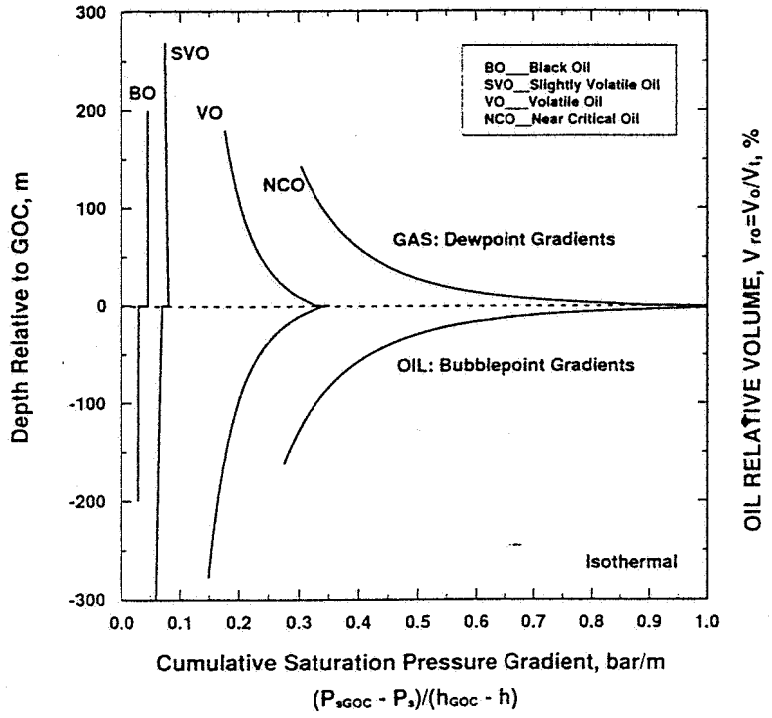

Fig. 2.7 Cumulative saturation pressure gradient versus depth relative to GOC (from Whitson and Belery, 1994).

equation of state. This includes measurements of volumetric properties, saturation pressure versus composition and K-values at different pressures. Notice however that equilibrium data only reflect fugacities indirectly (as ratios of fugacities are used instead of absolute fugacities).

Whitson and Belery (1994) and Whitson (1995) emphasize that measurements should be performed on samples that reflect the compositions at different depths in the reservoir of interest. Thus, if significant vertical compositional variations exist it is important that the samples should span the range of composition, temperature and pressure variations found in the reservoir. The data should then be applied in *simultaneous* tuning on VLE data from all samples, to obtain a single EOS characterization that correctly describes the whole reservoir. If this procedure is followed then the EOS should yield more accurate (a) solution of Eq. 2.23 for pressure and composition as a function of depth, and (b) the prediction of volumetric properties (e.g. density, gas-oil ratio) based on the results in (a).

2.3.2 Variations in Properties with Depth

Once the pressure and compositional variation with depth is known, other physical properties can be found by applying the cubic equation of state and, if necessary, through additional correlations. In this subsection we discuss typical variations with depth for key physical properties. We have used the four fluid systems presented in the previous subsection as the basis for this study.

Variations in fluid properties with depth is important for

- *Predictions of immiscible displacement processes* (water or gas injection). Immiscible displacement processes (Dietz, 1953) are most dependent on the viscosity ratio and the density difference between the reservoir fluid and the injectant.

- *Predictions of gas and oil properties at the surface.* The expected wellstream composition, gas-oil ratio and stock tank oil gravity from different depths in the reservoir form the basis for surface process requirements. Calculations should be applied at realistic separator conditions to yield representative results.

In addition, estimates of initial hydrocarbon in place and particularly condensate in place may be sensitive to compositional variation with depth, as discussed in Section 2.3.5. These points motivate the following discussion. We emphasize that large depth intervals has been applied in the investigations to cover the main effects for different fluid systems.

Fig. 2.8 shows calculated variations in reservoir fluid molecular weight for the four different fluid systems. Fig. 2.9 shows variations in reservoir fluid density with depth, calculated at reservoir pressure and temperature. Both figures demonstrate small and approximately linear property dependency with depth within each phase in the case of the BO and SVO systems. The volatile oil system shows larger, continuously-varying properties with depth, and the variations are not linearly dependent of depth. As a direct result of the compositional gradients, the largest gradients in molecular weight and density are found in the NCO example in the vicinity of the GOC. Tables 2.2 and 2.3 gives calculated fluid property variation with depth (below GOC), in the case of the BO, SVO, VOA and NCO systems. Notice also that in the NCO example we find the viscosity 100 m below the GOC to be approximately 50 percent larger

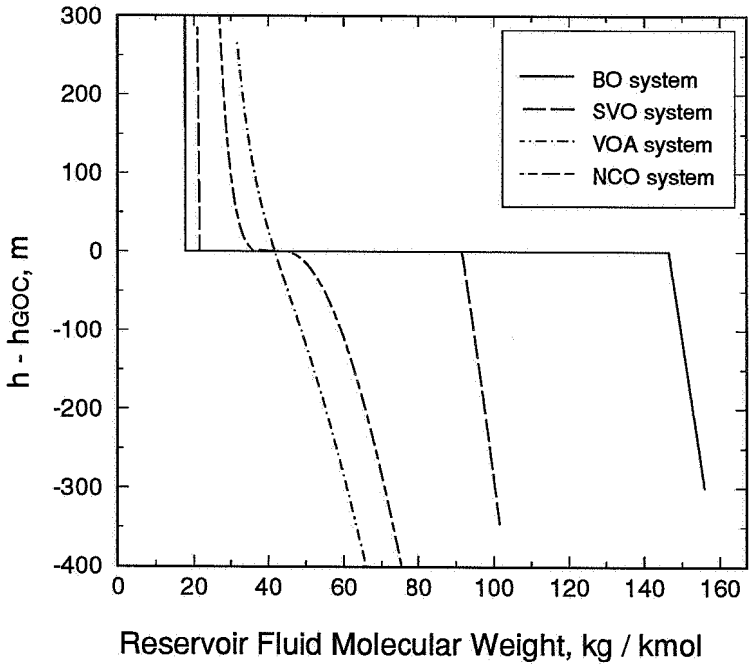

Fig. 2.8 Isothermal GCE results for mixture molecular weight variation with depth.

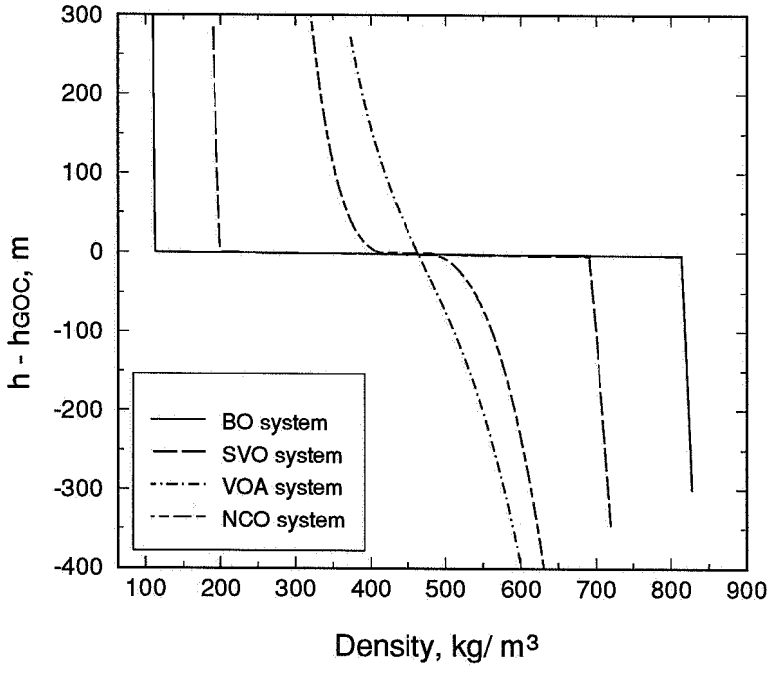

Fig. 2.9 Isothermal GCE results for reservoir fluid density variations with depth.

Table 2.2 Calculated property variation with depth below GOC in the BO and the SVO system. Isothermal GCE calculations.

Distance below GOC (m)	BO system			SVO system		
	M_o kg/kmol	ρ_o kg/m^3	p_b bara	M_o kg/kmol	ρ_o kg/m^3	p_b bara
0	146.5	813.5	160.0	91.6	689.7	254.5
10	146.8	814.0	159.7	91.9	691.0	253.8
25	147.3	814.7	159.3	92.3	692.2	252.7
50	148.0	815.9	158.6	93.1	694.8	251.0
100	149.6	818.4	157.1	94.7	699.4	247.5
200	152.7	823.2	154.3	97.5	708.5	241.5

Table 2.3 Calculated property variation with depth below GOC in the VOA and the NCO system. Isothermal GCE calculations.

Distance below GOC (m)	VOA system			NCO system		
	M_o kg/kmol	ρ_o kg/m^3	p_b bara	M_o kg/kmol	ρ_o kg/m^3	p_b bara
0	41.7	463.4	415.6	45.3	482.6	468
10	42.5	468.3	415.5	49.0	503.5	462
25	43.5	476.0	415.1	51.7	520.4	456
50	45.2	487.9	414.9	54.8	538.5	448
100	48.7	511.4	412.4	59.3	561.9	436
200	55.2	549.5	404.5	65.7	592.1	418

than the viscosity at the gas-oil contact.

Whitson and Belery (1994) gives calculations yielding significant variations in producing gas-oil ratio with depth for the fluid systems considered. Such variations will be important for surface process design. Fig. 2.10 shows our calculated results

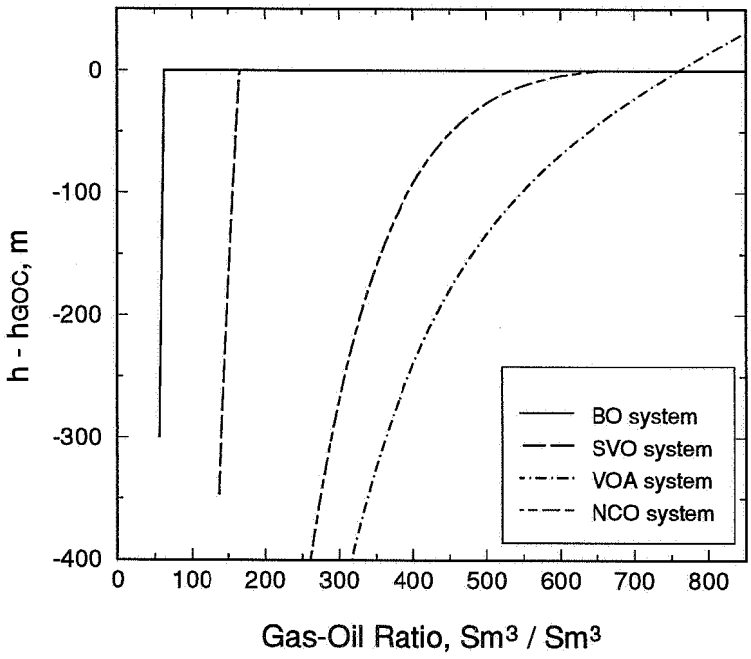

Fig. 2.10 Gas-oil ratio as a function of depth below GOC in four different fluid systems. Isothermal GCE calculations.

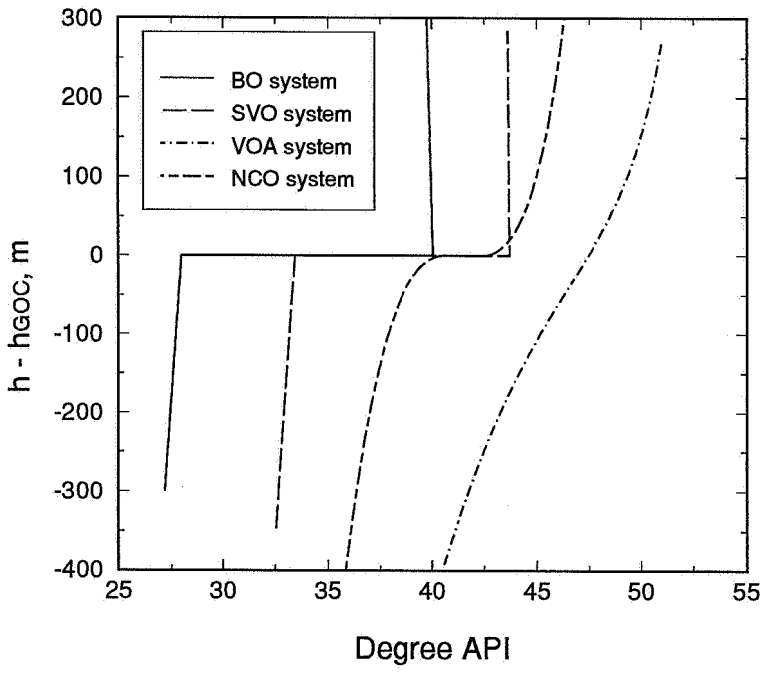

Fig. 2.11 Calculated API variation with depth. Isothermal GCE calculations.

for the produced gas-oil ratio as a function of depth. Both the volatile oil example and the near critical oil case show significantly variations with depth. Fig. 2.11 shows another surface quantity, the calculated stock tank oil API gravity as a function of depth. In both examples above we applied a single stage separator at standard conditions in the calculations. Notice that the VOA example gives the lowest stock tank oil specific gravity at these conditions, i.e. the highest degree API compared to the other fluid systems. The continuous variation with depth in degree API in this example is approximately equal to 10 °API, when comparing the values 300 m below and 300 m above the GOC.

In summary, these isothermal GCE calculations both demonstrate (1) how estimated property variation with depth can be significant in near critical fluid systems and less significant in highly undersaturated systems, and (2) how the variation in a series of different physical properties can be directly related to the compositional variation with depth.

2.3.3 A New Algorithm for Determination of Gas-Oil Contact

It is important to apply precise methods for determination of the gas-oil contact, as the position of the GOC is one of the key factors both in economic evaluation of a field and in practical production strategy of the reservoir. Several standard techniques for determination of a possible GOC exist, where formation pressures obtained from repeat formation tester (RFT) is the most common. With this method reservoir pressure (i.e. the mobile phase pressure at a given depth) is recorded as a function of depth. Distinct changes in the slope of the pressure versus depth gives knowledge about possible gas-oil contacts or water-oil contacts.

In this subsection we discuss methods for determining the GOC based on isothermal calculation methods and suggest new algorithms for locating the position of the GOC. When limited information about a newly discovered field exists, these methods can be used for GOC determination. An additional underlaying motivation for a search for a new algorithm is the potential for applying this parameter in EOS-regression (Whitson, 1995), which requires a fast *and* reliable GOC algorithm

Interval Halving

Whitson and Belery (1994) discussed possible methods for GOC determination, and suggested the following interval halving algorithm based on saturation pressure calculations:

1. Calculate the composition and pressure at top and bottom of the reservoir, applying the isothermal GCE method.

2. Calculate the saturation pressure at top and bottom of the reservoir, h^T and h^B. If the saturation type at these conditions equals, no GOC exist. If not, interval halving is initialized by performing an isothermal GCE calculation followed by a saturation pressure calculation, at depth $h = 0.5\ (h^T + h^B)$.

3. If the saturation type at h is a dewpoint, set $h^T = h$. Else, set $h^B = h$. Interval halving is performed with the new values for h^T or h^B, by setting $h = 0.5\ (h^T + h^B)$.

Point 3 is repeated until the difference between the new depth h at iteration n and the old depth at iteration $n\text{-}1$ is less than a convergence criteria, for example $\delta h=0.001m$. The number of iterations required to determine the gas-oil contact within this limit is given as $1.443\ ln\ ([h^T\text{-}h^B]/\ \delta h)$, i.e. 19 iterations if $h^T\text{-}h^B = 500$ m. This number will be independent of the fluid system considered.

This algorithm is failsafe provided the saturation type can be determined correctly. However, the method is somewhat slow, and improved algorithms can be found. Although the interval halving method was applied by Whitson and Belery, they noted that several possible techniques for locating the gas-oil contact can be tried; involving stability tests, negative flash calculations, saturation pressure calculations, modified phase envelope calculations or modified critical point calculations. An attempt to apply a modified phase envelope calculation to determine GOC's is discussed in the following.

Modified Phase Envelope Calculation

The equations describing isothermal gravity chemical equilibrium can be solved efficiently. The main equations are on the *same form* as the main equations in a saturation pressure calculation, and Michelsen's solution technique with successive substitution accelerated with GDEM for the composition and a Newton-Raphson method for the pressure update can be used, as discussed in the previous sections.

We tried to take this analogy one step further. Michelsen (1992) proposed an efficient and fast algorithm for calculation of accurate approximate phase envelopes for mixtures. The solution technique is based on a "smart" update and specifications for the incipient phase composition. Calculations start for example in the low

pressure/high temperature region, going through the critical point where the incipient phase composition equals the mixture composition, and ending up in the low pressure/low temperature region, by solving for p,T at each specification of the incipient phase. When using a linear or quadratic extrapolation for p,T, the algorithm is extremely fast compared to a series of ordinary saturation pressure calculation. An analog to this solution technique for compositional gradients can be found, and is based on the following observations for isothermal calculations

1. The fugacity is continuous over the whole reservoir height, also over the GOC. Thus the expression $f_i(h) = f_i(h^0) \exp(\frac{-M_i g (h-h^0)}{R T})$ is valid for all depths, h.

2. If a saturated gas-oil contact exists the composition is not continuous over the GOC. The analogy to the phase envelope calculations rests on the observation that the reservoir composition, z_k, versus depth (the "incipient phase composition" analogy) is approximately given as:

$$z_k = \frac{z_{k,refo} \left(\frac{z_k^B}{z_{k,refo}}\right)^{\alpha^B}}{\sum_k z_{k,refo} \left(\frac{z_k^B}{z_{k,refo}}\right)^{\alpha^B}} \qquad k=1,..,n \qquad h \in [h^B, h_{GOC}] \qquad (2.26)$$

$$z_k = \frac{z_{k,refg} \left(\frac{z_k^T}{z_{k,refg}}\right)^{\alpha^T}}{\sum_k z_{k,refg} \left(\frac{z_k^T}{z_{k,refg}}\right)^{\alpha^T}} \qquad k=1,..,n \qquad h \in [h^T, h_{GOC}] \qquad (2.27)$$

where T and B represent top and bottom of the reservoir, respectively. The subscripts *refg* and *refo* refer to one known reference condition in the oil zone and one in the gas zone. α^T and α^B represent specified numbers smaller than or equal to one (also

negative).

Eqs. 2.26 and 2.27 yield the correct composition at values of α equal to one and zero. We basically assume that for each component k there exists a relationship of the form $\ln Y_k = \ln z_{k,ref} + \alpha\,[\ln z_k^T - \ln z_{k,ref}]$ within each hydrocarbon phase. Here Y_k represents a composition, such that the normalized reservoir composition is given as $z_k = Y_k / \sum_k Y_k$ for each component k. In the case of reservoir fluid systems which are significantly away from critial conditions we find this approximation to give reasonable results within each phase, as shown in Appendix B. When *passing* through the GOC the calculated compositions are continuous with depth, but represent non-physical solutions.

The analogy with a saturation pressure and a phase envelope calculation suggests the following equations are nescessary to find an approximate solution for composition and reservoir pressure versus depth. Mole fractions should sum to unity and the equations for fugacity are given above.

$$d_k = f_k(z_k,h,p_{res}) - f_k(z_k^T,p^T,h^T)\,\exp\left(\frac{-M_k\,g\,(h-h^T)}{R\,T}\right) \qquad k=1,..,n \quad (2.28)$$

$$g_1 = \sum_k z_k^T\,d_k = 0 \quad (2.29)$$

$$g_2 = \sum_k z_k\,d_k = 0 \quad (2.30)$$

Eqs. 2.28 to 2.30 are used for calculations in the gas zone. The same expressions, changing the superscript T to B are used in the oil zone. This gives two equations and two unknowns for a given specification of α^T or α^B, when Eqs. 2.26 and 2.27 are used to determine reservoir composition. To initialize the calculations, composition and reservoir pressure at the top and the bottom of the reservoir and at the reference conditions are found from the ordinary GCE calculation method

The solution strategy is as follows:

1. Perform an ordinary GCE calculation and a saturation pressure calculation at the top and the bottom of the reservoir. If the phases are different, start the search for the GOC.

2. "March" from the top of the structure downwards into the gas zone, by specifying α^T initially equal 1.0, and then reducing the value in a stepwise manner. For each specification of α^T, g_1 and g_2 are forced to zero through a simple 2D Newton-Raphson method (with steplength control), which gives a solution for pressure and depth for the α^T spesification

3. Linear extrapolation of depth and reservoir pressure as a function of α^T is used for a new specification, to minimize the number of iterations required.

4. A corresponding calculation method is performed from the bottom of the reservoir.

5. The conditions for $\alpha^T$and α^B which yield the same reservoir pressure defines the condition for the gas-oil contact, see Fig. 2.12.

Clearly this is an approximate method, as both the composition estimate and the simplification of the problem to be solvable as a two-equation/two-unknown situation are not rigerous. To evaluate the method, it was compared with the ordinary interval halving method. Tests on several reservoirs fluids showed that the predicted GOC with the approximative method is within 0 - 1 m of the interval halving results in fluid systems with a saturated GOC far away from critical conditions. Computation time was found to be at least two times faster than the interval halving method. However, in near critical systems with large compositional gradients and a saturated GOC the predictive capability of the new method is worse. The region near the GOC with large compositional gradients is not approximated correctly if the reference conditons are away from this region. Consequently, the GOC determination is less accurate, as shown in Fig. 2.13. Here there is a significant difference of 2.7 m in GOC predictions with the new method and the interval halving method. Notice also that the method is only applicable in the case of a saturated GOC, as there is no well defined crosspoint for the reservoir pressure versus depth for a physical situation where there exist a *continuous transition* from a gas-like to an oil-like reservoir fluid versus depth.

In summary, and although interesting, the method is not robust enough as a general

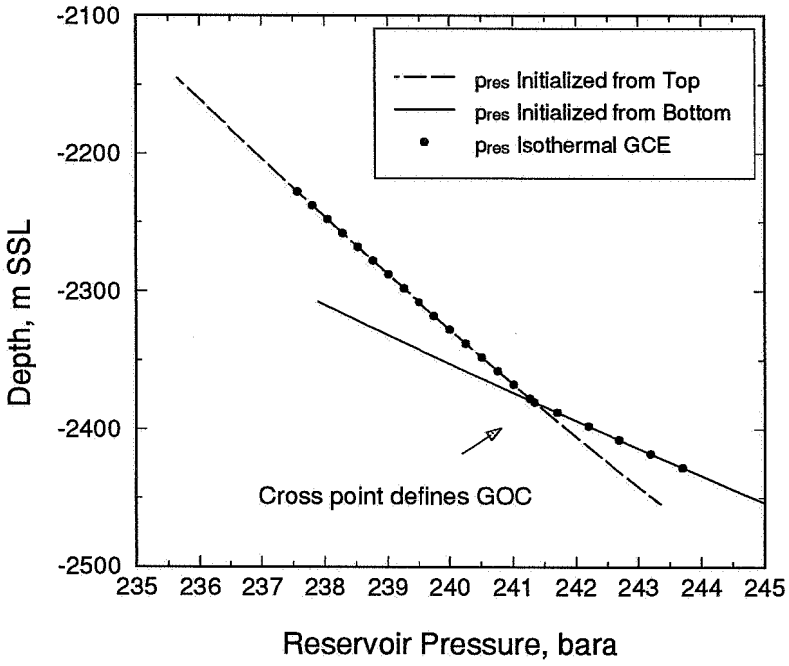

Fig. 2.12 The modified phase envelope method applied to a gas condensate reservoir.

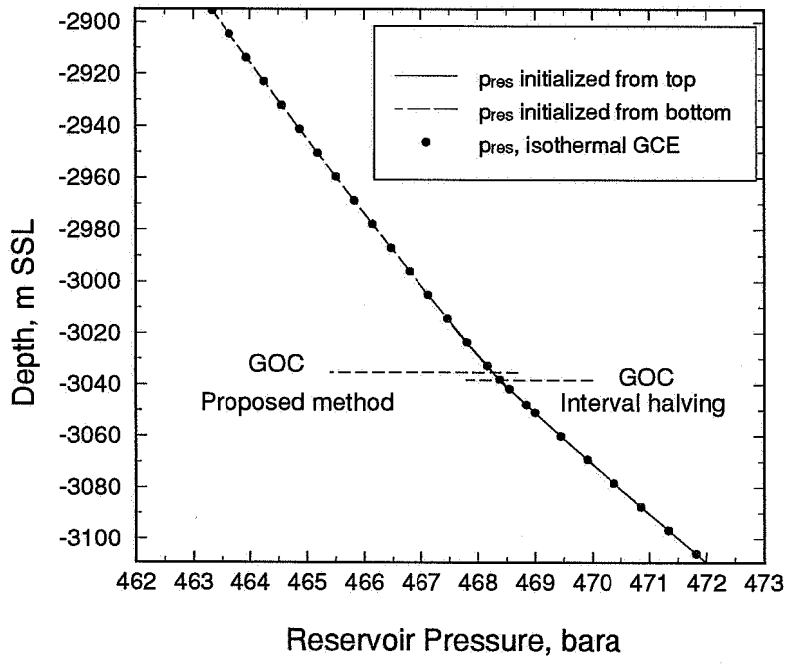

Fig. 2.13 The modified phase envelope method applied to a near-critical reservoir fluid system.

GOC-algorithm. In addition one needs two known reference conditions, one in the oil zone and one in the gas zone, instead of one. This motivates for a search for a more general procedure to determine the GOC accurately.

An Improved Method

A valid GOC algorithm should be able to compute the gas-oil contact accurately, independent of wheter the conditions at the GOC are saturated or not. The main behaviour of the K-values at the critical point suggests that it is possible to combine the characteristics at a saturated and undersaturated GOC, into one function. Consider the functions

$$\Delta p = \frac{(p_{res} - p_{sat})}{p_{res}} \tag{2.31}$$

and

$$\Delta C = \sum_{k=1}^{n} (\ln K_k)^2 \tag{2.32}$$

where p_{sat} and p_{res} represent the saturation pressure and reservoir pressure, respectively. K_k are the K-values of component k at the depth considered, evaluated *at the saturation pressure.*

In the case of a fluid system with a saturated GOC the Δp term goes towards zero approaching the GOC, and being equal to zero at the GOC. For a situation with an undersaturated GOC, the K-values for each component approaches 1.0 near the GOC. Hence, the term ΔC equals zero at the GOC in this situation. We now introduce a new function F, where for each depth F is given as

$$F(K, p_{res}, p_{sat}, T) = F(z, p_{res}, T) = \Delta p \cdot \Delta C \geq 0 \tag{2.33}$$

This function ensures a continuous behaviour going through zero at GOC *both* in the case of a saturated and an undersaturated GOC. F is a function of composition, temperature and pressure. All parameters needed to evaluate this function (for an

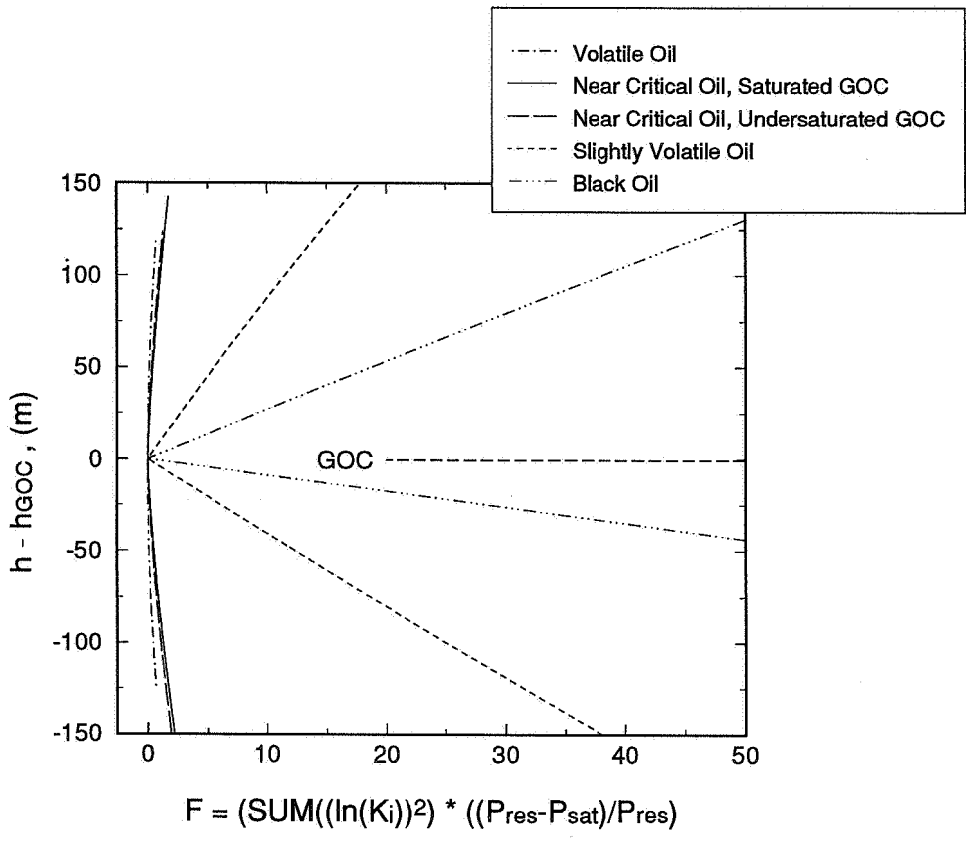

Fig. 2.14 Evaluation of F as a function of depth for different fluid systems. Isothermal GCE calculations.

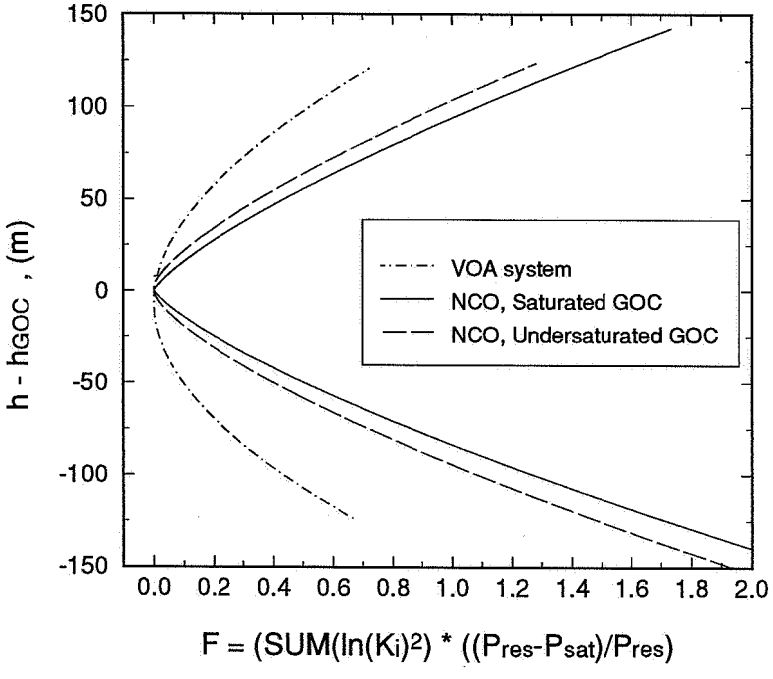

Fig. 2.15 Detail of F versus depth for saturated and near-saturated near-critical fluid systems.

arbitrary depth) can be found directly from an isothermal GCE calculation in combination with a saturation pressure calculation.

The behaviour of F as a function of depth has been studied for different reservoir fluid types, and typical behaviour is shown in Figs. 2.14 and 2.15. Included in these studies is also an example with the NCO fluid system presented earlier, but with reference pressure increased by 14 bar to artificially generate a near critical *undersaturated* GOC.

As seen from Figs. 2.14 and 2.15, F is continuous as a function of depth. F reaches its minimum equal zero at the GOC and increases when considering depths at increasing distance away from the GOC. For the black oil and the slightly volatile oil systems, F is found to be approximately linear with depth within each phase. For the volatile oil and near critical oil examples the behaviour of F versus depth is more non-linear. This is in agreement with the discussion in Sections 2.2.3 and 2.2.4 concerning gradients in composition and saturation pressure in different fluid systems.

As the function F(h) can be evaluated at any depth, it is possible to force the function to zero by a typical one-dimensional Newton-Raphson method.

The calculation technique for the proposed new method is as follows:

1. Calculate p_{sat} , p_{res} and composition. Identify the phase at top and bottom of the reservoir structure. If phases are identical the reservoir consist of one phase only, and no GOC exist. If not, evaluate the function F at top and bottom, and choose the point with smallest F, i.e. closest to GOC, as initial/base point.

2. Perturb the base point depth, evaluate F at perturbed depth, and use a Newton-Raphson method (with step-length control) to force F(h) to zero.

3. If F is less than 5 E-04, check if ΔC is smaller than Δp. If this is the case, this indicate that the GOC is undersaturated and it is extremely hard computationally to converge the problem further, so quit. If Δp is smallest, the GOC is saturated. Continue until F is less than 1 E-05.

For the case of a saturated GOC we find that the convergence criterium in step 3 ensures a predicted GOC +- 0.0005 m. See Table 2.4 and Figs. 2.16 to 2.19.

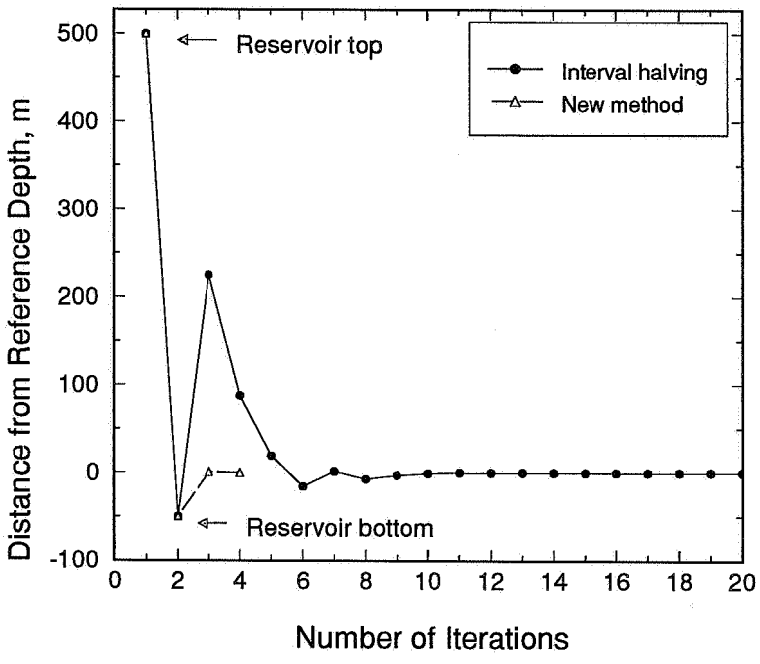

Fig. 2.16 Comparison between proposed GOC method and interval halving, BO system.

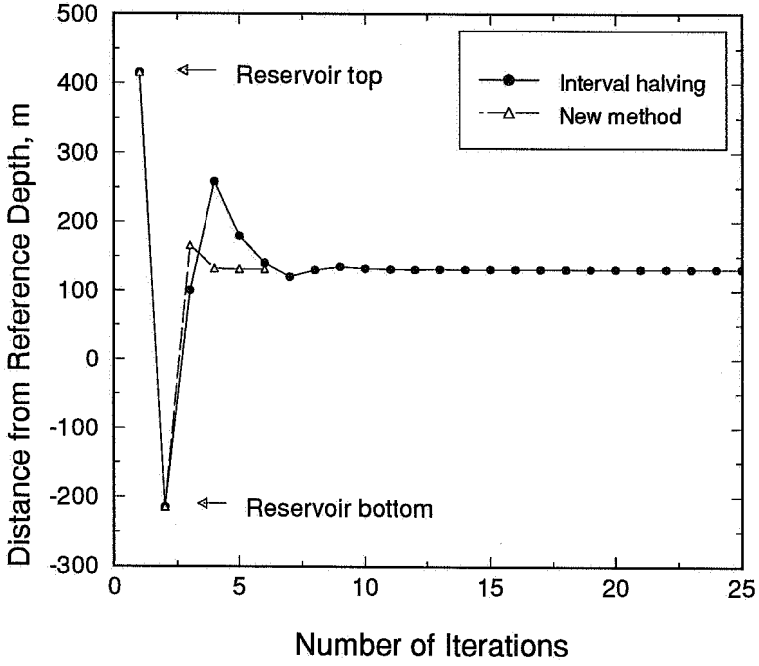

Fig. 2.17 Comparison between proposed GOC method and interval halving, slightly volatile oil system.

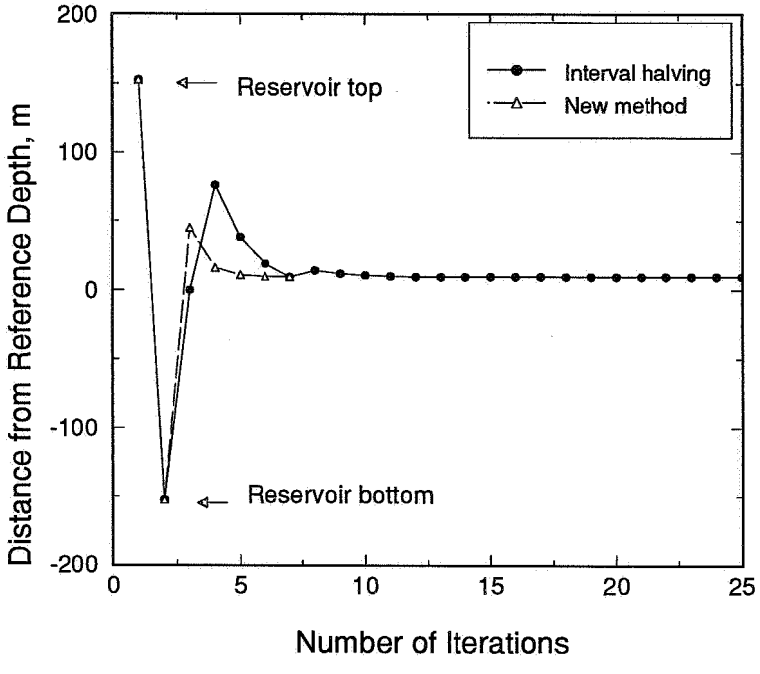

Fig. 2.18 Comparison between proposed GOC method and interval halving, saturated near-critical fluid system.

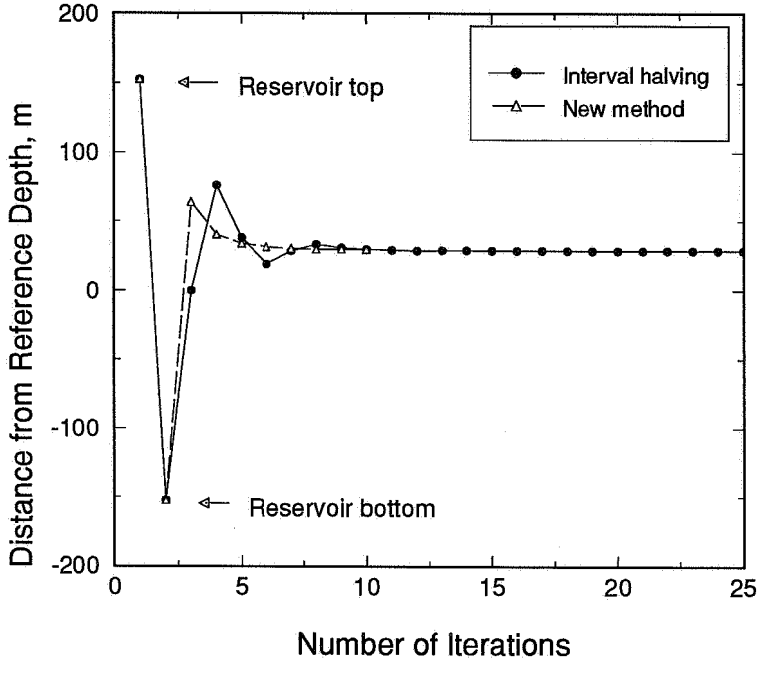

Fig. 2.19 Comparison between proposed GOC method and interval halving, near-saturated near-critical fluid system.

Table 2.4 Calculated position for GOC found with interval halving method, and with the proposed method using minimization of the function F.

System	GOC interval halving (m)	GOC new method (m)
Black Oil	-1549.9993	-1549.9995
Gas Condensate	-2380.5377	-2380.5378
Slightly Volatile Oil	-2503.7611	-2503.7611
Near Critical Oil 1*	-3038.2156	-3038.2151
Near Critical Oil 2 **	-3019.2418	-3018.4669
* : NCO example with saturated GOC, p_{ref} = 469 bara **: NCO example with undersaturated GOC, p_{ref} = 483 bara		

The applied Newton-Raphson method requires numerical derivatives of F with respect to *h*. This doubles the number of calculations compared to what is shown in Figs. 2.16 to 2.19. However, the calculations for the perturbed conditions are computationally cheap. Calculated reservoir pressure, saturation pressure and K-values at base point, serves as excellent initial conditions for the perturbed point calculations, and speeds up the calculation process significantly. When applying a Newton-Raphson method the number of iterations needed to achieve convergence will depend on the values of the first and second derivative of F with respect to depth. This number will be case dependent, and thus vary for different fluid systems. Due to the different curvature in the function F, the lowest number of iterations is needed in the BO system, while the largest number of iterations are reqired for the NCO system with an undersaturated GOC. This demonstrates that the proposed method is most beneficial in the case of reservoir fluids with small compositional gradients.

As seen from Fig. 2.19 and Table 2.4 the predictions from the new method differ somewhat (0.8 m) from the interval halving method when applied to the NCO system with undersaturated GOC. In these cases it is extremely hard to define a phase with 100% certainty. Therefore, the interval halving method is not more reliable than the new method because a wrong phase definition could result in the exclusion of a region where the GOC actually is positioned.

To summarize these examples demonstrate that the proposed method is as accurate as the interval-halving method. Computational speed is in all of the examples increased at least with a factor of 1.5 - 4 compared to the interval halving-method. The method is most beneficial in the case of saturated gas-oil contacts.

2.3.4 Effect of Sampling Errors on Compositional Gradients

In this subsection we discuss errors connected with sampling and their effect on isothermal gradient calculations.

Common sampling techniques are bottom hole sampling (typically applied in oil zones) or recombined separator samples from production tests (typically applied to gas condensate and oil reservoirs). Samples are usually taken from a completation interval and will at best represent an average composition over this perforated interval. Perforation intervals are known and reported, and may range from 1 to 50 m. Hence, standard sampling techniques are only able to define reference conditions with some uncertainty. As a result it is often difficult to obtain reliable and consistent measurements of composition with depth. This complicates the evaluation of compositional gradient models and their ability to describe actual compositional variations in petroleum reservoirs. New technology (e.g. RFT and MDT methods) have been developed and will hopefully lead to a more precise determination of initial compositional variation with depth in the future. These methods can be applied before casing is set, where samples can be taken dirctly from the porous medium at a spesific depth. Thus, theoretically these methods should be ideal for precise determination of compositional variations with depth.

As pointed out by Fevang and Whitson (1994), *any* uncontaminated fluid sample produced from a petroleum reservoir can and should be used to develop an EOS fluid characterization. However, a valid *compositional gradient calculation* requires an in situ representative sample as a reference point. The definition of an in situ representative sample is (Fevang and Whitson, 1994):

> *A sample that correctly reflects the composition of the reservoir fluid at the depth or depths being tested.*

The discussion of uncertainty in definition of in situ representative samples can be divided into five main parts: sampling method, perforation interval, reservoir geology, reservoir fluid state, and laboratory problems.

Sampling method. The conditions during sampling should be checked. Temperature, pressure and producing GOR should be stable during sampling. Flowing bottom hole pressure should be larger than saturation pressure to avoid multiphase flow near the wellbore.

Perforation interval. The perforated interval should ideally be as small as possible. The depth interval should be compared to the thickness of the producing layer, and compared to the position of the GOC to ensure that coning is not a problem.

Reservoir geology. Heterogeneties near the wellbore can result in complex fluid flow patterns. This can potentially generate a situation where the produced fluid composition at the sampling depth is not in situ representative for that depth. Communicating layered systems with high permeability contrast, or natural fractures close to the wellbore can induce similar uncertainties.

Reservoir fluid state. Near-saturated or saturated near-critical reservoir fluids will show large compositional variations for small differences in depth. For this condition a small error in the definition of the reference conditions may potentially cause large measurement errors in composition.

Laboratory measurement inaccuracies. There is some measurement uncertainty in the laboratory determination of dew point pressure for gas condensate samples. In addition, measurement errors in C_{7+} molecular weight and errors in recombination gas-oil ratio can generate (a) wrong composition, and as a direct result of this, (b) invalid saturation pressure for a given sample.

There will also be uncertainty connected to the instruments used to determine the reservoir pressure, temperature, and depth. Consequently, the sum of these factors will limit the accuracy of a possible in situ representative sample. Compositional gradient calculations can be sensitive to changes in the reference conditions and this should be taken into account in the evaluation of results.

A sensitivity analysis of errors in reference depth, pressures and composition for the NCO reference sample is given below. Potential changes in the resulting position of the gas-oil contact is studied in detail.

As samples are normally taken from perforation *intervals* there is a well-defined uncertainty in the reference depth of the produced reservoir fluid. In isothermal GCE calculations (Eq. 2.23) the distance from the reference depth is included in the calculations only. Consequently, a change in the reference depth causes only pressure and composition to be shifted upwards or downwards accordingly. Fig. 2.20 shows the result of changing the NCO reference depth from -3047.9 m to -3057.9 m. This change only shifts vertically the calculated results, including the GOC, 10 m

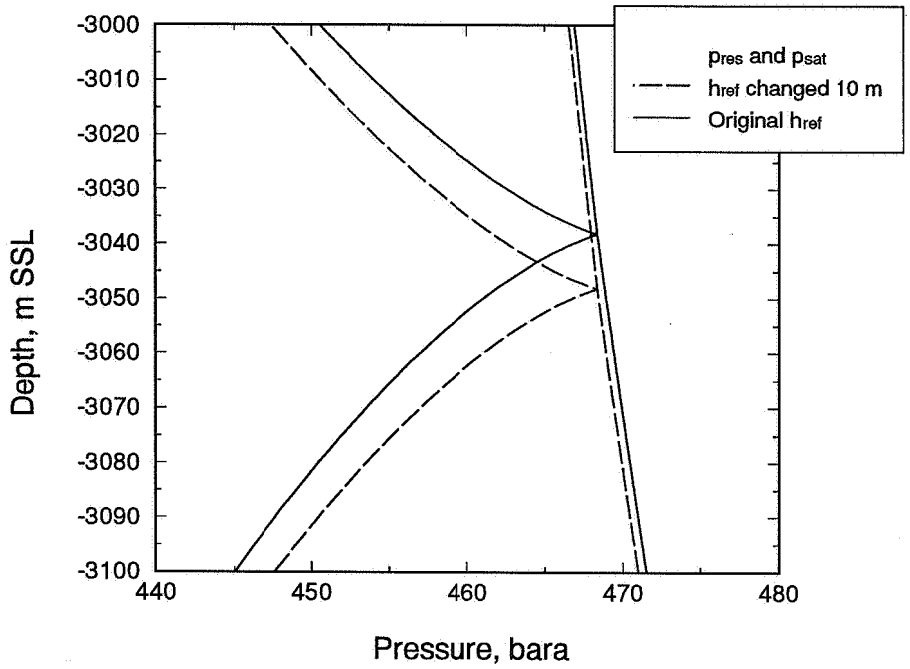

Fig. 2.20 Isothermal GCE calculations based on reference depth, and a shift downwards in reference depth of 10 m.

downwards. In isothermal GCE modelling the uncertainty in the position of the GOC equals the uncertainty in the reference depth.

In general, the difference between the reference depth and the position of the GOC, Δh_{GOC}, is given as

$$\Delta h_{GOC} = h^0 - h_{GOC} = f\left(\nabla p_{res}, \nabla p_{sat}, [p^0_{res} - p^0_{sat}] \right) \qquad (2.34)$$

where p^0_{res} and p^0_{sat} are the reservoir pressure and saturation pressure at reference depth, h^0. The gradients in reservoir pressure and saturation pressure will be a function of the compositional variation with depth within the considered depth interval.

An approximate expression for Δh_{GOC} can be found in the case of a saturated GOC by approximating the gradients in reservoir pressure and the saturation pressure as

$$(\nabla \bar{p}_{res}) = \frac{p_{GOC} - p_{res}^{0}}{h_{GOC} - h^{0}} \tag{2.35}$$

$$(\nabla \bar{p}_{sat}) = \frac{p_{GOC} - p_{sat}^{0}}{h_{GOC} - h^{0}} \tag{2.36}$$

where p_{GOC} is the reservoir pressure at the GOC. We eliminate the pressure at the GOC by combining Eqs. 2.35 and 2.36, and find

$$\Delta h_{GOC} = (p_{sat}^{0} - p_{res}^{0}) \left(\frac{1}{\nabla \bar{p}_{sat} - \nabla \bar{p}_{res}}\right) \tag{2.37}$$

Eq. 2.37 can be used to estimate the effect of an error in saturation pressure and reservoir pressure.

The uncertainty in reservoir pressure will normally be small. However, the uncertainty in saturation pressure can be significant. There are three potential sources for error connected to the saturation pressure, (a) measurement uncertainty in the laboratory, particularly in the case of gas condensate samples, (b) uncertainty in the EOS characterization which can easily have a few percent deviation in calculation of the saturation pressure, and (c) uncertainty due to wrong recombination of the sample (which yields wrong composition and hence wrong saturation pressure).

Errors in reference composition will influence the calculation of composition and saturation pressure with depth. To illustrate the influence of this effect Fig. 2.21 shows isothermal GCE calculations based on different compositions at the reference conditions. These reference compositions were generated by systematically introducing erroneous values in the recombination GORs. These calculations clearly demonstrate that the results are sensitive to changes in reference composition. The saturation pressure is a strongly dependent function of these changes, while the gradients in saturation pressure and reservoir pressure are more weakly dependent functions of the compositional changes. There is a discrepancy in the predicted GOC

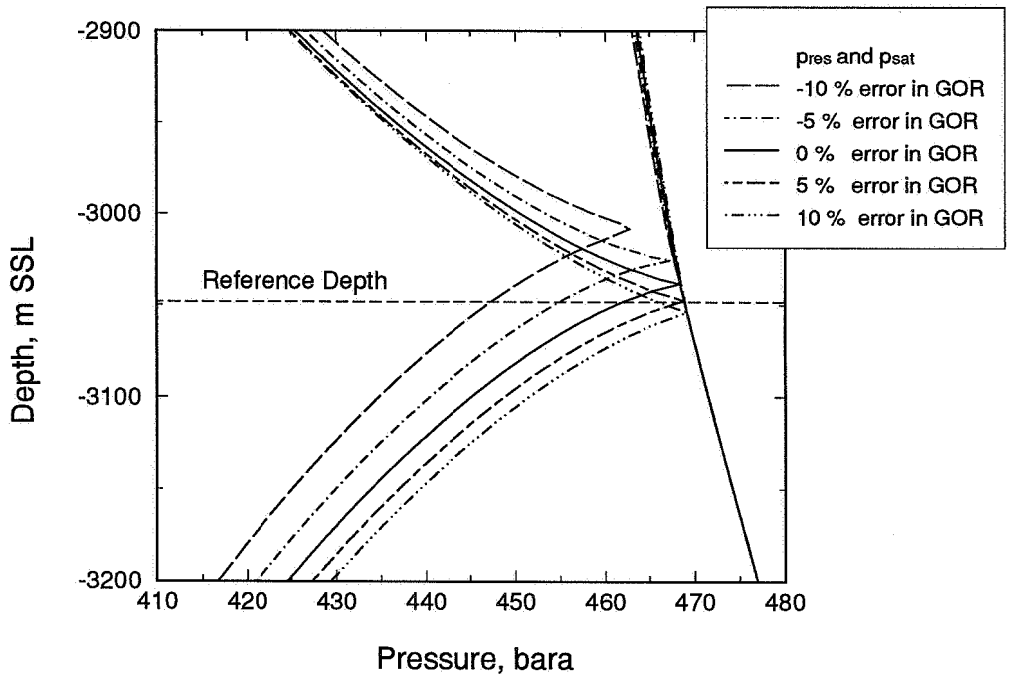

Fig. 2.21 Isothermal GCE calculations based on different reference compositions. The compositions were generated through errors in recombination GOR.

of approximately 50 m in the cases of ±10 percent error in recombination GOR. Notice also that in the case of a - 10% error in GOR the isothermal GCE algorithm predicts an undersaturated GOC, instead of a saturated GOC.

As shown in Fig. 2.21, the saturation pressure at reference condition, p^{0}_{sat}, changes as a function of the recombination GOR. We applied these changes in Eq. 2.37, in order to quantify the effect of an error in saturation pressure *alone*. The additional parameters in Eq. 2.37 were found from the isothermal GCE calculation with correct recombination GOR (and held constant). The resulting values for Δh_{GOC} are given in Table 2.5. The main conclusion from these calculations is that the effect of the error in saturation pressure alone will "dominate" the results. For example a change of 2 percent in p^{0}_{sat} will change the predicted position of the GOC by approximately 13 m. The additional compositional effects are significantly less than the saturation pressure effect, even in this near critical oil reservoir. In reservoirs with smaller compositional variations the saturation pressure effect is expected to be even more

Table 2.5 Calculated predictions of GOC as a function of (1) a change in saturation pressure alone, and (2) a change in composition *and* saturation pressure due to errors in recombination GOR.

% error in recombination GOR	p_b at reference depth (bara)	Δh_{GOC}, isothermal GCE (m)	Δh_{GOC}, Eq. 2.37 (m)
-10	447.33	- 39.8	- 31.6
-5	454.96	- 22.7	- 19.8
0	465.40	- 9.7	- 9.8
5	468.46	0.4	0.6
10	474.43	6.0	8.0

pronounced. In summary, our sensitivity study demonstrates that care should be taken when using gradient calculations based on a limited number of reference samples. Erroneous gradients will effect (1) model fluid property variations with depth, (2) the GOC, and (3) estimates of hydrocarbons in place. The results are particularly sensitive to errors in reference depth and saturation pressure at reference depth. Relatively small errors in these parameters can cause considerable errors. This suggests that potential in situ representative samples should be weighted extra in the EOS tuning procedure to optimize the saturation pressure fit for these particular samples.

We recommend that a quantification of the uncertainty limits be performed for each sample taken in the reservoir. When potential in situ representative samples are found, isothermal GCE calculations can be performed on each sample separately. The results should be compared to investigate if a consistent compositional variation with depth results, based on the estimated uncertainty limits.

2.3.5 Hydrocarbons-in-Place Calculations

In this subsection we discuss different methods for implementing compositional gradients to calculate hydrocarbons in place for a near critical reservoir mixture.

When a new petroleum reservoir has been discovered efforts are made to estimate the initial hydrocarbon reserves present, usually expressed as sales gas volumes and sales

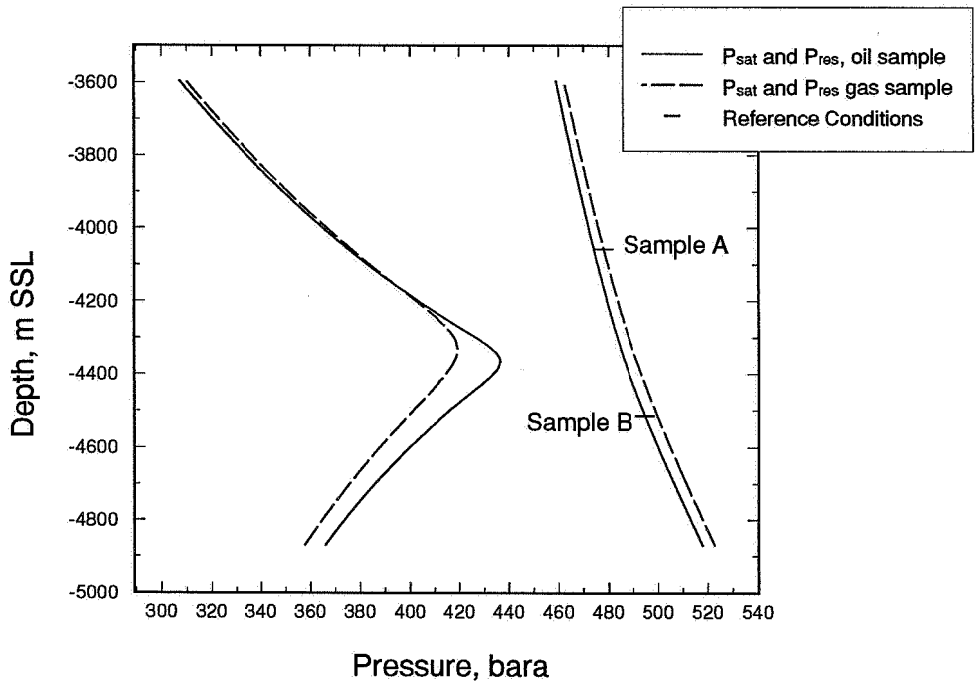

Fig. 2.22 Saturation pressure and reservoir pressure calculated by the isothermal GCE method, based on sample A and B, separately.

oil volumes (e.g. stock-tank oil), as these volumes represent the main justification for field development. In place calculations are dependent on reservoir geology and the nature of the reservoir fluid. The reservoir geology is difficult to define precisely and it will normally represent the largest uncertainty in the estimation of in place volumes. The size of different geological units in the reservoir are difficult to define accurately from seismic investigations and when applying information from a limited number of wells. Vertical and areal differences in porosity and water saturation may also exist. In addition, there can be a significant uncertainty connected to the fluid estimates, especially in near critical fields. The position of the gas-oil contact and the water-oil contact can also have large influence on the results.

Wheaton (1991) discussed in place calculations for two gas condensate fields including compositional variations with depth. The author applied isothermal compositional gradient calculations using two artificial 3-component systems, consisting of different mixtures of methane, butane and octane. When compositional variations were neglected Wheaton found that the estimate of initial in place volumes

could be in error up to 20%.

In the following discussion we present in place calculations based on actual data for a near critical reservoir. Two potentially in situ representative samples have been taken in this reservoir: (1) a lean gas condensate (sample A) taken from the upper part of the reservoir, and (2) a volatile oil bottom hole sample (sample B) taken at some distance below the undersaturated GOC. Fig. 2.22 shows isothermal GCE calculations performed separately on samples A and B. There is reasonably good consistency between the isothermal predictions, but there exists a discrepancy between the predicted undersaturated GOC of approximately 35 m. This discrepancy might indicate that the isothermal 1D model is not valid in this example. However, it might alternatively be related to uncertainty in determination of reference depth and saturation pressure, as discussed in the previous subsection.

By holding all geological parameters constant, and hence neglecting this uncertainty, it was possible to separately investigate the uncertainty in the in place calculations from the fluid part alone. Several methods for handling compositional gradients in this class of near critical reservoirs have been discussed in the industry (method 2 and 3 below). If only one sample exists for a near critical system a potentially large error in the in place estimates would be generated if a uniform composition is assumed throughout the reservoir. In the following study we considered three different methods for in place calculations:

- *Method 1.* Perform isothermal GCE calculations based on the reference sample. Reservoir fluid variation with depth is taken into consideration when estimating in place numbers.

- *Method 2.* Divide the near critical reservoir into two parts, one oil zone and one gas zone. The undersaturated GOC is found from isothermal GCE calculations and an average depth for the oil zone and the gas zone are calculated. At the average "gas zone depth" isothermal GCE calculations are performed to define the gas composition and this composition is assumed constant throughout the gas zone. Likewise, oil composition are calculated at average "oil zone depth" and assumed constant throughout the oil zone.

- *Method 3.* Use isothermal GCE calculations to calculate composition at average reservoir depth, and assume this composition to be constant throughout the reservoir.

Table 2.6 Calculated results for reserves in place based on the lean gas sample A.

	Method 1	Method 2	Method 3
Gg	1.0	1.011	
Go	1.0	1.033	
G	1.0	1.018	1.098
Ng	1.0	0.873	
No	1.0	1.022	
N	1.0	0.972	0.822

Table 2.7 Calculated results for reserves in place based on the oil sample B.

	Method 1	Method 2	Method 3
Gg	1.0	1.008	
Go	1.0	0.963	
G	1.0	0.995	1.108
Ng	1.0	0.873	
No	1.0	1.029	
N	1.0	0.979	0.720

The three methods were applied based on samples A and B, separately. A compositional simulator was initialized with compositions from the three methods and used to determine in place numbers. Tables 2.6 and 2.7 give the calulated in place results quantified as stock tank oil and separator gas. The results are given relative to the Method 1 results. We have applied a realistic multistage separator process in the calculations. The total stock tank oil volume, N, is the sum of the oil volume produced from the oil zone, N_o, and the oil from the gas produced from the gas zone, N_g. The total surface gas volume, G, is the sum of the gas volume produced from the oil zone, G_o, and the gas produced from the gas zone, G_g.

The result of the assumption in Method 3 is that the entire reservoir is treated as a rich gas condensate with uniform composition. As seen from the tables, Method 3 thus underpredicts oil in place numbers and overpredicts the gas in place estimates significantly compared to the other methods. Method 1 and 2 gives approximately the same results for the gas in place. However, Method 2 somewhat underpredicts the oil in place numbers compared to Method 1.

The calculations based on the oil sample B give lower estimates for oil in place and slightly higher estimates for gas in place than calculations based on gas sample A. This is mainly due to the predicted position of the undersaturated gas-oil contact which is lowest in the oil sample case.

In summary, we do not see any convincing reason for applying Methods 2 or 3 when calculating in place numbers. The methods unneccesarily oversimplefies the problem. Method 1 which takes compositional variations into account, is relatively easy to perform and is reccomended.

2.4 Implementation of Thermal Diffusion in Compositional Gradient Calculations

In this section we calculate and analyse the effect of thermal diffusion on vertical compositional gradients for a number of different fluid systems. Three different models for prediction of thermal diffusion have been applied in our calculations. The purpose has been (1) to investigate if the models predict consistent results when compared to each other, and (2) to analyse the effect of implementing these models in compositional gradient calculations. The results in (2) are compared to results from isothermal calculations results, to quantefy the differences between isothermal and thermal models.

2.4.1 Background of Thermal Diffusion

In the absence of gravity, a temperature gradient may induce a compositional gradient in a mixture caused by thermal diffusion. This effect was observed by Ludwig (1856) and later described by Soret (1879). The effect is known as the Soret-effect. Several authors addressed the phenomenon during the period 1950-70, both through theoretical work and experimental investigations on *binary mixtures*. de Groot (1950) outlined the most important equations provided by irreversible thermodynamics to describe the effect from a phenomenological approach. The majority of experiments in this period were performed with two-chamber cells separated by a membrane and with a controlled temperature gradient across the cell. Historically, the discussion of thermal diffusion is given in terms of α_k^T and k_k^T, the dimensionless thermal diffusion factor and ratio, respectively. At stationary state the compositional gradient in a temperature field is defined as

$$\nabla x_k = - x_k \cdot (1 - x_k)\ \alpha_k^T \frac{\nabla T}{T} = - k_k^T \frac{\nabla T}{T} \qquad k = 1,..,n \qquad (2.38)$$

where gravity is neglected. The thermal diffusion ratio is a function of composition, pressure, and temperature. Components with a positive k_i^T will concentrate in the coldest region.

In a series of articles Dougherty and Drickamer (1955) and coworkers published measurements of thermal diffusion factors in binary mixtures at high and low

pressures at room temperature. Measurements were performed on non-hydrocarbon mixtures, or on hydrocarbon / non-hydrocarbon binary systems. Typically, the mixtures were liquids far from critical conditions. Dougherty and Drickamer developed a theory for thermal diffusion based on *activation energy*. This theory is derived through a discussion of the energy involved in moving a molecule from one equilibrium position at one temperature to a new position at a new temperature. The authors relate the activation energy to viscosity and density and found good qualitative agreement with their measurements. Interestingly, they show measured examples where a sign change of the thermal diffusion factor is observed for a mixture when pressure is increased. The theory predicts this sign change, at least qualitatively.

Whitaker and Pigford (1958) reported measurements in a one-chamber cell where an optical technique was used to measure the compositional changes in binary mixtures. Their measurements of thermal diffusion factor in a binary mixture were in good agreement with the results of Dougherty and Drickamer. Whitaker and Pigford proposed a theory similar to Dougherty and Drickamer by introducing an additional "fitting-factor" in the energy calculations. The authors stated that (1) the model with activation energy oversimplifies the energy effects connected to molecular motion in a temperature field, and (2) the coupling between activation energy and viscosity is questionable.

Rutherford and Roof (1959) were apparently the first to do a thorough experimental investigation of binary *hydrocarbon* mixtures. Series of measurements were performed at relative high pressure and temperature, in liquid region and near the critical point of the binary mixtures. The authors made the important observation that the thermal diffusion factor in binary mixtures is inversely proportional to $x_1 \cdot (\partial \mu_1 / \partial x_1)$, which means that it goes to infinity at the critical point. By calculating the thermal diffusion factor as a constant divided by the expression above, the authors found reasonable correspondence with the experimental results when applying the Benedict -Webb-Rubin EOS to calculate the derivative of the chemical potential.

When Eq. 2.38 is included in Eq. 2.17 in the limit $n = 2$ and with no gravity, we find that Rutherford and Roof's observation that thermal diffusion factor is inversely proportional to $x_1 \cdot (\partial \mu_1 / \partial x_1)$ to be correct.

Using a two-chamber cell, Haase (1969) reported measurements of thermal diffusion in mixtures of methane-propane in the near critical region. A new theory for thermal diffusion in binary mixtures was proposed, relating thermal diffusion to partial molar

enthalpy and molecular weight. The majority of the measurements were in the *gas* phase region, and the theory gave qualitatively good results corresponding to the measured values in this region. However, in the one-phase "liquid-like" region in the vicinity of the critical conditions the theory highly overpredicted the magnitude of the thermal diffusion factor.

Kempers (1989) gave a review of theories and measurements on thermal diffusion, especially discussing Haase's theory. The author notes that molecular mass or size are the dominant parameters for thermal diffusion in gases while energetic interactions is the key factor in liquids. Kempers derived a new model for thermal diffusion similar to the Haase approach. The author demonstrated that this new theory slightly improved the predictions for thermal diffusion factor for near critical gases, when compared to Haase's model. However Kempers model also shows a weakness (as Haase's model) in the "liquid-like" region near the critical point. Furhtermore, only limited comparisons between the predictions from Kempers model and measurements on thermal diffusion in *liquids* were performed by Kempers.

At present, work on thermal diffusion has gained wider interest and is in progress. Two conferences in France have recently (1994 and 1996) been dedicated to the subject, and the main papers were published in a special edition of "Entropie" (1994). There is an ongoing discussion of (a) the sign of the thermal diffusion factor in liquids, (b) the magnitude of thermal diffusion factor, and (c) the potential impact of the porous medium on thermal diffusion factors (Costeseque, 1994; Faissat et al., 1994). There are very limited quality measurements at relevant reservoir conditions available on thermal diffusion. This is the case both in binary and multicomponent hydrocarbon mixtures. Hence, before additional relevant experiments are performed / published we have to rely on existing theories. The models of Dougherty and Drickamer, Haase, and Kempers are discussed in more detail in the next subsections to identify significant differences.

2.4.2 Thermal Diffusion in Binary and Multicomponent Mixtures

In this subsection we neglect gravity and consider the temperature effect on hydrocarbon mixtures alone. We apply Eqs. 2.16 and 2.17 derived previously. The term F_k^T (Eq. 2.17) involves the model for thermal diffusion for component k and is denoted F_k^H, F_k^K or F_k^D in the case of Haase's, Kempers or Dougherty and Drickamer's model, respectively.

Following Haase's theory, k_i^T is found by solving the equation :

$$\sum_{i=1}^{n-1} \left(\frac{\partial \mu_k}{\partial x_i}\right)_{p,T,x_{k\neq i}} k_i^T = \frac{1}{M}(M_k H_m - M H_k) = F_k^H \qquad k=1,..,n \qquad (2.39)$$

H_k is the partial molar enthalpy of component k, and H_m is given as: $H_m = \sum_k x_k H_k$.

M_k is the molecular weight of component k and M is the mixture molecular weight. Haase applied the centre of mass as reference condition in his derivations, and derived his theory in the framework of irreversible thermodynamics.

Kempers derived his expression for thermal diffusion ratio based on statistical physics. Kempers let the maximum number of microstates characterize the stationary state of the system, resulting in

$$\sum_{i=1}^{n-1} \left(\frac{\partial \mu_k}{\partial x_i}\right)_{p,T,x_{k\neq i}} k_i^T = \frac{1}{V_m}\cdot(V_k H_m - V_m H_k) = F_k^K \qquad k=1,..,n \qquad (2.40)$$

V_k is the partial molar volume of component k and V_m is given as $V_m = \sum_k x_k V_k$.

In terms of Faissat et al.'s (1994) parameters in Eq. 2.16, the theories of Haase and Kempers can be written as

$$Q_k^* = \frac{H_n}{M_n} - \frac{H_k}{M_k} \qquad (\textit{Haase}) \qquad (2.41)$$

and

$$Q_k^* = \frac{H_n}{V_n} - \frac{H_k}{V_k} \qquad (\textit{Kempers}) \qquad (2.42)$$

Notice however that Eq. 2.42 can not be applied directly in Eq. 2.16, as Kempers used a fixed volume as reference condition instead of the barycentric approach. Faissat et al. (1994) states that with Kempers choice of reference conditions, the forces X_k have to be replaced by X_k/v_k, to obtain independent forces. Here v_k is the partial specific volume of component k. With these forces we follow the same approach as in the derivation of Eq. 2.16 and get the following main equation valid for Kempers model :

$$\sum_{i=1}^{n-1} \left(\frac{\partial \mu_k}{\partial x_i}\right)_{p,T,x_{k\neq i}} \nabla x_i = (M_k - \rho V_k)\, g + V_k \left(\frac{1}{V_m} \sum_{i=1}^{n} x_k V_k Q_k^* - Q_k^*\right) \frac{\nabla T}{T} \qquad k = 1,..,n$$

This equation is consistent with Eq. 2.39 when gravity is neglected.

The main difference between Kempers and Haase's expressions is that Haase weighs the enthalpies with molecular weight and Kempers uses partial molar volumes. All parameters in both models can be found from thermodynamics alone, with the exception of ideal enthalpy, where correlations are used. The enthalpy calculation for component k can be divided into two parts, residual and ideal, given as

$$H_k^{res} = -R\,T \frac{\partial \ln \varphi_k}{\partial T} \qquad \text{and} \qquad H_k^{id} = -\int_{T_{ref}}^{T} C_{p_k}^{id}\, dT \tag{2.43}$$

where the partial molar enthalpy of component k is the sum of the two contributions. The residual part is found analytically from a cubic equation of state. The ideal part is found from an integration of the ideal gas heat capacity. This ideal heat capacity, C_{pk}^{id}, can be found from correlations. For light petroleum mixtures (N_2,CO_2,C_1,...,C_6) we apply the correlations given in Reid et al. (1976) . For the C_{7+} fractions the procedure of Kesler and Lee (1976) is used. This allows immediate calculations of the enthalpy, and thus the Soret-effect predicted with Haase and Kempers methods.

Belery and da Silva (1990) reviewed existing theory on thermal diffusion, and chose to extend the theory of Dougherty and Drickamer to multicomponent mixtures, instead of applying Haase or Kempers theories. Dougherty and Drickamer's original method uses the parameter "activation energy" in prediction of the thermal diffusion ratio. The partial molar activation energy is for each component k given as

$$\Delta U_k^* = \left(\frac{\partial \Delta U_m^*}{\partial n_k}\right)_{p,T,n_i} \tag{2.44}$$

The term ΔU_m^* is a function of the pressure and temperature dependent ratio between the mixture viscosity and density such that

$$\Delta U_m^* = R \left[\left(\frac{\partial \ln(\mu/\rho)}{\partial(1/T)}\right)_{p,x_k} - \left(\frac{\partial \ln(\mu/\rho)}{\partial p}\right)_{T,x_k} \right] \tag{2.45}$$

Belery and da Silva's extended expression for the thermal diffusion ratio in multicomponent mixtures is given as

$$\sum_{k=1}^{n-1} \left(\frac{\partial \mu_i}{\partial x_k}\right)_{p,T,x_{k\neq i}} k_k^T = -\frac{1}{2\bar{V}} \left(V_k \Delta U_m^* - V_m \Delta U_k^*\right) = F_k^D \qquad k=1,..,n \tag{2.46}$$

where $\bar{V} = \dfrac{M}{\sum_k (M_k/V_k)}$.

We can then calculate all terms in Eq. 2.46 from thermodynamic relations, plus a correlation for the viscosity to estimate the activation energy. Belery and da Silva used the Lohrenz-Bray-Clark (1964) correlation for viscosity which applies to both gases and oils in a consistent way.

In the following we calculate and analyse the thermal diffusion factor for a binary mixture using Eqs. 2.39, 2.40 and 2.46.

Thermal Diffusion Factor in Binary Mixtures

One main challenge connected to predictions of compositional variations with depth in real reservoir systems is to find a theory for the Soret-effect which is valid for a large region of pressure, temperature, and composition space. Petroleum reservoirs range from dry and wet gases, through gas condensate system, near critical oils,

volatile oils and black oil systems. It is therefore essential to use a generalized fluid model that predicts thermal diffusion accurately in all these examples.

The theories of Haase, Kempers and Dougherty and Drickamer follow different approaches to derive the expressions for thermal diffusion factor. These theories are not generally founded on basic thermodynamic principles that are widely accepted (as is the case of isothermal calculations). The three theories are all based on and compared to measurements in limited (p, T, z_i)-space. Only the theory of Dougherty and Drickhamer has, to our knowledge, been evaluated for reservoir fluids that span all types of realistic petroleum fluid systems (Whitson and Belery, 1994).

As discussed in Section 2.4.2, one of the most thorough experimental studies on hydrocarbon binary mixtures is the investigation of Rutherford and Roof (1959). These measurements are particularly interesting because they were performed at realistic reservoir conditions and covered relatively large regions of pressure and temperature. We chose to take this experimental study as the base for comparison of the predictive capability of the different models for thermal diffusion.

In advance of this study a consistency check was peformed by (1) testing our calculations of enthalpy on a series of mixtures against the results from the PVT package PVTSIM, and (2) computing thermal diffusion factor for all examples given in the Kempers (1989) article. The enthalpy calculation procedure is the same as the one used in PVTSIM, and our calculation results matched the PVTSIM enthaply results. Kempers used tuned EOS characterizations and measured data of enthalpy. He reported a number of calculated thermal diffusion factors applying both his own and Haase's theory. We found a match within 10 percent between our results and the ones reported by Kempers. This was considered to be a reasonably good match, as our calculations were based on *default* PVTx values for the examples investigated and correlations for the ideal part of the partital molar enthalpies. The sign of the thermal diffusion factor was in all cases found to be the same as reported by Kempers.

Fig. 2.23 shows three experimental series of data for constant temperature and variable pressure in the binary mixture C_1-nC_4, with $x_{C1} = 0.4$ (Rutherford and Roof, 1959). Notice that all experimental points are in the one phase region. One series of measurements were performed at pressures in the one phase near critical region. The experimental results are particularly susceptible to measurement inaccuracies close to critical conditions. This is due to the large changes in thermal diffusion factor for small variations in pressure or temperature. The other experimental series of this

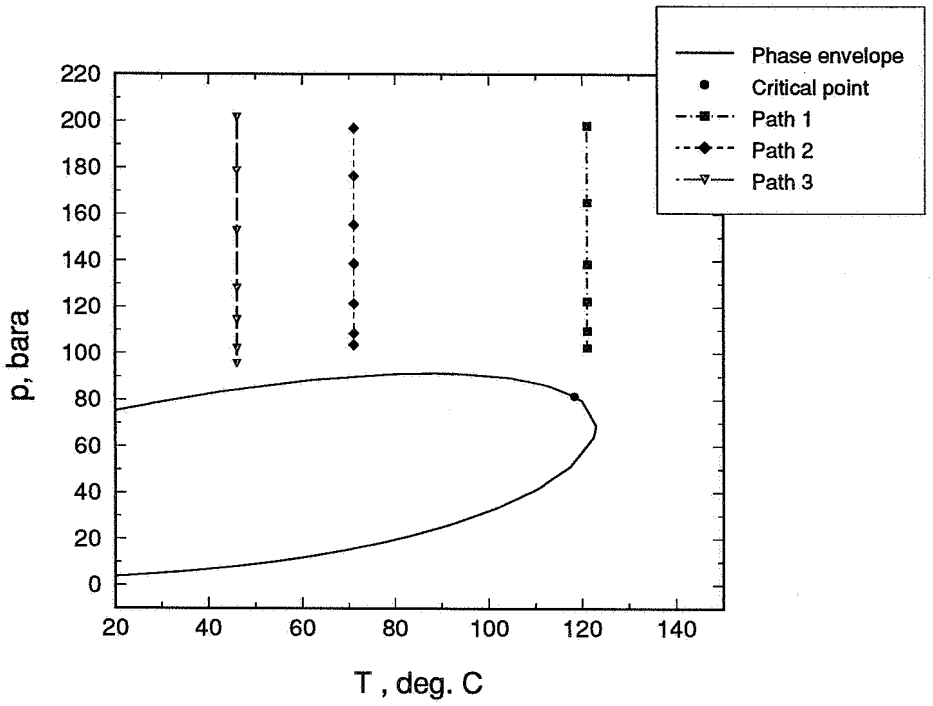

Fig. 2.23 Illustration of three series of experiments (Rutherford and Roof, 1959) for variable p,T conditions in a binary mixture of methane and butane.

mixture gave conditions in the liquid region, ranging from conditions close to the two phase region to highly undersaturated conditions.

Table 2.8 shows measurements and our calculated results for the thermal diffusion factor. Our results are plotted in Figs. 2.24 to 2.26. The following observations can be made based on these calculations :

1. *Near critical gas conditions:* Kempers model gives good estimates for the thermal diffusion factor in this case, slightly better than Haase's model. Dougherty and Drickamer's model highly overpredicts α^T in the vicinity of the critical point.

2. *Liquid conditions significantly away from critical point*: Kempers model overpredicts the measured results by a factor of 2-3. Haase and Dougherty and Drickamer's model both slightly overpredict the measured values, with the latter model giving the best results. At constant temperature the magnitude of the thermal diffusion ratio decreases as pressure increases.

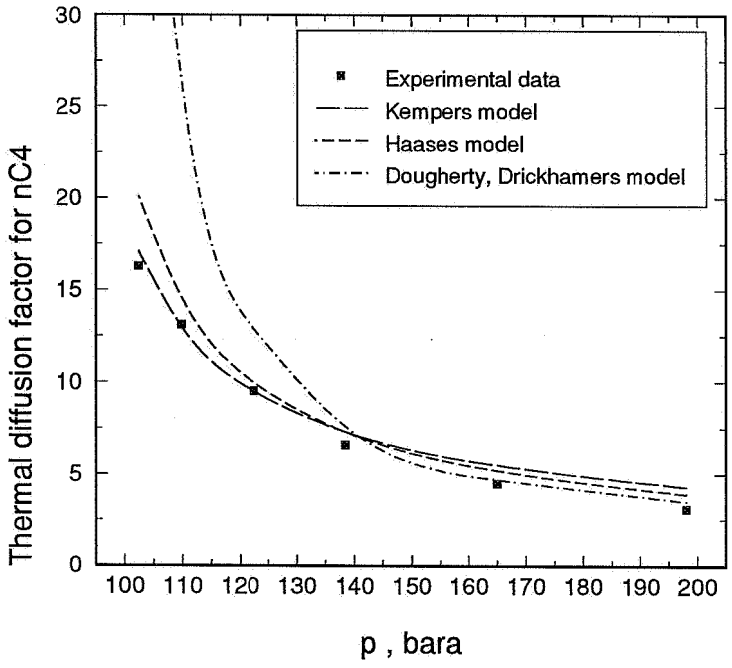

Fig. 2.24 Measured and calculated thermal diffusion factors, near-critical conditions.

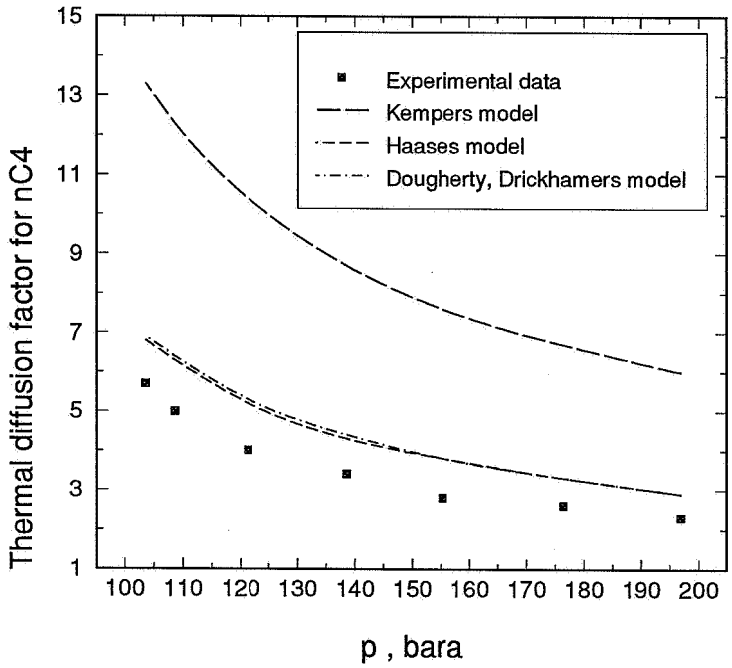

Fig. 2.25 Measured and calculated thermal diffusion factor at liquid conditions (experimental path 2, Fig. 2.23).

Table 2.8 Measured (Rutherford and Roof, 1959) and calculated values for nC_4 thermal diffusion factor in a binary mixture of methane and nbutane $x_{C1} = 0.40$.

T (° C)	Themal diffusion factor				
	p (bara)	Kempers	Haase	Dougherty, Drickamer	Experimental Value
121.1	102.4	17.1	20.1	51.2	16.3
	109.8	13.0	14.6	26.6	13.1
	122.4	9.5	10.0	12.9	9.5
	138.4	7.3	7.3	7.6	6.6
	165.0	5.5	5.2	4.7	4.5
	198.0	4.3	3.9	3.5	3.1
71.1	103.6	13.3	6.8	6.9	5.7
	108.6	12.3	6.3	6.4	5.0
	121.3	10.4	5.2	5.3	4.0
	138.6	8.7	4.3	4.4	3.4
	155.3	7.6	3.8	3.8	2.8
	176.4	6.7	3.3	3.3	2.6
46.1	95.5	11.5	4.6	4.4	3.6
	102.0	10.7	4.2	4.1	3.1
	114.4	9.7	3.8	3.6	2.9
	127.9	8.7	3.4	3.2	2.5
	152.9	7.5	2.9	2.6	2.2
	178.6	6.7	2.5	2.2	2.2
	201.7	6.1	2.3	1.9	2.1

In summary, we have shown that the three models for thermal diffusion in this case gave a consistent sign prediction. The results above show that methane concentrates in the warmest region in this case. As shown in Figs. 2.21 to 2.23 the magnitude of the results for thermal diffusion is model dependent. The calculated results suggest that the theories of Kempers and Dougherty and Drickamer give valid results at certain conditions and highly overpredict the thermal diffusion factors at other conditions. The main trend is that all methods to some degree overpredict experimental results. Haase's model is the best overall theory to apply in this particular binary mixture which consists of two light components only.

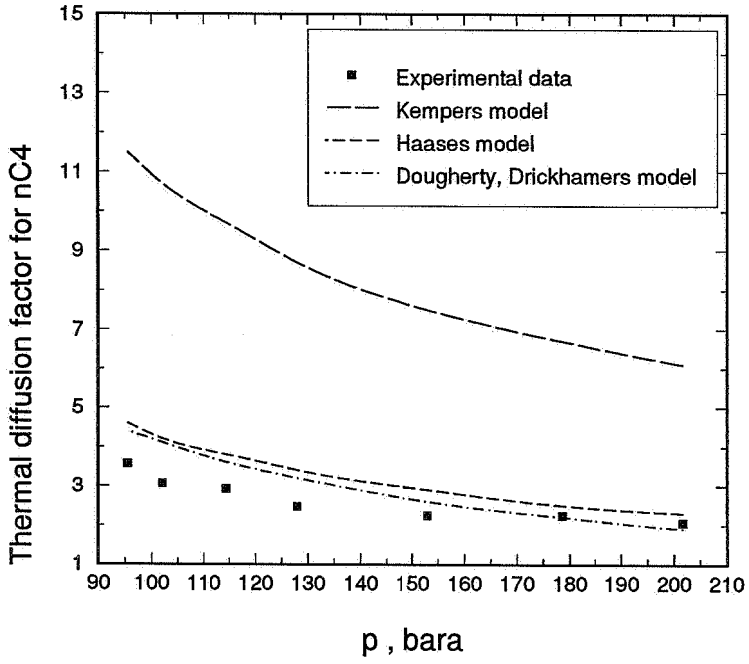

Fig. 2.26 Measured and calculated thermal diffusion factor at liquid conditions (experimental path3, Fig. 2.23).

2.4.3 Influence on Compositional Gradient Calculations

In this subsection we quantify and analyse the effect of implementing different models for thermal diffusion in compositional gradient calculations in realistic multicomponent systems.

Holt et al. (1983) were the first to include the thermal diffusion and gravity effect in compositional gradient calculations in petroleum reservoirs. They used a two-component model with methane and one pseudo component (chosen to be decane). Dougherty and Drickamers model was used to determine the thermal diffusion factor. Holt et al. used correlations and reported data on density and viscosity to quantify the parameters needed. The authors applied their simplified two-component model to the Valhall field. It was concluded that the thermal effect was approximately of the same magnitude as the gravity term in this case and *working in the same direction* (i.e. resulting in a compositional gradient larger than predicted by the isothermal model).

Interestingly, when using Haase or Kempers theories instead of Dougherty and Drickamers model we find a change in the sign of the thermal diffusion factor. For this system, consisting of one light and one heavy component, the sign predicted with the three methods is not consistent. Applying Haase or Kempers models thus results in compositional gradients smaller than predicted with an isothermal model.

We have applied the three models for thermal diffusion in numerous multicomponent systems by solving Eq. 2.17. The calculations presented below are given for (a) the VOA system, (b) the BO system ,and (c) the NCO system.

Belery and da Silva (1990) studied the VOA example and applied their model on this reservoir (the Ekofisk Field). The authors were the first to implement thermal diffusion and gravity in compositional gradient calculations for multicomponent systems. Their calculated results for the thermal diffusion ratio showed a significant non-linearity with depth. The results demonstrated a sign change in thermal diffusion ratio for methane and heavy components with increasing depth. This implies that thermal diffusion will oppose gravitational effects in parts of the reservoir and enhance compositional variations in other parts of the reservoir. From comparisons between field measurements and calculations Belery and da Silva proposed that their model overestimated the thermal effect by a factor of about four. The authors noted that both Haase and Kempers also had to reduce the calculated effect in the near critical liquid region to match measurements in binary mixtures.

Whitson and Belery (1994) applied the Belery-da Silva model on the NCO system and extended the analyses of the effects in the VOA example. The following discussion is a further study based on the articles above.

Compositional Gradients in Volatile and Black Oil Systems

In the VOA study we applied the temperature gradient reported by Belery and da Silva, equal to 0.037°C/m. Figs. 2.27 and 2.28 show our results for the thermal diffusion ratio for C_1 and the heaviest C_{7+} fraction as a function of depth. Both the models of Haase and Kempers give approximately linear variations of thermal diffusion ratio with depth. Both models predict thermal diffusion which opposes gravity over the entire reservoir depth. This leads to a significantly smaller compositional variation with depth than in the isothermal case. The Belery-da Silva model gives a Soret-effect similar to Haase and Kempers models in the upper part of the reservoir. However, the model predicts enhancement of compositional gradients

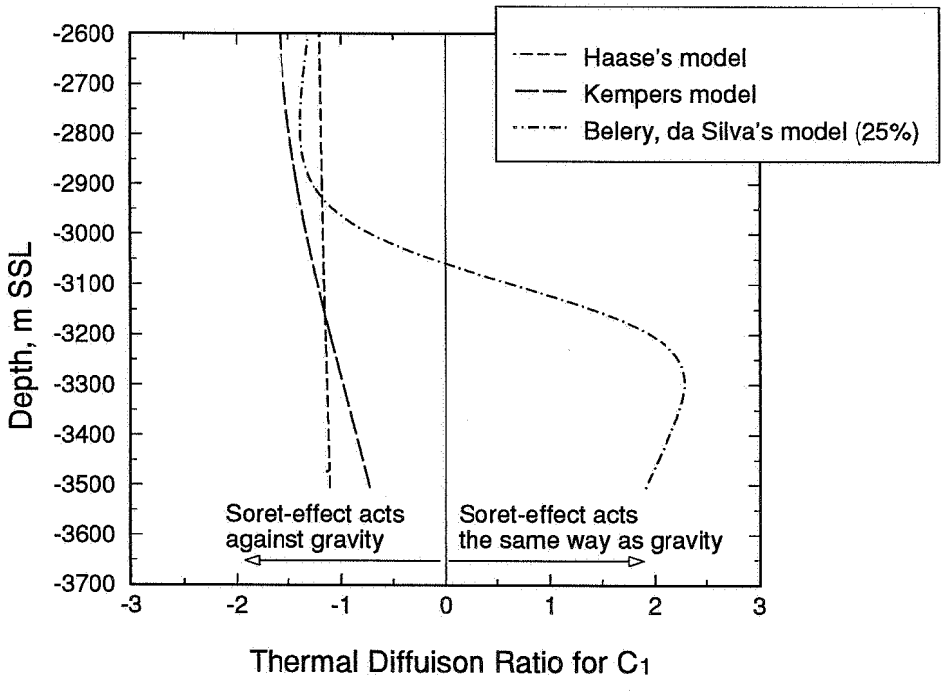

Fig. 2.27 Thermal diffusion ratio for methane versus depth.

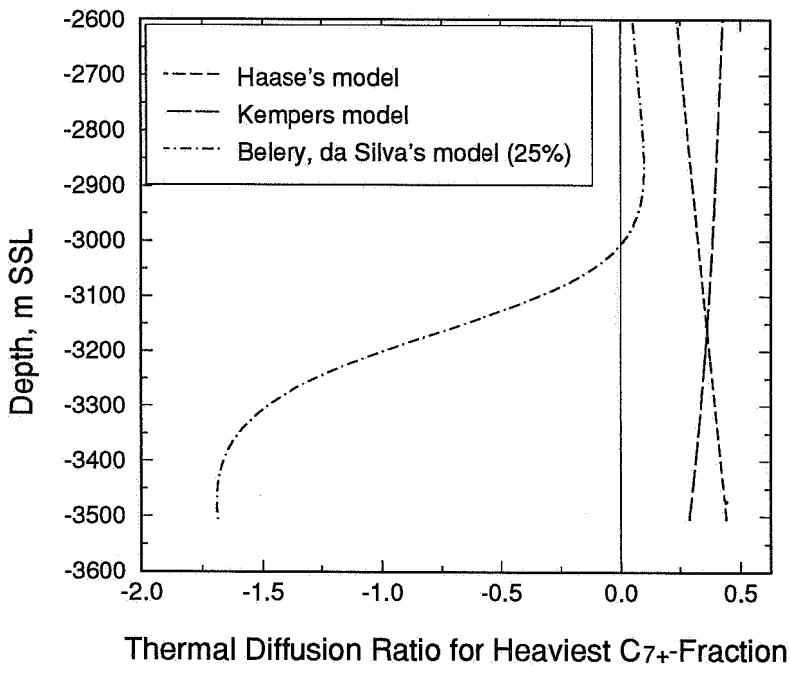

Fig. 2.28 Thermal diffusion ratio for the heaviest C_{7+} fraction, variation with depth.

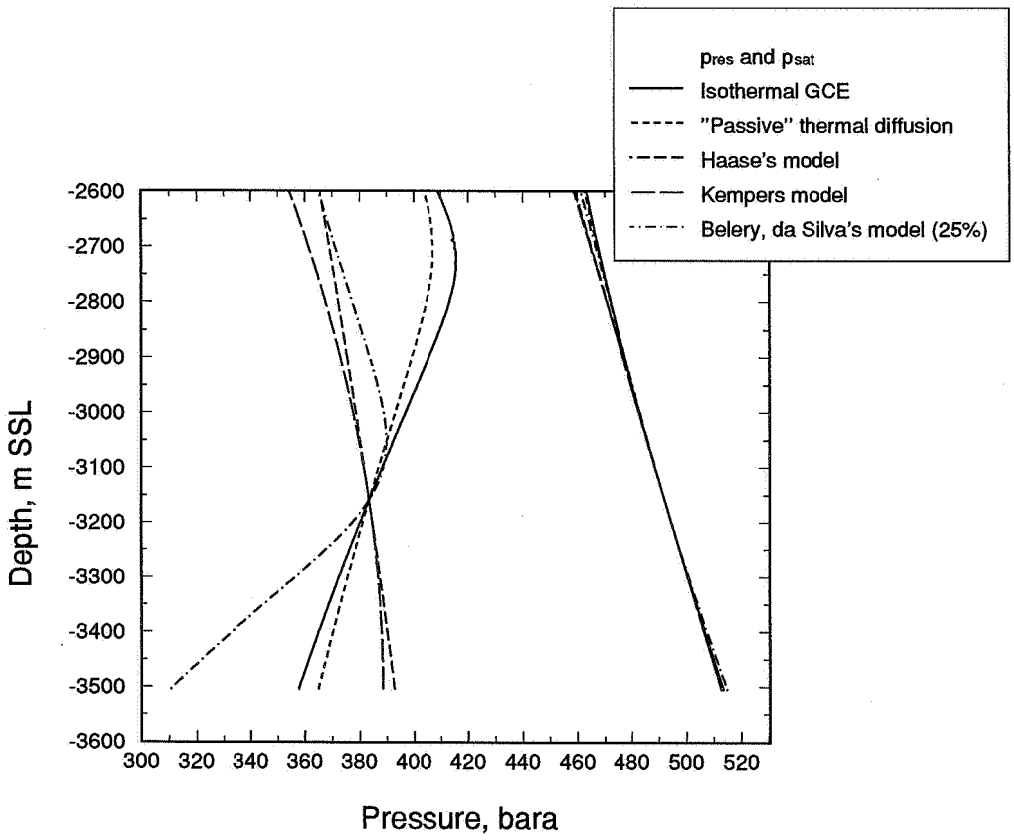

Fig. 2.29 Calculated reservoir pressure and saturation pressure versus depth

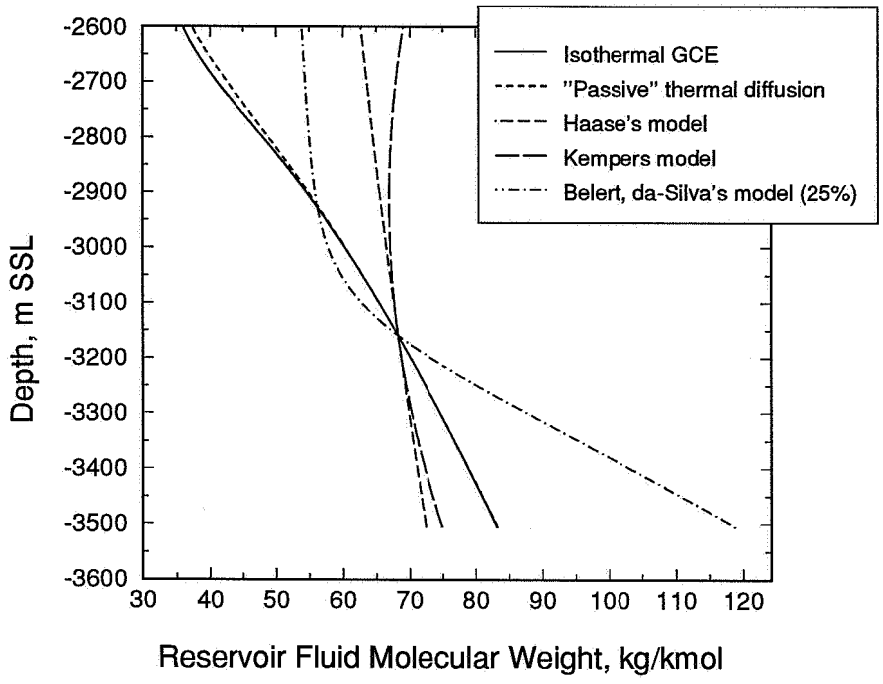

Fig. 2.30 Calculated mixture molecular weight variation with depth.

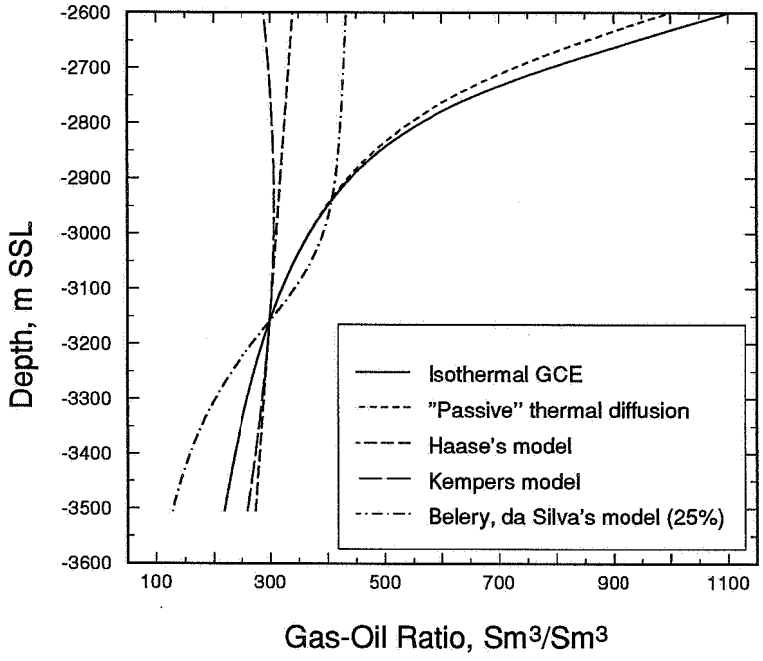

Fig. 2.31 Calculated gas-oil ratio variation with depth.

in the lower part of the reservoir, in contrast to the two other models.

Fig. 2.29 gives calculated variations in reservoir pressure and saturation pressure with depth. It is seen that the reservoir pressure is not changed significantly when applying the thermal models. The results for saturation pressure is significantly more model dependent. The effect of the different models are demonstrated clearly in Figs. 2.30 and 2.31, which give calculated variations with depth for reservoir fluid molecular weight and producing GOR[4]. In the upper "gas-like" part of the reservoir the application of *all* thermal models generate smaller gradients than predicted by the isothermal GCE method. Consequently, both producing gas-oil ratio and molecular weight is found to be approximately constant with depth in this region. The Kempers model gives a slightly higher molecular weight at the reservoir top than further down in the reservoir. This is a non-physical solution that will induce convection and in this

[4] Evaluated at first stage separator standard conditions.

situation a 1-D solution is not valid.

Proceeding downwards from the reservoir top, small variations in molecular weight and gas-oil ratio are predicted by the models of Haase and Kempers. The Belery-da Silva model predicts significantly larger changes in these properties than found by the isothermal GCE predictions.

In summary, both the *sign* and the *magnitude* of the predicted thermal diffusion factor in this example are different from the Belery-da Silva model when compared to the predictions with Haase and Kempers model. We also find the inclusion of a "passive" thermal diffusion to have negligible effect on compositional variation with depth in this example. This confirms Whitson and Belery's (1994) conclusion on "passive" thermal diffusion based on the NCO system.

Fig. 2.32 shows calculated thermal diffusion ratio as a function of depth in the 20 component BO example. Here a somewhat conservative temperature gradient of 0.03 °C/m was used. Calculations were performed 300 m downwards, starting from the GOC. In this fluid system the isothermal GCE model predicts a small compositional variations with depth. Thermal diffusion opposes the effect of gravity in the case of Kempers model, while compositional gradients are enhanced in the case of the Belery-da Silva model. Haase's model predicts a methane thermal diffusion ratio close to zero, changing sign with depth. Consequently, this model here predicts a slight increase in compositional gradients with depth, see Fig. 2.33. *This represents the only case we have found where Haase's model enhances compositional gradients.* From Fig. 2.33 it can further be seen that the model of Kempers almost balances the effect of gravity, which generates an approximately constant density variation with depth. If this thermal effect had been slightly larger it would induce unstable solutions with respect to density. We have observed the latter effect in some moderately GOR oil reservoirs (e.g. in the SVO case), when we apply Kempers model.

We emphasize that the calculated results using the Belery-da Silva model are uncertain for the BO system, as limited viscosity data were available. Consequently, the calculation of activation energy is uncertain. The results are, however, typical for low GOR oils, and show that the model can predict significantly larger compositional variations with depth than the isothermal model for this class of reservoir fluids. Large compositional variations with depth have been observed in some low-GOR oil reservoirs such as the Heidrun Field in the North Sea (Skjæveland and Kleppe, 1992). In the case of a static 1-D model the Belery-da Silva model for thermal diffusion

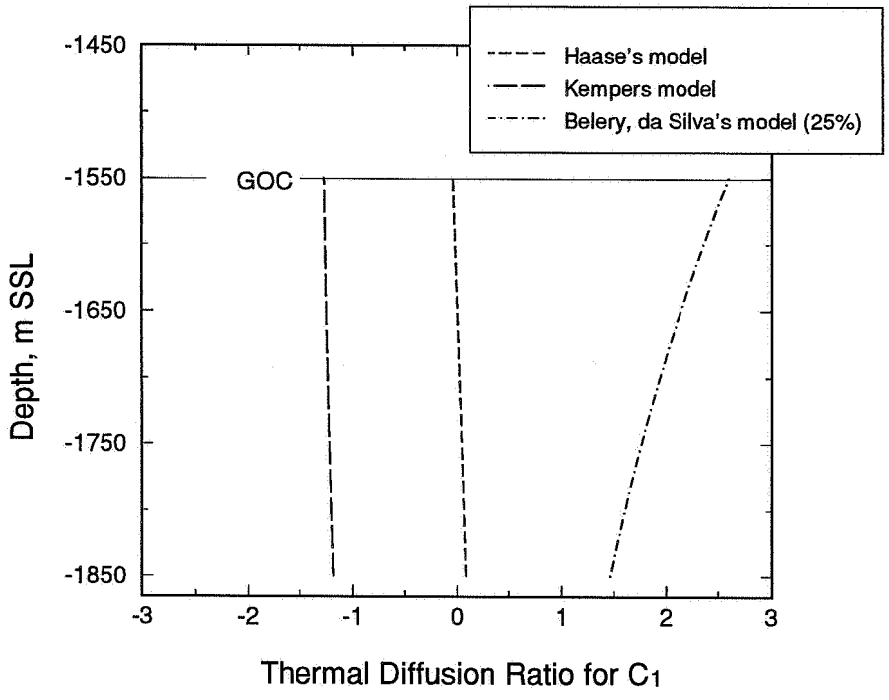

Fig. 2.32 Methane thermal diffusion ratio in the black oil reservoir.

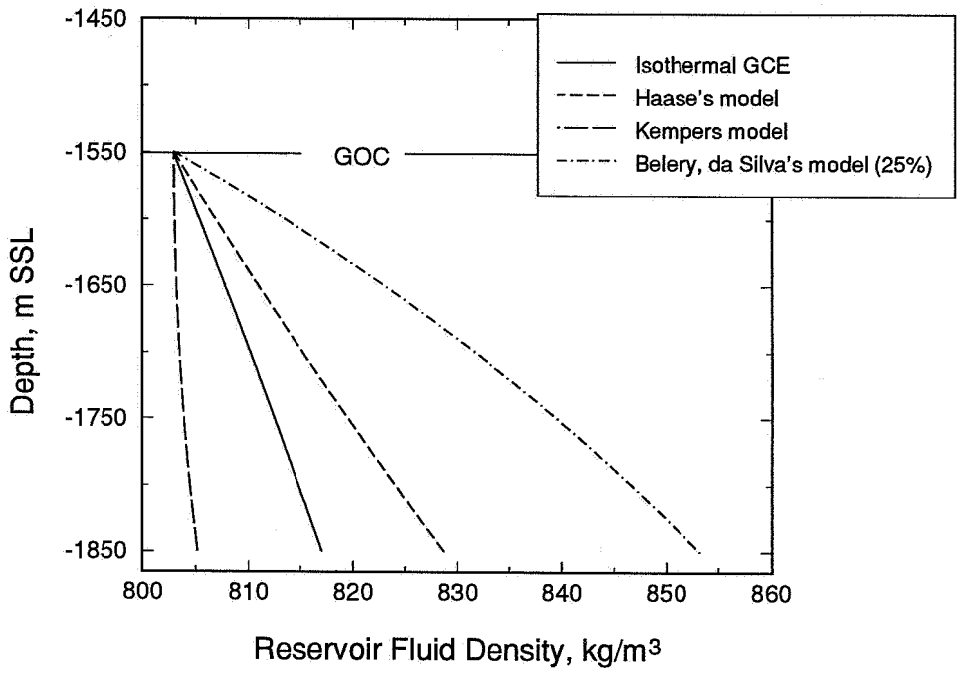

Fig. 2.33 Calculated reservoir fluid density variation with depth, applying the isothermal GCE method and different thermal models.

seems to be the only one that predicts significant gradients in these reservoirs.

Compositional Gradients in a Near Critical System

Fig. 2.34 shows calculated results for the methane thermal diffusion ratio versus depth in the NCO reservoir. We have used the same temperature gradient here as in the VOA example. Whitson and Belery (1994) performed both isothermal GCE calculations and calculations with the Belery-da Silva model for this fluid system. The authors concluded that the thermal diffusion term had to be reduced to approximately 5% of the original predictions to generate physical stable solutions with respect to density. Without any reduction the estimated thermal effect totally dominates the gravity term. The observation of large predicted thermal diffusion factor in the vicinity of critical conditions is consistent with our calculations for the binary mixture in Section 2.4.2.

Fig. 2.34 shows calculations where the Belery-da Silva thermal diffusion term has been reduced to 2% of its value. We find all models to give a thermal contribution that opposes the gravity effect thoughout the depth interval investigated. This can be seen from Fig. 2.35 where we plot the resulting variation in methane mole fraction with depth. Three conclusions can be drawn from these figures: (1) the predicted compositional variation is largest in the case of isothermal calculations, (2) the prediction of the gas-oil contact is moved upwards when thermal models are used (see Fig. 2.36), and (3) at the GOC the thermal diffusion ratio reaches its extremal value.

Notice that the Haase model predicts larger thermal effects than the Kempers model over the entire interval studied in this fluid system. The Belery-da Silva model (2%) gives similar results as the predictions by Kempers model. The three models predict consistent signs of the thermal diffusion ratio in the depth interval investigated. However the magnitude of the thermal diffusion term is significantly different for the three models.

Chaback (1992) estimated the magnitude of the thermal diffusion effect in a binary near critical gas condensate mixture and compared it with the effect of gravity. For a near critical equimolar methane-nbutane mixture Chaback found the gravity effect to be approximately two times the thermal effect. The author argued that this conclusion (if applicable to a complex reservoir mixture) shows that an isothermal GCE calculation can yield satisfactionary results for a near critical mixture. For mixtures with conditions far away from the critical region, Chaback argued that the

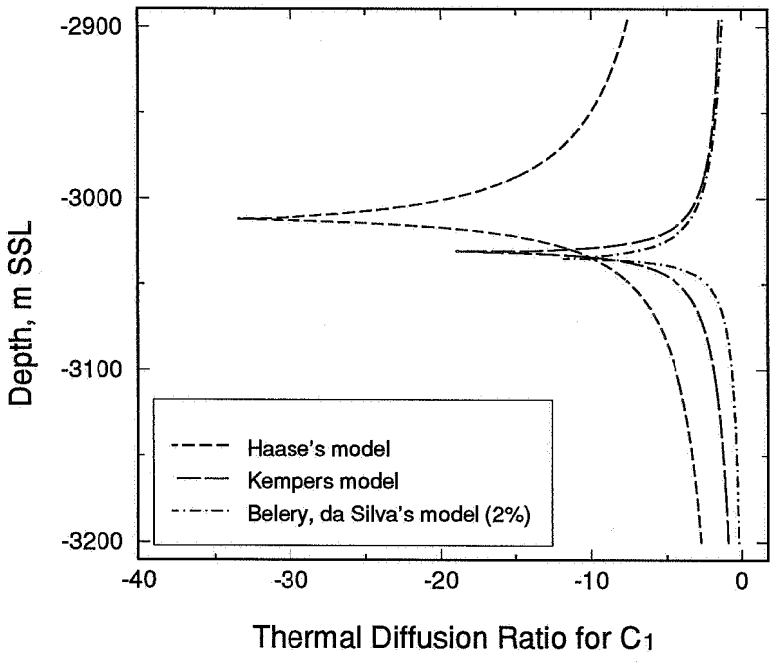

Fig. 2.34 Results for methane thermal diffusion ratio calculated with different thermal models.

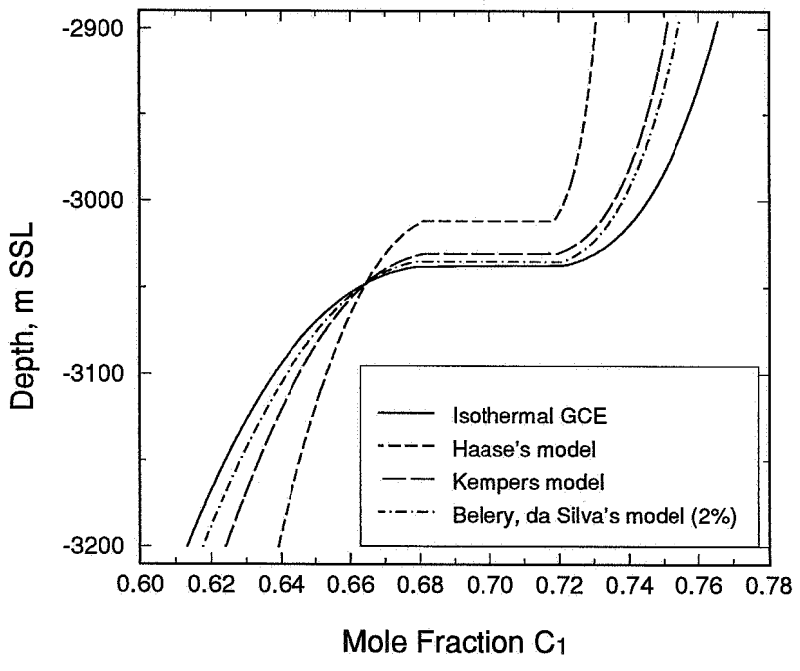

Fig. 2.35 Calculated methane mole fraction variation with depth.

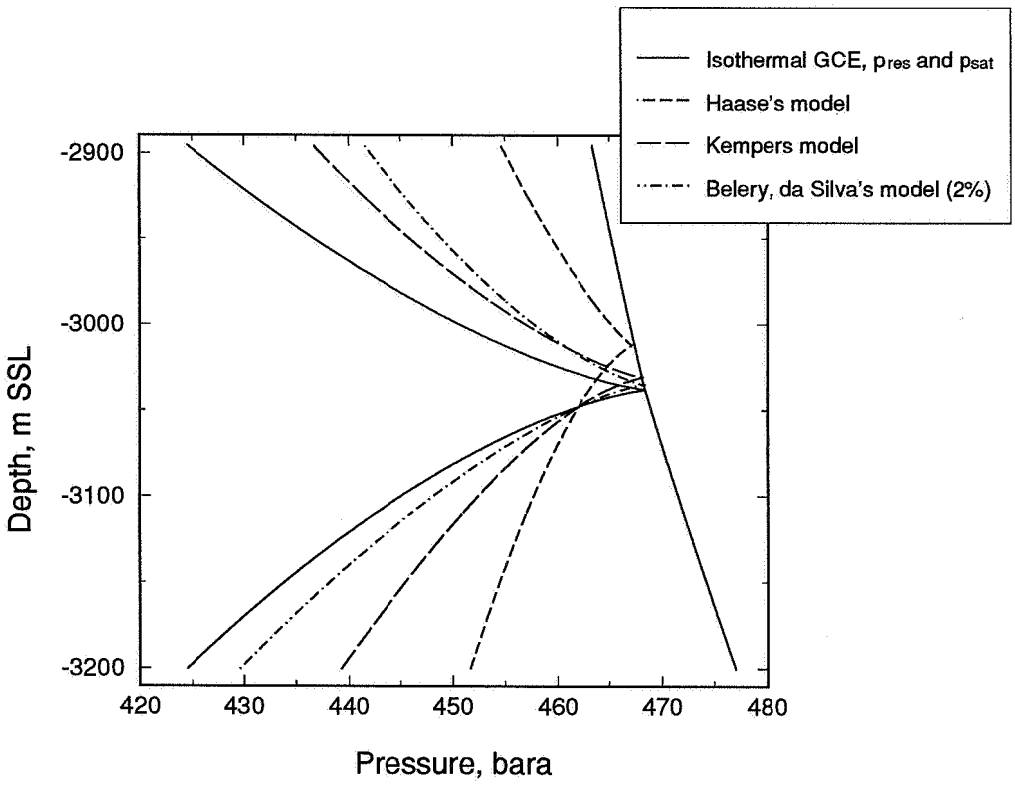

Fig. 2.36 Calculated reservoir pressure and saturation pressure variation with depth for the different thermal diffusion models and the isothermal GCE model.

terms can be of comparable size.

We find that going from a binary to a multicomponent mixture complicates these conclusions significantly. However, in the case of both Haase and Kempers models the predicted thermal effect close to the critical conditions in the NCO example are approximately half of the gravity term. At conditions significantly away from critical conditions the gravity and thermal terms *can* be of comparable size, e.g. as shown in the BO example with Kempers model.

Interestingly, we find a sign change in the thermal diffusion factor with the Belery-da Silva model in calculations far below the gas-oil contact in the NCO reservoir. Below -3450 m the Belery-da Silva model *enhances* compositional gradients, as in the lower part of the VOA reservoir and the oil zone of the BO example.

A number of observations which appears to be valid for most of the compositional gradient calculations made in this study are:

- Implementation of "passive thermal diffusion" does not change the *compositional* variation with depth significantly when compared to isothermal results. The temperature effect of saturation pressure and volumetric properties generates some deviation in phase properties from the isothermal predictions.

- The Haase and Kempers models for thermal diffusion usually predict a thermal effect that opposes the effect of gravity, both for reservoir gases and oils. However, we have found *a few* cases where both the Haase and Kempers models give a thermal diffusion effect that acts in the same direction as gravity.

- The thermal effect predicted by Kempers method can, far from near-critical conditions, be somewhat larger than and oppose the gravity effect. This has been found in the case of undersaturated oils and lean gases, and can induce non-physical (mechanically unstable) solutions

- The Belery-da Silva method *often* predicts positive and negative thermal diffusion ratios of methane and heavy components. Consequently, this model can enhance, reduce or completely reverse the compositional variations with depth (Whitson and Belery, 1994).

- At near critical conditions the Belery-da Silva model is found to predict thermal effects that are significantly larger than and consistently opposing the gravity effect. This often induces non-physical (mechanically unstable) solutions.

- At conditions significantly away from critical conditions the Belery-da Silva model predicts a thermal diffusion effect that typically opposes gravity in gases and typically enhances compositional gradients in oils.

- The isothermal GCE model will typically predict the largest compositional variations in *gases* compared with thermal models. The Belery-da Silva model will typically predict the largest compositional gradients in *oils* at conditions significantly away from critical conditions.

In conclusion, this study shows that the models of Haase, Kempers, and Belery-da Silva only gives consistently similar results for thermal diffusion ratios of *lean gases*. For a given (p,T,x_i) condition in *oils* the models do not provide internally consistent results with respect to the sign and magnitude of the thermal diffusion ratio. Consequently, it does not appear that *any* of the investigated models provide a generalized fluid model for calculation of vertical compositional variations with depth. To arrive at a generalized and consistent thermal diffusion model it will be necessary to obtain consistent and reliable measured data for liquids covering a large range of composition, pressure, and temperature gradients. Measurements should preferably be performed away from critical conditions to avoid experimental difficulties and hence reduce measurement uncertainties.

2.5 Conclusions and Recommendations

1. Saturated and near-saturated near-critical reservoir fluids show larger compositional variations than highly undersaturated systems. This can be understood directly from the governing equations for 1D isothermal GCE calculations. Variation in properties with depth such as saturation pressure, reservoir fluid density, mixture molecular weight, °API, and producing GOR can be directly related to the compositional variations and have been quantified for four reservoir fluid systems. The maximum variation in composition and other physical properties are found at a saturated gas-oil contact in a near-critical system.

2. Two new methods have been proposed for calculating the gas-oil contact for the isothermal model: (a) a modified phase envelope calculation procedure, and (b) a method that forces a function to zero through Newton-Raphson updates on depth. The function is a product of two terms which ensures that it goes to zero both in the case of a saturated and an undersaturated GOC. Method (a) was found not to be robust enough as a general GOC-algorithm. However, method (b) was found to be as accurate as an interval halving method, and with computation speed increased by a factor of 1.5 to 4.

3. Effects of sampling errors on isothermal compositional gradient modelling have been investigated. It has been shown that an error in the saturation pressure at reference depth can have significant effect on the prediction of the GOC. It is also demonstrated that uncertainty in definition of the reference depth will give a similar uncertainty in the GOC prediction. Erroneous reference conditions yield errors in modelling of fluid property variations with depth, prediction of the GOC, and as a result errors in hydrocarbons-in-place estimates.

4. Different methods for implementing compositional gradients to calculate hydrocarbons in-place volumes in a near critical reservoir fluid has been investigated. It has been demonstrated that the choice of method will influence significantly on the results. Based on our studies we recommend that compositional variations with depth should be taken into consideration when estimating hydrocarbon-in-place volumes.

The effect of implementing thermal diffusion in compositional gradient calculations have been analysed and quantified in different fluid systems. Three models for thermal diffusion has been discussed: the models of Haase, Kempers, and Dougherty and Drickamer (extended to multicomponent mixtures by Belery and da Silva). The

following conclusions have been made:

5. The effect of "passive thermal diffusion" is insignificant with respect to the calculations of compositional variation with depth, compared to isothermal GCE predictions.

6. The Haase and Kempers models for thermal diffusion both predict a thermal diffusion effect that *opposes* gravity in reservoir gases and oil. This observation holds for the majority of fluid systems investigated.

7. Non-physical (mechanically unstable) solutions for density can sometimes be predicted when applying Kempers model in fluid systems away from critical conditions, and almost always when applying the Belery-da Silva model in systems in the vicinity of a critical condition.

8. In fluid systems significantly away from critical conditions it has been shown that the Belery-da Silva model typically predicts a thermal effect that opposes gravity in gases and enhances compositional gradients in oils.

9. It has been shown that for lean reservoir gases the isothermal model will predict a larger compositional variation with depth than the thermal models.

10. The thermal models give internally consistent answers for thermal diffusion ratio *only* in the case of *lean gases* in the investigated examples, where thermal diffusion is found to oppose the effect of gravity. For *oils* the different thermal models have an *inconsistent sign and magnitude* of the thermal diffusion factor, when compared to each other.

11. Limited measurements on thermal diffusion exist, complicating the evaluation of the different thermal models. However, comparisons with an extensive experimental study of thermal diffusion factors in a binary system shows that neither the model of Kempers nor the model of Dougherty and Drickamer shows qualitative agreement with measurements in the entire investigated pressure and temperature region. In this study the Haase model gives the best agreement with the experimental results.

Based on the conclusions above, the following recommendations are given for further

research:

12. Additional experiments on thermal diffusion in binary and multicomponent systems should be performed to gain knowledge about (1) the sign, and (2) the magnitude of the thermal diffusion ratio. We recommend that measurements be performed at *liquid conditions*, where large inconsistencies are found between existing models. Particular care should be made to measure liquid thermal diffusion at conditions away from the critical point, and covering a large range of composition, pressure, and temperature.

13. Based on existing and new experiments thermal diffusion theories should be tested against the measurements. If necessary, a new thermal diffusion model should be developed based on the experimental results.

2.6 Nomenclature

c_k	=	volume shift parameter, component k
C_{pk}^{id}	=	ideal heat capacity, component k
C_{7+}	=	heptane and heavier components
d_k	=	difference in fugacities, component k
f_k	=	fugacity, component k
f_k^*	=	fugacity without any volume shift, component k
F_k^D	=	term with the Dougherty-Drickamer model for thermal diffusion, component k
F_k^G	=	gravity term, component k
F_k^H	=	term with Haase's model for thermal diffusion, component k
F_k^K	=	term with Kempers model for thermal diffusion, component k
F_k^T	=	term including model for thermal diffusion, component k
F	=	Function equal zero at the gas-oil contact (GOC)
g_1	=	function equal to zero, GOC-search algorithm
g_2	=	function equal to zero, GOC-search algorithm
g	=	gravitational acceleration
G_G	=	separator gas volume produced from gas zone
G_O	=	separator gas volume produced from oil zone
G	=	separator gas volume; Gibbs free energy
h_{GOC}	=	gas-oil contact depth
h^B	=	depth, reservoir bottom
h^T	=	depth, reservoir top
h^0	=	reference depth
h	=	depth
H_k	=	partial molar enthalpy, component k
H_k^{id}	=	ideal partial molar enthalpy, component k
H_k^{res}	=	residual partial molar enthalpy, component k
J_i	=	mass flux, component i
J_q	=	heat flux
k_k^T	=	thermal diffusion ratio, component k
k	=	permeability
K_k	=	K-value for component k
L_{ik}	=	phenomenological coefficients connecting forces and fluxes
L_{iu}	=	phenomenological coefficients connecting forces and fluxes
m_k	=	mass, component k
m	=	total mass
M_k	=	molecular weight, component k
n_k	=	moles of component k
n	=	total number of moles; number of components
N_G	=	stock tank oil volume produced from gas zone

N_O	=	stock tank oil volume produced from oil zone
N	=	stock tank oil volume
p_{res}	=	reservoir pressure
p_{sat}	=	saturation pressure
p^0	=	reference pressure
p	=	pressure
Q_k^*	=	"energy of transport", component k
Q^*	=	mixture specific heat of transport
R	=	the universal gas constant
Ra	=	Rayleigh number
S_k	=	partial molar entropy, component k
S	=	entropy
T	=	temperature
ΔU_k^*	=	partial molar activation energy, component k
v_k	=	velocity of component k; partial specific volume for component k
v	=	barycentre velocity
V_k	=	partial molar volume, component k
V	=	volume
x_k	=	composition, mole fraction component k
X_k	=	driving force acting on component k
X_u	=	driving force, a function of temperature and gradient in temperature
y_k	=	gas composition, mole fraction component k
Y_k	=	composition, component k, not normalized
z_k^0	=	reference mixture composition, mole fraction component k
z_k	=	total mixture composition, mole fraction component k

Greek

α^B	=	parameter used to determine composition in GOC-search
α^T	=	parameter used to determine composition in GOC-search
α_k^T	=	thermal diffusion factor, component k
β	=	coefficient of thermal expansion
γ_o	=	oil specific gravity
κ_m	=	thermal diffusivity for the total porous media (fluid and rock)
μ_k	=	chemical potential, component k
ν	=	kinematic viscosity
ρ_k	=	density, component k
ρ	=	density
ϕ_k	=	fugacity coefficient, component k

Subscript

GOC	=	gas-oil contact
g	=	gas
i,j,k	=	component number
o	=	oil
refg	=	gas at reference conditions
refo	=	oil at reference conditions
res	=	reservoir
sat	=	saturation

Superscript

B	=	bottom
D	=	Dougherty and Drickamer
G	=	gravity
H	=	Haase
id	=	ideal
K	=	Kempers
res	=	residual
T	=	top
0	=	reference conditions

Abbreviations

BIPS	=	binary interaction coefficients
BO	=	black oil
CCE	=	constant composition expansion
CVD	=	constant volume depletion
EOS	=	equation of state
GCE	=	gravity/chemical equilibrium
GDEM	=	general dominant eigenvalue method
GOC	=	gas-oil contact
NCO	=	near critical oil
SVO	=	slightly volatile oil
VLE	=	vapour-liquid equilibrium
VOA	=	volatile oil

2.7 References

Bath, P.G.H., Fowler, W.N., and Russell, M.P.M.: "The Brent Field, A Reservoir Engineering Review," paper EUR 164 presented at the 1980 SPE European Offshore Petroleum Conference and Exhibition, Sept. 21-24, London.

Bath, P.G.H., van der Burgh, J., and Ypma, J.G.J.: "Enhanced Oil Recovery in the North Sea," 11th World Petroleum Congress (1983).

Bedrikovetsky, P.G.: *Mathematical Theory of Oil and Gas Recovery*, Petroleum Engineering and Development Studies, No. 4, Cluwer Academic, Horthreht (1993).

Belery, P. and da Silva, F.V.: "Gravity and Thermal Diffusion in Hydrocarbon Reservoirs," paper presented at the Third Chalk Research Program, June 11-12, Copenhagen (1990).

Bjørlykke, K., Mo, A., Palm, E.: "Modelling of thermal convection in sedimentary basins and its relevance to diagenetic reactions", *Marine and Petroleum Geology*, **5**, (1988).

Chaback, J.J.: "Discussion of Treatment of Variations of Composition With Depth in Gas-Condensate Reservoirs," *SPERE* (Feb. 1992) 157-158.

Costeseque,P, El Maataoui, M., Riviere,E.: "Selective enrichments induced by thermogravitational diffusion in a porous medium on hydrocarbon species of crude oils; the spesific case of paraffin isomers", *Entropie*, (1994) **184/185**, 94-100

Creek, J.L. and Schrader, M.L.: "East Painter Reservoir: An Example of a Compositional Gradient From a Gravitational Field," paper SPE 14411 presented at the 1985 SPE Annual Technical Conference and Exhibition, Las Vegas, Sept. 22-25.

Crowe, A.M. and Nishio, M.: "Convergence Promotion in the Simulation of Chemical Processes-the General Dominant Eigenvalue Method," *AIChE J.* (1975) **21**, 528-533.

Dietz, D.N. "A Theoretical Approach to the Problem of Enchroaching and By-Passing Edge Water", *Akad. van Wetenschappen*, (1953), **83.**

Dougherty, E.L., Jr. and Drickamer, H.G.: "Thermal Diffusion and Molecular Motion in Liquids," *J.Phys.Chem.* (1955) **59**, 443.

Faissat, B., Knudsen, K., Stenby, E.H., Montel, F.: "Fundamental Statements about Thermal Diffusion for a Multicomponent Mixture in a Porous Medium," *Fluid Phase Equilibria*, **10**, 209-222, (1994).

Fevang, Ø. and Whitson, C.H.: "Accurate Insitu Compositions in Petroleum Reservoirs", paper SPE 22829 presented at the 1994 EUROPEC meeting (Oct. 25-27, 1994)

Førland, K.S., Førland, T., Ratkje, S.K.: *Irreversible Thermodynamics Theory and Applications*, John Wiley Ltd., Chapter 3 and 4, (1988)

de Groot, S.R. *Thermodynamics of Irreversible Process*, North Holland, (1950)

Haase, R., *Thermodynamics of Irreversible Processes*, Addison-Wesley. Chapter 4, (1969)

Hirschberg, A.: "Role of Asphaltenes in Compositional Grading of a Reservoir's Fluid Column," *JPT* (Jan. 1988) 89-94.

Holt, T., Lindeberg, E., and Ratkje, S.K.: "The Effect of Gravity and Temperature Gradients on Methane Distribution in Oil Reservoirs," unsolicited paper SPE 11761 (1983).

Horton, C.W. and Rogers, F.F.: "Convective currents in a porous medium", *J. App. Phys.* **16**, 367 (1945)

Høier, L. "Thermal Convection in Perturbed Systems", Thesis for the degree Cand. Scient. , Cooperative Phenomena Group, Department of Physics, University of Oslo (April, 1993)

Jacqmin, D.: "Interaction of Natural Convection and Gravity Segregation in Oil/Gas Reservoirs," *SPERE* (May 1990) **5**, No. 2, 233-238.

Kempers, L.J.T.M.:"A thermodynamic theory of the Soret effect in a multicomponent liquid", *J.Chem. Phys.* (1989) **90** (11), 6541-6548

Kesler, M.K. and Lee, B.I.: "Improve predictions of enthaply fractions", *Hydrocarbon Processing*, 153-158 (March 1976)

Lapwood, E. R.: "Convection of a fluid in a porous medium", *Proc. Camb. Phil. Soc.* **44**, 508, (1948)

Lee, S.-T., "Capillary-Gravity Equilibria for Hydrocarbon Fluids in Porous Media", paper SPE 19650 presented at the SPE Annual Conference, San Antonio, 8-11, Oct. 1989

Lohrentz, J., Bray, B.G., Clark C.R. "Calculating Viscosities of Reservoir Fluids from their Compositions", *JPT* (Oct. 1964), 1171-1176; Trans.,AIME, **231**

Ludwig, C.: "Diffusion zwischen ungleich erwarmten Orten gleich zusammengesetzer Losungen", *Siszber Akad. Wiss., Narutwiss.*, **20**, 539, (1856)

Metcalfe, R.S., Vogel, J.L., and Morris, R.W.: "Compositional Gradient in the Anschutz Ranch East Field," paper SPE 14412 presented at the 1985 SPE Annual Technical Conference and Exhibition, Las Vegas, Sept. 22-25.

Michelsen, M.L.: "Calculation of Phase Envelopes and Critical Points for Multicomponent Mixtures," *Fluid Phase Equilibria* (1980) **4**, 1-10.

Michelsen, M.L.: "The Isothermal Flash Problem. Part I. Stability," *Fluid Phase Equilibria* (1982) **9**, 1-19.

Michelsen, M.L.: "Saturation Point Calculations," *Fluid Phase Equilibria* (1985) **23**, 181-192.

Michelsen, M.L.: "A Simple Method for Calculation of Approximate Phase Boundaries," *Fluid Phase Equilibria* (1994) **98**, 1-11.

Michelsen, M.L. and Mollerup, J.: "Partial Derivatives of Thermodynamic Properties", (1986), *AIChE Journal*, **8**, 1389-1392

Montel, F., Caltagirone, J.P., Peybale, L.: "Prediction of Compositional Grading in a Reservoir Fluid Column", (1989), in *The Mathematics of Oil Recovery*, Clarendon Press Oxford, 1992.

Montel, F.: "Phase Equilibria Needs for Petroleum Exploration and Production Industry," *Fluid Phase Equilibria* (1993) No. 84, 343-367.

Montel, F. and Gouel, P.L.: "Prediction of Compositional Grading in a Reservoir Fluid Column," paper SPE 14410 presented at the 1985 SPE Annual Technical Conference and Exhibition, Las Vegas, Sept. 22-25.

Muskat, M.: "Distribution of Non-Reacting Fluids in the Gravitational Field," *Physical Review* (June 1930) **35**, 1384-1393.

Palm, E.: "On the tendency towards hexagonal cells in steady convection", *J. Fluid Mech.*, **8**, 183-192, (1960)

Peneloux, A., Rauzy, E., and Freze, R.: "A Consistent Correction for Redlich-Kwong-Soave Volumes," *Fluid Phase Equilibria* (1982) **8**, 7-23.

Rabinowicz, M., Dandurand, J-L., Jakubowski, M., Schott, J., Cassan, J-P., "Convection in a North Sea Oil Reservoir: Possible Interference on Diagenesis and hydrocarbon Migration", North Sea Chalk Symposium, Book **1** , (May 1985)

Reid, R.C., Prausnitz, J.M., Sherwood, T.K.: *The Properties of Gases and Liquids,* McGraw-Hill Book Company, 3rd edition (1976)

Riemens, W.G., Schulte, A.M., and de Jong, L.N.J.: "Birba Field PVT Variations Along the Hydrocarbon Column and Confirmatory Field Tests," *JPT* (Jan. 1988) **40**, No. 1, 83-88.

Rutherford, W.M. and Roof, J.G., "Thermal Diffusion in Methane-n-Butane Mixtures in the Critical Region", *J. Phys. Chem.* **63**, 1506-1511 (1959)

Sage, B.H. and Lacey, W.N.: "Gravitational Concentration Gradients in Static Columns of Hydrocarbon Fluids," *Trans.*, AIME (1938) **132**, 120-131.

Schulte, A.M.: "Compositional Variations within a Hydrocarbon Column due to Gravity," paper SPE 9235 presented at the 1980 SPE Annual Technical Conference and Exhibition, Dallas, Sept. 21-24.

Skjæveland, S.M. and Kleppe, J., "Recent Advances in Improved Oil Recovery Methods for North Sea Sandstone Reservoirs, *Spor Monograph*, Norwegian Petroleum Directorate (1992)

Soret, C.: *Arch. Sci. Phys.*,Geneve, **2**, 48-61 (1879)

Wheaton, R.J.: "Treatment of Variation of Composition With Depth in Gas-Condensate Reservoirs," *SPERE* (May 1991) 239-244.

Whitaker, S. and Pigford, R.L., "Thermal Diffusion in Liquids, Measurements and a Molecular Model", *Ind. Eng. Chem.*, **50**, 1026 (1958)

Whitson, C.H.: "PVTx: An Equation-of-State Based Program for Simulating & Matching PVT Experiments with Multiparameter Nonlinear Regression," Pera a/s, Trondheim, Norway (1995) **Version 95-01**

Whitson, C.H.: "Trends in Modeling Reservoir Fluids," paper presented at the Seventh Internation Conference on Fluid Properties and Phase Equilibria for Chemical Process Design, Snowmass, (June 18-23, 1995)

Whitson, C.H. and Belery, P.: "Compositional Gradients in Petroleum Reservoirs," paper SPE 28000 presented at the U. Tulsa/SPE Centennial Petroleum Engineering Symposium, (Aug. 29-31,1994), Tulsa.

Whitson, C.H. and Brule, M.R.: *Phase Behavior*, Monograph, SPE of AIME, Dallas (1994) **(in print)**.

Whitson, C.H. and Torp, S.B.:"Evaluating Constant Volume Depletion Data", *JPT* 610-620; *Trans.*, AIME, (1983)

Chapter 3

Developed Miscible Gas Injection

In this chapter we investigate the possibility for development of miscibility when a dry or an enriched gas is injected into an oil or a gas condensate reservoir. Simulation methods and calculation algorithms for determining miscibility are discussed, and consequences of variation in pressure, temperature and injection gas composition on the miscibility process are demonstrated and analyzed. Particularly focused is also the impact of vertical compositional gradients on miscibility, i.e. how miscibility can vary as a function of depth in petroleum reservoirs.

3.1 Introduction

Production from the majority of petroleum reservoirs in the North Sea include an injection process designed to enhance oil recovery beyond what would be recovered by pressure depletion. Several injection methods exist, including dry gas injection, water injection and alternating water gas injection (WAG). Dry gas may be injected as a secondary mechanism of recovery, or following water injection as a tertiary process. In fractured systems dry gas can be used to recover the oil in the matrix block by a complex process involving gas enrichment, lowered interfacial tensions and capillary forces, and gravity/capillary displacement.

If performed correctly, these injection processes can increase recovery significantly. Both water and separator gas will typically be available for injection if the gas is not sold directly. Considering the cost alone, these injectants are favourable compared to gases which must be enriched with solvents such as C_3 / C_4 NGLs (natural gas liquid).

Typically, these injection processes result in immiscible displacements, characterized by limited mass transfer between the reservoir fluid and the injectant. The ratio of the mobilities of the phases at the displacement front is the key parameter for evaluating

the feasibility of an immiscible injection alternative . An unfavourable ratio can lead to fingering (Saffman and Taylor, 1958), override and early gas/water breakthrough. In addition, complex reservoir geology including heterogeneties and fractures may dictate the efficiency of the process. In high-permeability reservoirs as found in the North Sea, density differences play a key role in the success of gas and water injection processes, where gravity forces may be more important than viscous.

Another characteristic behaviour of immiscible displacement processes is significant amounts of remaining reservoir oil (residual oil saturation), since capillary forces will hold some of the reservoir oil. This motivates the search for other injection methods which can reduce residual oil saturation.

An alternative to the traditional immiscible displacement processes is developed miscible gas injection. Such large scale miscible flood injections have been performed with success in several reservoirs, as discussed by Stalkup (1984).

Thermodynamically, the definition of miscibility is :

> **The condition when two fluids are mixed in any proportion and the resulting mixture is single phase.**

Two miscible phases will thus be characterized by zero interfacial tension and consequently zero capillary forces and zero residual oil saturation. On a microscopic pore scale a miscible displacement is characterized by recoveries close to 100 percent. On a reservoir scale the recovery is defined as the product of the microscopic displacement efficiency times the vertical sweep efficiency times the areal sweep efficiency (Craig, 1971; Stalkup, 1984). Thus, the overall recovery for a field will be a function of the amount of contacted reservoir fluid. This will strongly depend on the reservoir geology, well pattern, and viscous/gravity mobility ratios.

When a gas is injected into a reservoir fluid there are three possibilities. The gas (1) is miscible with the reservoir fluid at first contact, (2) develops miscibility through multiple contacts with the reservoir fluid, or (3) will displace the reservoir fluid immiscibly. Realistic alternatives for an injection gas will either be separator gas from the producing field or nearby fields, plant products from a process plant or dewpoint controller, CO_2 or N_2, or mixtures of these alternatives.

If it is possible to achieve miscibility with a mixture of available gas alternatives, this could improve or accelerate the overall recovery significantly and have large

consequences for the economy of a field, provided the sweep efficiencies are good. The possibility for improved recovery has to be compared to the extra cost of enriching the injection gas. The predicted economical result has to be compared with predictions from immiscible displacement methods, like injecting water and selling the gas directly. Thus the key parameters in the evaluation of a miscible gas-related enhanced oil recovery (EOR) process are :

(a) the lowest pressure at which miscibility can be achieved for a given injection gas, i.e. the **minimum miscibility pressure (MMP)**

or alternatively,

(b) the lowest possible enrichment level of an available injection gas to achieve miscibility at a relevant reservoir pressure, the **minimum enrichment level (MME)**.

To be able to make this EOR evaluation it is necessary to have correct methods to determine MMP and MME both experimentally, and by simulation using a valid equation of state model.

It should be noticed that this chapter mainly focuses on methods for finding miscibility on *a pore scale*. Heterogeneties and multiphase flow will be important in upscaling the results to reservoir size, but these upscaling effects are not discussed in this thesis. We have focused entirely on MMP and MME determination. Furthermore, we have chosen to restrict the discussion to hydrocarbon injection gases, since this seems to be the most realistic available injection alternative in most petroleum reservoirs in the North Sea.

Section two in this chapter gives a critical focus on one-dimensional ("slimtube") simulation techniques with compositional simulators to determine MMP, and emphasizes the importance of correct elimination of numerical dispersion. When discretizing the problem into a limited number of grid blocks, large uncertainties may be introduced. It will be shown how the number of grids has a large effect on the calculated MMP, and that there exists an uncertainty in determination of dispersion free MMP. A method is proposed for quantifying this uncertainty, and this method is applied to different oil-gas systems. Zick's formulation (1986) of the development of miscibility as a combined condensing/vaporizong mechanism is discussed. Also, the problems of using traditional single cell PVT calculation approaches, as compared to multi cell methods, are demonstrated through comparison between slimtube MMP calculations and multicell PVT results.

Part three focuses on and analyzes results generated with the Zick multicell algorithm. Results from standard slimtube simulations are compared for selected systems. MMP as a function of injection gas type is studied, i.e. MMP versus enrichment level of solvent in a dry gas. This type calculation is important in design of an optimum injection gas for miscible displacement in a given reservoir.

Since a large number of petroleum reservoirs are found to have vertical compositional gradients , the effect of such gradients on MMP/MME is studied in part four of this chapter. This includes MMP and MME variations both in oil reservoirs, gas reservoirs and reservoirs without a saturated GOC, continuously changing with depth from a wet gas to a volatile oil. The compositional variation with depth was generated with the static isothermal GCE model, as discussed in Chapter 2. MMP was calculated using Zick's multicell algorithm, and the results have been analyzed and compared with slimtube simulation results. This section mainly focuses on miscibility in oil reservoirs, or oil columns.

Special consideration has been given to miscibility in gas condensate reservoirs. The question at which pressure to do gas cycling is addressed in part five of the chapter, including a discussion of the need for reservoir pressure maintenance above the dew point pressure. MMP in depleted gas condensate reservoirs is studied through a series of constant volume depletion (CVD) simulations coupled with calculation of MMP using the Zick multicell algorithm. Also, grid effect and its consequence on large scale simulations of gas cycling are discussed. At pressures below the dewpoint the buildup on a pore scale of an oil bank at the miscible front is particularly interesting.

In section six we investigate and discuss the effect of temperature on miscibility, and show the effect of including a geothermal gradient on MMP as a function of depth. Four models for thermal diffusion have been used to determine the initial compositional variation with depth in different reservoirs, including passive thermal diffusion (Faissat et al., 1994), Haase's model (1969), Kemper's model (1989) and the Belery-da Silvas model (1990). These models were discussed in Chapter 2. The miscibility variations with depth for given injection gases have been determined and compared with ordinary isothermal model results.

The result of introducing compositional gradients in slimtube simulations or reservoir simulators are analyzed in part seven of the chapter. Especially interesting is the possibility of performing a vertical dry gas injection in a reservoir with gradual change from gas to oil. In addition, MMP variations in a depleted reservoir with initial compositional gradient are investigated. The process dependent nature of the

compositional variation with depth is demonstrated for this example, and its influence on MMP is analyzed. Also we discuss consequences of using non-representative samples (caused by incorrect recombination gas-oil ratio) and its effect on MMP.

Finally, the main results from the overall miscibility study are summarized in section eight of this chapter. Conclusions are drawn and suggestions for future work are given.

3.2 Calculating Minimum Miscibility Conditions

In this section we present the different calculation method for determination of minimum miscibility conditions. It is shown that single cell calculation algorithms can overpredict MMP significantly compared to slimtube simulations and the Zick multicell algorithm. A method is proposed to quantefy the extrapolation uncertainty connected to elimination of numerical dispersion in slimtube simulations. The Zick multicell algorithm is found to yield results for the MMP within the accuracy of the slimtube simulations.

3.2.1 Definitions and Background

If a gas is miscible at first contact with an oil, it is said to be **First Contact Miscible (FCM)** with the oil. The level of enrichment in an injection gas achieving FCM is typically too expensive to be a realistic alternative in large scale gas flooding.

If a dry or lean gas is injected into a porous medium saturated with oil, significant vaporization of intermediate components (C_6-C_{12}) may occur from the oil to the gas. The amount of this net mass transfer and how heavy the vaporized components may be is dependent on initial composition, pressure and temperature. If the pressure is high enough, the lean gas will be enriched enough to achieve miscibility at the displacement front. This is referred to as the **vaporizing gas drive (VGD) mechanism**. An example of a VGD displacement is shown in Figs. 3.1 a), b) and c). The process is close to a piston-like displacement, leaving small amounts of residual oil behind and yielding K-values equal to 1.0 at the leading edge of the miscible front. The oil saturation is close to zero in the gas region and exactly one in the oil region, with a small two-phase region near the displacement front. Miscibility occurs at the leading edge of the two phase region, as seen from Fig. 3.1c).

If a somewhat enriched gas, containing large amounts of C_2-C_4 is injected into an oil, some of the intermediate components in the gas may condense into the oil, resulting in an enrichment of the oil. If the injection pressure is high enough, miscibility can be achieved at the displacement front through this process. No residual oil is left behind the miscible front as seen in Fig. 3.2. This is referred to as the **condensing gas drive (CGD) mechanism.**

Traditionally, the VGD and the CGD mechanisms have been the only two definitions

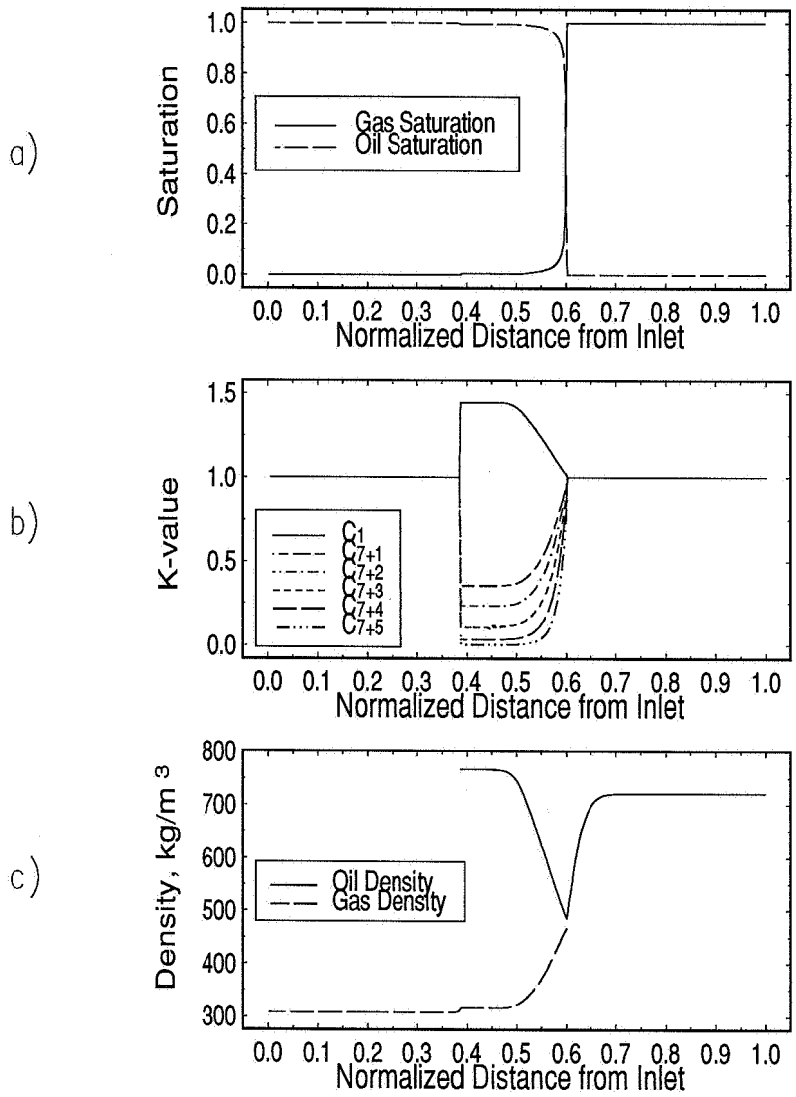

Fig. 3.1 Typical VGD slimtube profiles at 0.6 PV gas injected. a) oil and gas saturations, b) K-values, and c) oil and gas densities.

of developed miscible processes.

In 1986, Zick suggested that the vaporizing mechanism was correct for some dry gas injection process. However, for enriched gas injection processes Zick described the development of miscibility as a combination of condensation and vaporization. Zick also questioned the exsitence of the condensing drive mechanism in multicomponent petroleum systems. Zick's observations and conclusions were based on one-dimensional compositional simulations, traditional single-cell EOS simulation of the VGD and CGD mechanisms, and complete experimental verification of the simulated

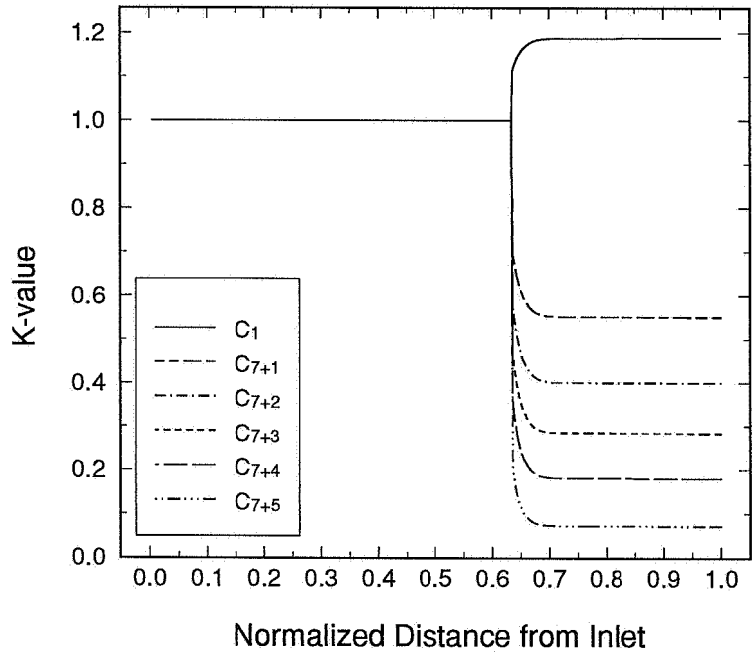

Fig 3.2 Typical profile of K-values in a slimtube simulation with the condensing gas drive mechanism.

results. The key point is that components are transferred both from gas to oil and from oil to gas, not only one way as is assumed in the traditional mechanisms. Zick showed that a somewhat enriched gas injection process could be divided into a zone with strong vaporization behind the front and strong condensation ahead of the front. As components are transported both ways between the phases, the net result is that both the oil and the gas near the displacement front are approaching each other in physical properties, yielding a near miscible situation with recoveries close to 100 percent. The resulting MMP in his examples was found to be significantly lower than the results from both the VGD and the CGD mechanism. It was further shown that the miscible process is usually a combined **condensing/vaporizing (C/V) mechanism**.

Consider Figs. 3.3 a), b) and c) that show a "snapshot" of a slimtube simulation at 0.6 pore volume (PV) injected, where an enriched gas has been injected into a slightly volatile oil system. The pressure is the "true" MMP. As seen in the figures, the displacement is characterized by a leading gas front ahead of the near miscible front

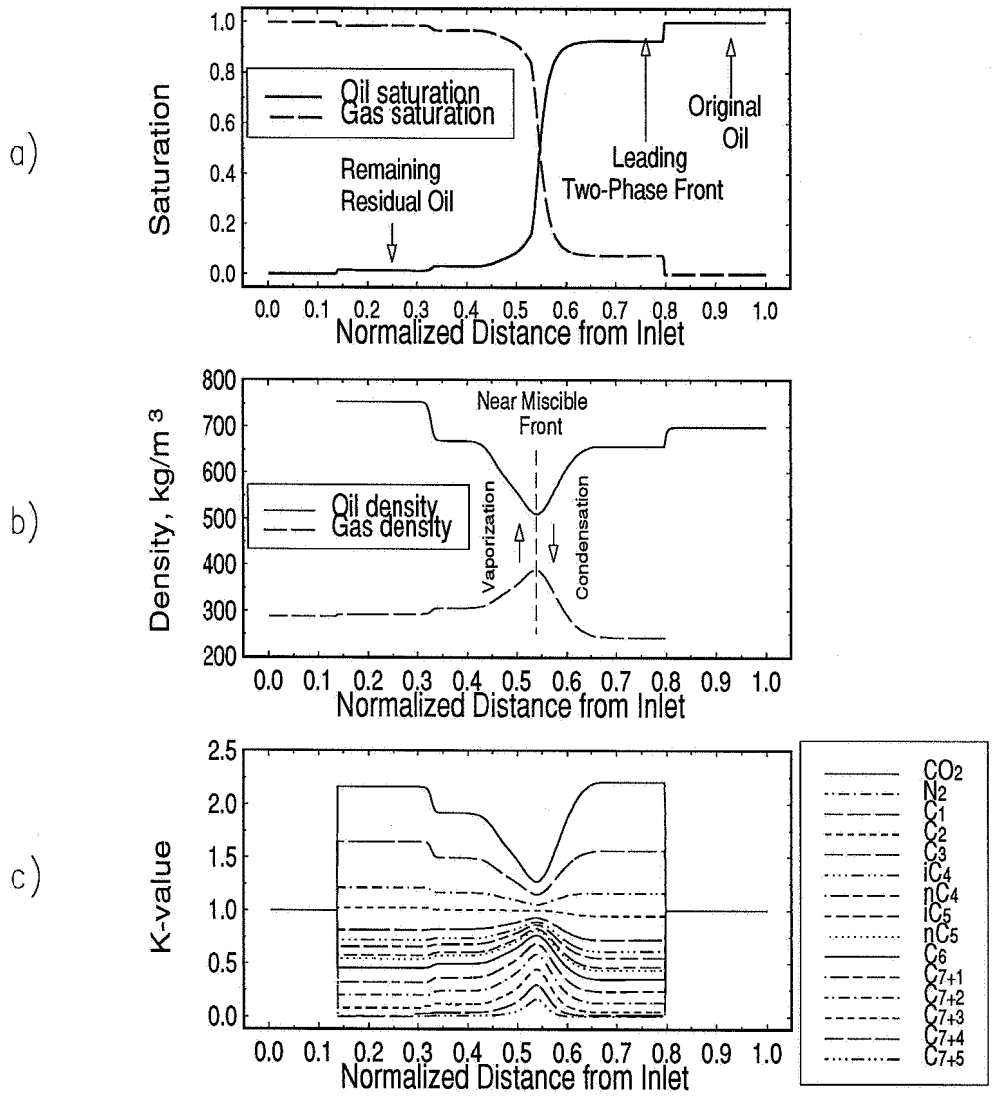

Fig. 3.3 Typical slimtube profiles for the C/V mechanism. a) saturations, b) densities and c) K-values.

with net condensation of intermediate components and a small trail of heavy residual oil left behind the front. Strong vaporization of intermediate and heavy components behind the front and strong condensation of intermediate and heavy components ahead of the front causes the K-values to go towards one at the near-miscible front, as demonstrated in Fig. 3.3 c). The transfer of the intermediate components is the key mechanism in this process. These simulation results are consistent with the development of miscibility as a combined condensing/vaporising mechanism, as described by Zick.

It is emphasized that there exists a significant grid effect in one-dimensional simulation of developed miscible gas displacement.. This causes the differences in density or K-values at the front to be larger than a "dispersion free" result would yield, and this will be discussed in Section 3.2.

3.2.2 Key Physical Parameters, Experiments and EOS Parameters

The previous subsection discussed definitions and main physical mechanisms in developed miscible gas injection. Here, we discuss the key parameters in miscibility studies and motivate for the choice of systems and parameters investigated later in this chapter. Also, an example of the impact of the number of components in an EOS characterization on calculated MMP is given to describe the importance of using enough components in the simulation of developed miscibility.

The main parameters affecting developed miscibility are

- **Reservoir Fluid Composition**
  When a gas is injected into a reservoir fluid, the resulting MMP can be significantly different for a heavy oil, a volatile oil, a near critical oil or a gas condensate reservoir fluid. If the reservoir fluid composition varies significantly with depth, the MMP/MME will also vary with depth. The reservoir fluid systems investigated in Chapter 2 include compositional gradients. These systems were used further in this chapter.

- **Injection Gas Composition**
  For a given reservoir fluid, development of miscibility can be different for a dry gas and an "enriched" injection gas. The choice of injection gas is mainly determined by what gases and solvents are available. In this chapter, four different injection gases have been used for all MMP/MME studies. The injection gas compositions are given in Table 3.1. Gas A represent a dry gas produced from a gas reservoir. Gas B is available first stage separator gas from an oil reservoir. Gas C is the rich gas composition reported by Hearn and Whitson (1994). Finally, Gas D represents a mixture of an available dry gas enriched with intermediate components from a dew point controller. Thus, mixtures of these gases should cover typical alternatives for compositions in large scale injection projects.

Table 3.1 Injection gases used in miscibility studies in this chapter.

Component	Gas A*	Gas B**	Gas C+	Gas D++
N2	1.58583	1.85790	0.7	0.24984
CO2	0.59725	3.79585	1.3	2.05874
C1	92.87720	55.51130	63.9	70.96587
C2	3.66376	11.48290	11.1	10.92781
C3	0.38875	13.41190	10.3	7.78334
IC4	0.33887	2.07080	3.6	1.33726
C4	0.08508	6.52458	5.3	3.71110
IC5	0.11535	1.68332	1.7	0.97486
C5	0.02264	2.38398	1.4	1.10205
C6	0.11333	0.50510	0.6	0.78439
F1 (C_{7+1})	0.12047	0.69520	0.0	0.10198
F2 (C_{7+2})	0.09140	0.07660	0.0	0.00278
F3 (C_{7+3})	0.00010	0.00057	0.0	1.575E-12
F4 (C_{7+4})	0.0000	1.71E-5	0.0	0.0000
F5 (C_{7+5})	0.0000	2.22E-17	0.0	0.0000

Notes:
* Gas A represents an available dry gas produced form a gas field.
**Gas B is a first stage separator gas from an oil reservoir
+ Gas C is a slightly modefied version of the rich gas reported by Hearn and Whitson, (1995)
++Gas D is a designed gas mixture consisting of an dry gas stream enriched with intermediate components from an available dew point controller.

- **Temperature**
  Reservoir temperature gradients may have a significant effect on MMP/MME, as will be discussed in Section 3.6. The geothermal temperature gradient will result in a temperature difference from top to bottom of a reservoir. As demonstrated in Chapter 2, thermal diffusion may also result in compositional gradients different from those found from isothermal models. This will thus have influence on the reservoir fluid composition and consequently on the MMP/MME. This motivates the investigation in Section 3.6 of temperature effects on MMP.

When performing compositional simulations using a cubic equation of state, the EOS-characterization may have large influence on the results. To ensure that the EOS can correctly predict the phase behaviour of mixtures occuring during the development of miscibility, relevant experiments should be performed. The EOS

should be tuned to match the experimental results. Zick (1986) and Hearn and Whitson (1995) emphasized that multi-contact swelling experiments should be performed, because a developed miscible process will happen through multiple contacts. Following these references, experiments should be performed at conditions in the vicinity of the critical point of a relevant oil/gas mixture. Saturation pressures, compositional data and volumetric PVT data should be recorded to ensure that the key phase behaviour connected to developed miscibility is measured. To obtain good EOS-predictions the EOS parameters, with particular focus on the C_{7+} critical properties and the binary interaction parameters, should be adjusted to match the measurements. If the EOS fails to predict these key data accurately then the EOS-calculated MMP will be uncertain and less reliable as a predictive tool.

Number of Components in EOS Characterization

Simulating large scale miscible projects requires a minimum number of components because of computer time and computer memory restrictions. Still, enough components have to be included to properly model the complex phase behaviour found in a developed miscible process.

Zick (1986) and Hearn and Whitson (1995) have found that 3 to 5 C_{7+} pseudocomponents could be enough to accurately determine MMP provided tuning to key experimental data has been performed correctly. In addition, the correct properties and amounts of the intermediates (C_2-C_6) both in the reservoir fluid and in the injection gas have to be reflected in the EOS to determine MMP accurately. This implies that there exists a case dependent lower limit for the number of EOS-components needed to correctly find the miscibility conditions for a system, probably six to eight with three C_{7+} pseudocomponents.

A typical example for the dependence of miscibility conditions on number of components is given below.

An original 15 component PR EOS-characterization with five C_{7+} components is assumed to predict miscibility condition accurately. This EOS was pseudoized by a PVT package from 15 to 5 components in steps of 2. The procedure is similar to the method described by Hearn and Whitson (1995) :

1. The original 15 component EOS characterization was used to simulate several relevant PVT experiments, including a multistage separator test, two differential liberation experiments (DLE) at relevant series of pressures, two

constant composition experiments (CCE) at relevant pressures, and two multicontact swelling experiments injecting a realistic injection gas. For definitions of the standard PVT experiments, see for example McCain (1990).

2. The compositional and volumetric PVT results from step 1 was stored and used as "data" in further regressions associated with the procedure of reducing the number of components ("pseudoization").

3. The original characterization was pseudoized to a lower number of components, and this new characterization was used in simulations of the same PVT experiments as in step 1.

4. The results in step 1 and step 3 were compared. Tuning on the main EOS parameters A, B and binary interaction coefficients was performed on the new pseudo components to match the PVT results from step 1. To match the viscosity data calculated in step 1, a separate viscosity fit was performed by adjusting critical volumes for the new pseudocomponents.

5. MMP was determined for each pseudoization step, injecting Gas D into a volatile oil sample. MMP was calculated with the Zick multicell algorithm (300 cells).

The process was then repeated, reducing the number of components further in steps of two, yielding an MMP for the 15, 13, 11, 9, 7 and 5 component EOS characterization. The results are given in Table 3.2.

Down to nine components, the MMP in this particular case did not change more than 5 bar as seen in the table. A deviation of 10 bar was found between the 15 and the seven component system. The general phase behaviour prediction with the five component system was significantly worse than the seven component system, and a relative large difference in MMP was found between the five and the 15 component system; 62 bar. Here, the five component system was found to give a too large deviation from the original MMP for engineering purposes. Hence, the seven component system was chosen for use in some particularly time-consuming simulations presented later in this chapter.

The resulting seven component mixture consisted of the following components: (C_1, N_2), (C_2, CO_2), (C_3), (iC_4, nC_4, iC_5, nC_5, C_6), (F1, F2), (F3, F4), (F5), where F1-F5 represent the original five C_{7+} fractions. The complete EOS fluid characterization

Table 3.2 Calculated MMPs for pseudoized systems, from 15 to 5 components. Volatile oil sample. Injection gas D. PR79 EOS, Appendix A. Zick multicell algorithm, 300 cells.

Number of components	C/V MMP bara (% deviation)
15 component system	337.1
11 component system	335.6 (- 0.4%)
9 component system	331.8 (- 1.6 %)
7 component system	327.1 (- 3.0 %)
5 component system	398.8 (+18.3 %)

for the 7 component system is given in Appendix A.

3.2.3 Evaluation of MMP/MME Calculation Algorithms

There exist several experimental and modelling methods for determining MMP and MME. The most important methods are discussed below, including experiments, forward and backward single cell PVT algorithms, multi cell PVT methods and slimtube simulations with elimination of numerical dispersion.

Experiments

Slimtube Experiment

A normal slimtube experimental setup consists of a 10-20 m coiled tubing with inner diameter of approximately 0.64 cm, packed with sand or a distribution of glass beads, see Yellig and Metcalfe (1980) . Initially the porous medium is saturated with the reservoir oil of interest, and gas is typically injected at a speed of 2-3 cm/min. Cumulative producing gas-oil ratio (GOR) and recovery factor (RF) is reported as a function of pore volume gas injected for a given pressure and pressure gradient.

There exists a physical dispersion in the slimtube experiment due to the presence of a porous medium that generates a certain width of the miscible front. To ensure that the entire front is included in the measurements, the experiment is normally carried out until 1.2 PV of gas has been injected. Four to six different pressures are often used, preferably two at miscible conditions and three to four at immiscible

conditions. For each pressure the measured RF at 1.2 PV injected ($RF_{1.2}$) is plotted against pressure. The minimum pressure where $RF_{1.2}$ flattens at a high values (90-100 percent) yields the MMP. Alternatively, experiments with injection gases at different enrichment levels could be carried out for a given pressure, and the RF at 1.2 PV injected is plotted against enrichment level to determine the MME.

Slimtube experiments are recognized to be a good method for determination of miscibility conditions, see Yellig and Metcalfe (1980), Auxiette and Chaperon (1981). Thus, carefully designed slimtube experiments should provide reliable estimation of the true MMP/MME. However, poor quality slimtube measurements may be highly susceptible to erroneous interpolation.

Notice also that a weakness of the slimtube experiment is the limited information obtained about the actual physical mechanisms taking place during the experiment.

Rising bubble apparatus has been suggested as an alternative to the slimtube experiment, by Novosad and Costain (1988) and Novosad et al. (1989). This experimental setup consists of a visual cell filled with reservoir fluid. Injection gas is then bubbled through the cell. The MMP is defined as the lowest pressure at which the gas bubble disappears in a "miscible" manner. The apparatus can be used for determination of the vaporizing only mechanism; the rising gas bubble is contacting original (uncontacted) oil, enriched, contacting more original oil, enriched and rising further, and so on. This can be recognized as an experimental procedure similar to the forward contact algorithm discussed below, and determines the VGD MMP/MME. Consequently, the method is not recommended for general determination of true miscible conditions.

Simulation and Modelling Procedures:

Forward and backward single cell calculation methods

Several authors have discussed calculation procedures for MMP and MME, and Stalkup (1982;1984) summarizes the majority of the main methods up to 1983. Most of these methods were based on correlations and K-value models, such as Benham et al. (1960), and later Kuo (1985).

Luks et al. (1987) and Jensen and Michelsen (1990a, 1990b) introduced computationally efficient algorithms for determining MMP with single cell methods, based on calculations with an equations of state. Most commercial PVT-programs

(PVT (1995), PVTSIM (1995)) with miscibility treatment, have single cell PVT algorithms to determine MMP for either the CGD or VGD mechanisms, and are based on these algorithms. The MMP is found from single cell backward or forward contact algorithms.

These algorithms are as follows:

Forward Contact: Injection gas is mixed with reservoir oil and a flash calculation is performed. Equilibrium gas from this flash calculation is mixed with original oil, and this procedure is repeated a number of times. This procedure represents a VGD mechanism.

Backward Contact: Injection gas is mixed with reservoir oil, and a flash calculation is performed. Equilibrium oil from this flash calculation is mixed with new original injection gas, and the procedure is repeated a number of times. This procedure represents the CGD mechanism.

Single cell backward or forward contact algorithms can be computed with an EOS and are widely used in the industry. As will be demonstrated in the followings sections, one major problem with these formulations has been that they can overpredict the MMP significantly compared to measurements, with exception for dry gas injections. This may lead to overdesign of enrichment requirement and can easily lead to the conclusion that miscible gas injection is not an economical alternative.

Multicell PVT cell methods:

Cook et al. (1969a;1969b) suggested multicell calculation approaches for studying vaporization processes. Based on Cook et al.'s suggestion Metcalfe et al. (1973) designed a multicell model for determination of miscibility. The results were plotted on ternary diagrams to determine MMP. However, an automated multicell PVT algorithm was not suggested in these papers.

Zick has developed an algorithm that mimics the development of miscibility as it appears in a slimtube simulation; this is usually the C/V (combined Condensing/Vaporizing) mechanism, but the VGD, CGD and FCM can also be identified by the method. The algorithm, which is unpublished, is based on a multicell approach, briefly described in the following (see also PVTx manual, 1995):

1. A series of cells are initially filled with the reservoir fluid of interest at a given pressure. Injection gas is brought into the first cell, mixed with the oil and a flash calculation is performed. The gas and/or some of the oil is passed on to the next cell, and contacted with that oil. This system is flashed and the process is repeated, by sending gas/oil on to the next cell. When all cells have been contacted, this result represents a single "time step".

2. The process is repeated with fresh gas injected into the already contacted oil in the first cell, the new mixture is flashed and gas/oil is passed on to the next cell, and so on. A dimensionless miscibility indicator is calculated for each cell at all contacts, and a historical minimum for each cell is found. The dimensionless miscibility indicator should be a factor that goes to zero at miscible conditions, e.g. the density difference between gas and oil.

3. Information from the historical minimum for the miscibility factor for each cell is used to extrapolate the indicator to an infinite number of grid cells/contacts. This dimensionless 'infinite' miscibility indicator should be zero at the MMP/MME.

4. The whole process is initialized again for a new pressure and repeated, giving a new miscibility indicator. The system pressure is then iterated further until the miscibility factor is below a convergence criterion, (theoretically zero). Then, the MMP for a given injection gas has been found.

Alternatively, the algorithm method can be applied for determination of the MME at a given pressure, by iterating on enrichment level for a given gas and solvent.

The Zick multicell method has been applied to a number of different reservoir fluid systems and the results have been compared with other methods in the next sections. Johns. et al (1992a, 1992b) have applied the method of characteristics for determination of MMP. Their results supports Zick's original description of the development of miscibility as a combined condensing/vaporizing mechanism. At present, their model can approximate MMP in mixtures with a maximum of four components, and has apparently not yet been applied to multicomponent reservoir fluids.

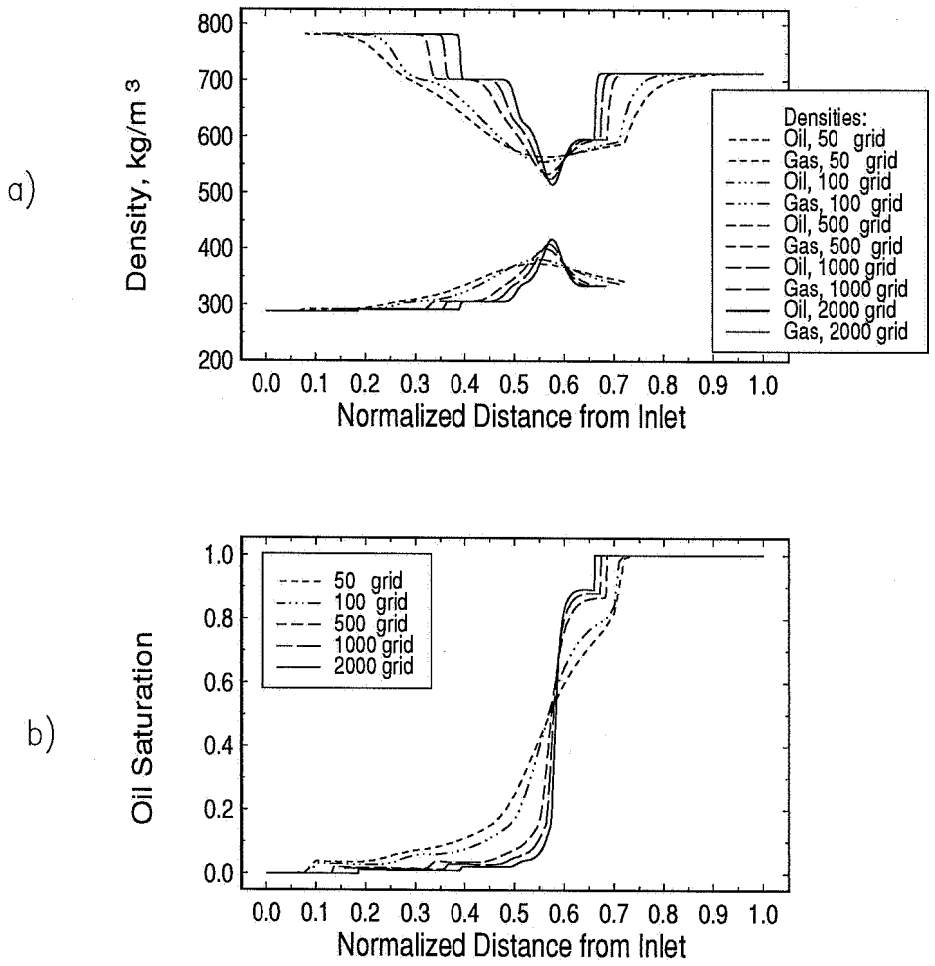

Fig. 3.4 Grid effect in slimtube simulations. Profiles at 0.6 PV gas injected in the SVO system: a) density and b) oil saturation.

Slimtube Simulations and Grid Effect

Compositional simulators can be used to determine an unambiguous MMP if performed correctly. The major problem with this type of simulations is severe case dependent grid effect, which may make interpretation of the simulated results difficult. This is demonstrated below.

Figs. 3.4 a) and b) show simulations of enriched gas injection in a SVO system at 0.6 PV injected for different numbers of grid blocks, ranging from 50 to 2000. As shown,

Table 3.3 Grid effect study for slimtube simulations at MMP = 430 bara. SVO sample. Injection gas A enriched with 40 percent gas B.

Number of grids	50	100	500	1000	2000	Extrapolated to infinity
$RF_{1.2}$	0.9230	0.9408	0.9700	0.9786	0.9843	1.00

the numerical dispersion generates a spread of the transition region where strong vaporization and condensation takes place. As stated by Johns et al. the length of this transition region should theoretically be zero in a dispersion free situation when diffusion and capillary pressure have been neglected. The main difference in the predicted profiles is that the front is "sharpened" when the number of grids is increased, resulting in the prediction of a more piston-like displacement front. At the near miscible front, the difference in density between oil and gas decreases when the number of grids is increased. This is also reflected in the results for the recovery factor, as shown in Table 3.3.

The consequence of the results given in the table is that the interpretation of the low grid simulations gives a significant *overprediction* of MMP. However, the run including 2000 grid blocks gave a recovery factor much closer to one, indicating that miscibility had been achieved. Slimtube simulations with several thousand grid cells can be time consuming. This motivates for methods that use information from simulations with lower number of grid cells to extrapolate the results to infinite number of grids. Such a method is discussed and evaluated in the following.

Slimtube Simulation Methods for Elimination of Numerical Dispersion

To avoid the grid effect problem in connection with slimtube simulations and MMP/MME determination Stalkup (1984) discussed a method for elimination of numerical dispersion through extrapolation from a finite number of grids to infinite number of grids. The purpose of the method is to eliminate errors caused by numerical dispersion. The trends in the variation of RF with grid number are used to extrapolate the results to an infinite number of grid blocks, in effect making the width of the transition zone small compared to the total number of cells.

The procedure used in this thesis has been as follows:

1. A run with a compositional simulator (ECL300) is initialized with 100 grid cells saturated with reservoir fluid, i.e. no water saturation. An EOS-characterization tuned to match relevant PVT properties for the system has to be performed in advance. Laboratory dimensions for the slimtube, properties for the porous material in the slimtube and typical laboratory injection rates are used in the initialization of the simulator. Straight line relative permeability curves with residual oil saturation equal 0.15 are used as standard. Capillary pressure and diffusion is neglected. An IMPES scheme (Implicit Pressure, Explicit Saturation) is used, with time steps chosen such that the displacement front at least stays within one grid cell for 10 time-steps.

2. Six to eight slimtube simulations with 100 grids are performed at different pressures, chosen such that 3 to 4 pressures give $RF_{1.2}$ in the region 0.6 to 0.9, and the other pressures give higher $RF_{1.2}$.

The recovery factor is defined as $RF_{1.2}=(a-b)/a$, where a is initial oil volume at reservoir conditions and converted to surface conditions, and b equals remaining oil at reservoir conditions at 1.2 PV converted to surface conditions.

3. The same pressures are run with 200 and 500 grids in the simulators, and $RF_{1.2}$ is recorded for each run.

4. $RF_{1.2}$ versus $1/\sqrt{N}$ is plotted (N = number of grids), and extrapolated to infinite number of grids for each pressure . This gives a value for RF_{∞} at each pressure.

5. The results in step 4 are plotted versus pressure, and MMP/MME is found in the same way as with slimtube laboratory results, as shown in Fig. 3.5 a).

6. Additional runs near the estimated MMP/MME at new pressures and/or for larger number of grids (typically 800 and/or 1000) are performed.

The method was applied in a simulation of dry gas injection in a SVO reservoir oil sample. The mechanism is VGD, and in this case there exists an approximately linear relationship between $RF_{1.2}$ and $1/\sqrt{N}$. This makes it relatively easy to extrapolate back to infinite number of grids, as shown in Fig. 3.5 b). At p=525 bara, an additional run with 800 grids was performed, and a weak curvature in the extrapolation of this pressure was allowed. The plot of RF_{∞} versus pressure gives a straight line from 0.77 to 1.0 and a straight line interpolation equal to 1.0 for higher pressures. As shown

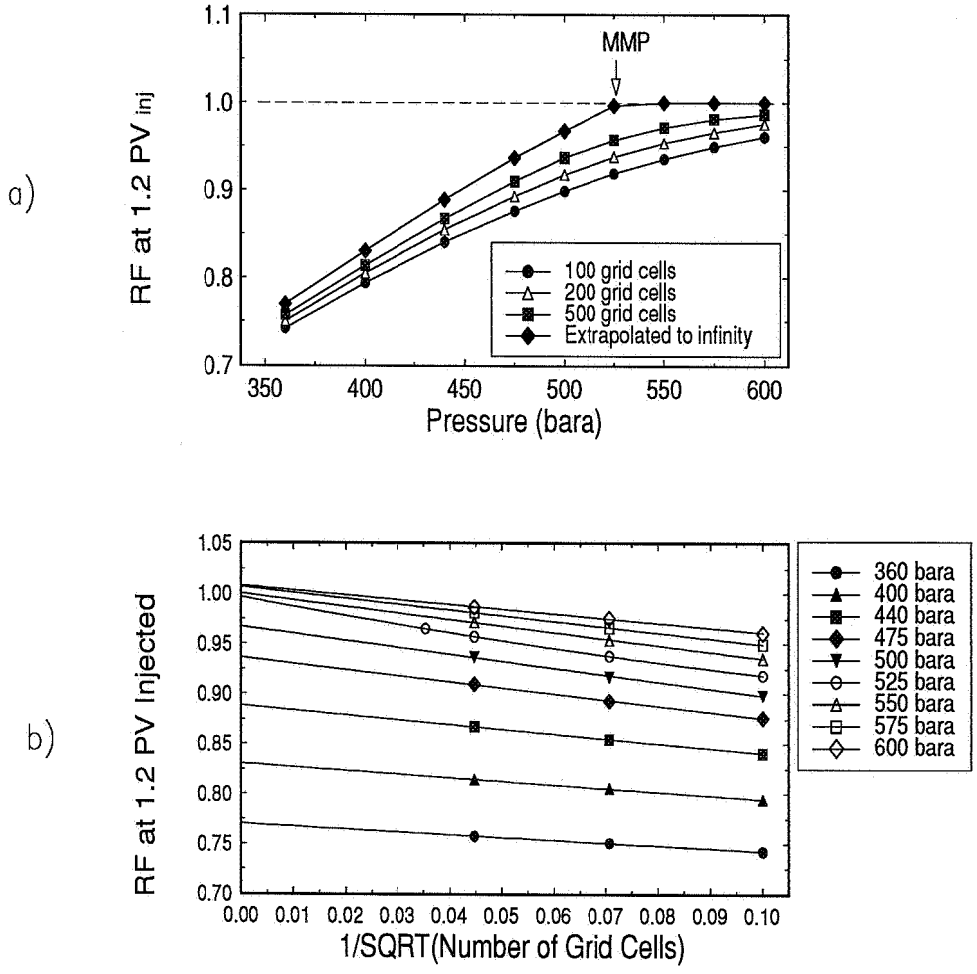

Fig. 3.5 MMP determination procedure applied on a system with dry injection gas injected into a SVO oil. a) graphical MMP determination, b) elimination of numerical dispersion through extrapolation.

in Fig. 3.5 a) this gives an MMP=526 bara. The same MMP is found when using realistic curved relative permeability curves, as shown in Fig. 3.6. Here, the change in relative permeability generates a change in the simulated values of $RF_{1.2}$ in the *immiscible* region. Thus, interpolation to determine MMP in the immiscible region is a function of relative permeability. However, at and above the MMP the predicted recovery factor is the same independent of relative permeability. Consequently, the *MMP is independent of relative permeability*. This motivates for our choice of simple straight line relative permeability curves.

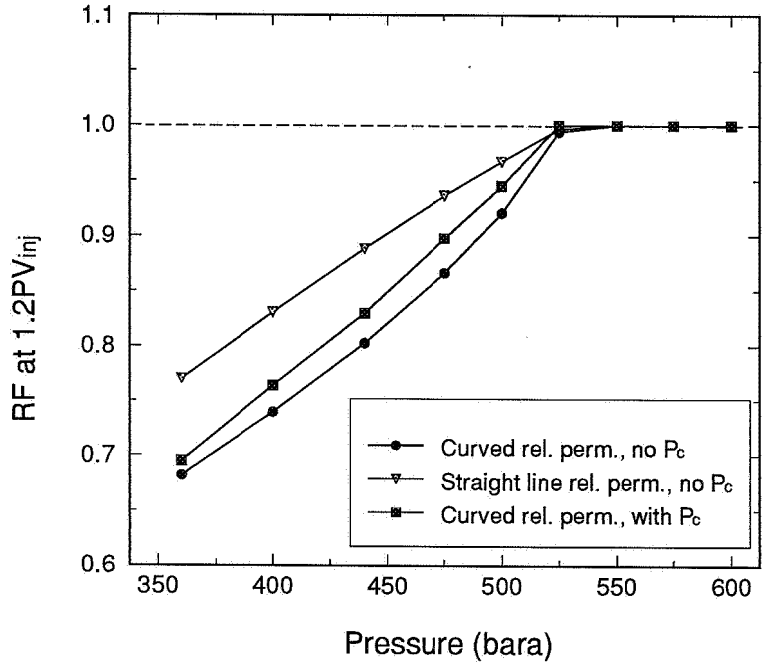

Fig. 3.6 Dispersion-free recovery factor versus pressure. Comparison between simulation results with curved and straight line relative permeabilities. Gas A injected into slightly volatile oil.

Notice that using the 100, 200 or 500 grid runs alone without any attempt to eliminate numerical dispersion would have given MMP larger than 600 bara. This demonstrates the need for elimination of numerical dispersion. Note also that numerical dispersion is most severe near the MMP/MME, which means that additional grid runs have to be performed in this region to verify the extrapolation procedure to infinite-grid recovery.

3.2.4 Quantification of Uncertainty in Slimtube Simulations

The SVO-dry gas example in the previous subsection was an example with relatively low grid effect. We find the grid sensitivity to be case dependent, and a typical plot of $RF_{1.2}$ versus pressure is not a straight line. Examples have been found where such plots are concave downwards or concave upwards. Deviations from straight line

behaviour may be significant and may effect the determination of MMP/MME.

Thus, interpretation of slimtube results can be sensitive to subjectivity. There does not appear to be a single consistent method that is commonly accepted for extrapolating to infinite grids. This uncertainty is reduced if additional runs near the apparent MMP are performed.

As a conclusion, we suggest that several extrapolations be performed, to systematically determine the case dependent uncertainty in the interpretation method. We are then able to give an uncertainty in the final MMP/MME result, for each set of simulations. This can be important in evaluation of the results and in comparison with both experiments and other modelling methods, like the Zick multicell algorithm. The choice of the extrapolation functions are motivated from our observations on typical shapes of $RF_{1.2}$ versus $1/\sqrt{N}$. In the majority of the cases three to five grid runs for each pressure has been simulated. Simple extrapolation methods that do not reqiure more than three to five data points have thus been chosen. Note that all methods which allow some curvature give RF_∞ equal a constant A for infinite grid. Also, straight line extrapolation has been included as this is widely used in the industry.

A Proposed Procedure for Quantification of Uncertainty in Slimtube Simulations

Let N be the number of grids. For each run do five (or eight if more than three different grid runs have been performed) different extrapolations to determine the RF_∞ for each pressure:

- best straight line for all data points at each pressure (Method 1).
- best straight line for data points from two highest values of N, only (Method 2).
- 2. order polynomial fit using

$$RF_\infty = A + \frac{B}{\sqrt{N}} + \frac{C}{N} \qquad (3.1)$$

a) using all grid points for each pressure (Method 3a).
b) using data points from the three highest values for N for each pressure, if more than three grid sizes run has been performed (Method 3b).

- Pade' approximation (Van Dyke, 1978),

$$RF_{\infty} = \frac{(A + \frac{B}{\sqrt{N}})}{(1 + \frac{C}{N})} \tag{3.2}$$

a) using all grid points for each pressure (Method 4a).
b) using data points from the three highest values of N for each pressure, if more than three grid sizes run has been performed (Method 4b).

- 3. order polynomial fit using

$$RF_{\infty} = A + \frac{B}{\sqrt{N}} + \frac{C}{(\sqrt{N})^2} + \frac{D}{(\sqrt{N})^3} \tag{3.3}$$

a) using all grid points for each pressure (Method 5a).
b) using data points from the three highest values of N for each pressure, if more than three grid sizes run has been performed (Method 5b).

Each extrapolation method thus gives a set of RF_{∞} with pressure variations. These data are used to determine an MMP for each method.

These methods have been used in all slimtube simulations for determination of MMP in this thesis. Two examples are given in Fig. 3.7 and Fig. 3.8 which demonstrates the variation in MMP dependent on the choice of extrapolation technique. Table 3.4 shows key results from the different methods applied on slimtube simulations of 11 different oil-gas systems. Note that the MMP predictions vary significantly within each case. The straight line extrapolation through all points most often give MMP predictions significantly higher than the other methods, and is not recommended.

Appendix C gives slimtube results and extrapolation for a number of different fluid

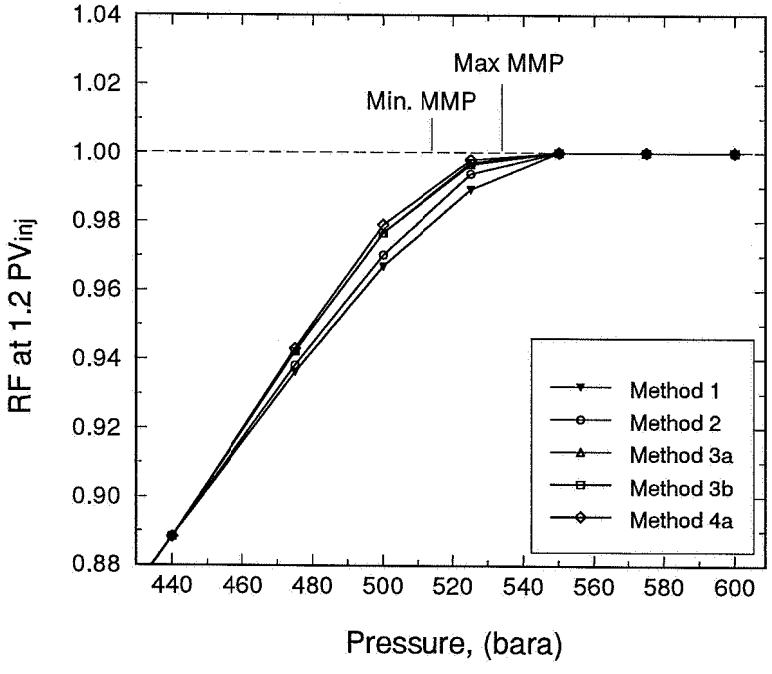

Fig. 3.7 Different extrapolation methods applied on slimtube simulation results for System 1 (Table 3.4).

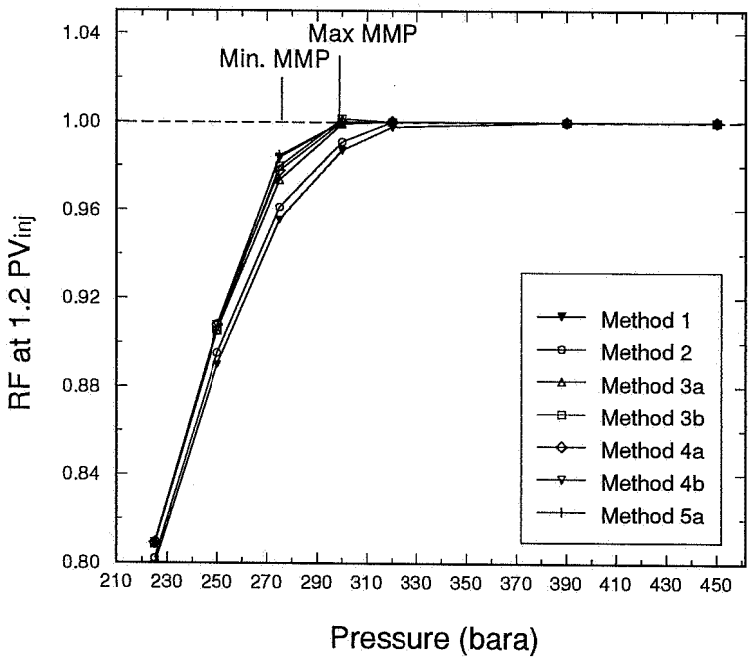

Fig. 3.8 Different extrapolation techniques applied on System 5 (Table 3.4).

Table 3.4 MMP results applying the method of slimtube simulation interpretation on 11 different systems. The oil systems were presented in Chapter 2, and the spesific depth for each sample is given. Reference conditions means sample at reference depth.

Oil/Gas System	Average MMP, Method 1-5 (bara)	Average MMP, Method 3-5 (bara)	MMP found with Method 3 (bara)
1	524 ± 10	519 ± 7	518
2	427 ± 15	420 ± 10	422
3	306 ± 15	306 ± 10	307
4	223 ± 20	231 ± 10	230
5	286 ± 10	282 ± 5	284
6	434 ± 30	428 ± 10	428
7	255 ± 10	253 ± 5	252
8	386 ± 20	381 ± 5	384
9	324 ± 15	322 ± 5	323
10	463 ± 20	457 ± 15	450
11	341 ± 20	336 ± 10	335

System Descriptions:

1 : SVO at reference conditions. Injection gas : Gas A
2 : SVO at reference conditions . Injection gas : Gas A enriched with Gas B, E=0.4
3 : SVO at reference conditions. Injection gas : Gas A enriched with Gas B, E=0.7
4 : SVO at reference conditions . Injection gas : Gas B
5 : VOA at reference conditions . Injection gas : Gas C
6 : VOA at reference conditions . Injection gas : Gas A enriched with Gas B, E=0.47
7 : VOA at -2895 mSSL . Injection gas : Gas C
8 : VOA at -2895 mSSL. Injection gas : Gas A enriched with Gas B, E=0.47
9 : VOA at -3505 mSSL. Injection gas : Gas C
10 : VOA at -3505 mSSL. Injection gas : Gas A enriched with Gas B, E=0.47
11 : 7 component VOA at reference conditions. Injection gas: Pseudoized Gas D, 7 components

systems, and clearly shows that there exist a curvature in the RF_∞ versus pressure results in all the investigated examples. Consequently, a method allowing some curvature in these extrapolations should be preferred, to describe the relevant behaviour correctly. We find the 2.order polynomial to approximately represent an arithmetic mean of the MMP predictions for each system, and this method is recommended if only one extrapolation method should be used. This method is shown in the graphs presented in Appendix C, consistently using the three highest possible values in the extrapolation procedure.

3.2.5 Comparison between MMP Predictions with Different Methods

Applying the different single cell VGD algorithm and Zick multicell algorithm on the oil-gas systems given in Table 3.4, MMP was calculated and compared with the main MMP results from the slimtube simulations. The results of this investigation of predictive capability for these systems are shown in Table 3.5.

Two observations may be drawn from this investigation :

i. For the fluid systems investigated in Table 3.5 the results from the VGD single cell method approximately equal the C/V MMP for lean gas injection, but are significant higher when richer injection gases are injected.

ii. Within extrapolation accuracy found with Method 1-5, the slimtube results are equal to the C/V algorithm results for all the fluid systems investigated above, see Fig. 3.9.

A grid effect also exists in the Zick multicell algorithm. Appendix D gives calculation examples of this grid effect for a series of different fluid systems. We find the grid effect in the multicell algorithm to occure at significantly lower number of cells than in slimtube simulations. Studying the multicell MMP predictions as a function of number of cells used in the calculations, we find that 100 to 300 cells should be sufficient to determine the MMP. Consequently, MMP determination using the Zick multicell algorithm has been performed with 100 to 300 cells in this chapter.

Another observation about the speed of the different MMP calculations methods and its consequences is: Single cell VGD and CGD methods can be computationally efficient and automated, but they generally give overpredicted MMPs for enriched gases.

Both experimental slimtube measurements and properly interpreted slimtube simulations provide reliable determination of miscibility conditions for a system, without assuming anything about the displacement mechanism. On the other hand, the methods are costly and time consuming. An experimental determination of *one* MMP/MME normally requires six runs at different pressures, or about one-two weeks in the laboratory. A slimtube simulation with correct elimination of numerical dispersion normally requires at least six-seven pressures, run with minimum 100, 200 and 500 grid cells each. That gives a minimum of 20 runs, including extrapolation to RF_{∞}, and interpolation to determine one MMP. Thus, slimtube

Table 3.5 Comparison between slimtube simulations results with estimated extrapolation uncertainty (Table 3.4), and MMP predicted with the VGD and the C/V algorithms, using 300 cells in the multicell method.

Oil/Gas System	SLIMTUBE SIMULATION		MULTICELL	SINGLE CELL
	Average MMP Method 1-5 (bara)	Average MMP, Method 3-5 (bara)	MMP C/V algorithm (bara)	MMP VGD algorithm (bara)
1	524 ± 10	519 ± 7	521	526
2	427 ± 15	420 ± 10	431	503
3	306 ± 15	306 ± 10	315	427
4	223 ± 20	231 ± 10	235	339
5	286 ± 10	282 ± 5	286	450
6	434 ± 30	428 ± 10	421	473
7	255 ± 10	253 ± 5	258	426
8	386 ± 20	381 ± 5	384	437
9	324 ± 15	322 ± 5	316	478
10	463 ± 20	457 ± 15	460	514
11	341 ± 20	336 ± 10	327	466

Note: Systems described in Table 3.4

simulations are also tedious and time-consuming and somewhat susceptible to subjective interpretation. The net result is that slimtube studies , both numerical and experimental, are often not performed for the entire range of pressure, temperature and compositions found in a reservoir. However, the Zick multicell algorithm is automated and computationally efficient, and opens for the possibility to investigate MMP/MME variations for a number of different fluid systems, as will be demonstrated in the following sections.

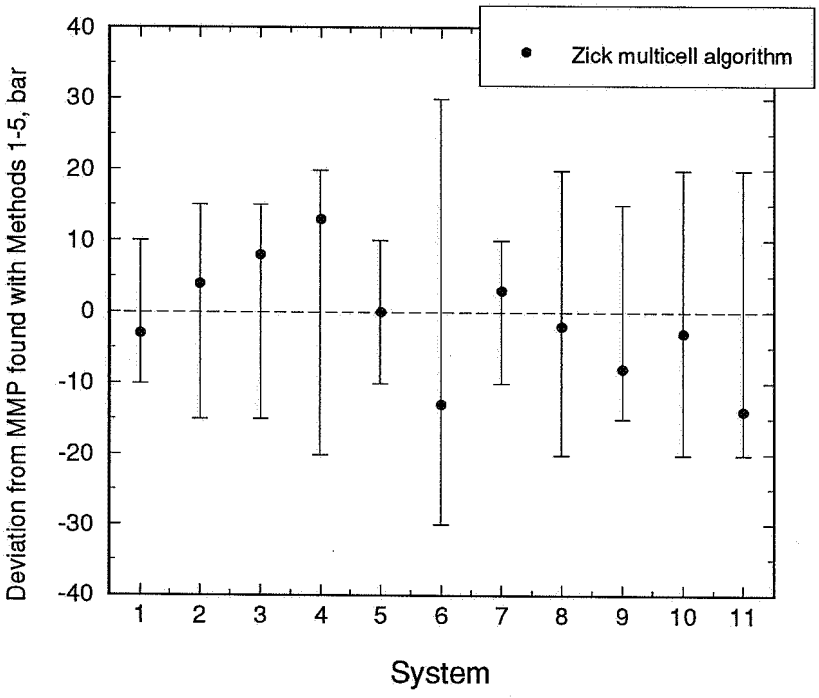

Fig. 3.9 Comparison between MMP determination with slimtube simulation and the Zick multicell algorithm. Oil-gas systems from Table 3.5. Uncertainty in slimtube MMP determination was found with Method 1-5.

3.3 Effects of Pressure and Injection Gas Composition on Miscibility

In this section we demonstrate and analyse the effect of variations in pressure and injection gas composition on miscibility. It is shown that single cell algorithms will only be sufficient for limited intervals of pressure and composition.

3.3.1 Pressure Effect on Developed Miscibility

This subsection demonstrates typical pressure effects on an oil mixture as it appears in slimtube simulations when an enriched gas is injected into the system. The main purpose has been to investigate the effect of pressure *at and above* the minimum miscibility conditions, in order to detect if significant differences are present in this pressure region.

Consider Fig. 3.10 that shows the graphical determination of MMP for the SVO system. Gas A is enriched with gas B with E=0.7, i.e. a rich gas is injected into the system. Extrapolation method 3a (Section 3.2.4) was used to determine RF_∞ for each pressure, and this gave an MMP of 315 bara. Simulations at three pressures in the miscible pressure region where selected for further investigation: (a) at the predicted MMP; p=315 bara, (b) at a somewhat higher pressure; p=370 bara and (c) at the MMP predicted with the VGD algorithm; p=427 bara.

"Snapshots" of saturation and density profiles at 0.6 PV injected in the 500 grid simulation are given at these pressures in Figs. 3.11 and 3.12. Oil composition, injection composition and temperature were held constant in these runs. Pressure is the only parameter varied.

Case (a) is similar to the case discussed in Section 3.2.1, and the 500 grid simulation shows a near-miscible situation with recovery factor just less than 1.0. As discussed in Section 3.2.1 this displacement is characterized by a leading gas front, strong condensation just ahead of a near-miscible front, strong vaporization just behind the near-miscible front, and a small oil saturation left behind the near-miscible front.

The change in characteristic profiles when pressure is increased from 315 bara to 370 bara is as follows: the extent of the condensing region and the leading gas front

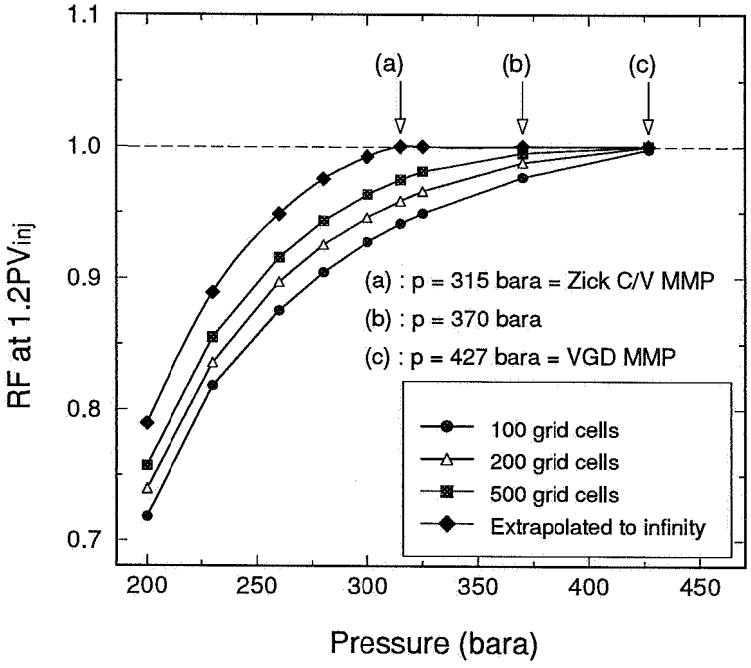

Fig. 3.10 Slimtube MMP determination for an enriched gas injected into a slightly volatile oil. (System 3, Table 3.5).

becomes smaller, the minimum difference in oil and gas density is smaller (and the K-values at the near-miscible front are closer to one). As shown in Fig. 3.11 the vaporization of the residual oil is stronger in case (b), resulting in a lower oil saturation behind the front. In summary, the displacement process is more "piston-like" .

Increasing the pressure further to the predicted VGD MMP leads to an almost 100 percent piston-like displacement front. No condensing region exists, and no leading gas front exists, as shown in Figs. 3.11 and 3.12. Almost all residual oil is vaporized, and there only exists a small two-phase region close to the displacement front.

When enriched gases are used, we find the slimtube profiles in Figs. 3.11 and 3.12 to be typical for simulations with a limited number of grids in the miscible pressure region. Due to the grid effect the displacement process appears different at different pressures, but the dispersion free RF_∞ equals 1.0 for all pressures above the MMP.

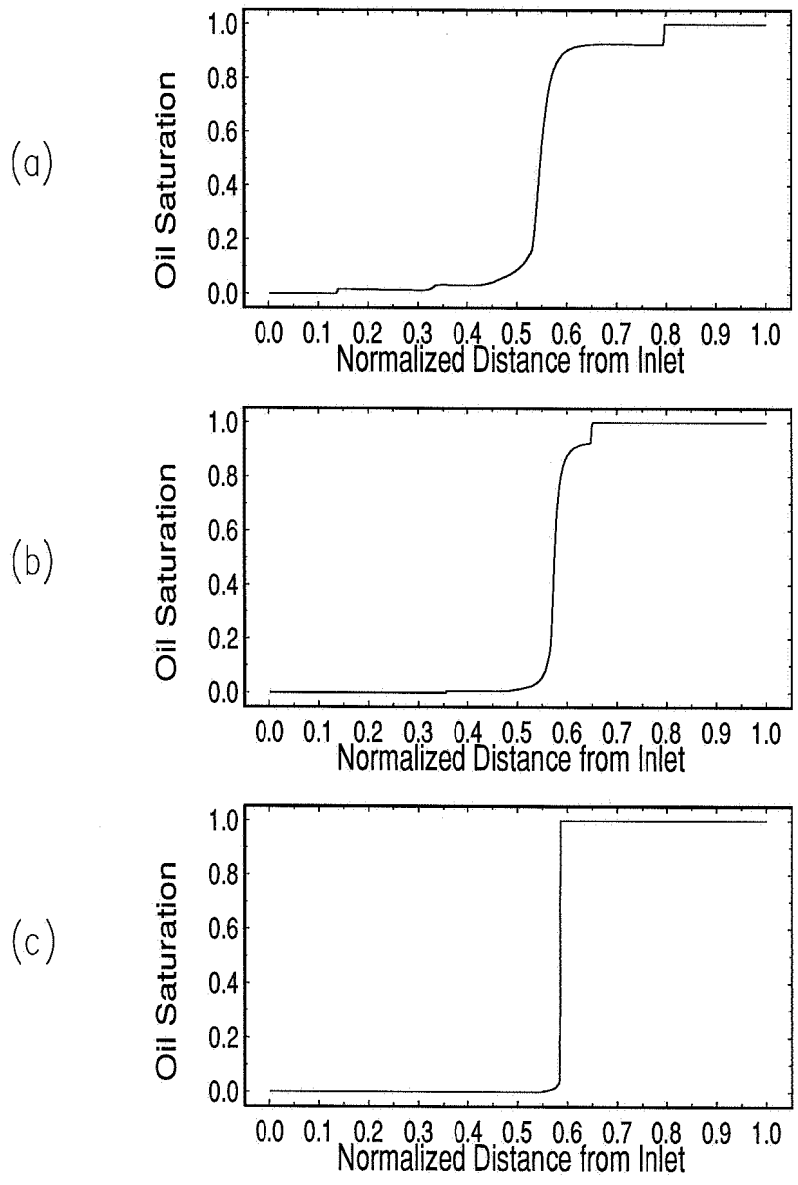

Fig. 3.11 Slimtube simulation profiles at 0.6 PV gas injected. 800 grids used in the simulations. Oil saturation at pressure (a), (b), and (c) given in Fig. 3.10.

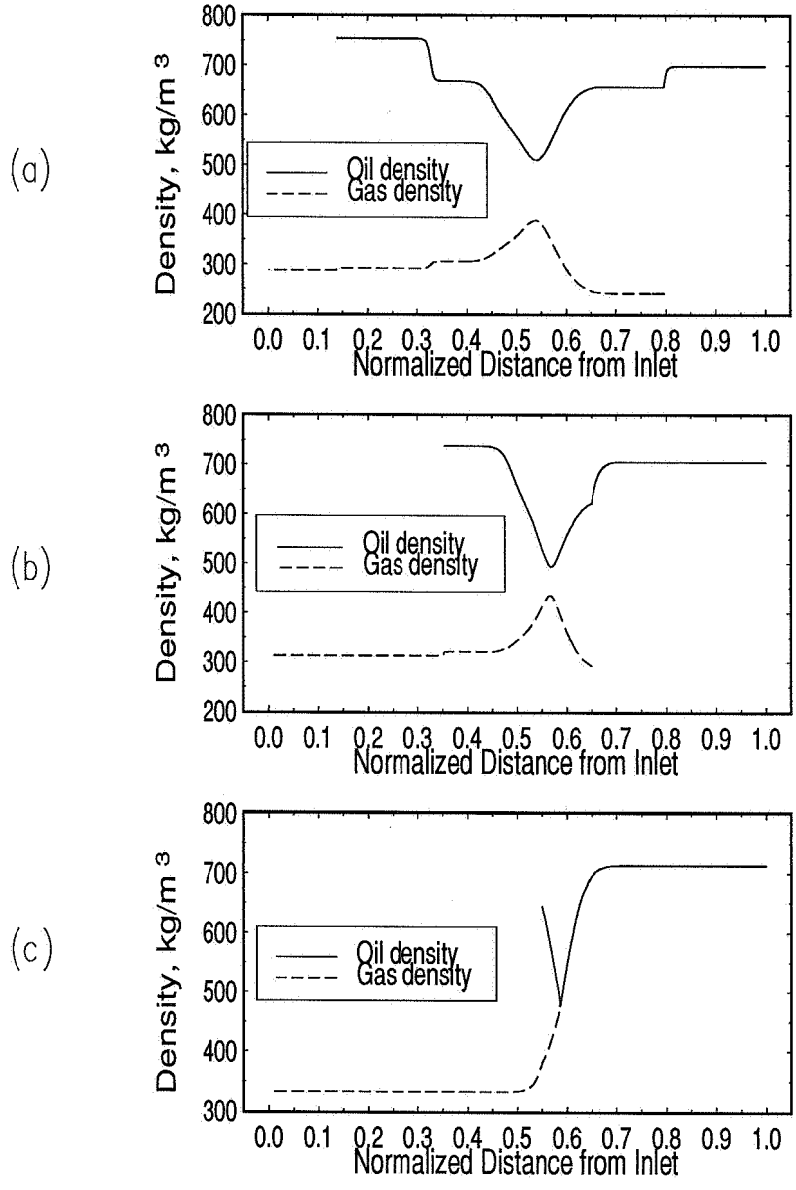

Fig. 3.12 Slimtube simulation profiles at 0.6 PV gas injected. 800 grids used in the simulations. Oil and gas densities at pressure (a), (b), and (c) given in Fig. 3.10.

3.3.2 Effect of Injection Gas Composition on MMP

Enrichment for an available injection gas can be used to design a miscible process when reservoir pressure is more-or-less fixed. The goal is to find a minimum-cost enrichment that creates developed miscibility at the pressure in the reservoir. Effects of changing the injection gas composition, while holding reservoir fluid composition and temperature constant, are investigated below. Three realistic 15-component reservoir fluid systems are considered :

- **Slightly Volatile Oil (SVO) Case**: A slightly volatile oil sample at depth -2695 mSSL (Sub Sea Level). The data was taken from the SVO reservoir presented in Chapter 2.

- **Near Critical Oil (NCO) Case**: A near-critical oil sample at depth -3105.5 mSSL, approximately 71 m below the saturated GOC, taken from the NCO reservoir presented in Chapter 2. The reservoir oil composition was found from isothermal GCE calculations.

- **Gas Condensate Case**: A near-critical gas condensate fluid at depth -2987 mSSL, approximately 51 m above the saturated GOC in the NCO example. Again, the gas condensate composition was calculated with the isothermal GCE method.

The compositions for these three different reservoir fluids are given in Table 3.6.

The calculation procedure for this investigation is the following:
The dry gas A was enriched with gas B as solvent. These gases is presented in Table 3.1. The enrichment level, E, represents the mole fraction of enrichment such that the resulting injection gas mixture, $y_{mix,k}$, for each component, k, is given as

$$y_{mix,k} = (1 - E)\, y_{drygas,k} + E\, y_{solvent,k} \qquad k = 1,..,n \tag{3.4}$$

where n is the total number of components. By varying E in steps of 0.02, 50 different injection gas mixtures were generated, as shown on Fig. 3.13. MMP was then calculated as a function of enrichment level, generating MMP as function of E (MMP(E)) for each reservoir fluid system.

Table 3.6 Reservoir fluid composition for three fluid systems.

Component	SVO	NCO	Gas Condensate
N2	0.2700E-02	0.5181E-02	0.6668E-02
CO2	0.7900E-02	0.1232E-01	0.1290E-01
C1	0.4634	0.6353	0.7491
C2	0.6150E-01	0.7802E-01	0.7688E-01
C3	0.4460E-01	0.4292E-01	0.3887E-01
IC4	0.8700E-02	0.9171E-02	0.7892E-02
C4	0.2270E-01	0.2206E-01	0.1839E-01
IC5	0.9600E-02	0.9324E-02	0.7359E-02
C5	0.1410E-01	0.1196E-01	0.9263E-02
C6	0.2100E-01	0.1525E-01	0.1106E-01
F1	0.4929E-01	0.5388E-01	0.3098E-01
F2	0.9245E-01	0.3733E-01	0.1589E-01
F3	0.9689E-01	0.2846E-01	0.8791E-02
F4	0.7032E-01	0.2225E-01	0.4499E-02
F5	0.3485E-01	0.1661E-01	0.1406E-02

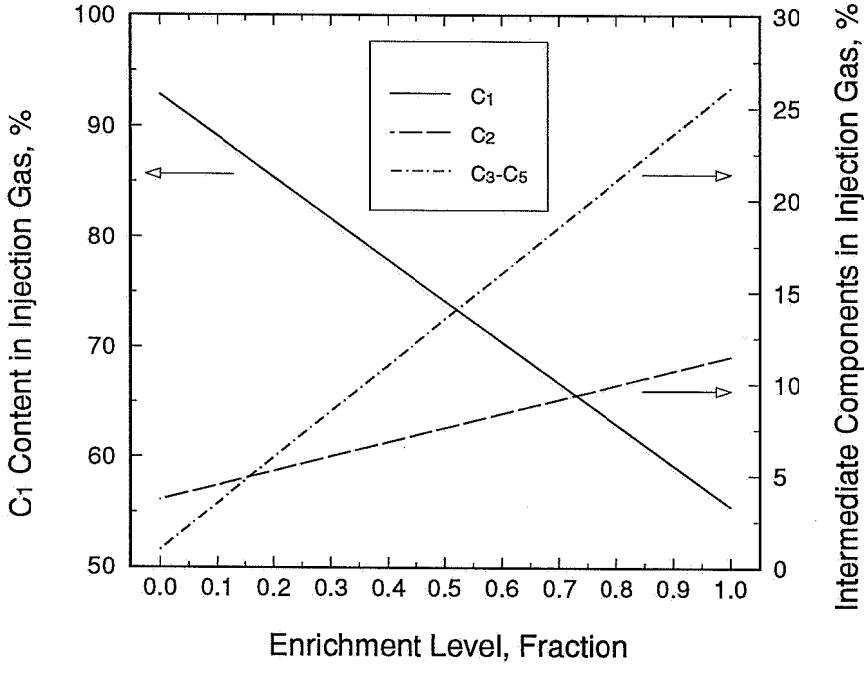

Fig. 3.13 Key components as a function of E in the designed injection gas.

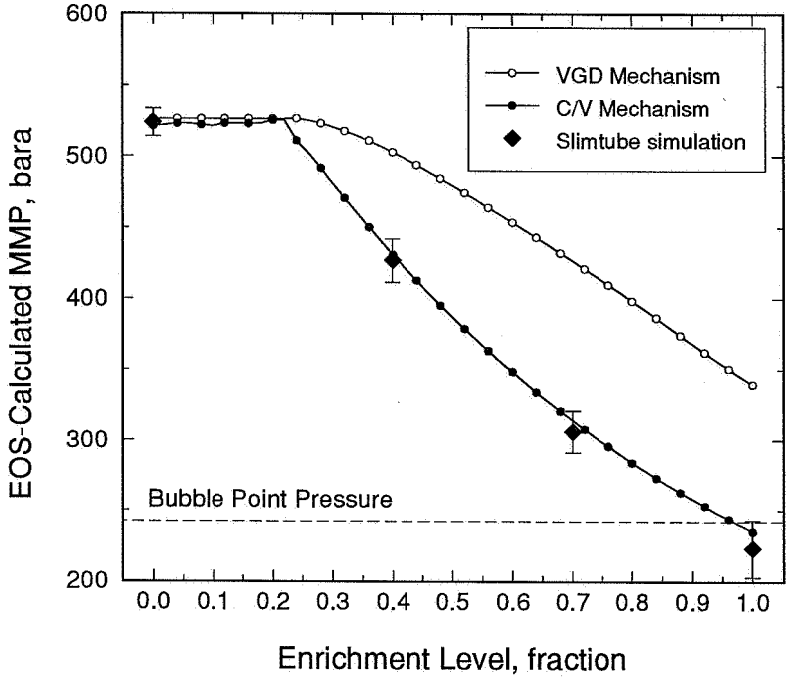

Fig. 3.14 MMP as a function of enrichment level (gas A enriched with gas B) for the SVO Case. 300 cells used in the Zick multicell algorithm. Slimtube MMP results with extrapolation uncertainty are taken from Table 3.5.

Fig. 3.14 shows the calculated results from this procedure when applying the VGD and the C/V algorithms for the SVO case. Included are slimtube results with estimated uncertainty for MMP at four different enrichment levels: 0.0, 0.4, 0.7, and 1.0. Within the extrapolation accuracy, the C/V MMP is equal to the slimtube MMP. As shown in the figure, the calculated C/V MMP remains approximately constant in the enrichment interval E= 0.0 to 0.22 and the results are approximately equal to the ones obtained with the VGD algorithm. For enrichment levels slightly above 0.22 the C/V mechanism predicts large changes of the MMP(E). The difference between the VGD MMP and the C/V MMP becomes large as enrichment level is increased, exceeding 100 bar for E=1.0.

For lean injection gases the VGD mechanism represents the correct miscible mechanism and the MMP does not vary significantly with enrichment. At a certain "crossover" enrichment level, E*, the injection gas becomes sufficiently enriched in

intermediate components to generate a mixed condensing / vaporizing mechanism. This decreases the MMP rapidly as enrichment level increases.

The existence of a crossover enrichment level E* was one of several interesting results from this study. The enrichment crossover effect was investigated further for the near-critical oil. Fig. 3.15 shows results of MMP(E) for this system. Again, there was an interval of low enrichment levels where all MMP predictions remain practically unchanged, beeing VGD. Exceeding a crossover level of E*=0.32 changes predictions with both the VGD and C/V algorithms. The VGD predictions decreases weakly as a function of enrichment level, until it reaches the bubble point pressure. The VGD mechanism does not ever predict MMP below the saturation pressure. However, the C/V MMP can be significantly below the bubble point pressure. As seen from the figure, the results from the VGD algorithm overpredicts the MMP significantly when compared to the C/V MMP predictions, above E=0.32.

MMP calculation below the saturation pressure is initialized with a CCE calculation of the reservoir fluid at the given pressure and temperature conditions. Gas is then injected into the two phase system, and the calculations proceed as usual.

Finally, the gas condensate case was investigated. Results are plotted in Fig. 3.16. As seen, the VGD MMP is never below the dew point pressure, and equals the dewpoint pressure for all enrichment levels. The CGD mechanism predicts an MMP equal to the VGD MMP up to a relative high enrichment level, E= 0.80. Exceeding this CGD "crossover" level leads to a decrease in predicted CGD MMP. Mark that the C/V MMP predictions are significantly lower than the CGD and VGD predictions for all enrichment levels above E*=0.4. Below E* all algorithms predict the same and constant MMP, equal to the dewpoint pressure. The C/V MMP results in Fig. 3.16 show that the MMP can be significantly lower than the dewpoint for enriched injection gases in gas condensate systems.

Fig. 3.17 shows the derivative of the C/V MMP(E) results with respect to enrichment level for the SVO, NCO and gas condensate cases. Note that the derivative is approximately zero, up to the crossover enrichment level, E*. In this enrichment region, small fluctuations are seen in the curves for the SVO case. The calculated MMP values in this region do not smoothly vary with enrichment level. This may be a weakness in the existing version of the Zick multicell algorithm. However, the MMP fluctuations are only present at enrichment levels below E*, and are not larger than ± 1 bar. As seen in the figure, exceeding the crossover level leads to an abrupt decrease in the MMP. Increasing the enrichment level further, results in a decreasing

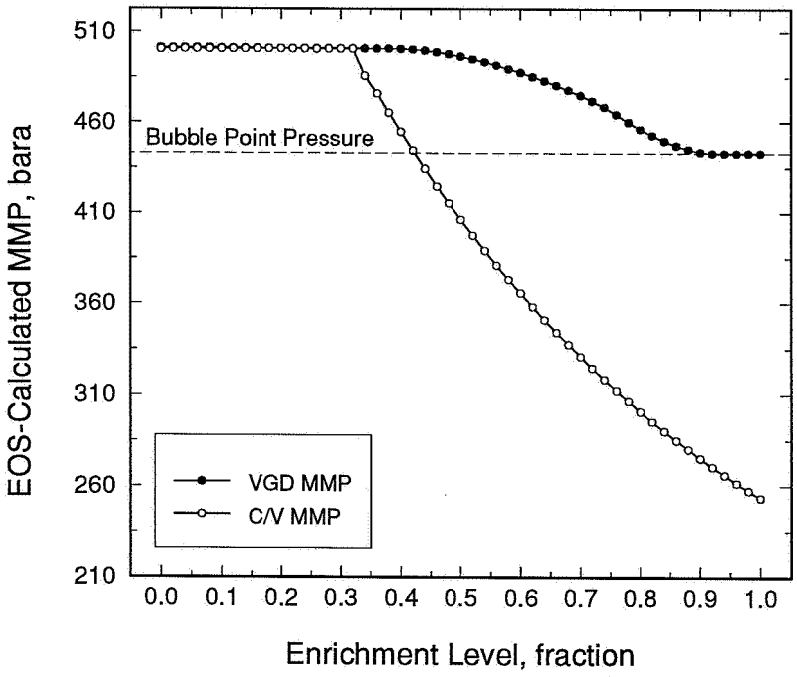

Fig. 3.15 VGD and C/V MMP (300 cells) as a function of E in the NCO Case.

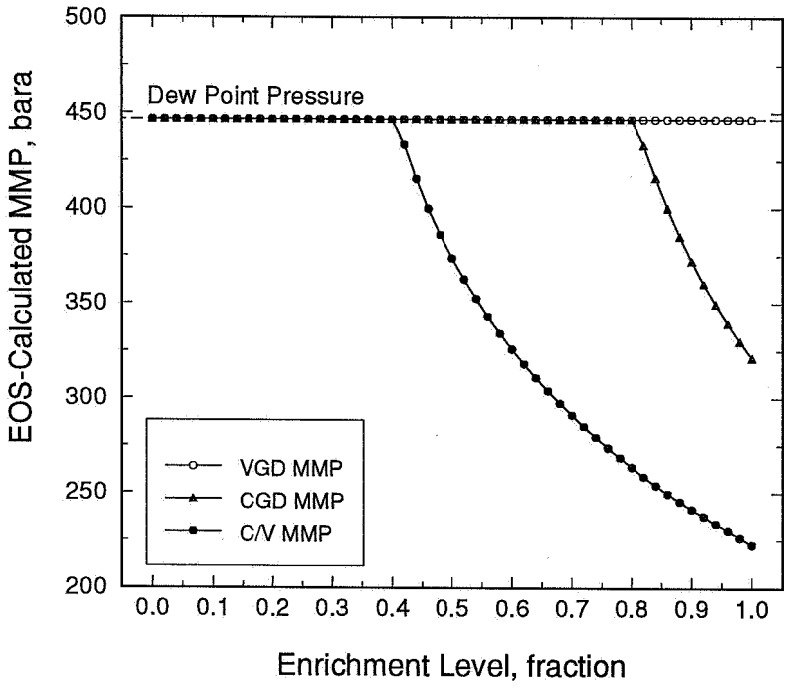

Fig. 3.16 VGD, CGD and C/V MMP versus E in the Gas Condensate Case. Zick multicell algorithm with 300 cells.

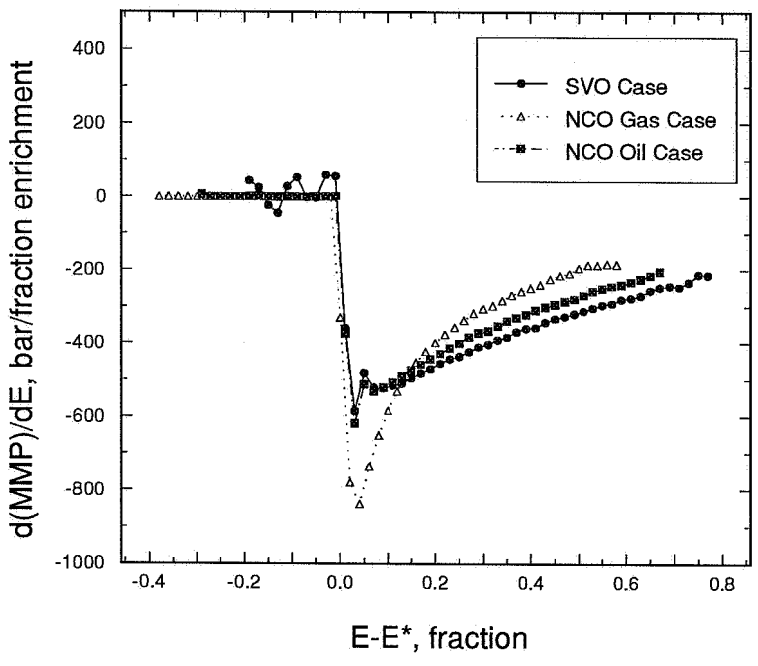

Fig. 3.17 Derivative of the C/V MMP's in Figs. 3.14 to 3.16, as a function of E.

slope of the MMP(E) curve.

To summarize, the following observations can be drawn from these calculations:

i. MMP VGD predictions are never below the saturation pressure. This can be understood directly from the forward contact algorithm, since enriched gas always is contacted with original reservoir oil only. This means that no initial two phase region will occur in the calculation, as can be seen from the previously shown snapshots of slimtube profiles where a vaporizing effect is characterized by a single phase region ahead of the miscible front.

ii. The C/V and CGD algorithms can predict MMP below saturation pressure.

iii. The true MMP (slimtube or C/V predictions) decreases with increasing enrichment of the injection gas, but stays approximately constant up to a threshold enrichment level, E*. This behaviour has been demonstrated for

three different reservoir fluid systems.

iv. The true MMP decreases significantly when exceeding the threshold enrichment level, E*.

v. The VGD and the CGD MMPs differ dramatically from both the C/V MMP predictions (and slimtube simulation MMP predictions) at enrichment levels above E*. The VGD and CGD MMPs overpredict the true MMP in this enrichment region. Consequently, E* determines the upper limit for enrichment level where the VGD or CGD algorithms are applicable.

These conclusions are confirmed in the next section where a number of different reservoir fluids ranging from dry gases to heavy oils have been investigated. Thus, these points are not only representative for the three systems alone, but confirmed in about 80 different cases, and appear to represent general behaviour for predictions of MMP as a function of enrichment.

As part of a practical and economical evaluation of the feasibility of a miscible gas injection project, the conclusions above suggest that E* for the system of interest should always be determined. An enrichment with E lower than E* will not reduce the MMP significantly, and hence not represent a beneficial economical situation. On the other hand, enriching the injection gas more than E* will lead to an abrupt drop in the MMP. Considering the phase behaviour effects alone, a slight increase in enrichment level in this region may have a large positive economical consequence. This should be important in design of the injection gas. Because the slope of the MMP(E) curves is largest for E close to E* and are reduced for increased enrichment levels, an analysis of the gain in MMP versus the cost of enriching the gas further is recommended always to be performed.

The results found for the MMP(E) also have to be compared with the existing reservoir pressure to find the enrichment required to lower the MMP below this pressure. If this value for E does represent a realistic economical alternative a possible injection gas has been designed which could be used in further studies. Figs. 3.14 to 3.16 demonstrate the problems in using single cell VGD or CGD methods in MMP predictions, as these methods may highly overpredict the MMP. Using the VGD or CGD algorithms may inccorectly lead to the conclusion that miscible gas injection is not economical or technically feasible.

3.4 Minimum Miscibility Conditions in Compositionally Grading Reservoirs

In Chapter 2 we discussed and demonstrated that significant vertical compositional gradients can exist in petroleum reservoirs. This section includes the effect of compositional gradients on miscibility conditions. The main goal has been to provide a general description of the MMP and MME variation with depth for different reservoir fluid system and injection gas compositions.

3.4.1 Method and Assumptions

Holding the reservoir fluid composition constant and vary the injection gas composition (Section 3.3.2), could be seen as an analogy to holding the injection gas composition constant and instead varying the reservoir fluid composition. It is the distribution and combination of components in *both* the injection gas and the reservoir fluid that determine the MMP or MME. This subsection gives the methods for our studies of *MMP as a function of depth* in compositionally grading reservoirs.

Compositional variations with depth for different reservoir fluid systems have been generated with the *isothermal GCE method*, assuming zero capillary pressure. Four reservoir fluid systems have been considered, ranging from a slightly volatile oil system with gas cap, showing limited compositional gradients, to a near critical reservoir with strong compositional gradients and with an undersaturated GOC. These reservoir fluids were presented in Chapter 2. We *mainly restrict the discussion to reservoir oils* in this section, but present results for the whole range of reservoir fluids, including gases, for convenience. Section 3.5 is dedicated to a discussion of MMP variations in gas condensate reservoirs. Also, thermal effects are neglected in this section, but discussed separately in Section 3.6. Notice that when referring to a variation with depth in this chapter we mean the variation occurring when going downwards in the reservoir.

The calculation method for determination of MMP/MME variations with depth (MMP(h) /MME(h)) has been as follows:

1. Use isothermal GCE to generate compositional variations with depth.

2. Pick compositions for a series of depths, covering the entire reservoir thickness.

3. Apply the Zick multicell (C/V) algorithm to the reservoir fluids at each depth for a series of injection gas compositions, and compare the calculations with slimtube simulations for selected systems.

To demonstrate the difference in predictions, a limited number of VGD and CGD results are included. Vertical fluid communication over large depth intervals has been assumed to evaluate miscibility variations for large compositional space.

As an introduction to the results in this subsection we will first discuss two figures, Figs. 3.18 and 3.19.

Fig. 3.18 shows calculated variations in MMP with depth for a VOA reservoir with continuous variation from gas to oil. Injection gas in this example was a mixture of gas A and B with enrichment level E=0.47. Within the extrapolation accuracy the slimtube simulations matched the C/V algorithm predictions at the three tested depths in the reservoir. The slimtube simulations were performed at 100, 200, 500 grids, and additional 800 and 1000 grids at selected pressures near apparent MMP. The C/V algorithm calculations were performed with 300 cells.

In Fig. 3.18 the VGD algorithm has been applied to determine MMP(h). As seen form the figure the resulting slope of the MMP(h) is approximately the same as the one found with the C/V algorithm in the oil zone. However, the VGD algorithm highly overpredicts the MMP.

The slope of MMP(h) is a result of the compositional gradients present in the reservoir. The lighter oil near the undersaturated GOC gives a lower MMP than the heavier oil near the bottom of the reservoir. This is caused by a more favourable composition distribution (intermediates mainly) in the light oil, compared to the heavier oil which contains more C_{7+} components. Table 3.7 shows the oil composition at three different depths in the reservoir. Note that the oil composition near the undersaturated GOC contain more C_1-C_6 and less C_{7+} than the deepest oil composition.

In the reservoir gas region in Fig. 3.18, the VGD MMP is equal to the dewpoint pressure. Thus, the injection gas is predicted to develop miscibility with the reservoir fluid at pressures only in the one-phase gas region. This behaviour is drastically

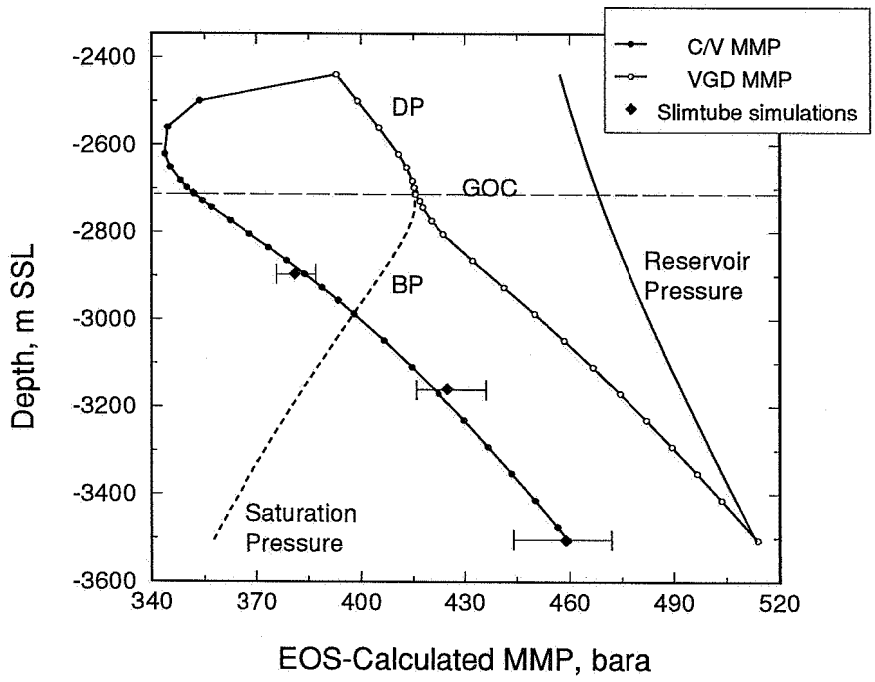

Fig. 3.18 MMP as a function of depth in the VOA reservoir. E=0.47 gas A enriched with gas B. Zick multicell algorithm with 300 cells.

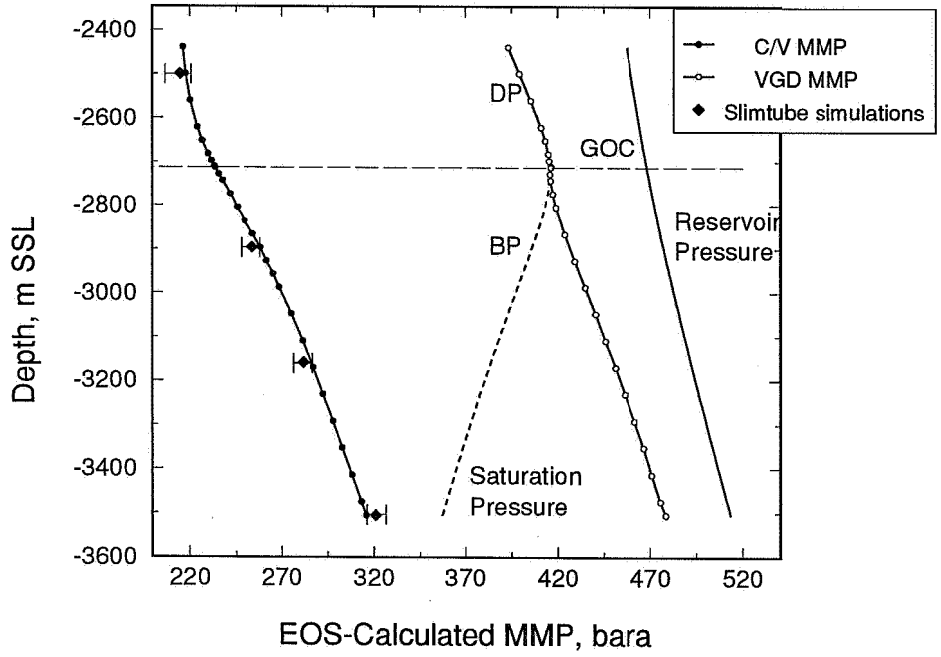

Fig. 3.19 MMP variation with depth in the VOA reservoir. Injection gas C. 300 cells applied in the Zick multicell algorithm.

Table 3.7 Reservoir fluid composition at three depths in the VOA oil column as predicted by the isothermal gravity/chemical equilibrium method.

Component	Oil composition at		
	-2895 m SSL	-3159 m SSL	-3505 m SSL
N2	0.9471E-02	0.9300E-02	0.9188E-02
CO2	0.2296E-02	0.2100E-02	0.1965E-02
C1	0.6262	0.5877	0.5553
C2	0.7955E-01	0.7570E-01	0.7186E-01
C3	0.4213E-01	0.4090E-01	0.3929E-01
IC4	0.9247E-02	0.9100E-02	0.8817E-02
C4	0.2106E-01	0.2090E-01	0.2035E-01
IC5	0.7632E-02	0.7700E-02	0.7583E-02
C5	0.1136E-01	0.1150E-01	0.1133E-01
C6	0.1698E-01	0.1750E-01	0.1744E-01
F1	0.5072E-01	0.5381E-01	0.5486E-01
F2	0.5229E-01	0.5866E-01	0.6207E-01
F3	0.4024E-01	0.5003E-01	0.5680E-01
F4	0.2164E-01	0.3519E-01	0.4823E-01
F5	0.9187E-02	0.1992E-01	0.3486E-01

different for the C/V MMP, where the MMP(h) has a minimum at -2620 m SSL, far into the two phase region. Going further upwards in the gas zone, the reservoir gas becomes leaner, and the C/V MMP increases and finally collapses to the results from the VGD mechanism at -2440 m SSL. The combination of a relatively lean injection gas and a lean reservoir gas does not generate a condensing region, and the vaporizing mechanism is the *only* mechanism taking place at and above -2440 m SSL for this particular injection gas. *This behaviour may bee seen as an analogy to the existence of a crossover enrichment level discussed in Section 3.3.2.*

Fig. 3.19 shows MMP calculations with injection of gas C into the same VOA reservoir system as above. The VGD predicted MMP(h) behaviour is here similar to the one found in the lean injection gas case. Notice that the MMP(h) curve in the oil zone has been shifted to the left compared to the VGD predictions for the lean gas example. Thus the VGD MMP results are lower than the initial reservoir pressures for all depths. Notice also that the VGD MMP is equal to the bubble point pressure when approaching the undersaturated GOC in the oil zone, and equal to the dewpoint pressure in the gas zone. This confirms the observations made in Section 3.3.2 that

the VGD predictions in general are not lower than the saturation pressure.

As shown in Fig. 3.19 the C/V predictions and slimtube predictions match at the three tested depths within the extrapolation uncertainty. The slope of the C/V MMP(h) results in the oil zone was found to be similar to the slope in Fig. 3.18 caused by the compositional gradients in the reservoir oil.

The rich gas injection gives C/V MMP(h) variations that are significantly lower than the variations in saturation pressure over the whole reservoir thickness. Because the injection gas is significantly richer in this case than in the case of Fig. 3.18, the C/V mechanism does not collapse into the VGD at the top of Fig. 3.19. However, if an analogy to the existence of a crossover enrichment level holds, the C/V MMP should finally collapse into the VGD mechanism when proceeding further up in the leaner gas zone.

The results from the VGD algorithm in this case overpredicts the appearant true MMP with an average difference of about 170 bar in the entire depth interval investigated. Again, this demonstrates the problems in using single-cell methods for determining miscibility.

The main conclusion to be drawn from Figs. 3.18 and 3.19 is that *compositional variations can generate relatively large variations of MMP with depth in a petroleum reservoir.*

The following sections gives MMP(h) for different reservoir fluid systems and up to 20 different mixtures of injection gases for each reservoir.

3.4.2 MMP with Depth in a SVO Reservoir with Gas Cap

The method given in Section 3.4.1 was applied on the SVO reservoir with gas cap presented in Chapter 2. 20 different mixtures of dry injection gas A and rich gas B were used in the MMP calculations for each depth. Fig. 3.20 a) shows C/V calculations for MMP(h). VGD calculations for the same cases were performed for comparison and are shown in Fig. 3.20 b).

The SVO reservoir has a relatively small and approximately linear compositional gradient. Consequently, we find that MMP is a weak and approximately linear function of depth within the oil zone. In this reservoir a discontinuity in composition

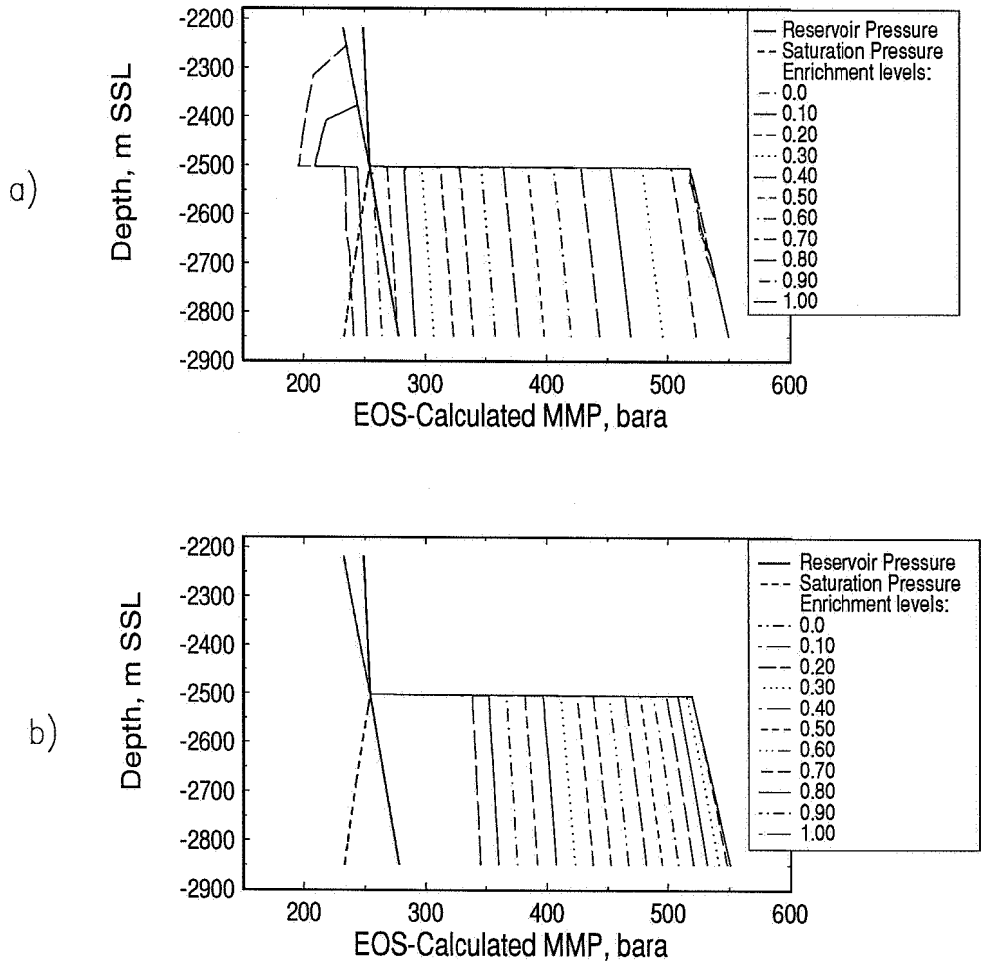

Fig. 3.20 MMP variation with depth in the SVO reservoir. a) C/V MMP (100 cells, Zick multicell algorithm), b) VGD MMP.

across the GOC is present. As shown in the figures this discontinuity also generates a discontinuity in MMP with depth across the GOC.

The VGD MMP predictions in the oil zone are significantly higher than the C/V predictions for MMP when enriched gases are injected; approximately 170 bar on average. The VGD MMP for the richest gas investigated is higher than the reservoir pressure over the entire oil column, thus leading to the wrong conclusion that miscibility is not possible to achieve in this reservoir for any of the available gas mixtures.

The C/V mechanism predicts MMP's lower than reservoir pressure in the oil zone, but only for rich gases with E larger than 0.85-0.90. This shows that generating a miscible process in this particular reservoir will be possible, but questionable and expensive, from an economic point of view.

An interesting feature of this particular reservoir was identified by comparing the C/V MMP(h) values with the reservoir pressure. The slope of MMP(h) compared to the slope of the curve showing reservoir pressure versus depth leads to the conclusion that injection gases with enrichment levels close to 0.85-0.90 can develop miscibility in the lowest parts of the oil zone, even though MMP is higher than the reservoir pressure in the upper parts of the oil zone. Theoretically, this suggests a scenario with developed miscible gas injection in the lower part of the reservoir.

Also notice that by going in the horizontal direction for an arbitrary chosen depth in the oil zone (Fig. 3.20 a)) one yields the same main MMP variation with enrichment level as the one discussed in Section 3.3.2. In Fig. 3.20 a) there exists a 'crossover' enrichment level, E*, approximately equal to 0.2 in the oil zone. Below this limit the C/V MMP collapses to the VGD MMP. As in Section 3.3.2, small fluctuations in the C/V calculations are present below E*, but as shown in Fig. 3.20 a) the fluctuations are small.

For engineering purposes, the MMP(h) in the SVO oil zone for a given injection gas may be treated as a constant. The small compositional variations do not generate large MMP variations with depth. The next subsections show examples with volatile and near critical oils where vertical compositional variations are larger and accordingly, the MMP variations with depth are more pronounced.

3.4.3 MMP with Depth in a NCO Reservoir with Gas Cap

The near critical oil reservoir with a saturated GOC was investigated with respect to MMP variations for 20 different mixtures of gas A and gas B. This reservoir was presented in Chapter 2. The procedure given in Section 3.4.1 was applied to determine MMP(h). Calculated results for the C/V mechanism are given in Fig. 3.21 a), and results for the VGD mechanism are shown in Fig. 3.29 b).

VGD Calculations

Consider Fig. 3.21 b). Starting from the reservoir top and proceeding downwards, it

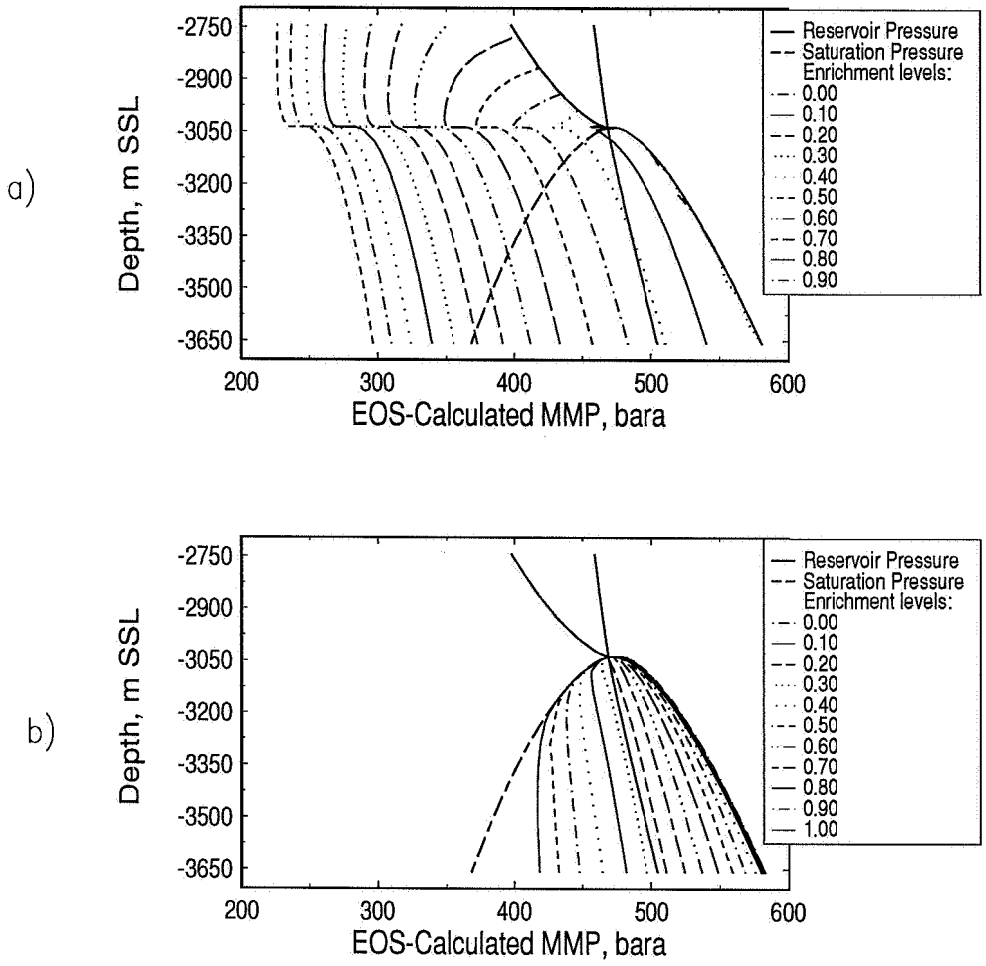

Fig. 3.21 MMP variation with depth in the NCO reservoir for a series of mixtures of injection gas A and B. a) C/V MMP determined with the Zick multi-cell algorithm, 100 cells, b) VGD MMP.

is seen that the MMP(h) variation calculated with the VGD method is equal to the dewpoint pressure in the gas zone. For lean gases, the MMP(h) is larger than the bubble point pressure when proceeding further down in the reservoir oil zone. In this part of the reservoir rich gases give a calculated MMP(h) that follows the bubble point pressure line. Dependent on injection gas enrichment level the VGD MMP(h) deviates from the saturation pressure further down in the oil zone, and the position for this deviation is deepest in the reservoir for the richest gas.

C/V Calculations

As discussed in Chapter 2 this NCO reservoir is characterized by larger compositional gradients than the SVO reservoir, and has the largest compositional variations in the vicinity of the GOC. This is reflected in the C/V MMP calculations, as shown in Fig. 3.21 a).

Consider the oil zone in Fig. 3.21 a). For lean gases with E < 0.30 the C/V predictions are equal to the VGD MMP. For richer injection gases the C/V MMP(h) results are lower than the VGD MMP. In the oil zone the C/V MMP(h) has its minimum at the GOC. Going downwards from the GOC, the MMP predictions increase rapidly as a function of depth in the vicinity of the GOC, but show a smaller increase further down in the oil zone. Notice that the general shape of the MMP(h) curves below the GOC is not linear with depth. This is due to the nonlinear compositional variation with depth in this reservoir.

Because the reservoir fluid composition is discontinuous across the GOC, the MMP(h) is also discontinuous at this depth going from one phase to another in the vertical direction. The calculated discontinuity in MMP *at the GOC* is much smaller for the NCO reservoir than for the SVO reservoir. The contrast over the GOC in physical properties like composition and density is small in the NCO case compared to the SVO case. Therefore, a smaller difference in MMP above and below the GOC is observed in the NCO case compared to the SVO case.

For injection gases with enrichment levels between 0.35 and 0.40, the C/V predictions show that a miscible zone below the GOC will be present. The minimum MMP will be at the GOC, and MMP increases with depth in the oil zone. Proceeding further down in the reservoir the MMP(h) will eventually exceed the reservoir pressure for a given enrichment level. This MMP(h) behaviour is fundamentally different from the MMP(h) in the SVO reservoir where the opposite behaviour was found.

Riemens et al. (1988) discussed the possibility for miscible gas injection in a Middle East reservoir and found a miscible zone just below the GOC. This is a similar result to the one we find in the NCO example, but unfortunately the method for MMP determination was not given in the paper.

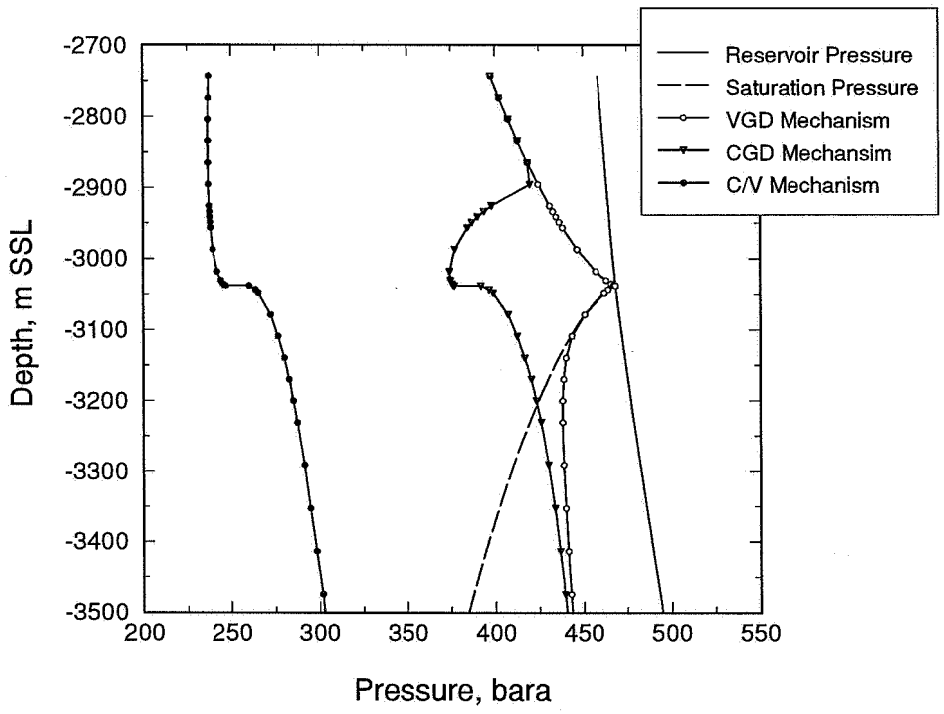

Fig. 3.22 Comparison between VGD, CGD, and C/V MMP(h) variations in the NCO reservoir. Injection gas: gas A enriched with gas B, E=0.9

CGD Calculations

To focus on the possible differences between results from the VGD, CGD and C/V algorithms, a series of calculations for MMP(h) were performed with all algorithms. One typical example for a rich gas injection is shown in Fig. 20. As seen from the figure, the MMP(h) calculated with the CGD algorithm is not limited downwards by the saturation pressure. Thus, the CGD predictions in this case are significantly lower than the VGD results over a large depth interval in the reservoir, approaching the VGD predictions in the lower parts of the oil zone and collapsing into the dew point pressure close to the top of the reservoir.

However, notice that the CGD predictions in this case are significantly larger than the C/V predictions over the whole reservoir thickness.

Number of Calculations Needed to Generate One Figure

The C/V MMP results shown in Fig. 3.21 a) have been generated for 20 mixtures at 34 depths, i.e. 680 MMP calculations for this figure. This is a typical number in most of the figures in this section. To determine the MMP for 680 fluid systems with slimtube simulation would be computationally very time consuming. In this case it would require approximately:

> 680 fluid systems at minimum 7 pressures and at least 3 different grid runs for each pressure, giving 14280 slimtube simulation runs

Each run would involve manual interpretation and extrapolation for the 680 different cases only to generate this *one* figure. We find the fully automated C/V algorithm to be 20-100 times faster than a slimtube simulation on computers with comparable capabilities in computational speed and efficiency. This demonstrates the strength in the C/V algorithm as a tool for MMP determinations for a large number of different fluid systems.

3.4.4 MMP with Depth in a VOA Reservoir with Undersaturated GOC

This subsection extends the discussion of the volatile oil reservoir presented in Section 3.4.1. The reservoir does not have a saturated GOC. The compositional variations are continuous over the entire reservoir thickness, and consequently so are also the MMP variations with depth.

Fig. 3.23 shows MMP(h) calculations for 20 different mixtures of the dry gas A and the rich gas B, using the C/V algorithm. As seen from the figure, the predicted MMP(h) has many similarities to the NCO example in Section 3.4.3 when considering behaviour away from the GOC.

However, the calculated gradient in MMP(h) close to the undersaturated GOC is smaller than the gradient in MMP(h) close to the saturated GOC in the NCO example. Analysing the compositional variation with depth in the two cases we find that this should be expected. Chapter 2 established that compositional gradients will be largest at the critical point. The *minimum distance* between the saturation pressure and the reservoir pressure at the GOC will be larger in the case of an undersaturated GOC than in a saturated one. This yields larger compositional gradients in the vicinity of a saturated GOC than at an undersaturated GOC. Consequently, the

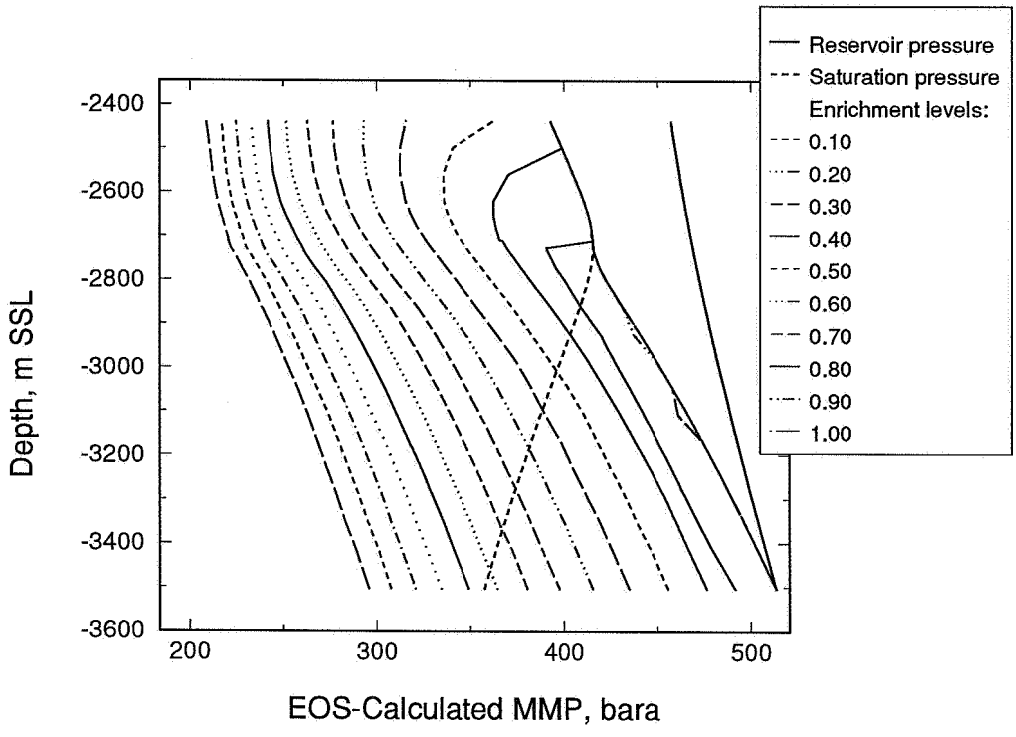

Fig. 3.23 Calculated C/V MMP(h) variations for a series of mixtures of gas A and gas B. Zick multicell algorithm with 100 cells.

calculated MMP(h) should show smaller gradients near the GOC in the VOA case than in the NCO case.

Notice also that continuing upwards from the GOC into the "gas-like" region, the MMP continues to decrease. The particular behaviour of MMP(h) in the gas region of this reservoir is addressed in Section 3.5.

This VOA reservoir is a special case, as all injection gas mixtures predict miscibility for practically the entire reservoir thickness. If similar reservoirs fluid systems exist with homogeneous geological properties, they could be very interesting targets for a miscible flooding process. In addition, reservoirs with an undersaturated GOC should also be considered as targets for *vertical* miscible flooding processes, as discussed in Section 3.7.3.

3.4.5 MME Variations for Different Reservoir Systems

The results presented in the four previous subsections can be used to manually determine MME as function of depth in different reservoir fluid systems (MME(h)). In this subsection we discuss this variation with depth. The following discussion has been limited to oil zones.

The determination method for MME(h), using MMP(h) results, was as follows:

1. For each depth, plot the calculated MMP for each enrichment level.

2. For each depth, find the MMP that is equal to the reservoir pressure. From the plot generated in step 1., determine the solvent enrichment needed to generate that pressure.

This method generates an MME variation with depth for the actual reservoir pressure profile, as demonstrated for the NCO reservoir in Fig. 3.24. This figure shows the same data as presented in Fig. 3.21 a) earlier, but now plotting MMP(E) for a number of depths in the oil zone instead of MMP(h). The crossover enrichment level, E*, is found to be approximately constant over the entire oil column, but near the GOC the value of E* increases. Notice that the general shape and behaviour of these MMP(E) curves are consistent with the conclusions drawn in Section 3.3.3.

The variation of the minimum enrichment level with depth for the SVO reservoir and the NCO reservoir was found with this method, using the *initial* reservoir pressure variation with depth.

In the SVO reservoir case, the slope of the initial reservoir pressure with depth and the slope of the MMP(h) curves, generates a slight *decrease* of MME with depth. We find the maximal difference in MME in the oil zone to be less than 0.05. Therefore, the MME variations with depth do not practically play an important role in this particular reservoir.

In the NCO case, there is a significant MME variation below the GOC. The MME varies from approximately 0.25 at the GOC to 0.42 at the bottom of the oil zone. The largest changes are found in the vicinity of the GOC. These differences represents a significant *increase* of MME with depth. Hence, economically it may be advantageous to perform a miscible gas injection in the upper part of the oil zone in this reservoir.

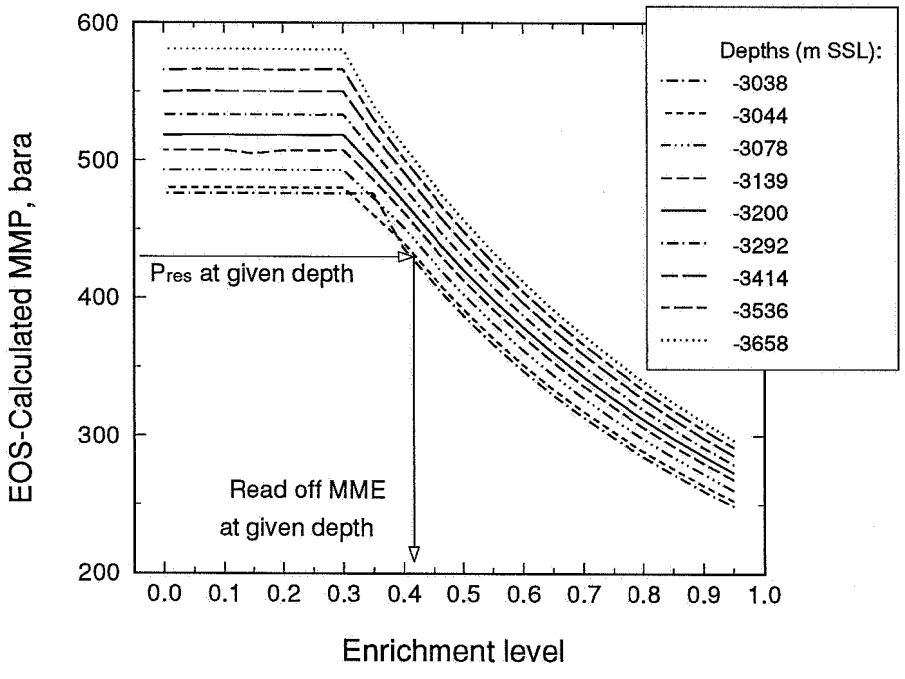

Fig. 3.24 C/V MMP as a function of enrichment level for a series of depths in the NCO oil zone. Zick multicell algorithm, 100 cells. At each depth the enrichment level that generates MMP equal to the reservoir pressure is found, determining the MME at each depth.

3.5 Miscibility in Gas Condensate Reservoirs

Minimum miscibility conditions in gas condensate reservoirs have traditionally been considered to exist only above the dewpoint pressure. Consequently, the majority of gas cycling projects are designed with the a priori assumption that miscibility can only be achieved by maintaining reservoir pressure above the dewpoint. Our results contradict this traditional view for enriched injection gases.

3.5.1 MMP with Depth in Gas Condensate Reservoirs

MMP variation with depth is a direct result of compositional variations with depth, if thermal gradients are neglected. Section 3.4 established that MMP increases monotonically with depth in oil reservoirs. In gas condensate reservoirs the VGD MMP is equal to the dewpoint pressure and consequently the VGD MMP will also increase monotonically with depth. We find that the MMP variation with depth is *not* a monotonic function with depth in gas condensate reservoirs if the C/V mechanism is present.

Fig. 3.25 shows calculated results for C/V MMP(h) in the gas cap of the NCO reservoir previously presented in Section 3.4.3. A series of mixtures with gas A and B were used in the calculations. Fig. 3.26 plots the same data as MMP variation with enrichment level, MMP(E), for selected depths in the gas cap.

The MMP(E) plot demonstrates the main behaviour of MMP variations in gas condensate reservoirs. Going upwards in the gas condensate reservoir the reservoir gas becomes leaner, and hence a richer injection gas is needed to generate a combined condensing vaporizing mechanism. Thus, the crossover enrichment level, E*, increases upwards in the gas zone, as shown in Fig. 3.26. This means that the C/V-collapse into the VGD mechanism will take place at richer and richer enrichment levels of the injection gas when going upwards in the gas zone. This behaviour is different from the E*(h) behaviour in the NCO *oil* zone discussed in Section 3.4.4, where the E* was found to be approximately constant with depth.

This means that a rich gas condensate reservoir system will have a lower E* than a leaner reservoir gas, for a given injection gas and solvent. The leaner reservoir gas will have a lower E* than a dry reservoir gas.

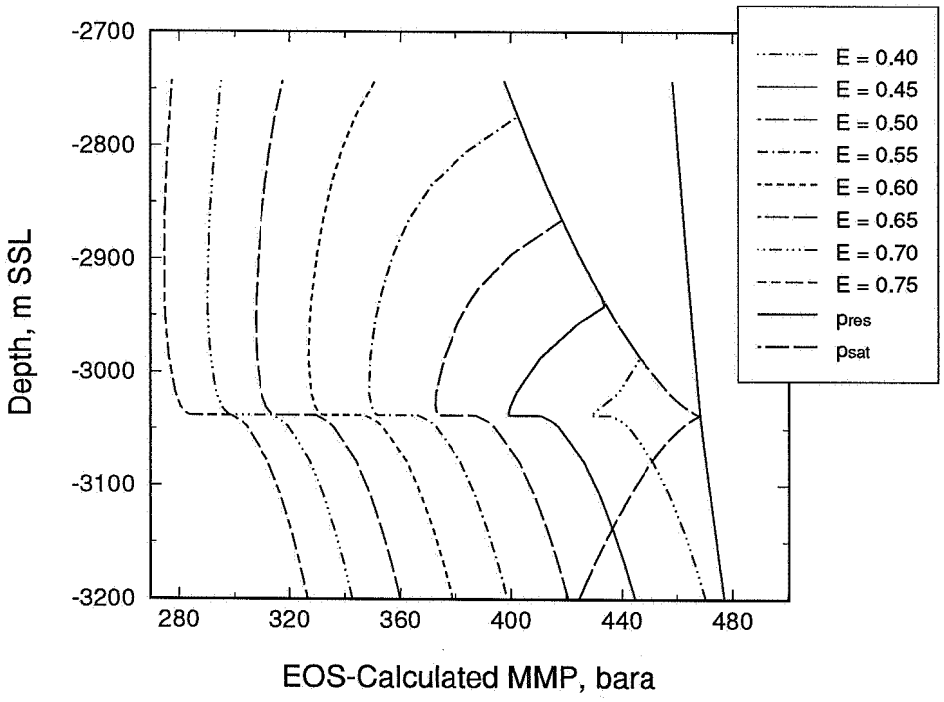

Fig. 3.25 C/V MMP(h) variations in the gas cap of the NCO reservoir.

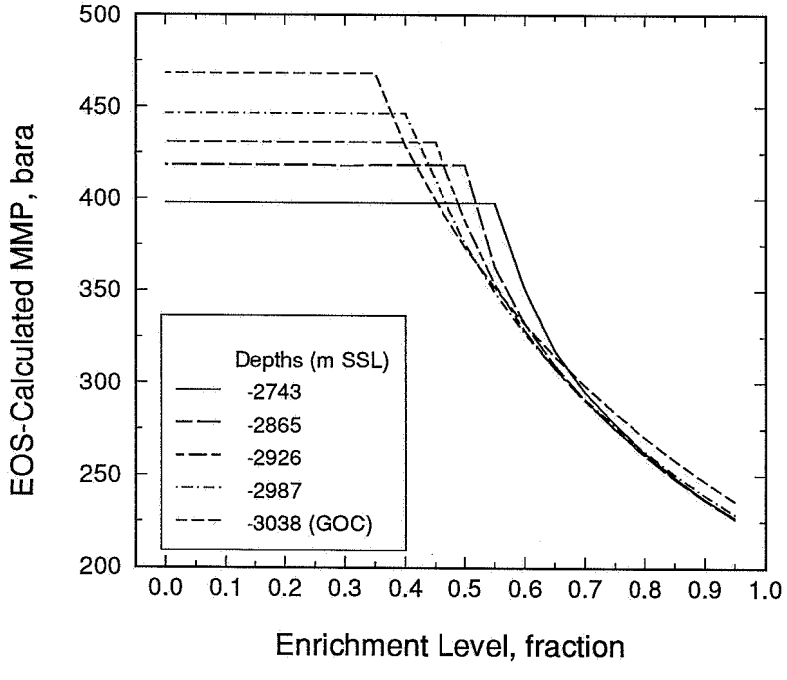

Fig. 3.26 MMP variation with enrichment level at selected depths in Fig. 3.25.

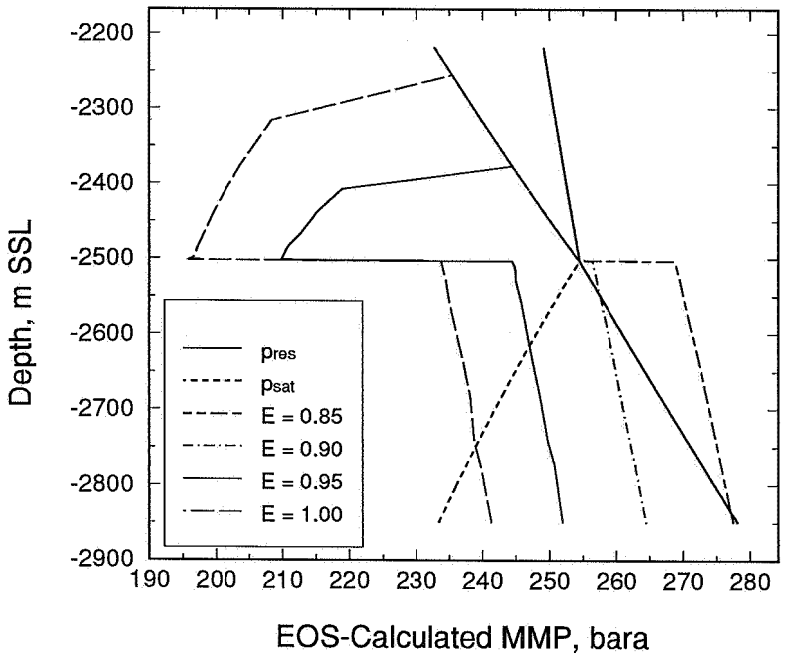

Fig. 3.27 MMP(h) variations in the SVO reservoir, injecting strongly enriched gases. (gas A enriched with gas B).

This is shown in Fig. 3.27, where C/V MMP(h) in the lean gas zone of the SVO reservoir is plotted. Notice that the same injection gases were used in the NCO and the SVO study. Above the GOC, only the injection gas mixtures with enrichment level above 0.9 give a C/V MMP different from the VGD MMP. This should be compared with the E* of 0.35-0.60 in the rich gas condensate example above. Proceeding upwards from the GOC in the SVO reservoir, the reservoir gas becomes leaner. Above approximately -2255 m SSL, the E* reaches 1.0, which means that none of the available injection gas alternatives will give an MMP below the dewpoint pressure.

One general observation drawn from the examples above is that there exist two possibilities for C/V collapse into the VGD mechanism; a) if the *injection gas* is so lean that no condensing region will be generated, or b) if the *reservoir fluid* is so lean that the condensing region ahead of the front will not be present for the particular injection gas of interest.

The discussion above suggests that MMP(h) in gas zones will have minimum values at some depth for each injection gas case, and that the C/V MMP(h) will eventually collapse into the VGD mechanism upwards in the gas zone. This is actually observed in Fig. 3.25 where for E larger than E* it is shown that the C/V MMP(h) has local minimum values for each injection gas. Due to the compositional variation with depth, the reservoir gas will be richest at the GOC, where in this case the gas has a favourable component distribution in intermediate components. As shown in the Fig. 3.25, the minimum in C/V MMP will be at the GOC for lean injection gases. For rich injection gases, we find the MMP variation in this reservoir to be approximately constant with depth over large depth intervals. However, the discussion in this section suggests that the general E*(h) behaviour due to the compositional gradients will cause the C/V MMP to eventually collapse into the VGD MMP, when proceeding significantly higher up in the reservoir.

We conclude that the C/V algorithm can yield values for MMP that are significantly lower than the dewpoint pressure. According to these results the MMP is consequently *not* limited downwards by the dewpoint pressure if an enriched gas is injected into a gas condensate system.

3.5.2 Grid Effect in Gas Condensate MMP Determination

To disregard or confirm the C/V results for MMP in gas condensates, a series of slimtube simulations were performed. This subsection presents typical slimtube results and gives a discussion of grid effect. We restrict the discussion to the VOA case at a selected depth of -2500 mSSL, i.e. a lean gas condensate. Slimtube MMP determination for three different injection gases are provided; with (a) gas C as injection gas, (b) E=0.55 gas A enriched with gas B and (c) E=0.47 gas A enriched with gas B. Thus, the only difference between the three cases is the injection gas, yielding MMP's that increase as the injection gas becomes leaner. MMP results for these cases are given in Table 3.8. As seen from the table, the C/V algorithm predictions and the slimtube results match each other within extrapolation accuracy. The slimtube results are discussed below.

Fig. 3.28 shows slimtube determination of MMP in case (a). A series of pressures were run with this rich gas injected, starting close to the reservoir pressure and reducing the pressure stepwise below the dewpoint pressure. As shown in the figure, the dispersion free recovery factor was found to equal 1.0 for pressures significantly below the dewpoint pressure. This confirmed that MMP below dewpoint is possible

Table 3.8 MMP determination in gas condensate system with different methods for case (a), (b) and (c).

Injection gas	MMP (bara)		
	VGD algorithm	C/V algorithm	Slimtube simulation+
Gas C	399	218	213 ± 7
E=0.55, Gas A, Gas B	399	305	300 ± 15
E=0.47, Gas A, Gas B	399	355	356 ± 25

Notes:
+: Extrapolation accurancy determined with method 3-5, (Section 3.2.4)

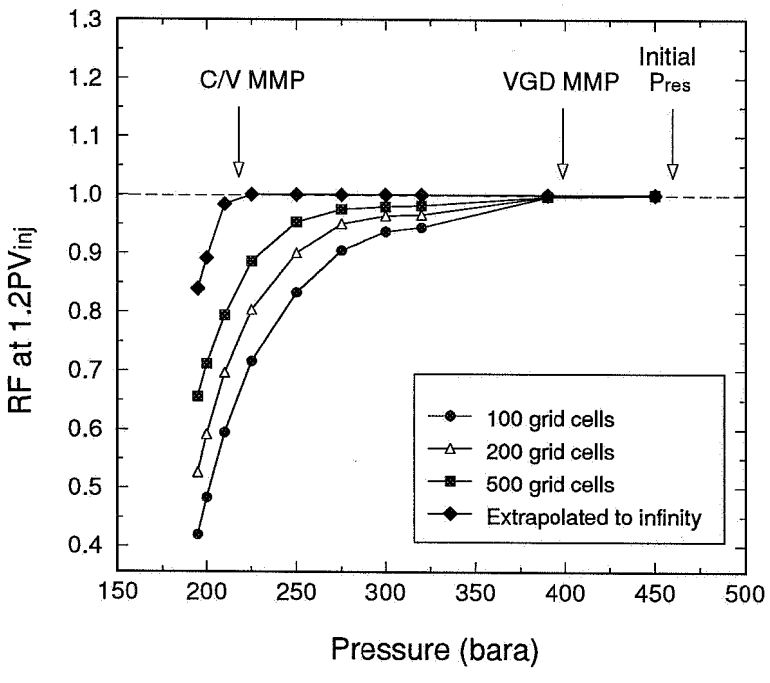

Fig. 3.28 Slimtube MMP determination for a gas condensate system (case (a)).

to achieve in gas condensate systems with rich injection gases.

Grid effect in gas condensate reservoirs was found to be large. Figs. 3.29 and 3.30 show extrapolation and MMP determination for slimtube results in case (b). The slimtube simulations were run with up to 3000 grid cells. As seen from Fig. 3.29 there exist a large change in recovery factor for all pressures considered when the cell number is increased. Thus, in this example a slimtube run with too few grids can easily lead to underpredictions of the recovery factor and consequently significant overprediciton of MMP. The results also demonstrate that straight line extrapolation to determine RF_∞ is not sufficient for correct extrapolation.

We find the grid effect to be pronounced in systems consisting of lean injection gases and lean gas condensates yielding systems with E slightly higher than E*. At these conditions the MMP(E) variation will be large, as discussed previously. Also, the condensing edge of the miscible front will be small. If the length of the condensing region is comparable with the size of the grid block the effect may be lost in the simulations and only the vaporizing effect will be predicted, as suggested by Zick (1997). Consequently, it is particularly important to do grid refinement in such situations. Due to the small liquid dropout volumes in gas condensate systems at pressures just below the dew point pressure, extreme grid refinement is needed to capture the condensing effect in this region.

Case (c) represents an example with large grid sensitivity. In this particular case the condensing region is not captured in the lowest-grid cells simulations. As seen in Fig. 3.31 the net result is almost flat RF curves in the extrapolation to infinity, going up to 3000 grids. Consider the RF curves for p=350 bara and 370 bara in this figure.

The grid effect appears to be small, but is actually relatively large and is only captured using additional grid blocks.

This is seen when doing additional runs with 5000 grid blocks at the selected pressures. For p=350 bara the recovery factor increases significantly, lowers the MMP, and generates an MMP close to the C/V algorithm prediction, as seen in Fig. 3.32. For p=370 bara, i.e. above the apparent MMP, the RF is not increasing significantly at the 5000 grid simulations. This can be caused by the lower liquid dropout volume in the latter case. Fig. 3.33 shows snapshots of the two slimtube simulations at 350 and 370 bara. Notice that the minimum density difference between gas and oil is smaller at 350 than 370 bara. We interpret this as a grid effect, and not a true physical effect.

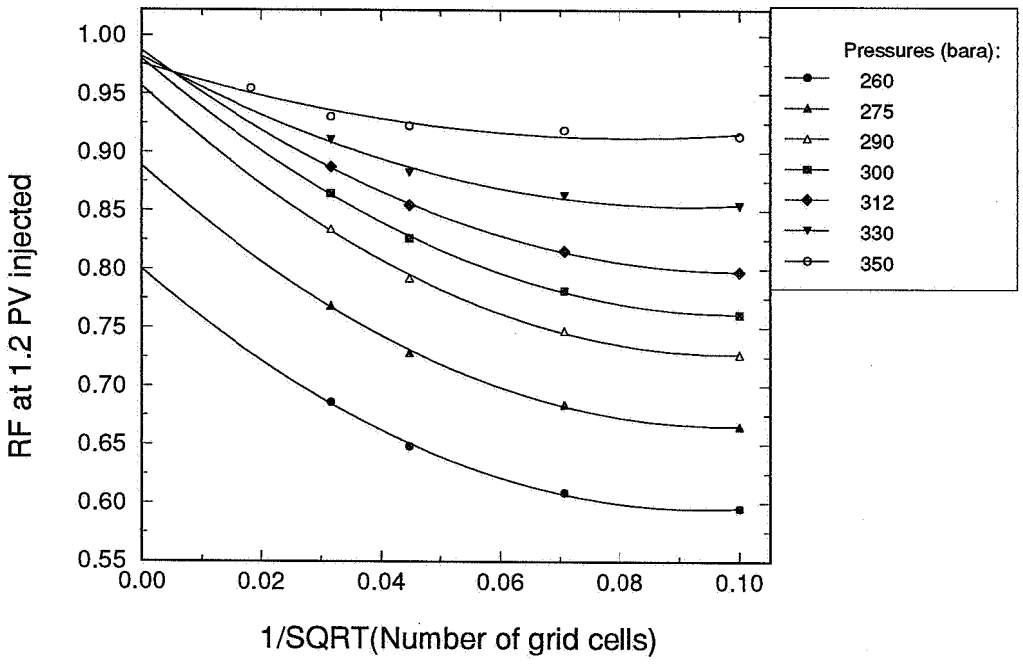

Fig. 3.29 Elimination of numerical dispersion in slimtube simulations of case (b).

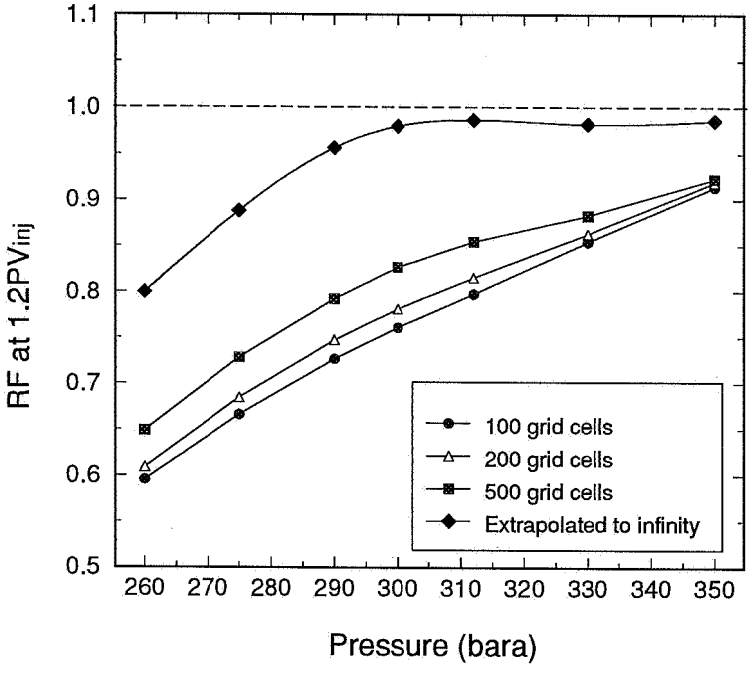

Fig. 3.30 Slimtube MMP determination in case (b). The results in Fig. 3.29 are used to determine the dispersion-free MMP for the gas condensate system.

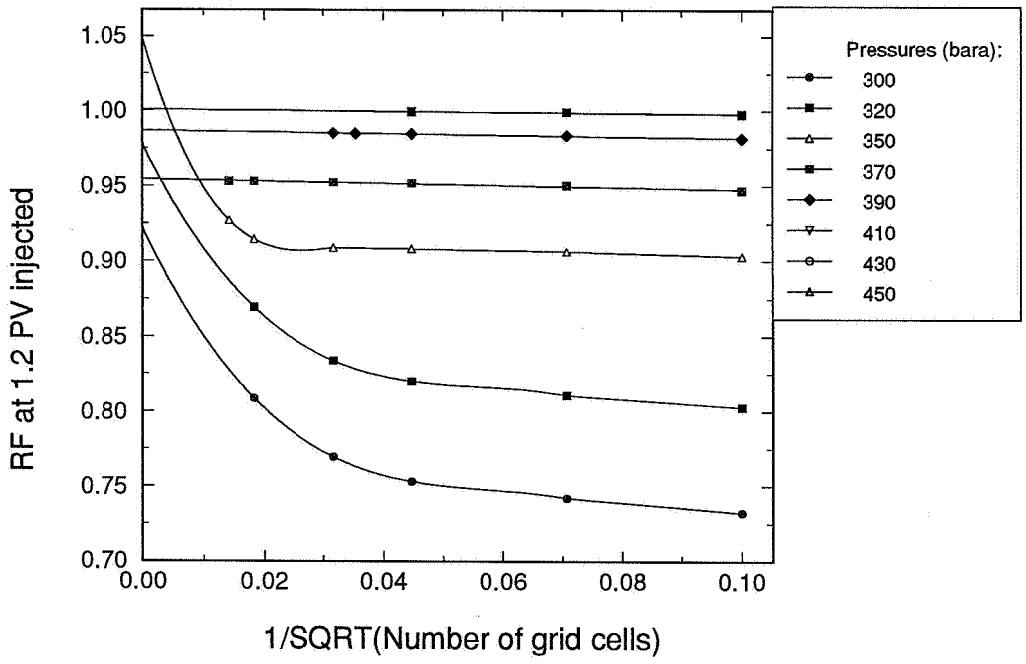

Fig. 3.31 Elimination of numerical dispersion, case (c) slimtube simulation results.

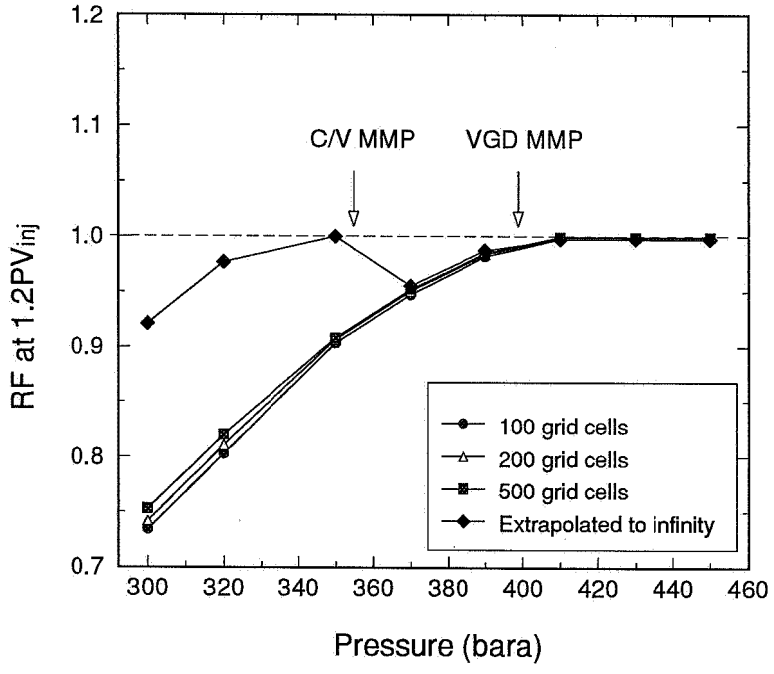

Fig. 3.32 Slimtube MMP determination, case (c), based on the results in Fig. 3.31.

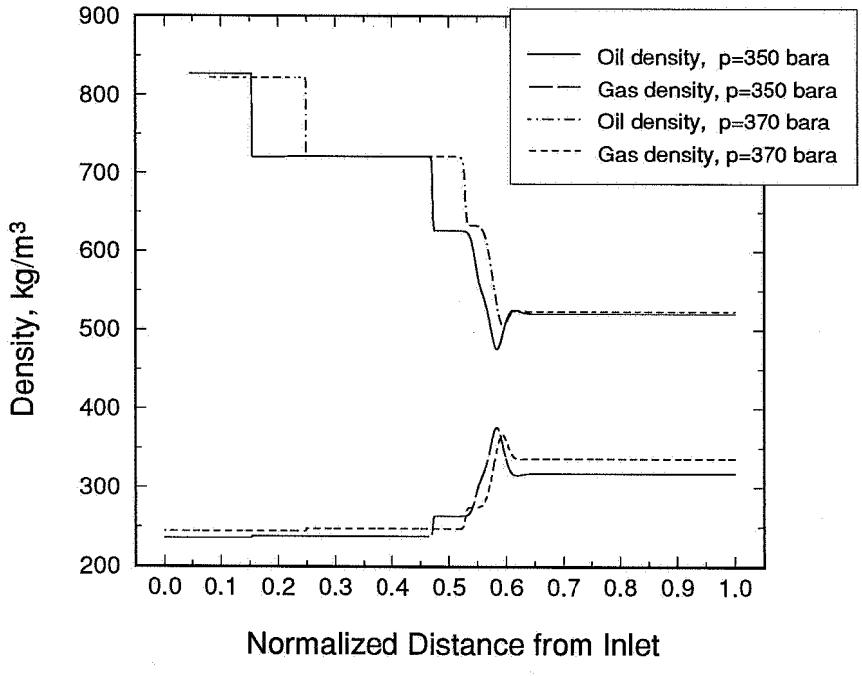

Fig. 3.33 "Snapshots" of slimtube simulations of case (c) at two different pressures. 0.6 PV gas injected. 5000 grids used in the simulations.

To further investigate the grid effect in case (c) a slimtube simulation initialized with 100 percent oil was performed. The oil composition was taken from a flash of the gas condensate system considered at pressure equal to the C/V MMP. The results are shown in Fig. 3.34. Note that the grid effect in this case is much smaller than in the former case, and that the predicted MMP=355±5 bara matches the C/V MMP. These observations can be drawn from this particular simulation; 1) the increase in condensate volume decreased the grid effect, and 2) the oil phase properties give approximately the same MMP as the total system MMP.

The C/V algorithm has a special unpublished treatment of gas condensate reservoirs to minimize the grid effect. We find that for gas condensate systems there is a significant grid effect in this algorithm also, but occuring at lower number of grids than typical slimtube results. Fig. 3.35 shows MMP(h) over the whole VOA reservoir thickness predicted with the C/V algorithm for E=0.47. 25, 50, 100, 200 and 300 cells were used in the calculations. It is seen that the grid effect is larger in the gas

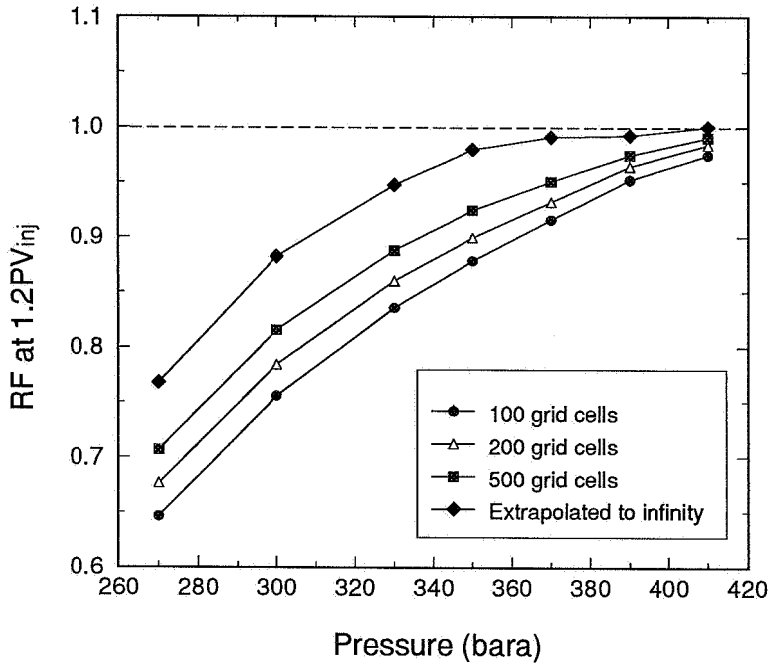

Fig. 3.34 Slimtube simulation initialized with 100 percent oil, case (c).

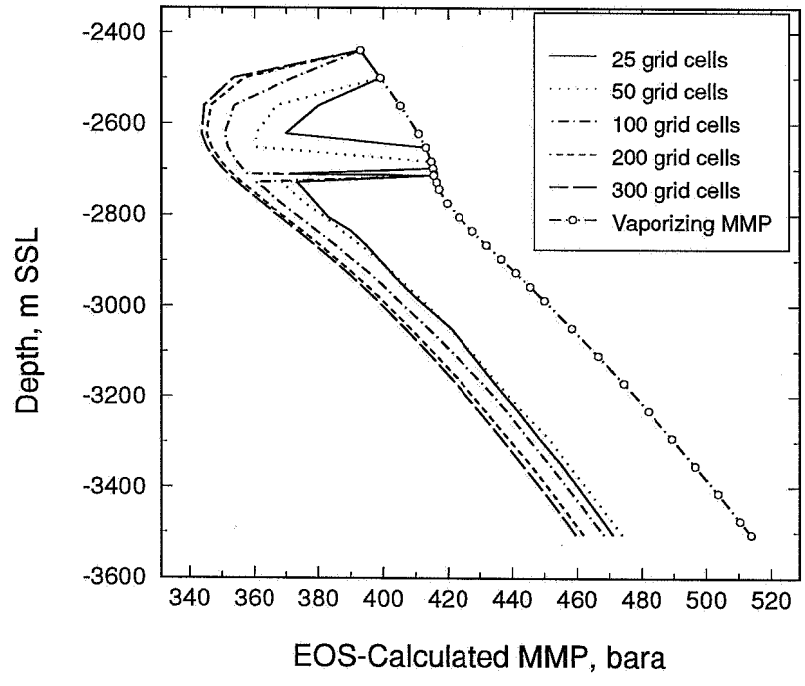

Fig. 3.35 Grid cell sensitivity test for the Zick multicell algorithm. E=0.47 gas injected in the VOA reservoir. Isothermal GCE calculations.

zone than in the oil. Particularly large grid effect is seen in the vicinity of the undersaturated GOC, and in the upper parts of the gas zone. For too few cells, the MMP(h) is easily overpredicted, equal the VGD mechanism. Note also that the predictions converge towards a consistent solution when increasing the cell numbers to 200-300 cells. This suggests that the key physical mechanism should be covered if the number of grids is high enough.

The discussion above demonstrated that grid effect can be large in gas condensate systems. In full field scale compositional reservoir simulations, a limited number of grids are usually used, and this may be a problem. If only a small number of grids are used, the MMP can be highly overpredicted. This can lead to the conclusion that gas cycling below dewpoint pressure will not develop miscibility, although there could be a possibility of the opposite.

Liquid Buildup at the Miscible Front

Simulations of miscible gas injection in 1D gas condensate systems show one interesting behaviour; namely liquid buildup at the miscible front. Fig. 3.36 shows slimtube profiles for a 500 grid simulation of case (a). The figure demonstrates liquid buildup at the miscible front, yielding a local high oil saturation region propagating through the system at the miscible front. The oil saturation ahead of the miscible front is unchanged, and the initial free equilibrium gas is displaced ahead of the front. This lead to a producing GOR that is constant in the simulations until approximately one pore volume has been injected. When the oil bank reaches the outlet of the slimtube, the producing GOR drops rapidly until the oil bank has left the slimtube, and the GOR increases rapidly.

Injecting a leaner gas at the same depth it is found that the buildup of an oil bank is smaller. Fig. 3.37 shows a snapshot of 0.6 PV gas injected for case (b). Notice that the buildup of the local high oil saturation takes place at the *condensing region* of the miscible front.

Fig. 3.38 shows the change in the liquid buildup predictions for different number of grid cells in case (c). It is seen how the bank is sharpened for increased number of cells, and how the local oil saturation at the miscible front is increasing when larger number of cells are used. Large compositional variations are thus taking place over small widths, and this demonstrates the need for large grid refinement in such systems.

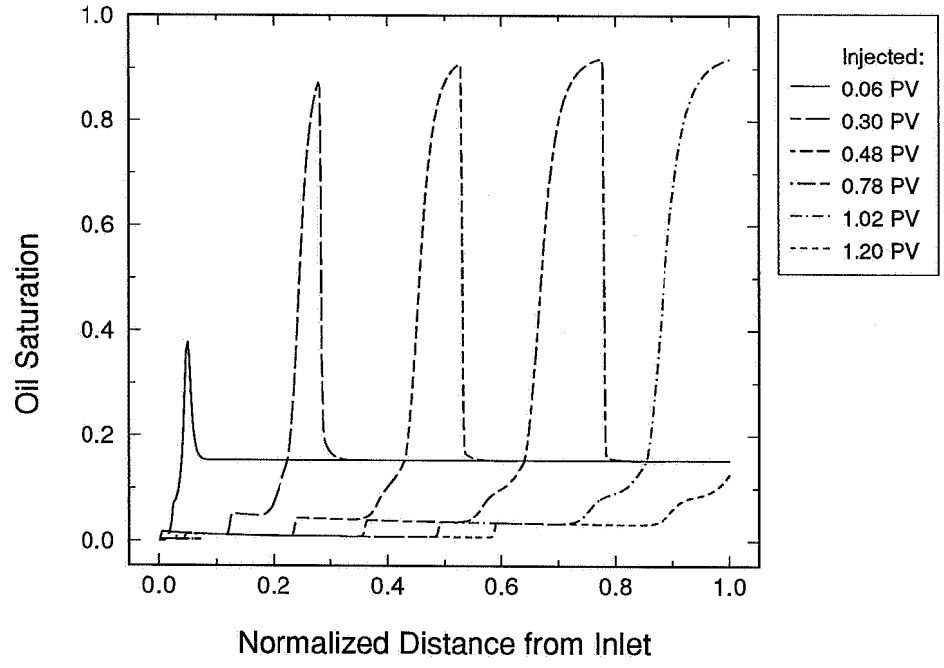

Fig. 3.36 "Snapshots" of oil saturation in a 500 grid slimtube simulation at p = 220 bara, case(a).

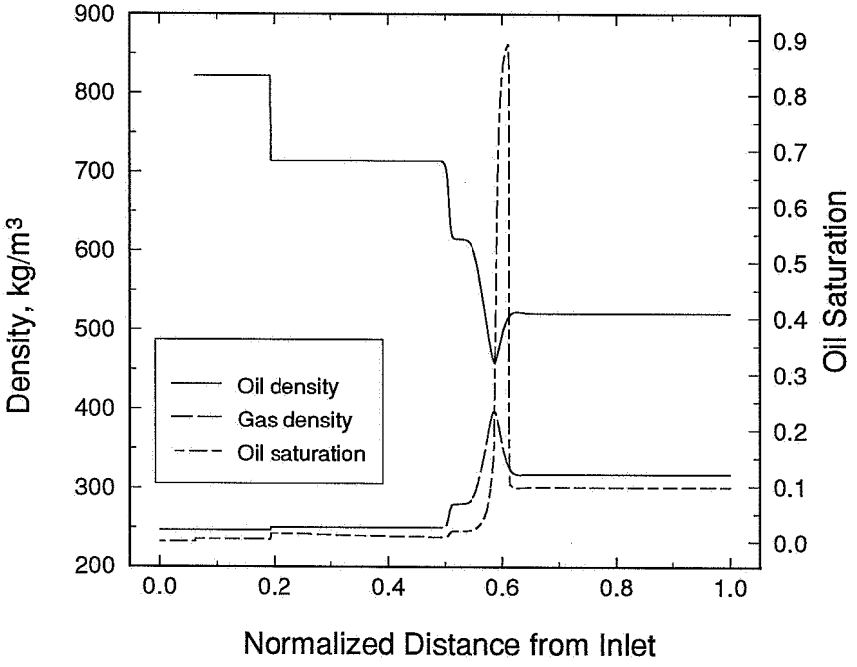

Fig. 3.37 "Snapshot" (0.6 PV) of densities and oil saturation in slimtube simulations of case (b) at p = 350 bara. 3000 grids used in the simulations.

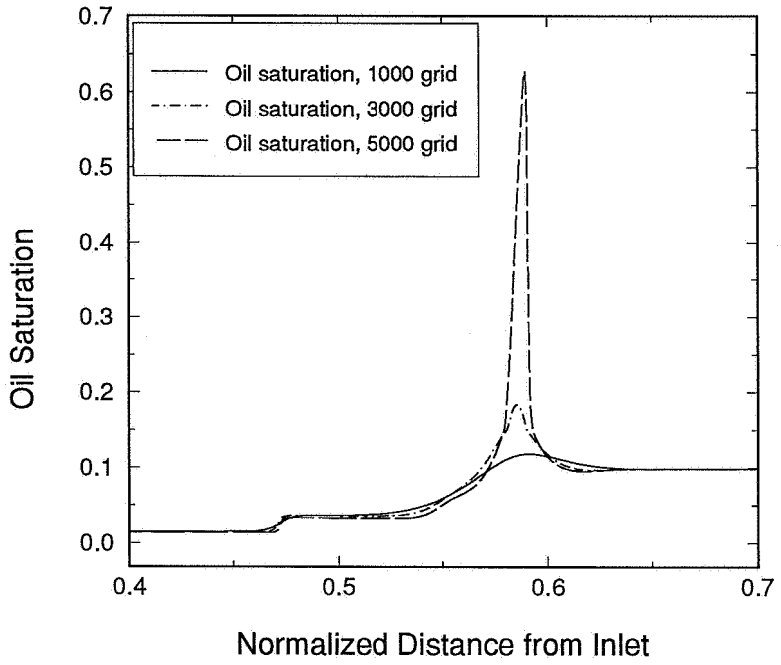

Fig. 3.38 "Snapshots" of oil saturation for different number of grids applied in slimtube simulations of case (c). p = 350 bara.

This behaviour is different from an ordinary oil-gas system, and should be taken into consideration. The effect should be tested in initially two phase slimtube experiments, to investigate if this is a general physical behaviour in two-phase gas condensate systems.

3.5.3 Miscibility in Depleted Gas Condensate Reservoirs

Because overall reservoir composition can change considerably when a gas condensate reservoirs undergoes depletion, CVD simulations were used to generate compositions to quantify the effect on MMP. A CVD experiment represents a simplified model for depletion of a gas condensate reservoir, as discussed by Whitson and Torp (1983).

The NCO reservoir gas cap (Fig. 3.25) was investigated at three different depths. At

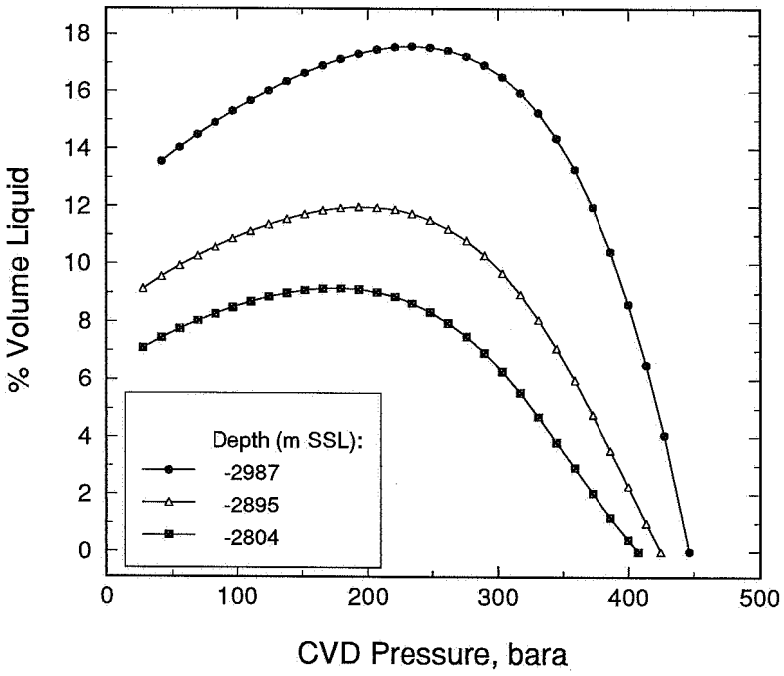

Fig. 3.39 Percent volume liquid in CVD calculations, for compositions at three different depths above the gas-oil contact in the NCO reservoir.

each depth a CVD experiment was simulated with a series of pressures, and overall cell composition at each pressure determined. For each CVD pressure a C/V MMP calculation was made for a series of injection gases, initialized with the overall CVD cell composition as reservoir fluid.

Fig. 3.39 shows percent liquid dropout at three different depths in gas condensate CVD calculations. Note the large difference in liquid dropout between the gas condensate sample 50 m above the saturated GOC, and the liquid dropout for the lean gas approximately 180 m higher in the reservoir. Figs. 3.40 a), b), and c) give the calculated MMPs for the gas condensate case, at -2987 mSSL, -2895 mSSL and -2804 mSSL, respectively. As seen from the figures the MMP does not increase during depletion for rich gases when the C/V mechanism exists.

These results show that the system C/V MMP below the dewpoint is not affected significantly by changes in the overall composition. The reason is probably that the

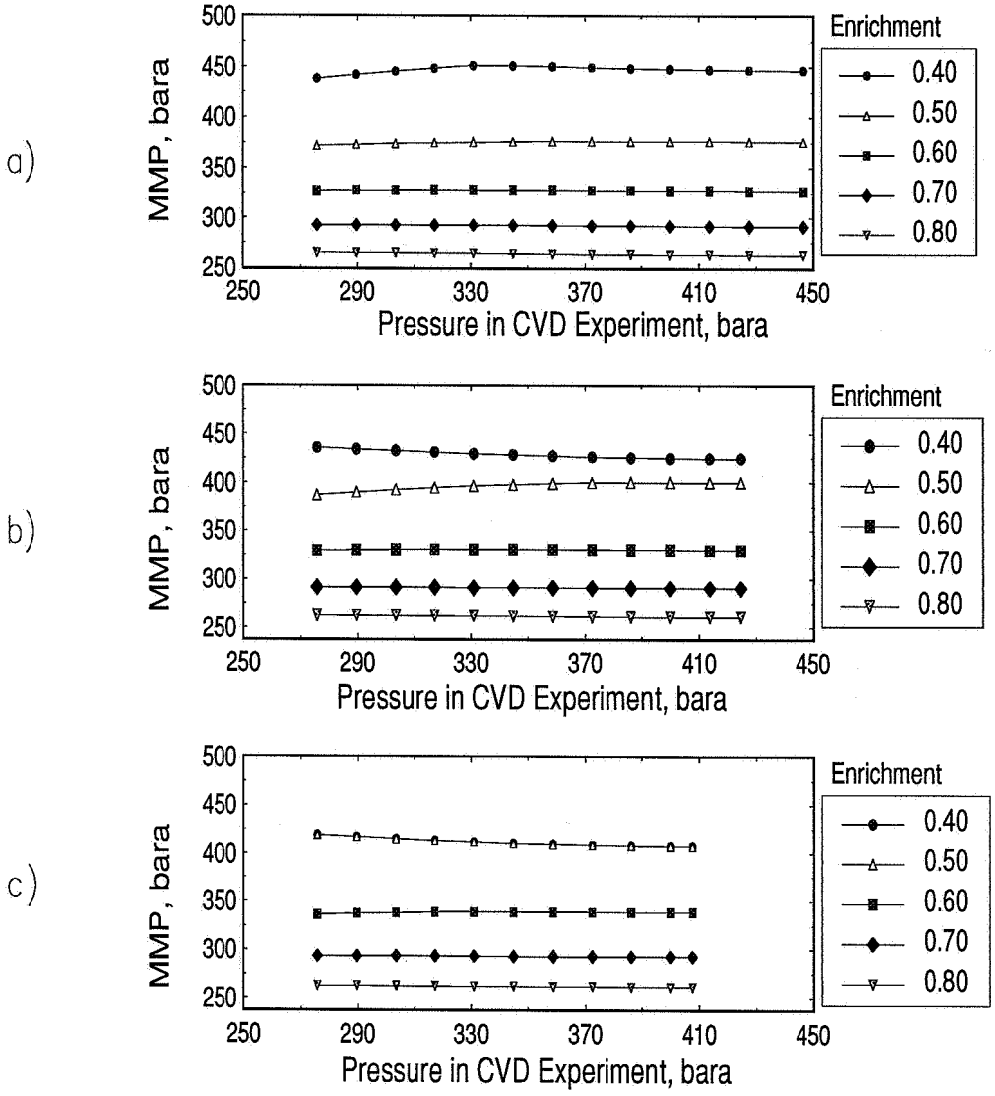

Fig. 3.40 C/V MMP (300 cells) as a function of pressure in the CVD experiments. The composition at each CVD pressure in Fig. 3.39 was used to initialize an MMP calculation for a number of enriched separator gases (Gas A enriched with gas B). Compositions at a) -2987 mSSL, b) -2895 mSSL, and c) -2804 mSSL.

"stock tank oil" (STO) composition does not change radically during the process, as the STO properties have a strong influence on the C/V MMP.

3.5.4 Consequences for Gas Cycling Processes

Candidates for gas cycling are typically medium to rich gas condensates, as the potential for significant additional STO recovery exists for this class of reservoir fluids. To avoid large pressure compression requirements a first stage separator gas can often be a realistic candidate for injection.

The C/V and slimtube MMP calculations presented in the previous sections show that MMP's can be significantly lower than the dewpoint pressure in gas condensate reservoirs, if the injection gas is significantly enriched. This is in contrast to the traditional way of thinking, where gas cycling processes are assumed to have an MMP equal to the dewpoint.

If the true MMP is significantly lower than the dewpoint pressure this may have a significant impact on the design of gas cycling projects; pressure maintenance above the dewpoint pressure is not necessary yet miscible recoveries can still be obtained. This would result in (1) lower injection pressure requirements, and (2) make-up gas requirements reduced or eliminated.

To our knowledge, miscibility conditions below the dewpoint for gas condensates have not been reported previously in the literature. Before any general conclusions can be drawn about the consequences of our calculations, we recommend that slimtube measurements on gas condensates be performed. Also, more work is needed on upscaling the results to reservoir scale, to determine the link between microscopic and macroscopic effects. In summary, our calculations show a *potential* for improved economics in gas cycling projects using an enriched injection gas.

3.6 Temperature Effect on Miscibility

Previous sections have demonstrated the effect of pressure, injection gas composition and reservoir fluid composition on miscibility processes while holding the temperature constant. In this section we analyse the temperature effect on miscibility. The temperature effect on MMP(E) and MMP(h) is investigated for different injection gases and reservoir fluids. Finally, MMP(h) for compositional gradients calculated with thermal diffusion models has been studied and compared to MMP(h) resulting from the isothermal GCE method.

In Chapter 2 we discussed implementation of thermal diffusion in multicomponent compositional gradient calculations. It was emphasised that there is a lack of valid experiments to confirm the models for thermal diffusion. Consequently, the predictions of Soret-effect is uncertain. Still, it is interesting to quantify the effect of thermal diffusion and thermal gradients on MMP(h) and MMP(E) calculations.

Natural geothermal gradients exist in all petroleum reservoirs, leading to a vertical temperature variation which can be significant in reservoirs with large vertical extent. In addition, cold water injection can generate a cooled region near the injection well, which potentially can have an effect on the miscibility condition. These points motivates the following discussion.

3.6.1 Temperature Effect on MMP with Injection Gas Enrichment

Fig. 3.41 a) shows MMP calculations for the SVO case presented in Section 3.4.2. Reservoir temperature of 95.0°C and five lower temperatures were applied in the calculations.

For dry gases a slight increase in the VGD MMP is found at decreasing temperature, as seen in Fig. 3.41 a). For richer injection gases the reduction in temperature results in a *decreased* MMP compared to the MMP at reservoir temperature. This effect increases with enrichment level of the injection gas. Fig. 3.41 b) shows the C/V MMPs and temperature effect as percent deviation from MMP at reservoir temperature.

The temperature effect was verified by a number of slimtube simulations. Injection

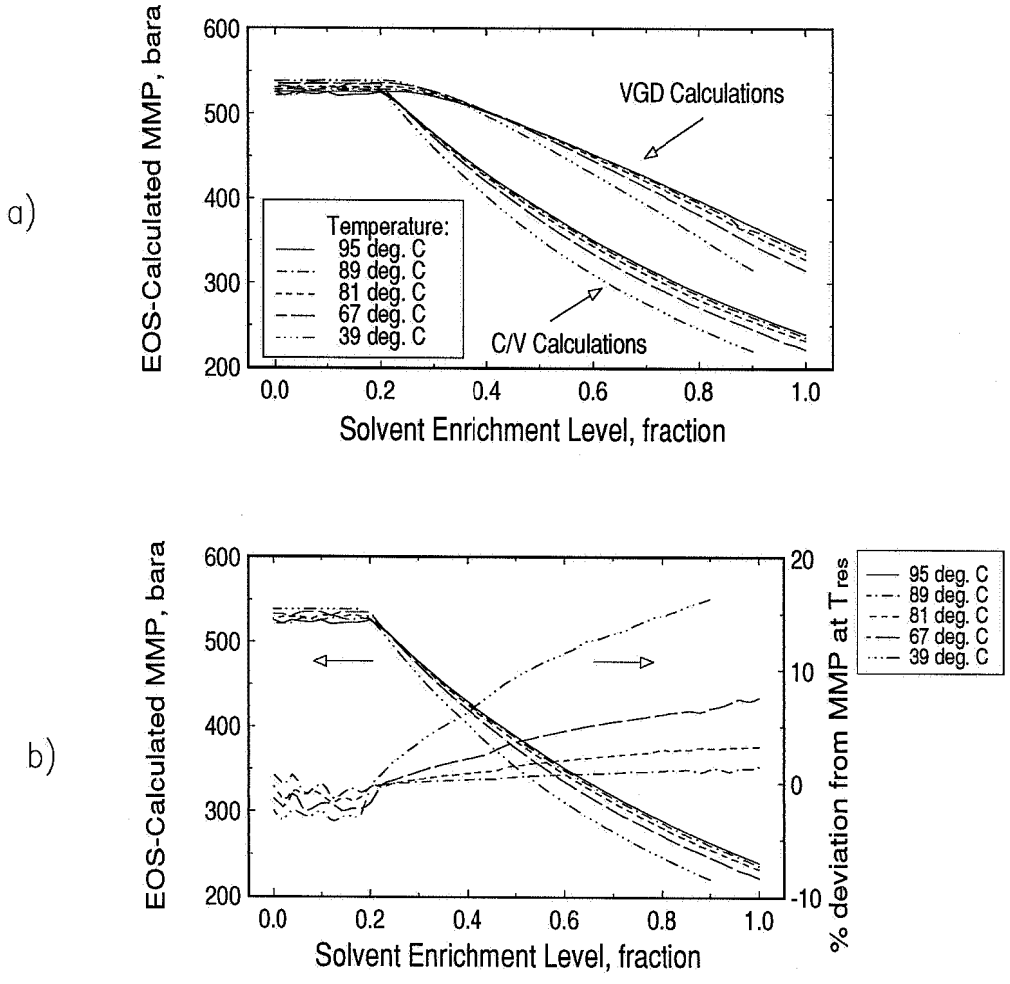

Fig. 3.41 Temperature effect on VGD and C/V MMP(E) variations. 300 cells used in the Zick multicell algorithm. Separator gas A enriched with gas B.

gas was gas A enriched with gas B with E=0.4. Figs. 3.42 a) and b) show density and saturations for two slimtube runs with slightly volatile oil at reference temperature and at 39.4 °C. The main effect of a decrease in temperature is similar to an increase in pressure. A reduction in temperature here leads to a shorter extent of the condensing region and the vaporizing region, with the net effect of a more piston-like displacement. For richer injection gases we find this effect to be more pronounced, as seen in Fig. 3.41 b). The density difference between the oil and gas decreases, which generates higher recovery. Consequently, the MMP for this system *decreases* when temperature decrease, as shown in Fig. 3.42.

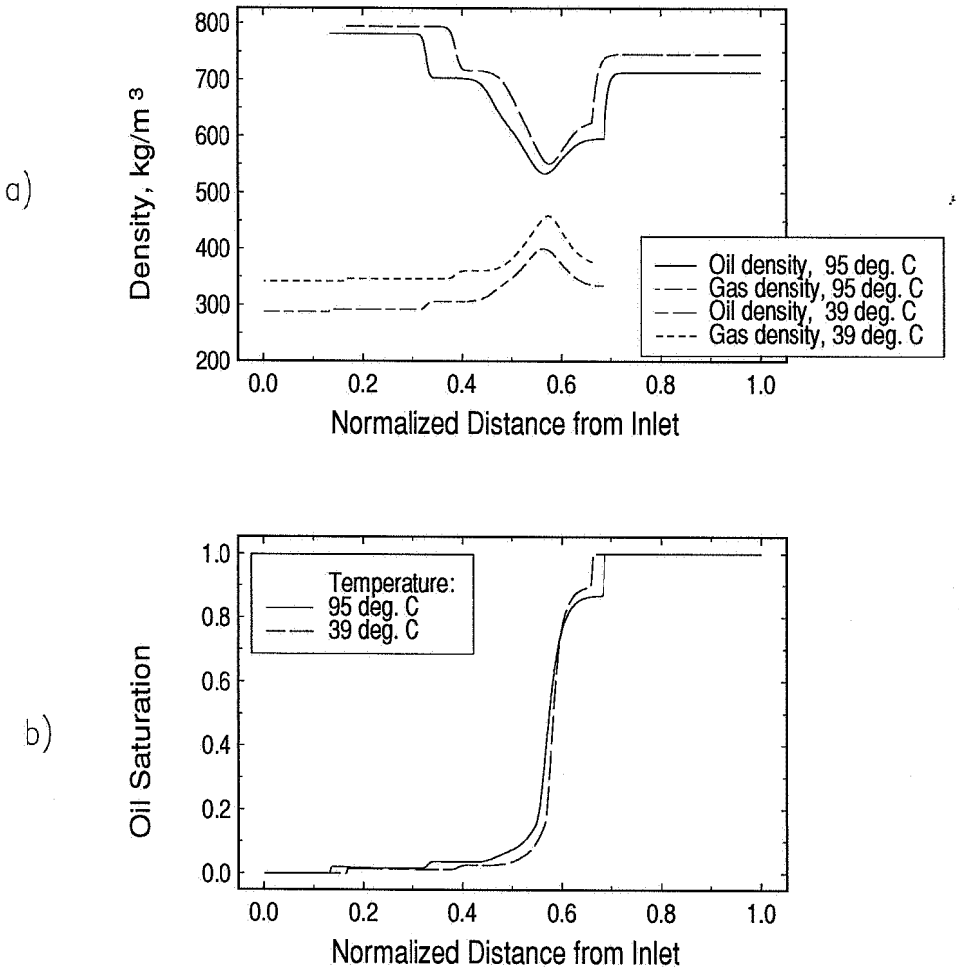

Fig. 3.42 "Snapshot" (0.6 PV) in slimtube simulations of a) densities, and b) oil saturations, at two different temperatures. 1000 grids used in the simulations. E=0.4 gas A enriched with gas B.

A similar behaviour was found in a gas condensate. Fig. 3.43 shows MMP versus enrichment level calculated with the Zick multicell algorithm. The gas condensate composition was taken from isothermal GCE calculations, approximately 45 m above the gas-oil contact in the NCO reservoir. Injection gases were mixtures of gas A and gas B. An increase in temperature generates a lower dewpoint pressure and consequently a lower VGD MMP. Notice that the value of E* is increased significantly when the temperature is increased with 55 °C in this example. For $E > E^*$ the C/V MMP increases when temperature is increased, which is consistent with the results in the slightly volatile oil example above.

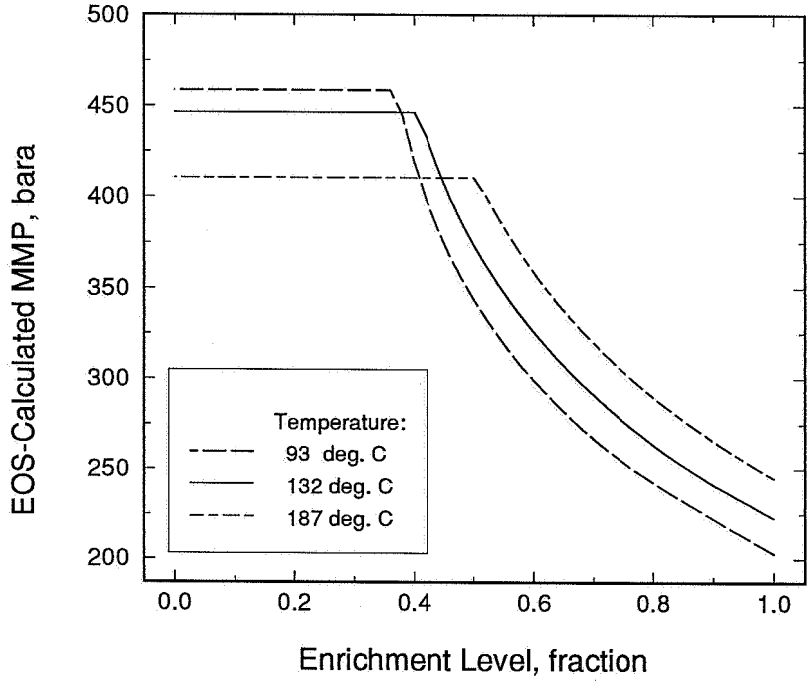

Fig. 3.43 C/V MMP(E) variations for a gas condensate sample. 300 cells applied in the Zick multicell algorithm.

3.6.2 Effect of "Passive" Thermal Diffusion on MMP with Depth

Including the natural geothermal gradient in a petroleum reservoir gives a lower temperature at the top of the reservoir than at the bottom. For a constant reservoir fluid composition and rich injection gas, the MMP will decrease upwards. If compositional gradients exist this will also have influence on the MMP(h), as discussed earlier. MMP(h) will thus generally have a larger variation with a temperature gradient than without, for rich injection gases.

Fig. 3.44 a) shows the effect of including a "passive" thermal diffusion in compositional variations, and its effect on MMP(h) for rich injection gases in the SVO reservoir. The compositional variation with depth was generated neglecting thermal diffusion but including a thermal gradient. It is seen that MMP(h) variation increases in these cases. Fig. 3.44 b) demonstrates the effect when a dry gas is injected into the SVO reservoir. The inclusion of a temperature gradient in this case

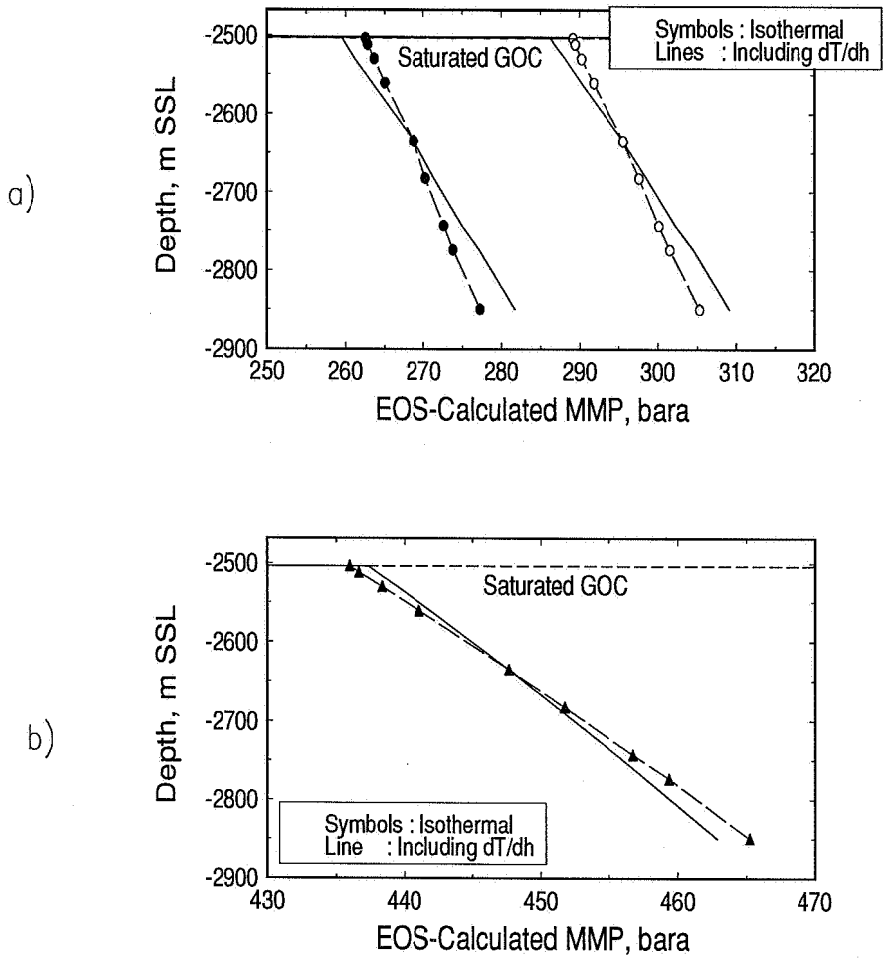

Fig. 3.44 Comparison between MMP(h) generated with isothermal GCE calculations and "passive" thermal diffusion in the SVO reservoir. a) two strongly enriched injection gases, b) a dry injection gas.

generates a slightly smaller MMP(h) variation than the isothermal MMP(h).

Fig. 3.45 shows MMP(h) variations in the VOA reservoir for two rich injection gases, with and without a temperature gradient in the calculations. Changes in MMP(h) are significant, and the trend is the same as for the rich gas SVO example.

To summarize, inclusion of a temperature gradient in the MMP(h) calculations, neglecting thermal diffusion, may change the miscibility conditions significantly provided that (1) the injection gas is rich *and* (2) the vertical extent of the reservoir is large.

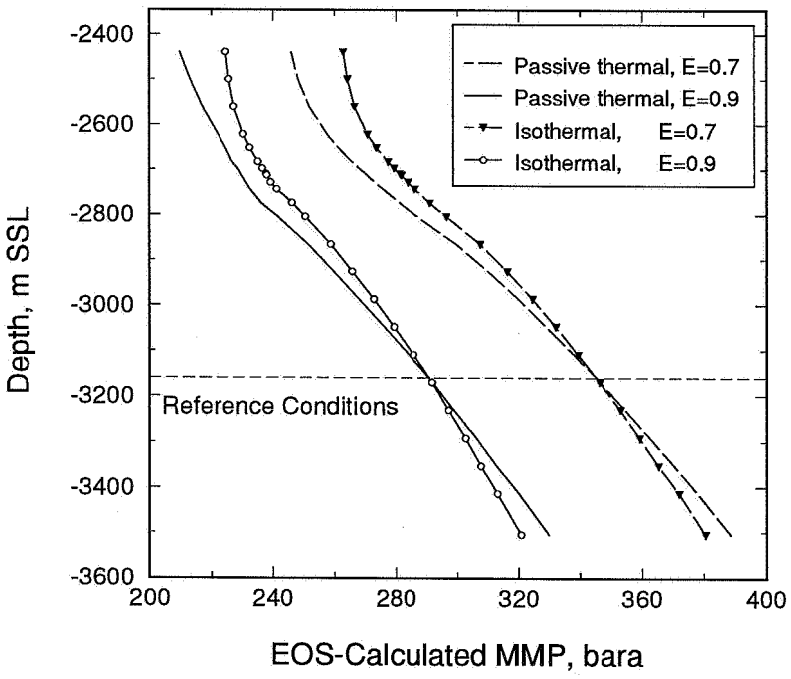

Fig. 3.45 Comparison between MMP(h) variations calculated with isothermal GCE and "passive" thermal diffusion. Injection gas A enriched with gas B.

3.6.3 Including Thermal Diffusion in MMP with Depth Calculations

Inclusion of thermal diffusion in compositional gradient calculations can change the results significantly, as discussed in Chapter 2. This will also have an influence on the miscibility calculations. The previous subsection demonstrated that a thermal gradient *alone* will affect MMP(h) calculations. In this subsection we investigate the effects of including thermal diffusion in MMP(h) calculations in the VOA reservoir.

Three cases have been used to generate the compositional variations with depth in the VOA reservoir; Haase's method, Kemper's method and Belery da Silva's model. The significance and results of applying thermal diffusion to gradient calculations has been discussed in detail in Chapter 2. Fig. 3.46 gives a typical result for MMP(h) in the VOA reservoir with a rich gas (E=0.7) injected. Implementation of thermal diffusion in this reservoir results in the following MMP(h) behaviour :

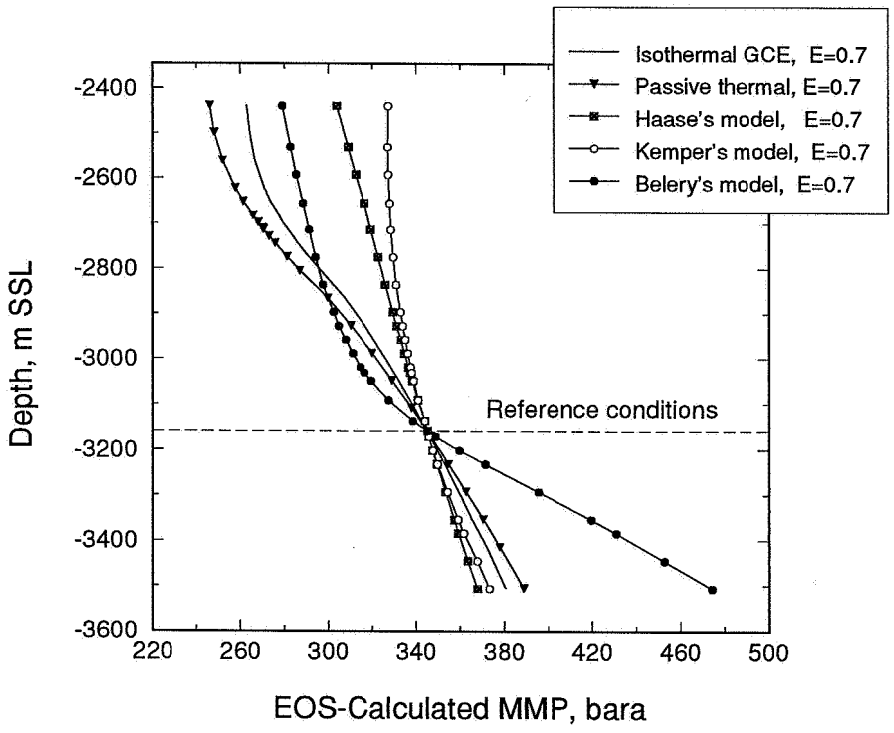

Fig. 3.46 C/V MMP(h) variations in the VOA reservoir, different thermal models.

1. In the gas zone, the thermal methods above generate a decrease in compositional variations with depth. Consequently, the MMP variations in this region is largest using the isothermal GCE method to generate MMP(h).

2. In the oil zone, all investigated thermal models except the Belery-da Silva's method generate a decrease in compositional variations with depth. In this case Haase and Kempers' models for thermal diffusion generate an MMP variation with depth smaller than the isothermal MMP(h) variation.

As a result of the points above, we find that using Haase and Kempers methods results in small MMP variations with depth throughout the whole reservoir thickness. Applying the Belery-da Silva model for thermal diffusion generates a smaller MMP(h) variations than the isothermal MMP(h) in the *upper part* of the reservoir. However, the Belery-da Silva model predicts a strong increase in compositional gradients in the *lower part* of the reservoir. As shown in Fig. 3.46, the calculated MMP varies strongly with depth in the oil zone and the variations are significantly larger than the isothermal MMP(h) variations.

3.7 Discussion and Analyses

In this section we discuss and analyse the effects on MMP of implementing compositional gradients in slimtube simulations and reservoir simulators. Also, rate dependency in vertical gas injection simulations and its effect on miscibility are demonstrated. Vertical dry gas injection in a reservoir with vertical continuous transition from gas to oil has been given particular attention. Finally, MMP(h) in a depleted system with initial compositional gradient is calculated, and the effect of production process is demonstrated. Also, the effect of applying erroneous values for gas-oil ratio in recombination and its effect on MMP is adressed.

3.7.1 Horizontal Gas Injection in Compositionally Graded System

The effect on MMP in a system with compositional gradients is investigated in this subsection.

MMP variations with depth and enrichment level of injection gas has been studied in previous sections, based on "single depth calculations". Compositions at one depth were used to initialize an MMP calculation for that specific depth, and by multiple calculations at a series of different depths the MMP(h) curves were generated, as discussed in Section 3.4.1

Two horizontal slimtube simulations were initialized with compositional gradients and run (1) to investigate the effect on MMP, and (2) to compare the MMP with results from "single depth calculations". Each simulation was initialized with compositions from 50 different depths generated with the isothermal GCE calculations. The system investigated was the VOA reservoir in the depth interval -2895 m SSL to -3505 m SSL. Injection gas was chosen as Gas A enriched with gas B, with E=0.47. Notice that the MMP for the VOA system had earlier been determined by slimtube simulations at the top and bottom of the selected depth interval (Table 3.4). In these cases with *uniform* composition the MMP was found to be 381 ± 5 bara and 457±15 bara at the top and bottom of the depth interval, respectively. The MMP is significantly below the bubble point pressure for the composition at -2895 m SSL, and significantly above the bubble point pressure at -3505 m SSL.

The two slimtube simulation cases with compositional gradient were as follows:

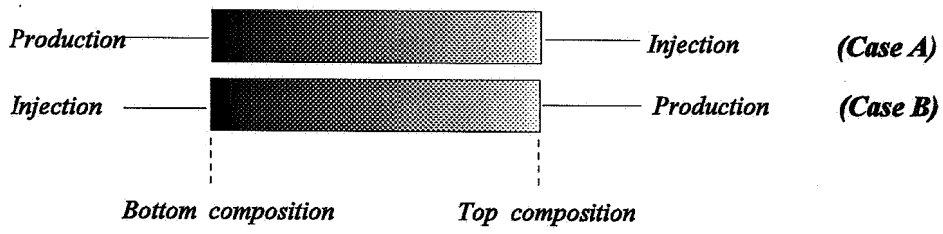

Fig. 3.47 Schematic illustration of Case A and B; i.e. slimtube simulation initialized with compositional gradients. Grey tone represents density.

- **Case A**. Horizontal slimtube initialized with compositionally grading reservoir fluid. Injection gas: slightly enriched separator gas (E=0.47). Injection point corresponing to composition at -2895 m SSL in the isothermal GCE calculations, and production at the -3505 m SSL oil composition side.

- **Case B.** Identical to Case A, but with injection and production points switched, i.e. injection at composition from -3505 m SSL.

Illustration of Cases A and B is given in Fig. 3.47. Case A is more physically relevant than Case B, as the typical gas injection process is vertically downwards. In such situations the gas will contact lighter oil at the injection point than it does further down in the reservoir.

Each case was run at a series of relevant pressures for 100, 200 and 500 grid cells. As in the uniform composition cases, additional 800 grid runs were performed in the close vicinity of the apparent MMP. The extrapolation methods were identical to the uniform composition cases. (Extrapolation method 3-5, see Section 3.2.4). The dispersion free recovery factors obtained with extrapolation method 3 are plotted in Figs. 3.48 a) and b).

We now consider Fig. 3.48 a). The dispersion free recovery factors resulting from the

a)

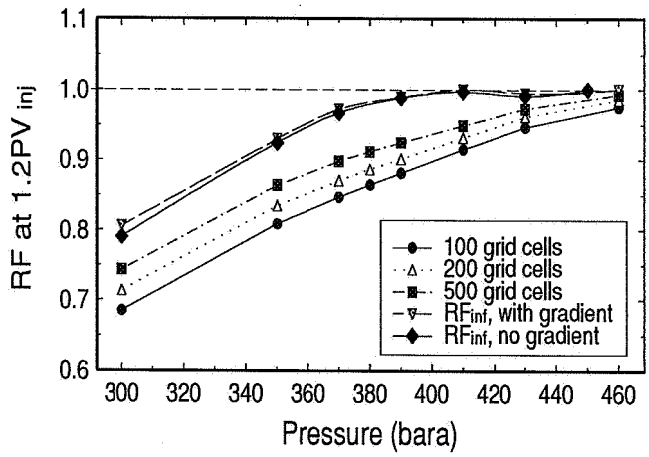

b)

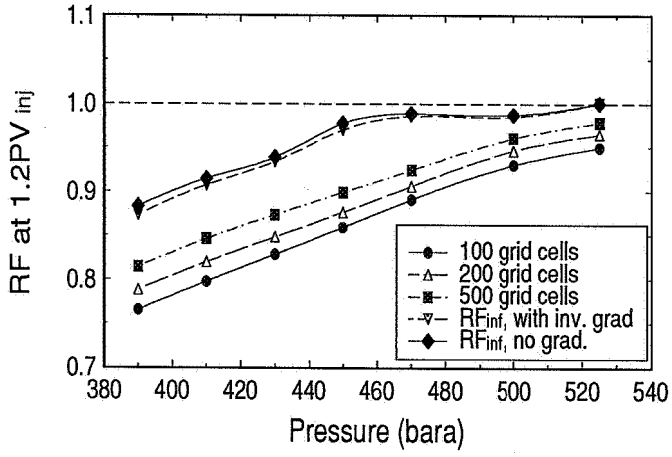

Fig. 3.48 Slimtube simulations for MMP determination. a) Case A, and b) Case B.

Case A study give slightly higher recoveries for each pressure than the no-gradient case. The difference decreases in the vicinity of the apparent MMP. We find the MMP in Case A to be 384 ± 5 bara, which is within the extrapolation accuracy when compared to the uniform composition results for MMP at -2895 m SSL.

In Fig. 3.48 b) the Case B study is seen to generate slightly lower recoveries for each pressure than the one found for the uniform composition case. The MMP was found to be 464 ± 15 bara, approximately 7 bar higher than the no-gradient case at -3505 m SSL. The compositional gradient with highest oil density at the injection point has a slightly negative effect on MMP, but the deviations from the no-gradient predictions are within the estimated extrapolation accuracy.

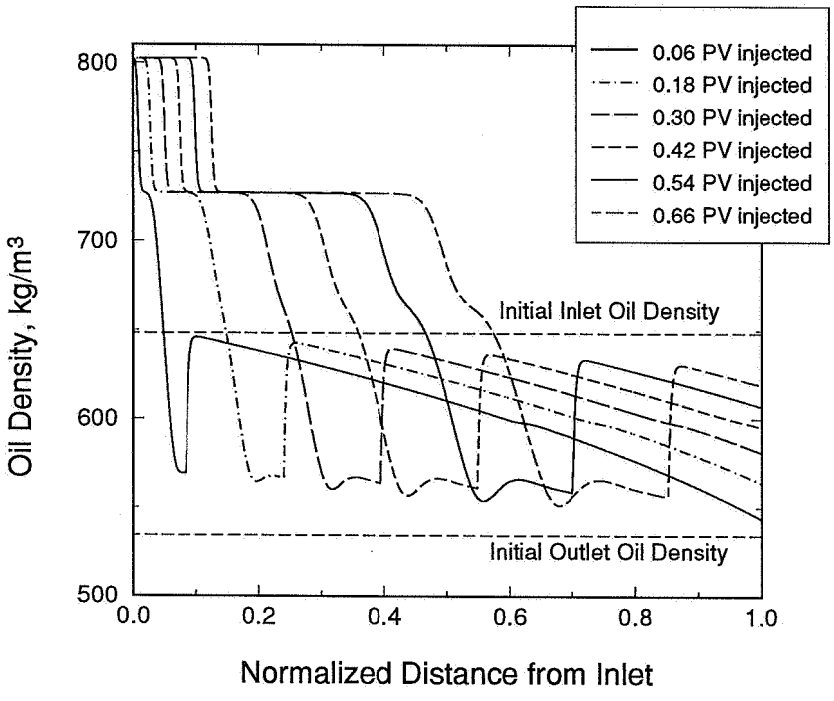

Fig. 3.49 "Snapshots" of oil density at different PV gas injected. 800 grid slimtube simulation of Case B at 460 bara.

These simulation results can be understood from the theory of development of miscibility in a 1D situation. As pointed out by Zick (1997), information is only travelling one way in a 1D slimtube simulation. Consequently the composition for example in the middle of the slimtube can not have any influence on the development of miscibility near the injection point. Since a miscible front theoretically should be developed over a zero distance length in a situation with no diffusion and dispersion (Johns et al., 1992), the system MMP should be determined by the composition near/at the injection point.

To investigate this effect further we considered "snapshots" of oil density for different injection times at MMP in Case B, see Fig. 3.49. We emphasize that there exists a numerical dispersion in this figure which in effect generates a certain width of the near-miscible front, and with a compositional gradient over this width. Still, the figure explains the main behaviour of the process. The near-miscible front at each snapshot is found at the position of *minimum* oil density. The high density oil near

the inlet is close to the near-miscible front at all times and thus is the main factor for determination of the MMP. As seen from the figure, the position of the near miscible-front changes as more gas is injected into the system such that the oil ahead of the front is displaced miscibly. As a result, the composition in the middle of the slimtube will never be in the vicinity of the miscible front.

In summary, the 1D miscibility process is mainly dictated by the composition in the vicinity of the injection point and consequently determines the MMP. This should be an important observation when applying the previously generated MMP(h) results.

3.7.2 Rate Dependence in Vertical Gas Injection

Slimtube experiments are normally carried out at high injection rates in horizontally coiled tubing. This implies that gravity should play a minor role in these measurements. Also, normal slimtube simulations are chosen to be horizontal and with similar injection rates as used in the laboratory. Horizontal miscible gas injections with enriched gases are characterized by a leading two phase front and a combined condensing/vaporizing mechanism, as discussed in Section 3.2.1. However, the typical gas injection scenario in a reservoir is *vertical* and performed at rates significantly lower than laboratory rates.

Intuitively, the effect of gravity could have an effect on the miscibility behaviour going from a horizontal to a vertical injection case. The main idea in this subsection has been to establish if the MMP and key physical mechanisms will be different in a vertical and a horizontal case. This is important both for the evaluation of the applicability of normal slimtube results in reservoir systems *and* in the applicability of the Zick multicell algorithm. Particular interest was connected to the possible deterioration of the condensing region in vertical enriched gas injection processes and its effect on MMP; possibly collapsing the MMP into the vaporizing MMP.

T*heoretically* the dispersion-free extent of the miscible front should be zero if diffusion and capillary forces are neglected, yielding a completely horizontal miscible front in a situation with vertical injection . Thus, theoretically, gravity can not play an important role in this situation. This was investigated through slimtube simulations for the 7 component VOA system (presented in Section 3.2.2) with injection of a 7 component pseudoized version of gas D, Table 3.1.

Recapitulating Table 3.5, the horizontal slimtube simulation of the 7 component

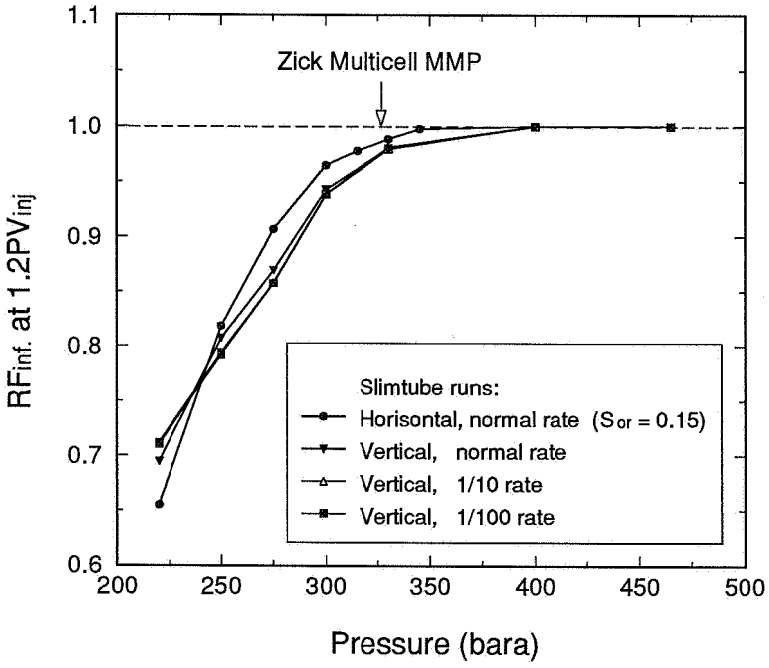

Fig. 3.50 Dispersion-free RF for horizontal and vertical slimtube simulations with different gas injection rates. Elimination of numerical dispersion are based on 100, 200 and 500 grid simulations.

VOA system with injection of Gas D gave an MMP=336 ± 10 bara. The C/V algorithm predicted an MMP=327 bara and the VGD algorithm predicted an MMP equal to 466 bara.

A system identical to the horizontal case with respect to all parameters was used in the vertical simulations. These parameters are all parameters in PVT characterization, compositions, temperature, pressure, number of grids and extrapolation method for elimination of numerical dispersion. Injection was run at normal slimtube rates, a rate reduction factor of 10 and a rate reduction of 100. The reducible oil saturation was set to 0.3 to be able to differ between immiscible and miscible results. Notice that the MMP is significantly lower than the bubble point pressure for this system. For pressures in the two phase region a segregation process will take place, being significant for slow injection rates and long time intervals. We detected some numerical problems when reducing the injection rate with 100. Reducing the injection

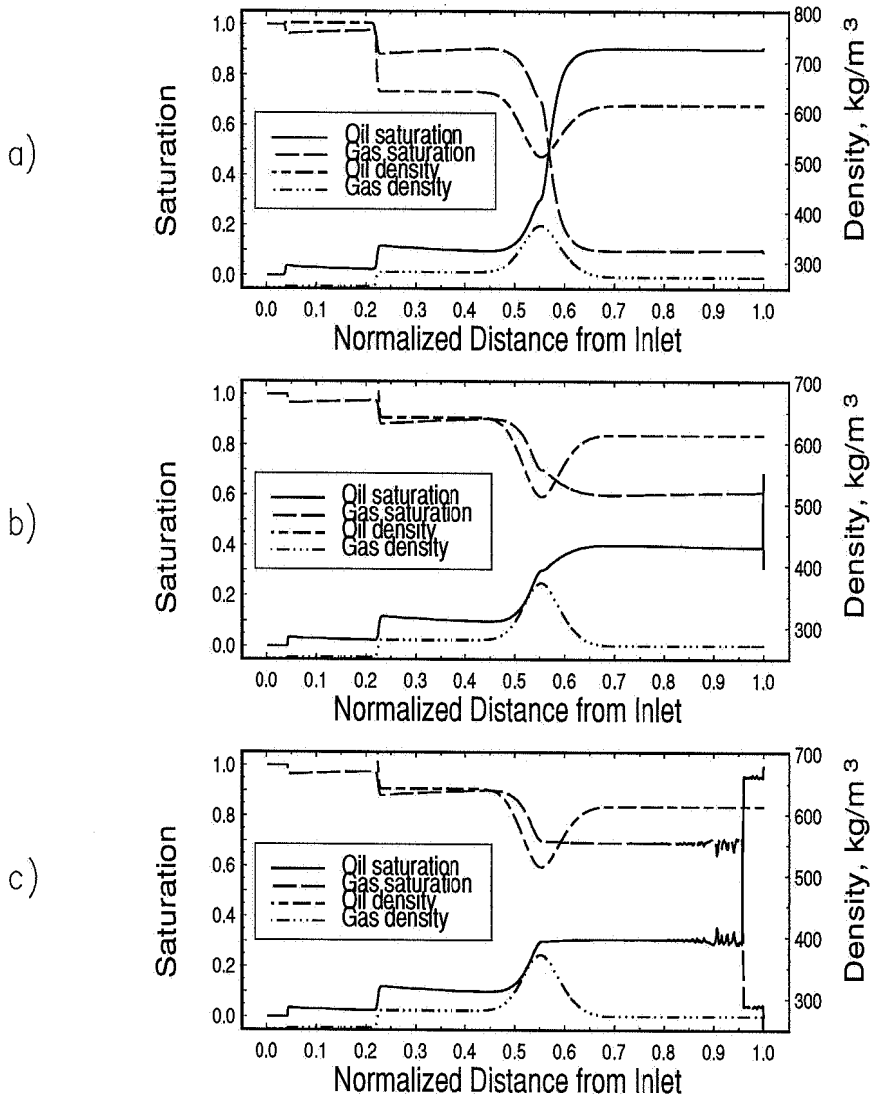

Fig. 3.51 "Snapshots" of oil and gas densities and saturations at 0.6 PV gas injected. p=330 bara. a) normal injection rate, b) rate reduction of 10, and c) rate reduction of 100.

rate further, we detected severe numerical difficulties using the ECL300 compositional simulator. Thus, this investigation was limited to a rate reduction of 100.

The RF extrapolated to infinite grid cells is plotted versus pressure in Fig. 3.50 for the cases ranging from laboratory rate to 100 times reduction. Although there exists

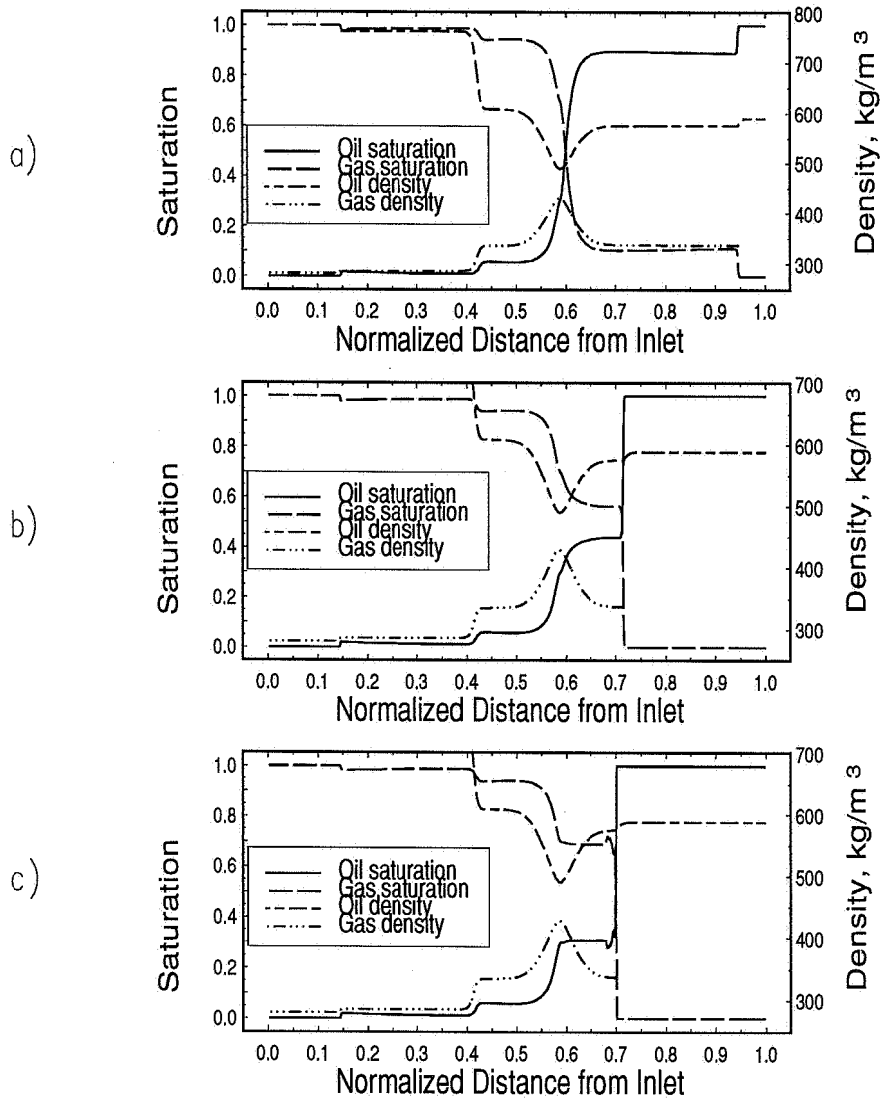

Fig. 3.52 "Snapshots" of oil and gas densities and saturations at 0.6 PV gas injected. p=400 bara. a) normal injection rate, b) rate reduction of 10, and c) rate reduction of 100.

a small difference in results in the immiscible pressure region, the three different vertical cases give the same MMP equal to 328 ± 10 bara. Within the extrapolation accuracy, this value matches the horizontal MMP and the prediction from the Zick multicell algorithm.

To understand the origin of this result, consider Figs. 3.51, 3.52 and 3.53 which show

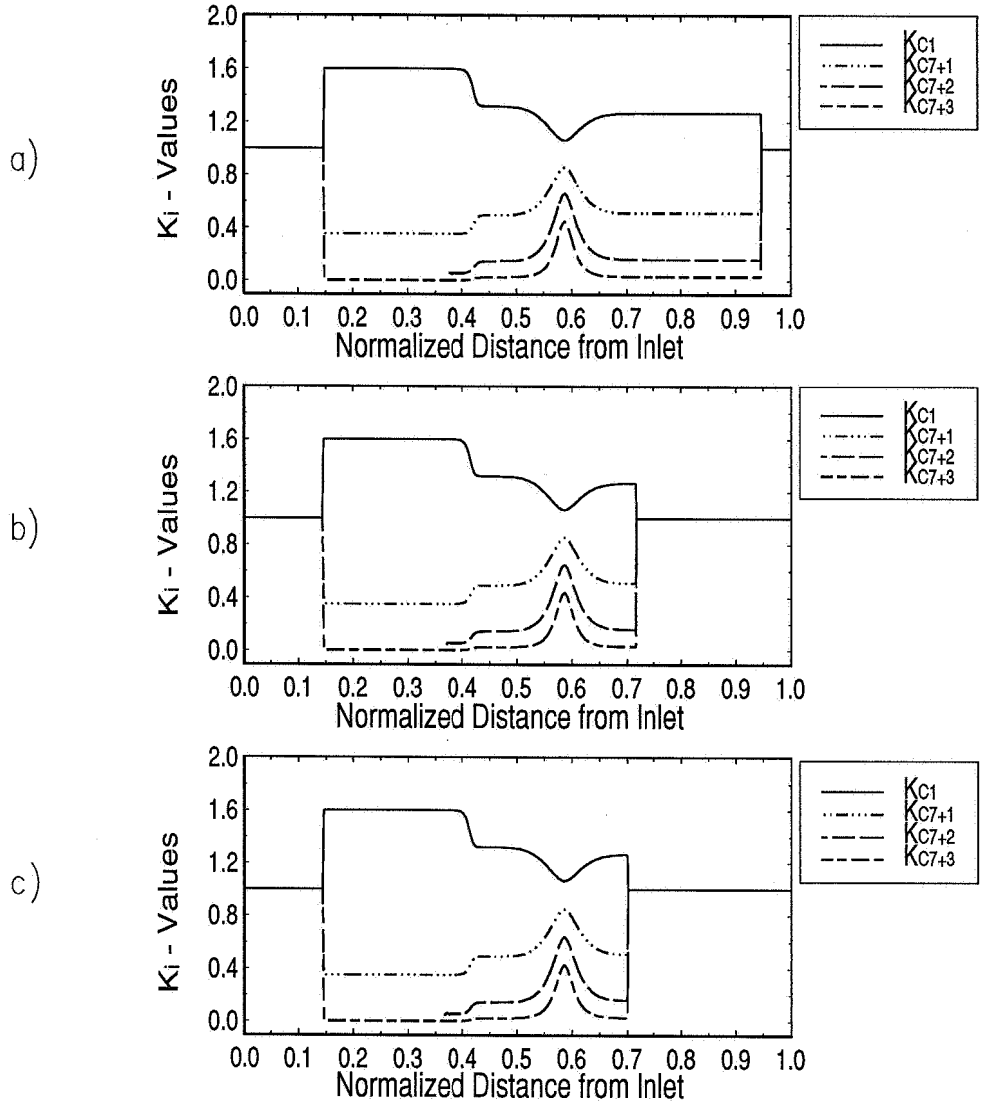

Fig. 3.53 "Snapshots" of K-values at 0.6 PV gas injected. p=400 bara. a) normal injection rate, b) rate reduction of 10, and c) rate reduction of 100.

selected slimtube profiles for different rates at p=400 bara, approximately 70 bar above the MMP and p=330 bara, approximately equal to the MMP. The figures represent typical results in this study.

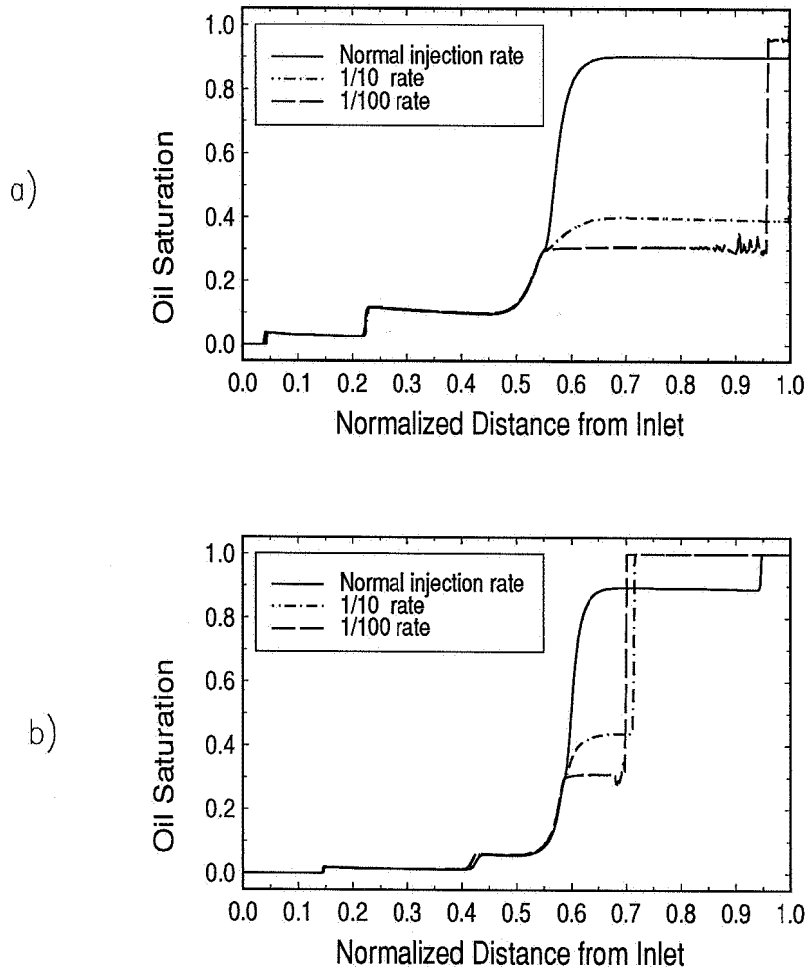

Fig. 3.54 "Snapshots" of oil saturations at 0.6 PV gas injected. Vertical slimtube simulations run with three different gas injection rates. a) p=330 bara and b) p=400 bara.

The following observations can be drawn from these figures:

1. *K-values*: At each pressure in the miscible pressure region, the K-values for the three different injection rates are practically unaltered in the vicinity of the near miscible front, although the extend of the condensing side of the front is different from case to case.

2. *Oil saturation ahead of the near miscible front*: At high injection rates, free gas saturation exists ahead of the near miscible front. In this region an

immiscible displacement takes place, and at high injection rates the oil saturation is here significantly higher than the S_{or}. Reducing the injection rate leads to a more piston-like displacement in this region due to the gravity effect, with oil saturation approaching S_{or}. The extent of the free gas saturation ahead of the near miscible front decreases when injection rates decreases.

3. *Oil saturation behind the near miscible front*: The near miscible front yields saturation significantly lower than S_{or}. Although the saturation profiles *ahead* of the near miscible front are radically different, the saturation profiles *behind* the near miscible front is approximately equal in the three rate cases considered, as demonstrated in Figs. 3.54 a) and b).

As a direct result of Point 3 only small deviations in recovery at 1.2 PV are observed and the MMP is approximately constant for the cases investigated.

This demonstrate that the MMP predicted by the Zick multicell algorithm, horizontal slimtube simulations and vertical simulations performed at different rates match each other within the extrapolation accuracy. These vertical rate dependency studies did not show any apparent destruction of the condensing side of the near miscible region, and thus the mixed mechanism was practically unaltered.

3.7.3 Vertical Injection in a System with Undersaturated GOC

In this subsection we investigate the possibility of performing a vertical dry gas injection in a system with gradual change from gas to oil, i.e. in a reservoir with undersaturated gas oil contact.

One of the most interesting aspects of this class of reservoirs is the similarity to the definition of first contact miscibility. There exists a continuous change with depth for all key physical parameters like density, composition and gas-oil ratio. Thus, the top composition is first contact miscible with the composition below, which again is FCM with the composition below, and so on, through the whole reservoir thickness.

Theoretically, using a gas equal to the reservoir top fluid a vertical injection at pressures above saturation pressure could be first contact miscible with depth, yielding 100 percent recovery. However, a more realistic economical alternative would be to inject a dry gas instead. This case is analyzed in the following.

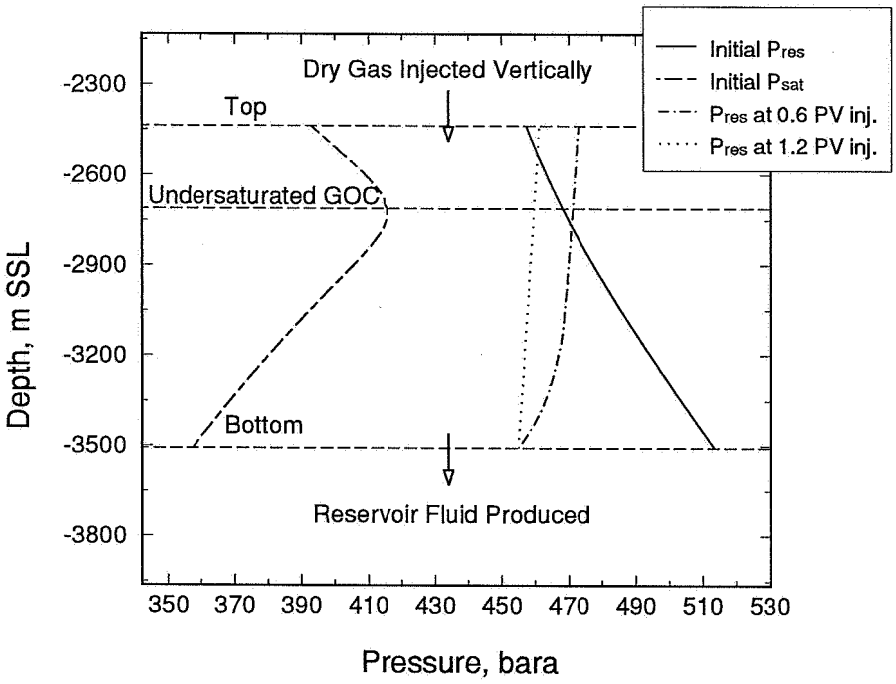

Fig. 3.55 Illustration of the simulation of vertical dry gas injection in the VOA reservoir.

The 15 component VOA system with compositional gradient determined by isothermal GCE calculations, was used to initialize a simple vertical 1D reservoir simulation. The reservoir top was set to -2438 mSSL and reservoir bottom to -3505 mSSL. Dry Gas A was injected vertically at the top of the system at an injection rate of 60 cm/day, as shown in Fig. 3.55. Permeability was set to 100 md and the minimum bottom hole pressure was set to 455 bara. 200 grids were used in the simulations, each with a vertical distance of 5.33 m.

Fig. 3.56 a) shows variation of the total methane reservoir composition with depth for different PV of dry gas injected. Fig. 3.56 b) plots the density variation with depth at different times. The figures demonstrate how the whole initial reservoir fluid column is shifted downwards in position as a result of the vertical dry gas injection. The position of the undersaturated GOC moves downwards as a function of the amount of gas injected. Continuing the injection further resulted in recoveries close to 100 percent, with a total replacement of the reservoir fluid to injection gas in the

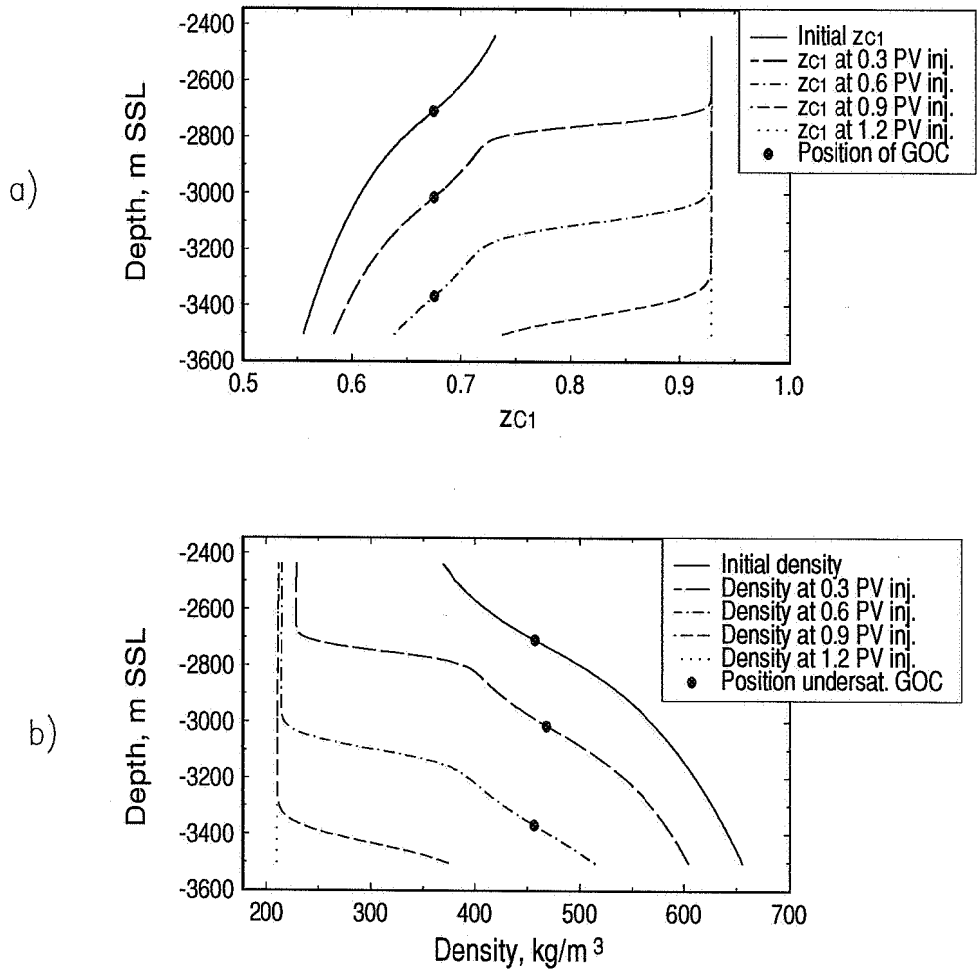

Fig. 3.56 "Snapshots" of a) methane mole fraction and b) density variation with depth for different PV dry gas injected vertically. 200 grid simulation.

system.

This behaviour can be understood by considering the reservoir fluid density with depth for 0.3 PV gas injected, as shown in Fig. 3.57. Here, the upper part of the reservoir has been replaced by dry gas. Below the dry gas zone there exists a transition zone from dry gas density to the gas density initially at top of the reservoir. The dry gas has displaced the top reservoir gas downwards, resulting in a FCM displacement further down in the reservoir. The initial reservoir fluid density with depth has been changed somewhat due to pressure change in the reservoir, but still yielding a continuous vertical density difference with depth within the original reservoir fluid column. The main result is that the whole initial reservoir fluid is

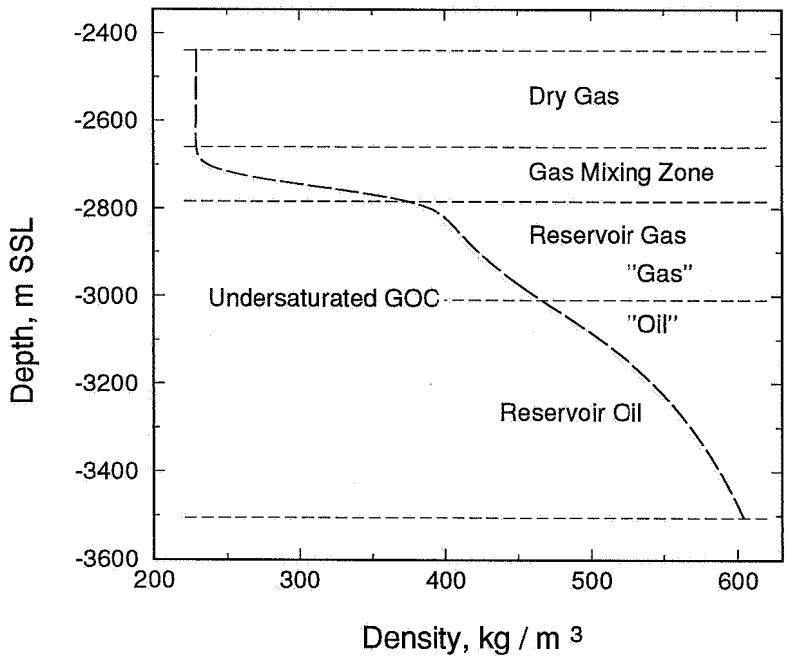

Fig. 3.57 Reservoir fluid density variation with depth at 0.3 PV gas injected.

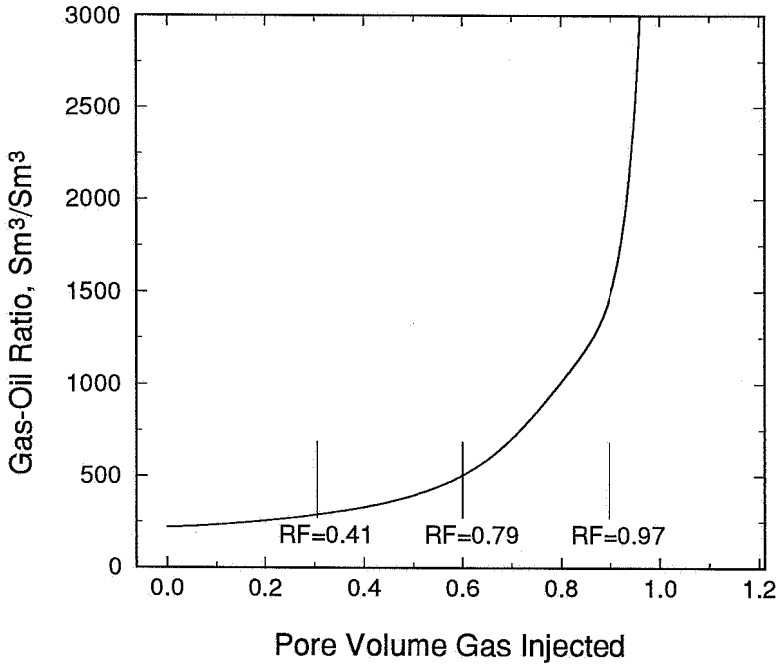

Fig. 3.58 Producing gas-oil ratio as a function of PV gas injected.

shifted downwards and the lower part of the column is produced at the bottom of the reservoir.

Fig. 3.58 shows simulated results for producing gas-oil-ratio as a function of pore volume dry gas injected. Notice that the producing GOR increases continuously with time until all the reservoir fluid has been replaced by the injection gas. Injection of 0.9 PV dry gas resulted in a RF of 0.97. These results are positive and interesting from a fluid perspective. However, it is emphasised that this study only takes the fluid properties into account, and the results are representative only for an ideal reservoir with homogeneous geological reservoir properties. If a more complex reservoir geology is present including heterogeneties, or high and low permeable zones or fractures, the high recovery can be reduced. Gas breakthrough can destroy the FCM effect, and a dry gas injection could contact the oil directly, resulting in lower recovery.

3.7.4 MMP Variations in Depleted Oil Systems with Initial Compositional Gradient

In this subsection we investigate the significance of previously presented MMP(h) variations *below* bubble point pressure in initial oil systems with compositional gradients.

The MMP(h) calculations presented in Sections 3.4 to 3.6 were initialized through series of calculations with the following procedure: For each pressure in the iteration process for determination of MMP, the Zick multicell algorithm was initialized with a CCE experiment in order to determine the two-phase reservoir compositions. Hence, this method neglects the possibility for general redistribution in composition with depth caused by gas segregation or local convective mixing during the production life of the reservoir.

If production and/or injection processes generate a compositional variation with depth that is significantly different from the one predicted with the "CCE-method" above, the MMP(h) variations is expected to deviate from the curves generated by this "CCE method". To investigate and quantify this possible deviation three depletion simulations were run on simple 1D oil systems with initial vertical compositional variation, as will be discussed below.

The fluid system chosen was the 15 component VOA fluid system, with top chosen

at -2923 mSSL and bottom at -3505 mSSL, i.e. an initial one phase oil. Isothermal gravity chemical equilibrium calculations were used to initialize a 200 grid compositional simulation with initial compositional gradient. The simple geometrical 1D system was produced by depletion by three well completion production cases to investigate the resulting compositional variation with depth, and thus the MMP(h) variation in these systems:

- **Case A** : Production from the deepest grid block only, with constant rate. Permeability equal 500 md. No injection.

- **Case B** : Similar to case A, but with permeability set to 5000 md, to artificially generate a secondary gas cap.

- **Case C** : Production from all grid blocks, with constant total rate and high permeability, equal to 5000 md. No injection.

All cases were produced down to an average reservoir pressure of approximately 275 bara. At this pressure the production was stopped and the resulting compositional variation with depth was used to initialize C/V MMP(h) studies. MMP(h) variation for different injection gases where calculated with the C/V mechanism, using (1) the *two phase oil* compositional variation with depth, and (2) the *total mixture* compositional variation with depth.

During depletion the reservoir pressure reaches the initial bubble point pressure first in the upper part of the reservoir. This yields a situation where gas starts to go out of solution at this depth. Decreasing the reservoir pressure further it will eventually become lower than the initial reservoir pressure over the whole reservoir thickness. In our example the lighter oil in the upper part of the system will have more light components to give away than the heavier oil at the bottom. Consequently, the compositional gradient will generate a *variation in saturation with depth* below initial bubble point, see Fig. 3.59. The shape of this curve is dictated by the initial compositional variation with depth and the production strategy.

Figs. 3.59 to 3.61 show results for Case A at an average reservoir pressure of 275 bara. In this case some gas migrates upwards in the system resulting in a high gas saturation at the top of the reservoir. As seen from Fig. 3.60, the compositional variation with depth for the two-phase oil was found to be approximately equal to the CCE results. The total mixture compositional variation with depth caused by the saturation gradient with depth, was found to be approximately equal to the initial

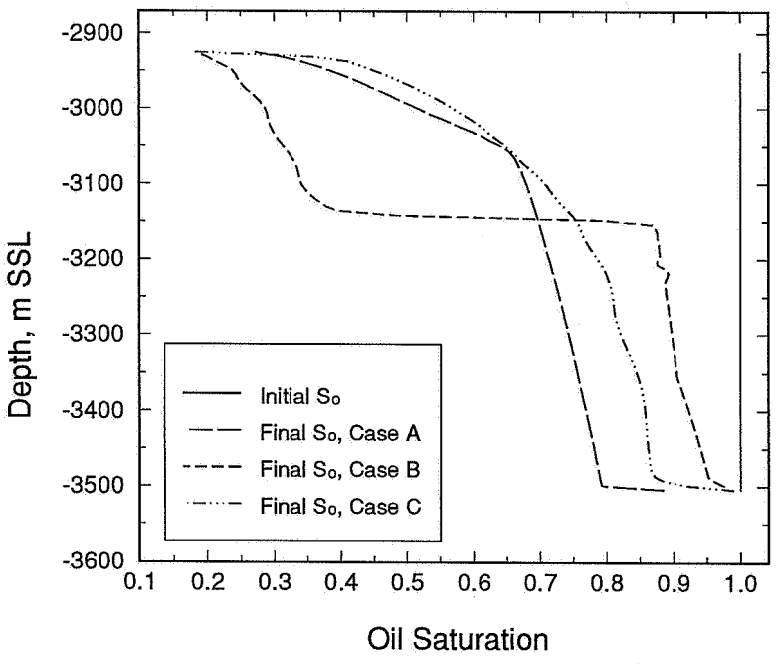

Fig. 3.59 Final oil saturations in depleted oil reservoir, cases A, B, and C.

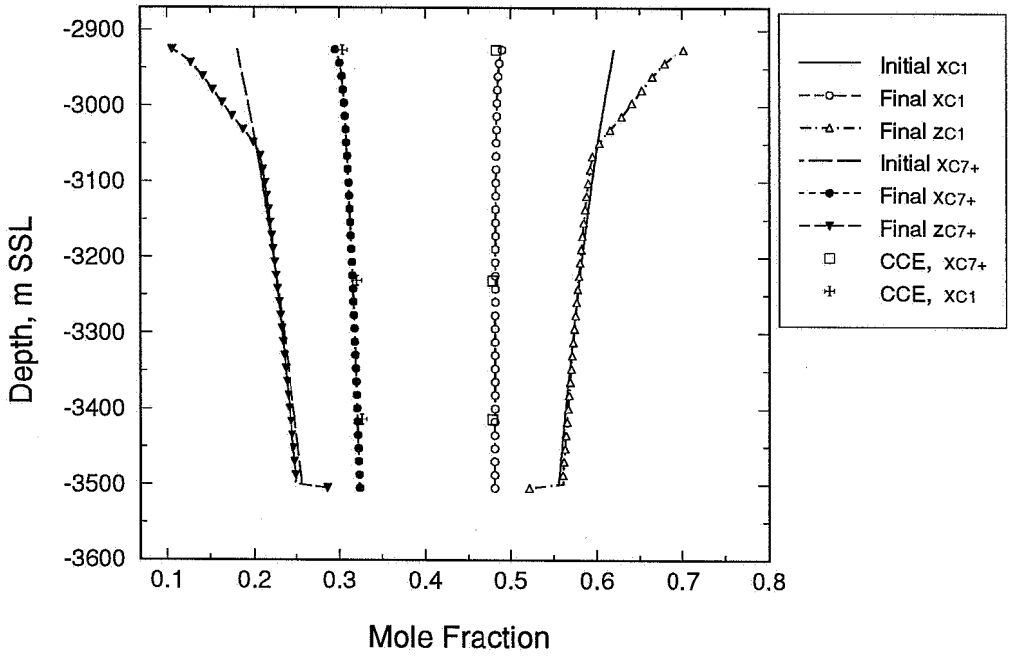

Fig. 3.60 C_1 and C_{7+} mole fraction variation with depth, Case A.

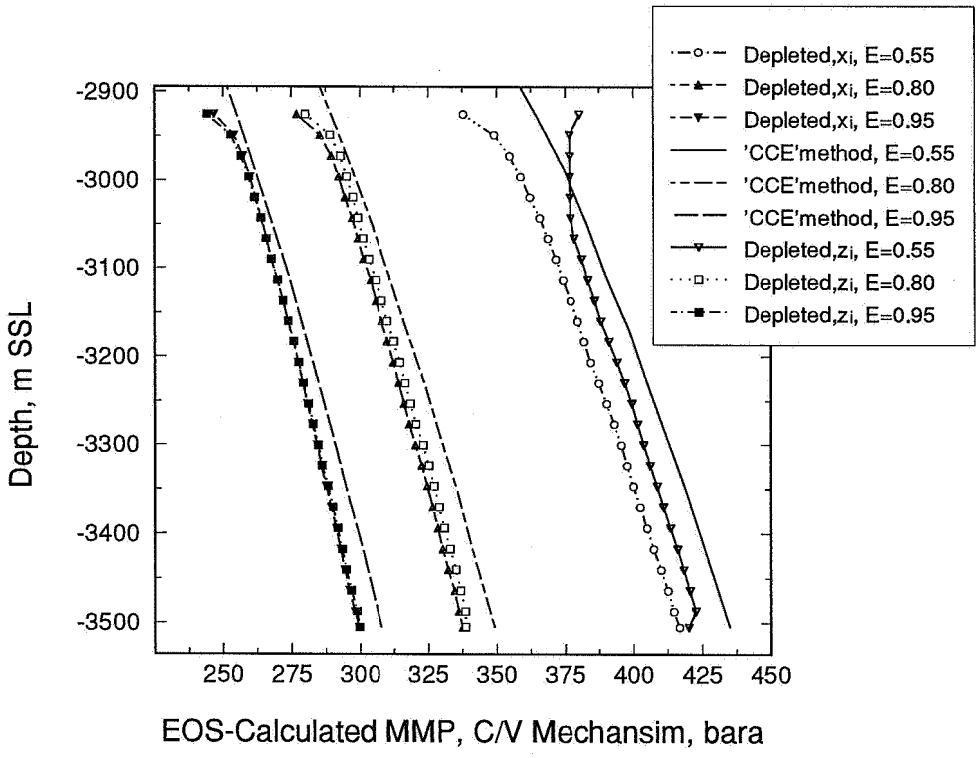

Fig. 3.61 Calculated MMP(h) variations based on oil composition and total mixture compositional variation with depth. Depleted state, Case A.

variation with depth. Exceptions are found in the producing grid block, and in the upper part of the system.

Notice that in case A the MMP(h) is approximately equal using the resulting oil composition and the total mixture composition. Also, the resulting MMP(h) variations in case A are found to be only slightly lower than the previous MMP(h) calculated in Section 3.4.4, as demonstrated in Fig. 3.61. Here, only the two richest gases gave MMP(h) below the initial bubble point pressure over the whole thickness. We thus focus on these injection alternatives in our discussion.

Figs. 3.62 to 3.63 show results for Case B. The main difference from case A is that the higher permeability resulted in a generation of a secondary gas cap with a distinct gas oil contact. Thus, the z_i in this case vary discontinuously with depth at the final reservoir pressure. However, the calculated MMP(h) based on both x_i and z_i gave a similar behaviour as the MMP(h) found in case A for the rich injection gases. Again,

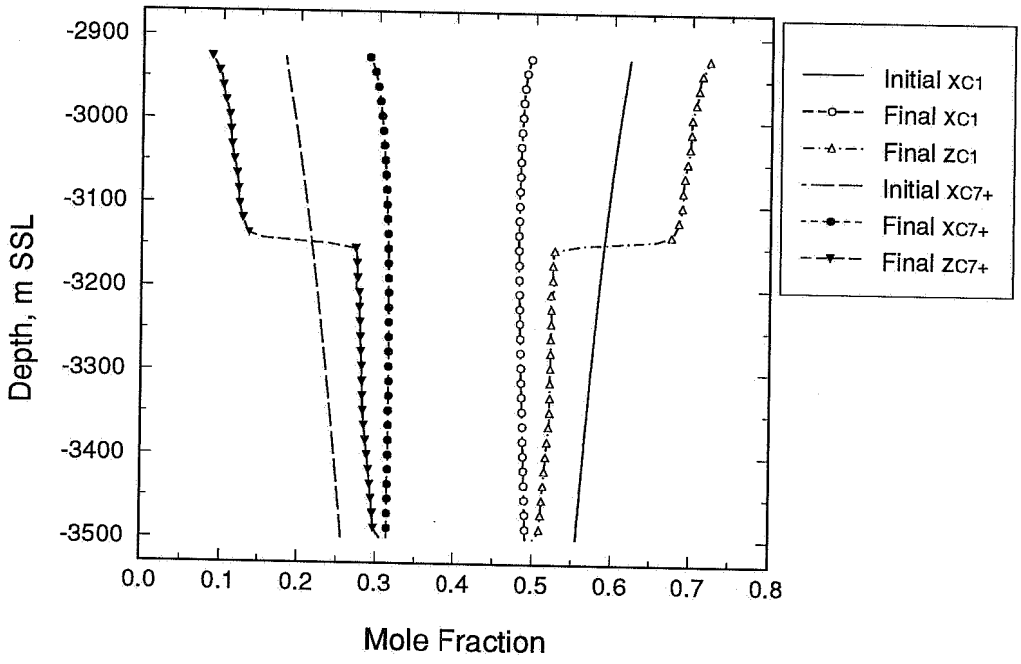

Fig. 3.62 C_1 and C_{7+} mole fraction variation with depth, Case B.

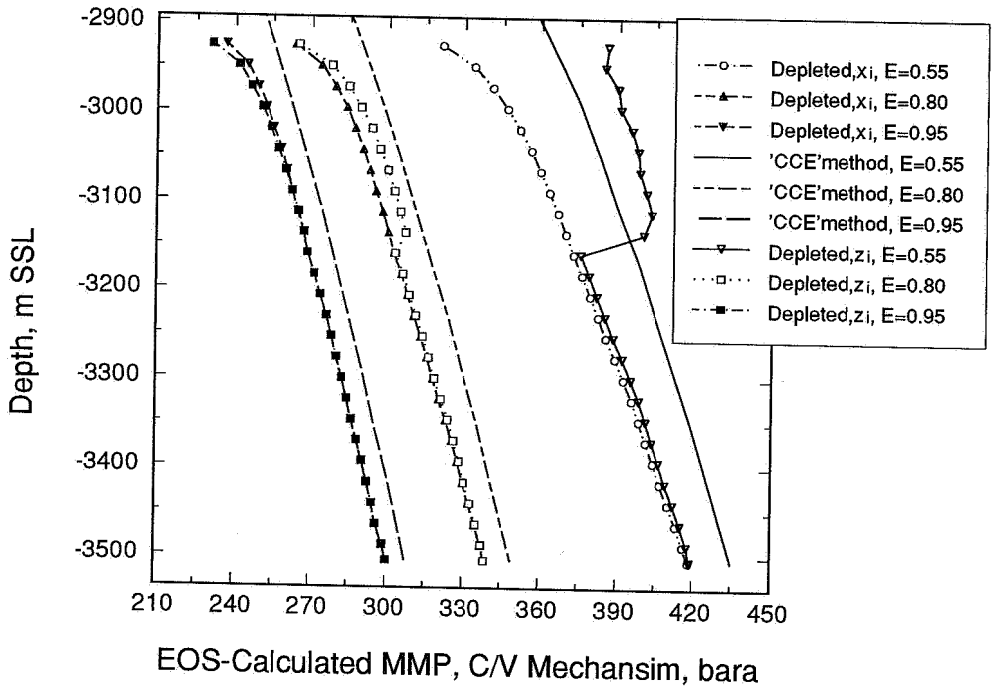

Fig. 3.63 Calculated MMP(h) variations based on oil composition and total mixture compositional variation with depth. Depleted state, Case B.

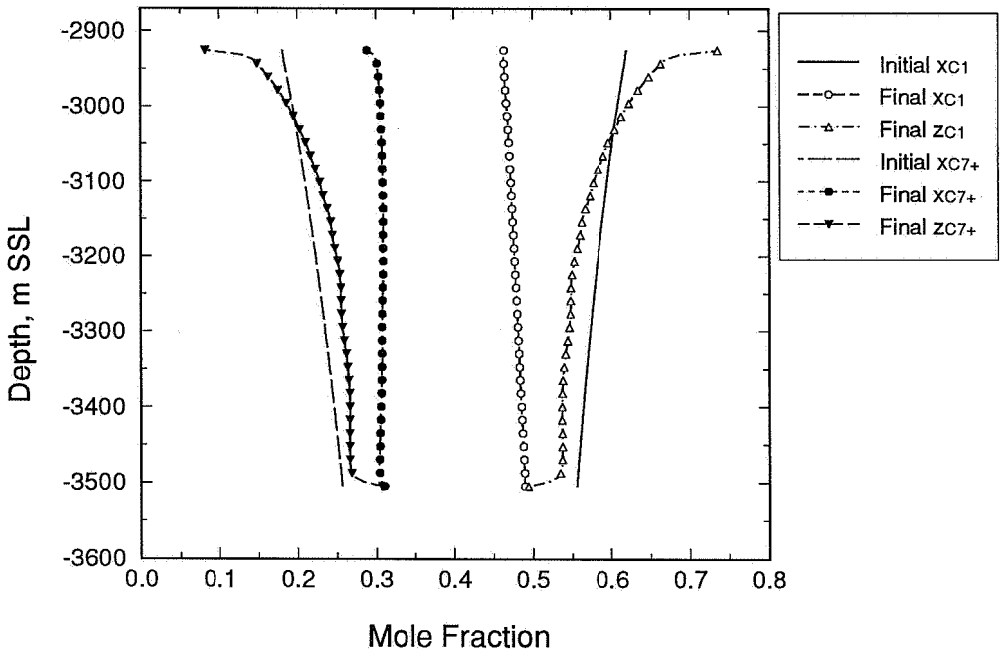

Fig. 3.64 C_1 and C_{7+} mole fraction variation with depth, Case C.

the resulting MMP(h) was only slightly different from the previous MMP(h) calculations in Section 3.4.4.

Case C represents a situation where larger parts of the two-phase region gas are produced during the depletion process and with production from all grid blocks. The lighter oil at the top of the system can give away more light and intermediate components than the heavier oil further down in the system. These components are produced mainly as gas, and the gas production is larger in case C than in Case A and B. The result is almost a disapperance of the compositional variations with depth in each phase, as seen in Fig. 3.64. Also, notice the variation in oil density with depth, Fig. 3.65. The calculated variations in MMP(h) applying the two phase oil composition showed constant values with depth. This is radically different from Case A and B, as seen in Fig. 3.66. MMP(h) calculations based on the total mixture composition did not deviate significantly from the oil case, with the exception near the system top. This deviation was found to be a result of the gas migration.

In summary, this investigation demonstrates the general case dependency of MMP

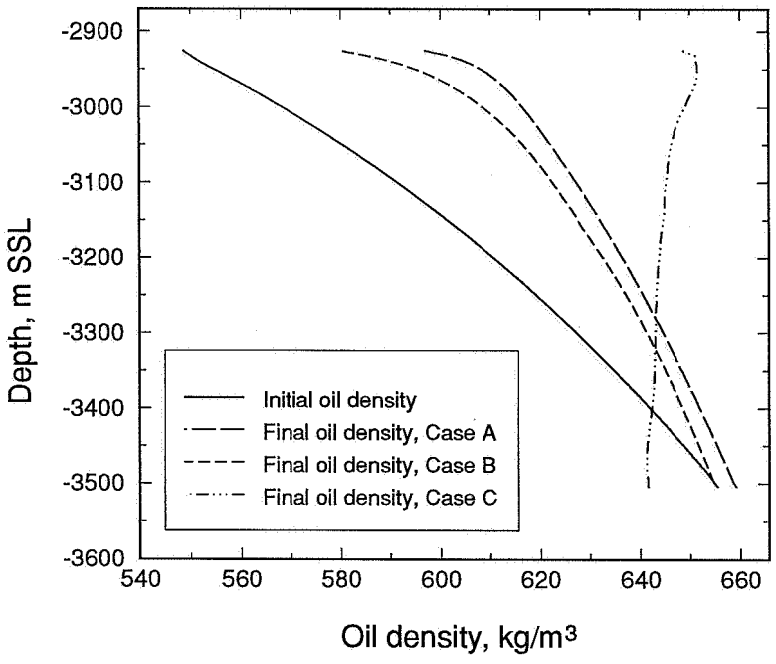

Fig. 3.65 Final oil densities in the depleted oil reservoir, cases A, B, and C.

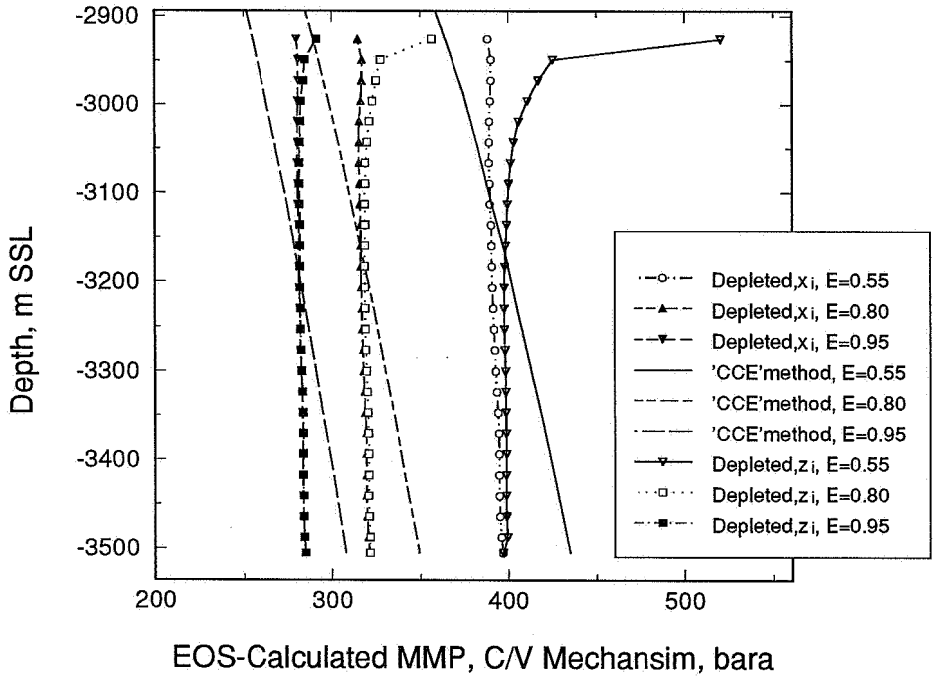

Fig. 3.66 Calculated MMP(h) variations based on oil composition and total mixture compositional variation with depth. Depleted state, Case C.

in the initial two-phase region assuming a very simplified geometrical system. When rich gases were injected, the cases with production from the lowest grid block alone gave MMP(h) variations that did not vary much from the C/V MMP(h) found in Section 3.4.3. The case with production from all grid blocks demonstrated the generation of approximately constant physical properties within each phase in the two-phase region. The direct consequence of this was constant MMP(h) variations for each injection gas.

3.7.5 Recombination Gas-Oil Ratio Effect on MMP

In this subsection we analyse and quantify the effect on C/V MMP calculations due to the use of wrong gas-oil ratio in recombination of reservoir samples.

In Section 3.2.2 we discussed sensitivity of EOS-characterization and number of components on calculated MMP results. As demonstrated in Chapter 2 there will also exist an uncertainty in the reservoir fluid composition due to possible problems during sampling, large completion intervals, and variations in gas-oil ratio during sampling. Consequently, wrong gas-oil ratio is one possible source for yielding wrong reservoir composition. It is thus important to quantify the influence of this effect on miscibility conditions.

The example is taken from the near-critical reservoir, using a reference sample approximately 30 m below the saturated GOC as the main sample. This reservoir yields large variations in gas-oil ratio with depth due to large compositional gradients. Hence, the uncertainty in precise gas-oil ratio determination is large in this example. A systematical study of using erroneous values for gas-oil ratio in recombination was performed in order to investigate how the reservoir fluid composition at the reference point changed. Deviations in the gas-oil ratio up to + - 20 percent, in steps of 5 percent, were used to generate a series of compositions using the equation. (The same compositions were used previously in Chapter 2.3.4).

MMP calculations with the Zick multicell algorithm (200 grid cells) were performed for all generated reservoir fluid composition, using four different injection gases: Gas A enriched by Gas B for the cases of E = 0.0, 0.2, 0.4, 0.7.

Calculated MMP variations as a function of percent error in recombination gas-oil ratio are plotted in Figs. 3.67 to 3.70, together with calculated percent deviations from the correct MMP.

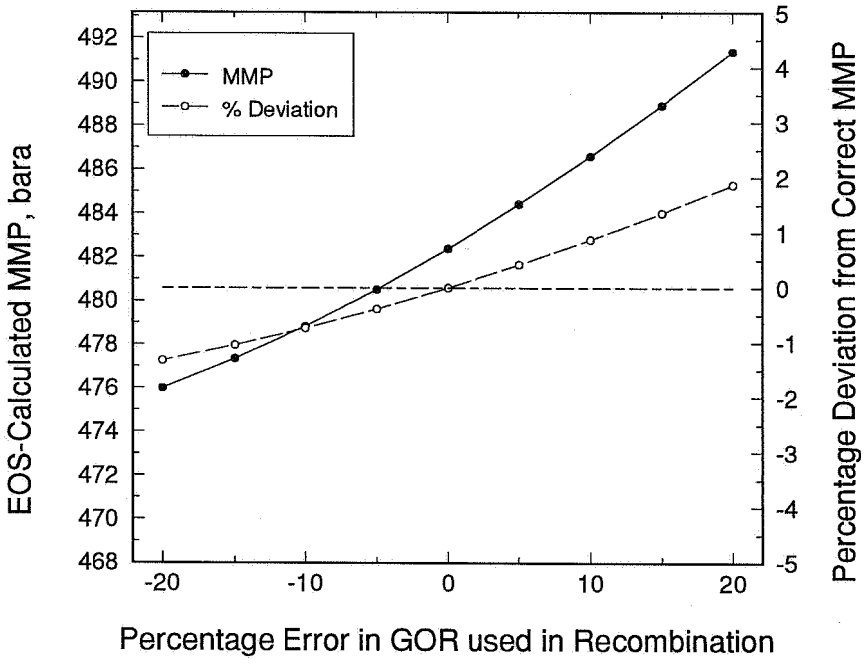

Fig. 3.67 C/V MMP as a function of error in recombination GOR. E=0.0.

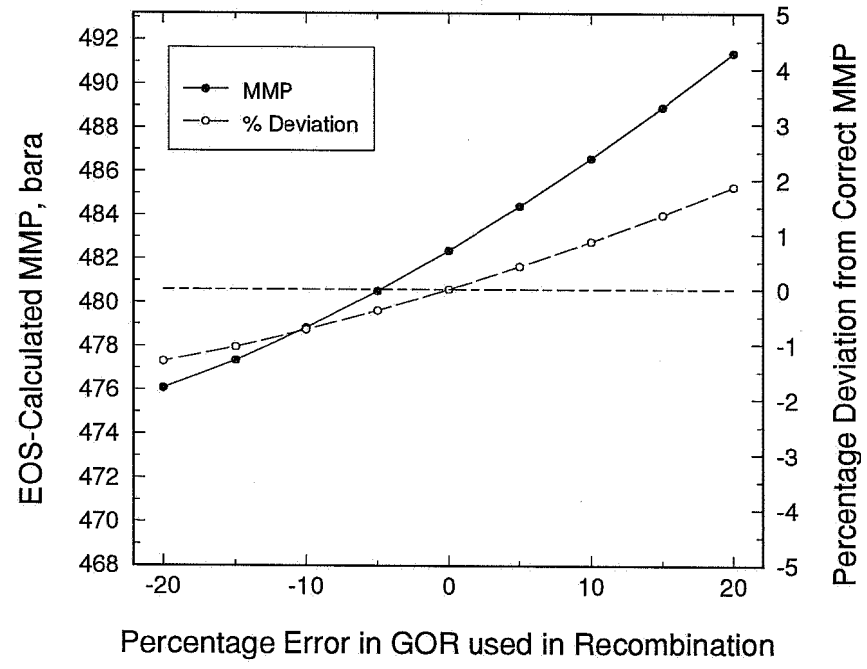

Fig. 3.68 C/V MMP as a function of error in recombination GOR. E=0.2

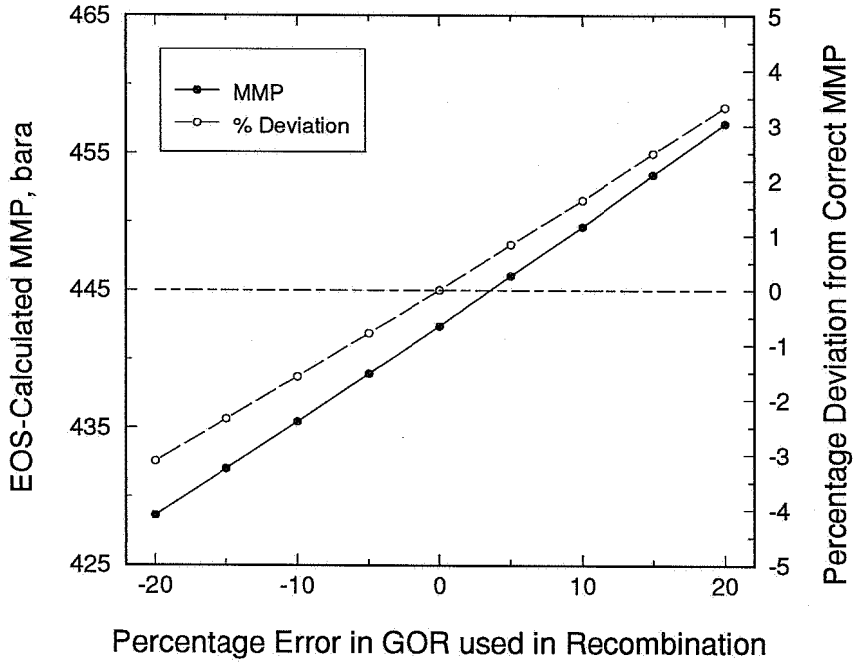

Fig. 3.69 C/V MMP as a function of error in recombination GOR. E=0.4.

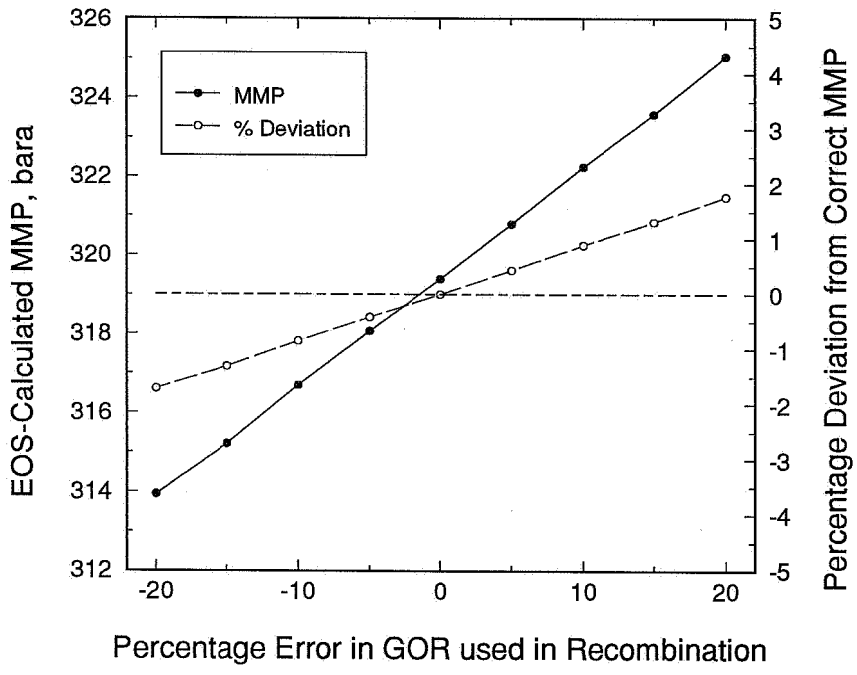

Fig. 3.70 C/V MMP as a function of error in recombination GOR. E=0.7.

As shown in the figures, the percent deviation from correct MMP as a function of error in recombination is case dependent with respect to injection gas, but are not larger than approximately ± 4 percent in the examples investigated. This shows that a recombination error will have a relatively small influence on the calculation of MMP.

3.8 Conclusions and Recommendations

1. Relative permeability and capillary pressure have *no impact* on one-dimensional miscible gas displacements, and consequently no impact on determination of the minimum miscibility conditions.

2. A procedure is proposed to quantify the uncertainty in extrapolation for elimination of numerical dispersion. It is shown that a significant case-dependent uncertainty exists in MMP determination by slimtube simulations, due to the method used for eliminating numerical dispersion.

3. Single cell (VGD and CGD) calculation algorithms have been found to highly overpredict MMP for enriched gases. The VGD MMP will *always* be larger than or equal to the saturation pressure, independent of the injection gas composition.

4. The development of a miscible process is most often a combination of a condensing and vaporizing (C/V) mechanism, where components are transported between both phases and intermediate component transfer is a key mechanism (Zick, 1986). The Zick multi-cell algorithm is found to predict MMP within the extrapolation uncertainty of slimtube results for a series of different fluid systems, ranging from gas condensates to low-GOR oils. We find that computational speed is 20 to 100 times faster than slimtube simulations.

5. MMP decreases with increasing enrichment level of the injection gas, but remains approximately constant below a threshold enrichment level, E*. This value determines the upper limit for enrichment level where the VGD algorithm is applicable. Above E* the developed miscible process is a combined C/V mechanism, and the true MMP decreases significantly as a function of E. This behaviour of MMP as a function of enrichment level is found in *all* investigated fluid systems. We recommend that E* be determined when miscible gas injection is evaluated as a potential EOR candidate. Above E* a small increase in enrichment level can give a *large decrease in MMP*, and this represents a region in enrichment level which potentially can result in large economic gain for a small additional cost.

6. The variation in MMP with depth can be directly related to the compositional variation with depth. It is demonstrated that the MMP variation in a slightly volatile oil reservoir is negligible, while relatively large variations in MMP were found in a volatile-oil system and a near-critical oil system. Based on isothermal GCE

calculations we find that MMP increases monotonically with depth in oils.

7. The variation in MME with depth can be found from comparison between the reservoir pressure and the MMP variations. In a near-critical reservoir with saturated GOC it is shown that there will be a significant MME increase with depth below the GOC. It hence may be economically advantageous to perform a miscible gas injection in the upper part of the oil zone in this reservoir.

8. The VGD MMP equals the dewpoint pressure in gas condensate systems. The C/V mechanism can yield *MMPs that are significantly lower than the dewpoint pressure* if an enriched gas is injected into a gas condensate system. The Zick multicell C/V MMP results in gas condensates have been confirmed with slimtube simulations. Miscibility conditions below the dewpoint show a potential for improved economics in gas cycling processes using an enriched injection gas.

9. Slimtube simulations in gas condensates suffer severely from grid effects. The grid effect is particularly pronounced when the injection gas enrichment level is slightly higher than E*. "Snapshots" of slimtube simulations show the buildup of an oil bank at the condensing edge of the miscible front. Large compositional variations are taking place over small distances, and grid refinement is needed to capture the C/V mechanism. If too few grids are used then an erroneous MMP equal the VGD MMP can be predicted. This grid effect can potentially be a problem in full-field simulations with large grid blocks.

10. The calculation of MMP in gas condensate systems below the dewpoint suggests that the oil properties dominate the MMP. This has been tested in a limited number of slimtube simulations, and further work is needed to confirm the results. We also find that the C/V MMP in a gas condensate reservoir does not change significantly during a reservoir depletion process.

11. The temperature effect on MMP(E) and MMP(h) has been investigated. When injecting an enriched gas it is shown that the main effect of a decrease in temperature is similar to an increase in pressure. It is demonstrated how the inclusion of thermal models in the calculations of vertical compositional variations may have a large impact on MMP(h) results.

12. The effect of compositional gradients in 1D slimtube simulations on MMP has been analysed. It is found that a miscible process is mainly dictated by the composition in the vicinity of the injection point, as this composition remains close

to the miscible front at all times. The fluid originally ahead of the miscible front will be displaced miscibly, and consequently has no influence on the MMP.

13. The possibility of performing a vertical dry gas injection in a system with an undersaturated GOC was investigated. One-dimensional vertical slimtube simulations gave recoveries close to 100 percent, at pressures above the saturation pressure.

14. Vertical slimtube simulations performed at variable injection rates were found to predict the same MMP as horizontal slimtube simulations. Injection rates were performed at typical laboratory rates, and at rates 100 times lower. The vertical simulations did not show any destruction of the condensing side of the near-miscible front, and consequently the mixed mechanism was practically unaltered in the case of rich gas injection.

The following recommendations are given for further research:

15. Slimtube experiments with gas condensate systems should be performed to confirm/disregard the MMP predictions below dewpoint pressure. Injection gas can be a realistic first stage separator gas, slightly enriched with intermediate components C_3 to C_5.

16. Slimtube experiments should be performed to investigate why and how retrograde condensate properties dominate MMP predictions below the dewpoint in gas condensates.

3.9 Nomenclature

a	=	initial oil volume in slimtube simulations converted to surface conditions
A	=	numerical constant in expression for RF_∞; dimensionless EOS-constant describing molecular attractive forces
b	=	remaining oil volume at 1.2 PV injected in slimtube simulations, converted to surface conditions
B	=	numerical constant in expression for RF_∞; dimensionless EOS-constant describing molecular repulsive forces
C	=	numerical constant in expression for RF_∞
D	=	numerical constant in expression for RF_∞
E	=	enrichment level
E^*	=	crossover enrichment level
$E^*(h)$	=	crossover enrichment level variation with depth
F_g	=	moles of gas relative to total number of moles
K_k	=	K-value for component k
M_o	=	oil molecular weight
N	=	number of grid cells in slimtube simulations
n	=	number of components
p	=	pressure
$RF_{1.2}$	=	recovery factor at 1.2 PV gas injected
RF_∞	=	recovery factor extrapolated to infinite number of grid cells
S_o	=	oil saturation
S_{or}	=	residual oil saturation
T	=	temperature
x_k	=	oil mole fraction, component k
y_k	=	gas mole fraction, component k
$y_{drygas,k}$	=	dry injection gas mole fraction, component k
$y_{mix,k}$	=	mixture gas mole fraction, component k
$y_{solvent,k}$	=	gas solvent mole fraction, component k
z_k	=	total mixture mole fraction, component k

Greek

γ_o	=	oil specific gravity

Subscript

b	=	bubble point
d	=	dew point
g	=	gas
i,j,k	=	component number
o	=	oil

res = reservoir
sat = saturation

Abbreviations

CCE = constant composition expansion
CGD = condensing gas drive
CVD = constant volume depletion
C/V = combined condensing vaporizing
DLE = differential liberation experiment
EOS = equation of state
EOR = enhanced oil recovery
FCM = first contact miscible
GCE = gravity chemical equilibrium
GOC = gas-oil contact
GOR = producing gas-oil ratio
IMPES = implicit pressure explicit saturation
MME = minimum miscibility enrichment
MME(h) = minimum miscibility enrichment variation with depth
MMP = minimum miscibility pressure
MMP(E) = minimum miscibility pressure variation with enrichment level
MMP(h) = minimum miscibility pressure variation with depth
NCO = near critical oil
NGL = natural gas liquid
PR = Peng-Robinson
PV = pore volume
PVT = pressure, volume, temperature
RF = recovery factor
SRK = Soave-Redlich-Kwong
SSL = sub sea level
STO = stock tank oil
SVO = slightly volatile oil
VGD = vaporizing gas drive
VOA = volatile oil
WAG = water alternating gas

3.10 References

Auxiette, G. and Chaperon, I.: "Linear Gas Drives in High-Pressure Oil Reservoirs Compositional Simulation and Experimental Analysis," paper SPE 10271 presented at the 1981 SPE Annual Technical Conference and Exhibition, San Antonio, Oct. 5-7.

Bath, P.G.H., van der Burgh, J., and Ypma, J.G.J.: "Enhanced Oil Recovery in the North Sea," 11th World Petroleum Congress (1983).

Belery, P. and da Silva, F.V.: "Gravity and Thermal Diffusion in Hydrocarbon Reservoirs," paper presented at the Third Chalk Research Program, June 11-12, Copenhagen (1990).

Benham, A.L., Dowden, W.E., and Kunzman, W.J.: "Miscible Fluid Displacement - Prediction of Miscibility," *Trans.*, AIME (1960) **219**, 229-237.

Cook, A.B., *et al.*: "Effects of Pressure, Temperature, and Type of Oil on Vaporization of Oil During Gas Cycling," *RI 7278* (1969a).

Cook, A.B., Walter, C.J., and Spencer, G.C.: "Realistic K-Values of C_{7+} Hydrocarbons for Calculating Oil Vaporization During Gas Cycling at High Pressure," *JPT* (1969b) No. July, 901-915; *Trans.*, AIME, **246**.

Craig, F.F.Jr.: *The Reservoir Engineering Aspects of Waterflooding*, SPE Monograph Series, 3 (1971)

Dake, L.P.: *Fundamentals of Reservoir Engineering*, Elsevier Scientific Publishing Company, Amsterdam (1978).

Van Dyke, M: *Perturbation Methods in Fluid Mechanics*, Parabolic Press, 2nd edition, 205-207, 247 (1978)

Faissat, B., Knudsen, K., Stenby, E.H., Montel, F.: "Fundamental Statements about Thermal Diffusion for a Multicomponent Mixture in a Porous Medium," *Fluid Phase Equilibria*, **10**, 209-222, (1994).

Hearn, C.L. and Whitson, C.H.: "Evaluating Miscible and Immiscible Gas Injection in Safah Field, Oman," paper SPE 29115 presented at the 1995 13th SPE Symposium on Reservoir Simulation, San Antonio, Feb. 12-15.

Haase, R., *Thermodynamics of Irreversible Processes*, Addison-Wesley. Chapter 4, (1969)

Jensen, F. and Michelsen, M.L.: "Calculation of First Contact and Multiple Contact Miscibility Pressures," *In Situ* (1990a) **14**, 1-17.

Jensen, F. and Michelsen, M.L.: "Calculation of First Contact and Multiple Contact Miscibility Pressures," Fourth European Symposium on Enhanced Oil Recovery, Hamburg, Oct. 27-29 (1990b).

Johns, R.T., Fayers, J.F., and Orr, F.M., Jr.: "Effect of Gas Enrichment and Dispersion on Nearly Miscible Displacement in Condensing/Vaporizing Drives," paper SPE 24938 presented at the 1992 Annual Technical Conference and Exhibition, Wash. D.C. (Oct. 4-7).

Johns, R.T., Orr, F.M., Jr., and Dindoruk, B.: "Analytical Theory of Combined Condensing/Vaporizing Gas Drives," paper SPE 24112 presented at the 1992 SPE/DOE Symposium on Enhance Oil Recovery, Tulsa (April).

Kempers, L.J.T.M.,"A thermodynamic theory of the Soret effect in a multicomponent liquid", *J.Chem. Phys.* (1989) **90** (11), 6541-6548

Kuo, S.S.: "Prediction of Miscibility for the Enriched-Gas Drive Process," paper SPE 14152 presented at the 1985 SPE Annual Technical Conference and Exhibition, Las Vegas, Sept. 22-25.

Luks, K.D., Turek, E.A., and Baker, L.E.: "Calculation of Minimum Miscibility Pressure," *SPERE* (Nov. 1987); *Trans.*, AIME, **283**.

McCain, W.D. Jr., *The Properties of Petroleum Fluids*, PennWell, 2. ed., (1990)

Metcalfe, R.S., Fussell, D.D., and Shelton, J.L.: "A Multicell Equilibrium Separation Model for the Study of Multiple Contact Miscibility in Rich Gas Drives," *SPEJ* (June 1973) 147-155; *Trans.*, AIME, **255**.

Novosad, Z. and Costain, T.G.: "New Interpretation of Recovery Mechanisms in Enriched Gas Drives," *J. Can. Pet. Tech.* (March-April 1988) **21**, No. 2, 54-60.

Novosad, Z. and Costain, T.G.: "Mechanisms of Miscibility Development in Hydrocarbon Gasdrives: New Interpretation," *SPERE* (Aug. 1989) **4**, No. 3, 341-347.

Orr, F.M., Jr., Johns, R.T., and Dindoruk, B.: "Miscibility in Four-Component Vaporizing Gas Drives," paper SPE 22637 presented at the 1991 SPE Annual Technical Conference and Exhibition (Oct. 6-9).

Orr, F.M., Jr. and Taber, J.J.: "Displacement of Oil by Carbon Dioxide," Annual Report for Oct. 1980 - Sept. 1981 prepared for the U.S. DOE under Contract No. DE-AS19-80BC10331, Bartlesville, OK (1981).

Peterson, A.V.: "Optimal Recovery Experiments with N_2 and CO_2," *Pet. Eng. Intl.* (Nov. 1978) 40-50.

Riemens, W.G., Schulte, A.M., and de Jong, L.N.J.: "Birba Field PVT Variations Along the Hydrocarbon Column and Confirmatory Field Tests," *JPT* (Jan. 1988) **40**, No. 1, 83-88.

Saffman, P.G. and Taylor G. I:. "The penetration of a fluid into a medium or Hele-Shaw cell containing a more viscous fluid.", *Proc. R. Soc.* Lond. 245, 312-329 (1958)

Stalkup, F.I.Jr.: "Status of Miscible Displacement," paper SPE 9992 presented at the 1982 SPE International Petroleum Exhibition and Symposium, Beijing, China, March 18-26.

Stalkup, F.I.Jr.: *Miscible Displacement*, Monograph, SPE, Richardson, TX **8** (1984)

Vogel, J.L. and Yarborough, L.: "The Effect of Nitrogen on the Phase Behavior and Physical Properties of Reservoir Fluids," paper SPE 8815 presented at the 1980 SPE Annual Technical Conference and Exhibition, Tulsa, April 20-23.

Whitson, C.H.: "PVTx: An Equation-of-State Based Program for Simulating & Matching PVT Experiments with Multiparameter Nonlinear Regression," Pera a/s, Trondheim, Norway (1995) **Version 95-02**.

Whitson, C.H.: "Trends in Modeling Reservoir Fluids," paper presented at the Seventh Internation Conference on Fluid Properties and Phase Equilibria for Chemical Process Design, Snowmass, June 18-23, (1995)

Whitson, C.H. and Belery, P.: "Compositional Gradients in Petroleum Reservoirs," paper SPE 28000 presented at the 1994 U. Tulsa/SPE Centennial Petroleum Engineering Symposium, Aug. 29-31, Tulsa.

Whitson, C.H. and Brule, M.R.: *Phase Behavior*, Monograph, SPE of AIME, Dallas (1994) **(in print)**.

Whitson, C.H. and Torp, S.B.: "Evaluating Constant Volume Depletion Data", *JPT* (1983), 610-620; *Trans.*, AIME

Yellig, W.F. and Metcalfe, R.S.: "Determination and Predicting of CO_2 Minimum Miscibility Pressures," *JPT* (Jan. 1980) 160-168.

Young, L.C.: "A Study of Spatial Approximations for Simulating Fluid Displacements in Petroleum Reservoirs," *Computer Methods in Applied Mechanics and Engineering* (1984) **47**, 3-46.

Zick, A.A.: "A Combined Condensing/Vaporizing Mechanism in the Displacement of Oil by Encriched Gases," paper SPE 15493 presented at the 1986 SPE Annual Technical Conference and Exhibition, New Orleans, Oct. 5-8.

Zick, A.A.: Personal communication (1995-97).

Appendix A

Complete EOS Fluid Characterization

In this appendix we give the complete EOS characterization for the main fluid systems investigated in Chapter 2 and 3. This includes: a black oil (BO) system, a slightly volatile oil (SVO) system, a volatile oil (VOA) system, and a near-critical oil (NCO) system. Reference depth, pressure, temperature and compositions for these systems were given in Chapter 2. Also included is the EOS characterization for the pseudoized 7 component VOA system presented in Chapter 3.

Table A.1 Complete EOS characterization for the 22 component BO system.

Comp	Mol. Weight	Critical Temp. (K)	Critical Pressure (kPa)	Acentric Factor	Vol.Trans. Shift s=c/b	CA	CB	Specific Gravity	Boiling Point (K)	Critical Volume (m3/kmol)
N2	28.01	126.3	3399.1	0.0450	-0.00800	1.0000	1.0000	0.4700	77.4	0.0901
CO2	44.01	304.2	7381.5	0.2310	0.08300	1.0000	1.0000	0.5072	194.7	0.0940
C1	16.04	190.6	4604.3	0.0115	0.02300	1.0000	1.0000	0.3300	111.7	0.0993
C2	30.07	305.4	4880.1	0.0908	0.06000	1.0000	1.0000	0.4500	184.6	0.1479
C3	44.10	369.8	4249.2	0.1454	0.08200	1.0000	1.0000	0.5077	231.1	0.2029
iC4	58.12	408.1	3648.0	0.1756	0.08300	1.0000	1.0000	0.5631	261.4	0.2627
C4	58.12	425.2	3796.9	0.1928	0.09700	1.0000	1.0000	0.5844	272.7	0.2547
iC5	72.15	460.4	3381.2	0.2273	0.10200	1.0000	1.0000	0.6247	301.0	0.3058
C5	72.15	469.7	3368.8	0.2510	0.12100	1.0000	1.0000	0.6310	309.2	0.3040
C6	86.18	507.4	3012.3	0.2957	0.14700	1.0000	1.0000	0.6640	341.9	0.3701
F1	96.00	542.5	3570.0	0.4682	0.03192	1.0000	1.0000	0.7822	365.6	0.3510
F2	107.00	560.9	3216.0	0.5001	0.06961	1.0000	1.0000	0.7960	390.0	0.3931
F3	121.00	581.6	2854.9	0.5401	0.10565	1.0000	1.0000	0.8081	415.6	0.4417
F4	146.54	615.8	2428.5	0.6133	0.13839	1.0000	1.0000	0.8285	460.6	0.5357
F5	189.42	663.5	2017.5	0.7275	0.14846	1.0000	1.0000	0.8534	519.9	0.6764
F6	235.81	707.5	1776.2	0.8424	0.12917	1.0000	1.0000	0.8734	571.8	0.8159
F7	275.51	741.9	1662.2	0.9337	0.09797	1.0000	1.0000	0.8902	611.2	0.9242
F8	323.28	780.3	1571.2	1.0345	0.05506	1.0000	1.0000	0.9066	653.1	1.0469
F9	379.17	821.8	1503.7	1.1374	0.00079	1.0000	1.0000	0.9229	695.1	1.1731
F10	447.39	869.5	1453.6	1.2397	-0.06706	1.0000	1.0000	0.9398	738.8	1.3048
F11	552.88	938.7	1414.0	1.3394	-0.17129	1.0000	1.0000	0.9615	794.2	1.4686
F12	767.90	1073.9	1395.7	1.2638	-0.36563	1.0000	1.0000	0.9958	894.2	1.7800

Summary of Binary Interaction Parameters:

	N2	C02	C1	C2	C3	iC4	C4	iC5	C5	C6	F1	F2	F3	F4	F5	F6	F7	F8	F9	F10	F11	F12
N2	0.000																					
CO2	0.000	0.000																				
C1	0.020	0.150	0																			
C2	0.060	0.150	0	0																		
C3	0.080	0.150	0	0	0																	
iC4	0.080	0.150	0	0	0	0																
C4	0.080	0.150	0	0	0	0	0															
iC5	0.080	0.150	0	0	0	0	0	0														
C5	0.080	0.150	0	0	0	0	0	0	0													
C6	0.080	0.150	0	0	0	0	0	0	0	0												
F1	0.080	0.150	0	0	0	0	0	0	0	0	0											
F2	0.080	0.150	0	0	0	0	0	0	0	0	0	0										
F3	0.080	0.150	0	0	0	0	0	0	0	0	0	0	0									
F4	0.080	0.150	0	0	0	0	0	0	0	0	0	0	0	0								
F5	0.080	0.150	0	0	0	0	0	0	0	0	0	0	0	0	0							
F6	0.080	0.150	0	0	0	0	0	0	0	0	0	0	0	0	0	0						
F7	0.080	0.150	0	0	0	0	0	0	0	0	0	0	0	0	0	0	0					
F8	0.080	0.150	0	0	0	0	0	0	0	0	0	0	0	0	0	0	0	0				
F9	0.080	0.150	0	0	0	0	0	0	0	0	0	0	0	0	0	0	0	0	0			
F10	0.080	0.150	0	0	0	0	0	0	0	0	0	0	0	0	0	0	0	0	0	0		
F11	0.080	0.150	0	0	0	0	0	0	0	0	0	0	0	0	0	0	0	0	0	0	0	
F12	0.080	0.150	0	0	0	0	0	0	0	0	0	0	0	0	0	0	0	0	0	0	0	0

Table A.2 Complete EOS characterization for the 15 component SVO system.

Comp	Mol. Weight	Critical Temp. (K)	Critical Pressure (kPa)	Acentric Factor	Vol.Trans. Shift s=c/b	CA	CB	Specific Gravity	Boiling Point (K)	Critical Volume (m3/kmol)
N2	28.01	126.3	3399.1	0.0450	-0.19300	1.0000	1.0000	0.4700	77.4	0.0901
CO2	44.01	304.2	7381.5	0.2310	-0.08200	1.0000	1.0000	0.5072	194.7	0.0940
C1	16.04	190.6	4604.3	0.0115	-0.15900	1.0000	1.0000	0.3300	111.7	0.0993
C2	30.07	305.4	4880.1	0.0908	-0.11300	1.0000	1.0000	0.4500	184.6	0.1479
C3	44.10	369.8	4249.2	0.1454	-0.08600	1.0000	1.0000	0.5077	231.1	0.2029
iC4	58.12	408.1	3648.0	0.1756	-0.08400	1.0000	1.0000	0.5631	261.4	0.2627
C4	58.12	425.2	3796.9	0.1928	-0.06700	1.0000	1.0000	0.5844	272.7	0.2547
iC5	72.15	460.4	3381.2	0.2273	-0.06100	1.0000	1.0000	0.6247	301.0	0.3058
C5	72.15	469.7	3368.8	0.2510	-0.03900	1.0000	1.0000	0.6310	309.2	0.3040
C6	86.18	507.4	3012.3	0.2957	-0.00800	1.0000	1.0000	0.6640	341.9	0.3701
F1	98.55	563.2	3177.6	0.2753	0.01861	1.0000	1.0000	0.7576	375.3	0.3914
F2	135.84	638.3	2619.0	0.3761	0.04281	1.0000	1.0000	0.8068	443.4	0.5158
F3	206.65	736.5	1963.7	0.5552	0.07923	1.0000	1.0000	0.8564	542.5	0.7476
F4	319.83	837.0	1451.9	0.8021	0.09803	1.0000	1.0000	0.9019	653.0	1.0623
F5	500.00	936.9	1106.6	1.1080	0.06813	1.0000	1.0000	0.9464	766.9	1.4086

Summary of Binary Interaction Parameters:

	N2	C02	C1	C2	C3	iC4	C4	iC5	C5	C6	F1	F2	F3	F4	F5
N2	0.000														
CO2	0.000	0.000													
C1	0.025	0.105	0.000												
C2	0.010	0.130	0.000	0											
C3	0.090	0.125	0.000	0	0										
iC4	0.095	0.120	0.000	0	0	0									
C4	0.095	0.115	0.000	0	0	0	0								
iC5	0.100	0.115	0.000	0	0	0	0	0							
C5	0.110	0.115	0.000	0	0	0	0	0	0						
C6	0.110	0.115	0.000	0	0	0	0	0	0	0					
F1	0.110	0.115	0.020	0	0	0	0	0	0	0	0				
F2	0.110	0.115	0.028	0	0	0	0	0	0	0	0	0			
F3	0.110	0.115	0.040	0	0	0	0	0	0	0	0	0	0		
F4	0.110	0.115	0.052	0	0	0	0	0	0	0	0	0	0	0	
F5	0.110	0.115	0.064	0	0	0	0	0	0	0	0	0	0	0	0

Table A.3 Complete EOS characterization for the 15 component VOA system.

Comp	Mol. Weight	Critical Temp. (K)	Critical Pressure (kPa)	Acentric Factor	Vol.Trans. Shift s=c/b	CA	CB	Specific Gravity	Boiling Point (K)	Critical Volume (m3/kmol)
N2	44.01	304.2	7381.5	0.2310	-0.08030	1.0000	1.0000	0.5072	194.7	0.0940
CO2	28.01	126.3	3399.1	0.0450	-0.11425	1.0000	1.0000	0.4700	77.4	0.0901
C1	16.04	190.6	4604.3	0.0115	-0.15762	0.9149	0.9600	0.3300	111.7	0.1117
C2	30.07	305.4	4880.1	0.0908	-0.10886	1.0000	1.0000	0.4500	184.6	0.1547
C3	44.10	369.8	4249.2	0.1454	-0.08015	1.0000	1.0000	0.5077	231.1	0.2062
iC4	58.12	408.1	3648.0	0.1756	-0.05991	1.0000	1.0000	0.5631	261.4	0.2631
C4	58.12	425.2	3796.9	0.1928	-0.05991	1.0000	1.0000	0.5844	272.7	0.2551
iC5	72.15	460.4	3381.2	0.2273	-0.04433	1.0000	1.0000	0.6247	301.0	0.3108
C5	72.15	469.6	3368.8	0.2510	-0.04433	1.0000	1.0000	0.6310	309.2	0.3090
C6	86.18	507.4	3012.3	0.2957	-0.03170	1.0000	1.0000	0.6640	341.9	0.3811
F1	96.63	554.8	3174.2	0.2707	-0.00211	1.0000	1.0000	0.7462	369.5	0.4008
F2	142.23	640.9	2343.4	0.4195	0.07245	1.0000	1.0000	0.7863	453.7	0.6024
F3	228.81	756.8	1569.9	0.6716	0.15658	1.0000	1.0000	0.8386	577.5	0.9886
F4	367.20	877.9	1065.1	1.0197	0.23271	1.1437	1.0189	0.8940	715.8	1.5063
F5	587.50	1002.7	780.2	1.2887	0.30154	1.1437	1.0189	0.9528	858.5	2.0132

Summary of Binary Interaction Parameters:

	N2	C02	C1	C2	C3	iC4	C4	iC5	C5	C6	F1	F2	F3	F4	F5
N2	0.000														
CO2	0.000	0.000													
C1	0.105	0.025	0.000												
C2	0.130	0.010	0.003	0.000											
C3	0.125	0.090	0.008	0.001	0.000										
iC4	0.120	0.095	0.014	0.004	0.002	0.000									
C4	0.115	0.095	0.014	0.004	0.002	0.000	0.000								
iC5	0.115	0.100	0.019	0.008	0.004	0.001	0.001	0.000							
C5	0.115	0.110	0.019	0.008	0.004	0.001	0.001	0.000	0.000						
C6	0.115	0.110	0.024	0.011	0.005	0.002	0.002	0.000	0.000	0.000					
F1	0.115	0.110	0.005	0.014	0.008	0.003	0.003	0.001	0.001	0.000	0.000				
F2	0.115	0.110	0.008	0.025	0.015	0.009	0.009	0.005	0.005	0.003	0.002	0.000			
F3	0.115	0.110	0.011	0.041	0.029	0.021	0.021	0.016	0.016	0.012	0.009	0.003	0.000		
F4	0.115	0.110	0.014	0.059	0.047	0.037	0.037	0.030	0.030	0.025	0.022	0.011	0.003	0.000	
F5	0.115	0.110	0.018	0.078	0.065	0.055	0.055	0.048	0.048	0.041	0.037	0.025	0.012	0.003	0.0

Table A.4 Complete EOS characterization for the 15 component NCO system.

Comp	Mol. Weight	Critical Temp. (K)	Critical Pressure (kPa)	Acentric Factor	Vol.Trans. Shift s=c/b	CA	CB	Specific Gravity	Boiling Point (K)	Critical Volume (m3/kmol)
N2	28.01	126.3	3399.1	0.0450	-0.19300	1.0000	1.0000	0.4700	77.4	0.0901
CO2	44.01	304.2	7381.5	0.2310	-0.08200	1.0000	1.0000	0.5072	194.7	0.0940
C1	16.04	190.6	4604.3	0.0115	-0.15900	1.0000	1.0000	0.3300	111.7	0.0993
C2	30.07	305.4	4880.1	0.0908	-0.11300	1.0000	1.0000	0.4500	184.6	0.1479
C3	44.10	369.8	4249.2	0.1454	-0.08600	1.0000	1.0000	0.5077	231.1	0.2029
iC4	58.12	408.1	3648.0	0.1756	-0.08400	1.0000	1.0000	0.5631	261.4	0.2627
C4	58.12	425.2	3796.9	0.1928	-0.06700	1.0000	1.0000	0.5844	272.7	0.2547
iC5	72.15	460.4	3381.2	0.2273	-0.06100	1.0000	1.0000	0.6247	301.0	0.3058
C5	72.15	469.7	3368.8	0.2510	-0.03900	1.0000	1.0000	0.6310	309.2	0.3040
C6	86.18	507.4	3012.3	0.2957	-0.00800	1.0000	1.0000	0.6640	341.9	0.3701
F1	117.98	595.7	2691.2	0.3456	0.04682	1.0000	1.0000	0.7611	410.1	0.4743
F2	180.12	692.2	1990.2	0.5140	0.09973	1.0000	1.0000	0.8123	505.9	0.7018
F3	250.66	768.3	1532.6	0.6912	0.14837	1.0000	1.0000	0.8462	589.1	0.9523
F4	346.62	842.4	1185.1	0.9077	0.18602	1.0000	1.0000	0.8776	674.8	1.2507
F5	547.83	944.1	858.9	1.2704	0.19255	1.0000	1.0000	0.9207	795.3	1.6913

Summary of Binary Interaction Parameters:

	N2	C02	C1	C2	C3	iC4	C4	iC5	C5	C6	F1	F2	F3	F4	F5
N2	0.000														
CO2	0.000	0.000													
C1	0.025	0.105	0.000												
C2	0.010	0.130	0.000	0											
C3	0.090	0.125	0.000	0	0										
iC4	0.095	0.120	0.000	0	0	0									
C4	0.095	0.115	0.000	0	0	0	0								
iC5	0.100	0.115	0.000	0	0	0	0	0							
C5	0.110	0.115	0.000	0	0	0	0	0	0						
C6	0.110	0.115	0.000	0	0	0	0	0	0	0					
F1	0.110	0.115	0.034	0	0	0	0	0	0	0	0				
F2	0.110	0.115	0.050	0	0	0	0	0	0	0	0	0			
F3	0.110	0.115	0.063	0	0	0	0	0	0	0	0	0	0		
F4	0.110	0.115	0.075	0	0	0	0	0	0	0	0	0	0	0	
F5	0.110	0.115	0.093	0	0	0	0	0	0	0	0	0	0	0	0

Table A.5 Complete EOS characterization for the 7 component VOA system.

Comp	Mol. Weight	Critical Temp. (K)	Critical Pressure (kPa)	Acentric Factor	Vol.Trans. Shift s=c/b	CA	CB	Specific Gravity	Boiling Point (K)	Critical Volume (m3/kmol)
C1N2	16.12	189.9	4590.8	0.0119	-0.15920	1.1047	0.9998	0.3311	111.3	0.1216
C2CO2	31.60	305.2	5261.8	0.1122	-0.11068	1.0551	1.0135	0.4579	186.1	0.1599
C3	44.10	369.8	4249.2	0.1454	-0.08600	1.0000	1.0000	0.5077	231.1	0.2469
F1	69.39	461.7	3401.8	0.2383	-0.04424	0.9479	0.9738	0.6184	303.4	0.3077
F2	126.58	622.2	2572.2	0.3778	0.07294	1.0019	1.0684	0.7815	433.7	0.3808
F3	271.32	801.6	1475.2	0.7639	0.15589	0.9325	0.9487	0.8689	622.9	1.1040
F4	550.00	955.2	910.1	1.2575	0.16343	1.0000	1.0000	0.9359	800.8	2.2012

Summary of Binary Interaction Parameters:

	C1N2	C2C02	C3	F1	F2	F3	F4
C1N2	0.000						
C2CO2	0.016	0.000					
C3	0.001	0.019	0				
F1	0.001	0.018	0	0			
F2	0.032	0.019	0	0	0		
F3	0.094	0.020	0	0	0	0	
F4	0.126	0.020	0	0	0	0	0

Appendix B

Compositional Predictions with Proposed GOC Algorithm

In this appendix we give additional results for compositions in a GOC search performed with the modified phase envelope algorithm. The algorithm was presented in Chapter 2. For comparison, results from isothermal gravity/chemical equilibrium calculations are included in the figures.

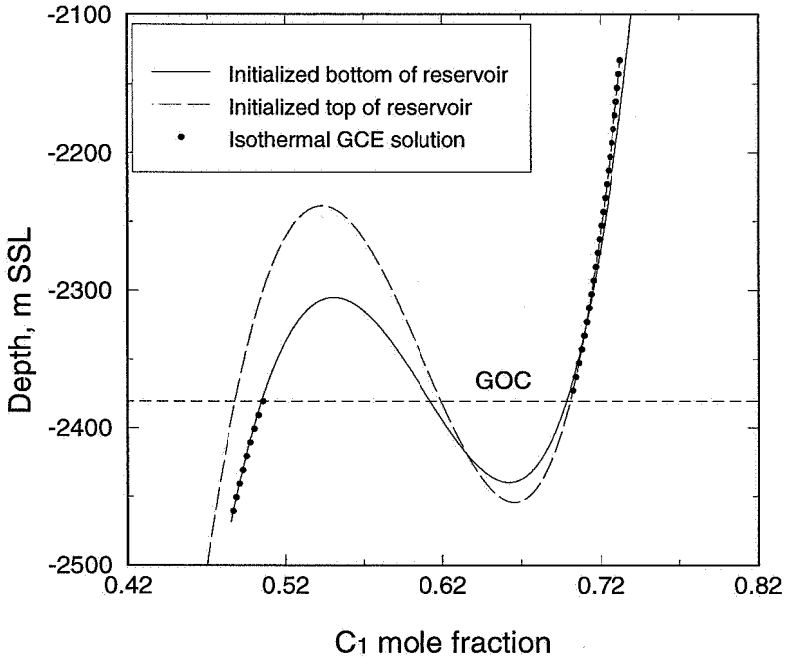

Fig. B.1 C_1 variation with depth predicted by the modified phase envelope algorithm. Gas condensate system with a saturated gas-oil contact (presented in Chapter 2). For comparison, results from isothermal gravity/chemical equilibrium calculations have been included.

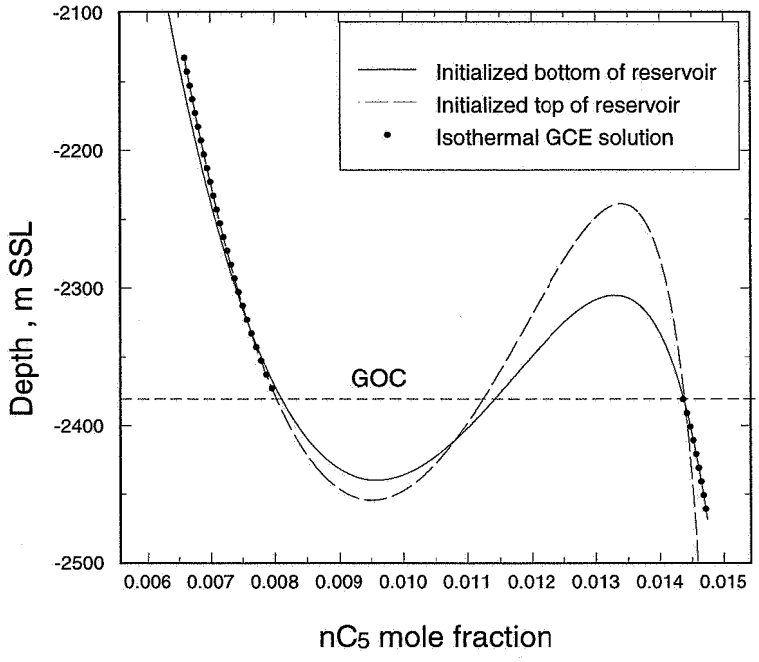

Fig. B.2 nC_5 variation with depth predicted by the modified phase envelope algorithm. Gas condensate system with a saturated gas-oil contact (presented in Chapter 2). For comparison, results from isothermal gravity/chemical equilibrium calculations have been included.

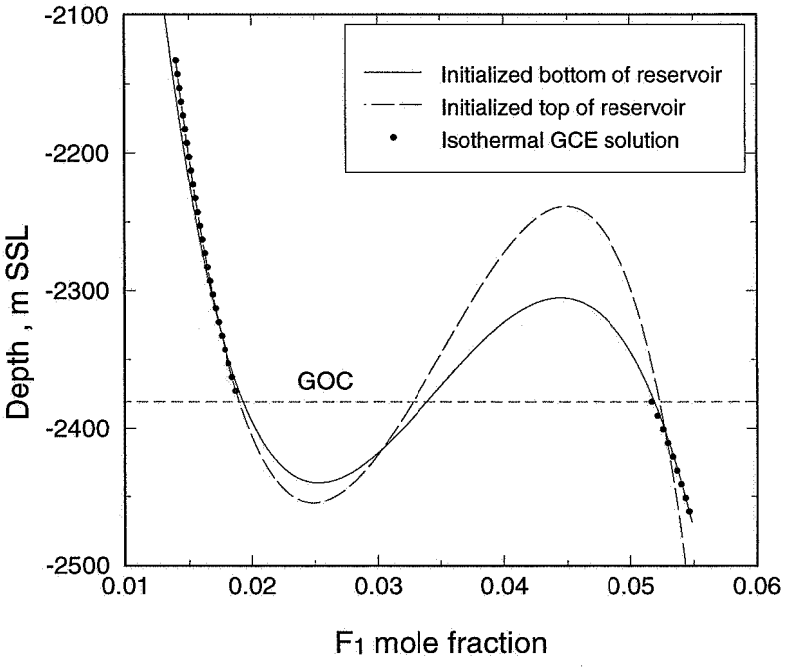

Fig. B.3 F_1 (i.e. the lightest C_{7+}-fraction) variation with depth predicted by the modified phase envelope algorithm. Gas condensate system with a saturated gas-oil contact (presented in Chapter 2). For comparison, results from isothermal gravity/chemical equilibrium calculations have been included.

Appendix C

MMP Determination for Slimtube Simulations

Slimtube simulation results for a number of different fluid systems investigated in Chapter 3 are given in this appendix. Linear or second order polynomial fits are used to eliminate numerical dispersion in the simulation results. The dispersion-free recoveries are applied to determine the minimum miscibility conditions.

Note: If only enrcihment level is given in the figure text, we mean that an injection gas has been designed with basis in gas A and gas B.

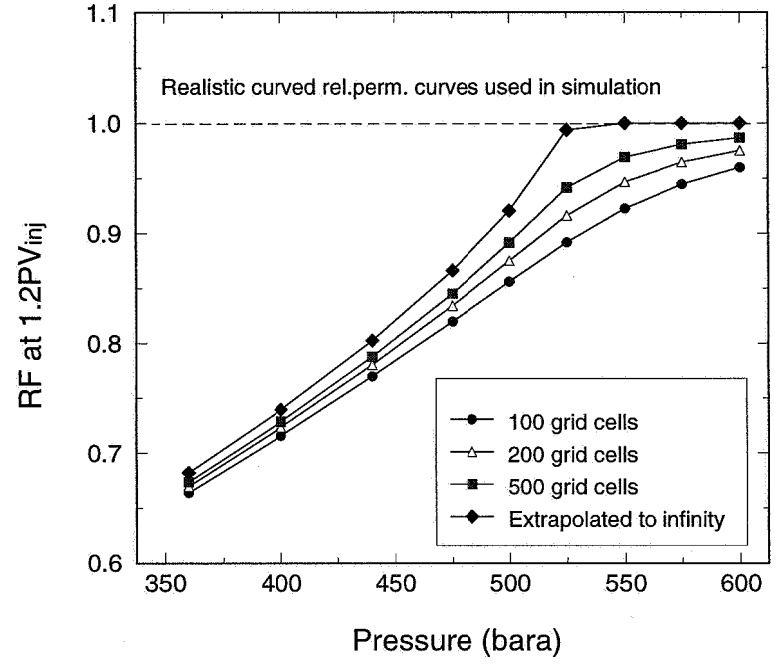

Fig. C.1 MMP determination for SVO system at ref. conditions. Injection gas A.

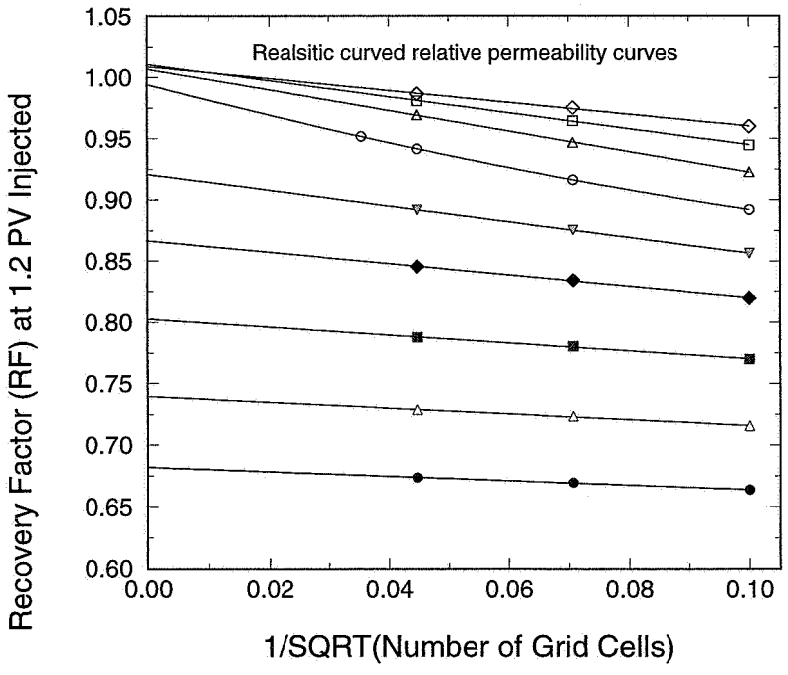

Fig. C.2 Elimination of numerical dispersion for the system in Fig. C.1

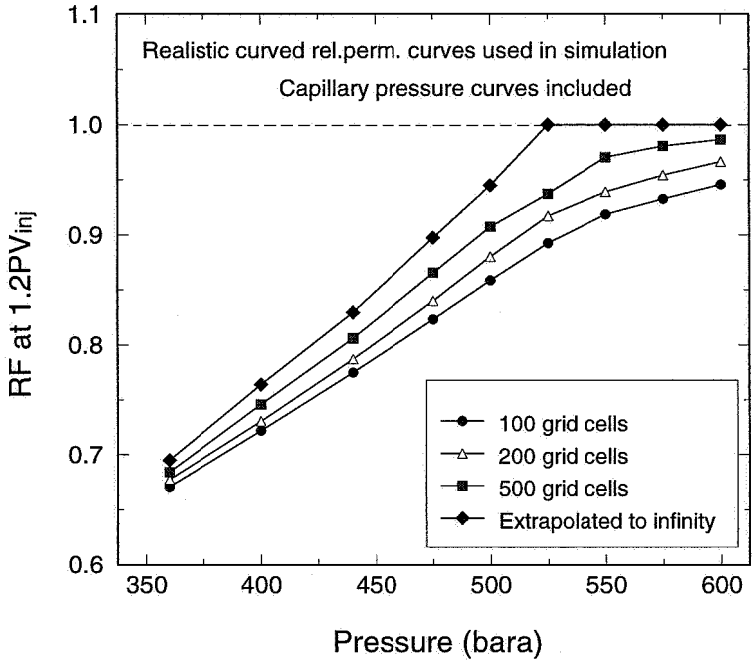

Fig. C.3 MMP determination for SVO system at ref. conditions. Injection gas A

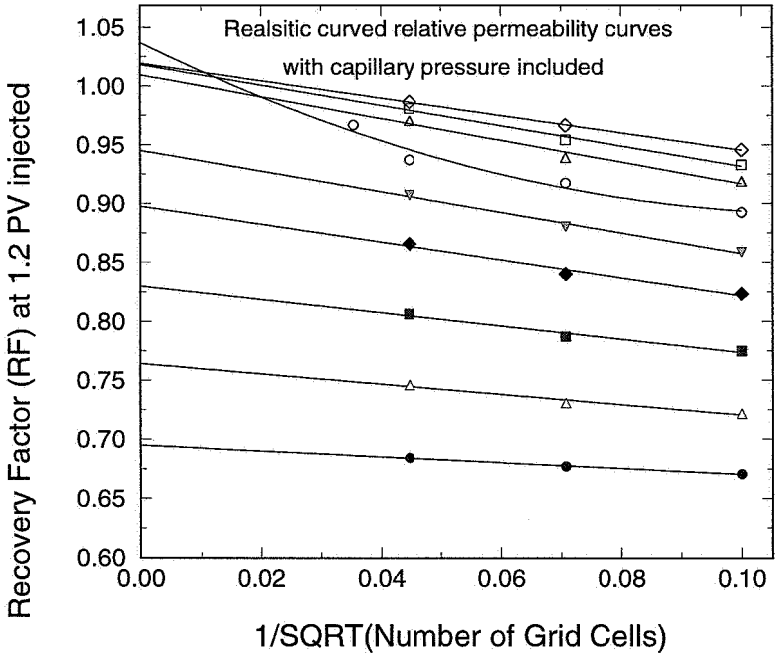

Fig. C.4 Elimination of numerical dispersion for the system in Fig. C.3.

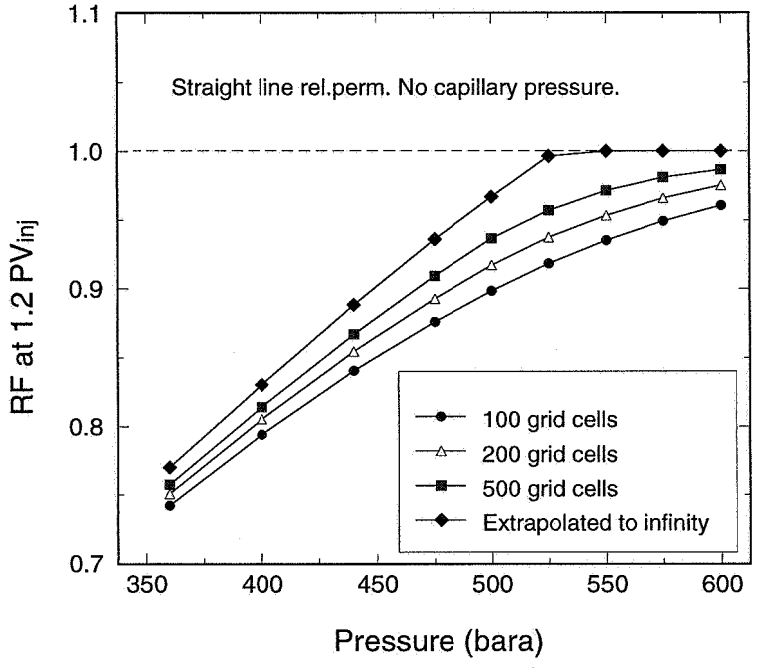

Fig. C.5 MMP determination for SVO system at ref. conditions. Injection gas A

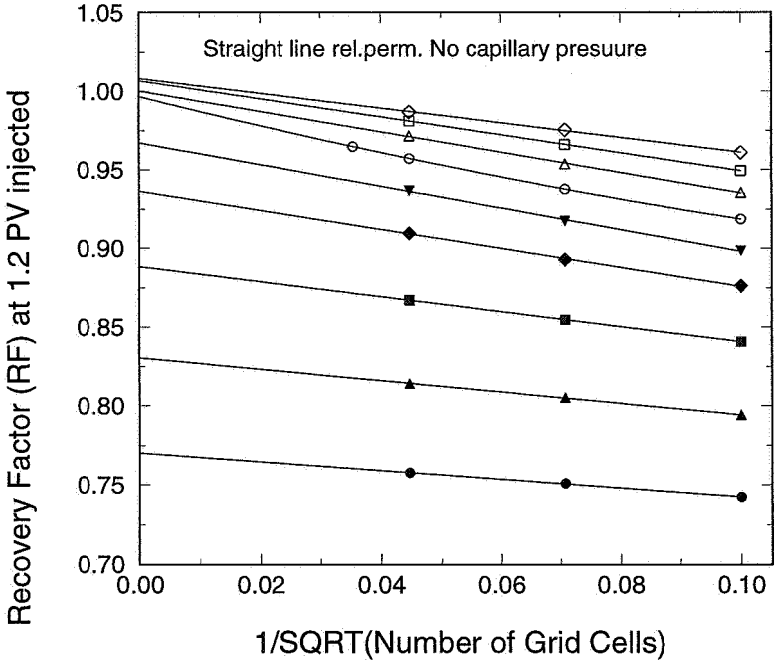

Fig. C.6 Elimination of numerical dispersion for the system in Fig. C.5.

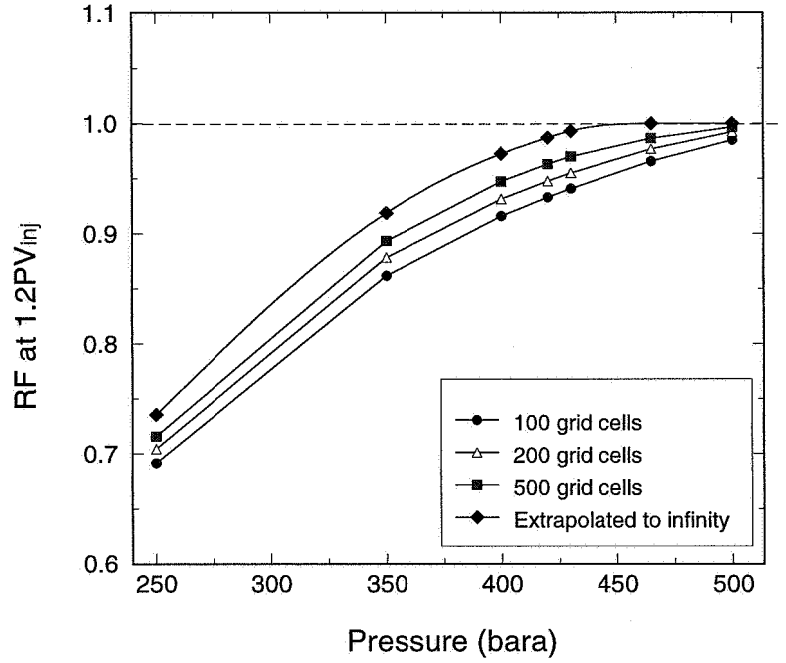

Fig. C.7 MMP determination for SVO system at ref. conditions. E=0.4.

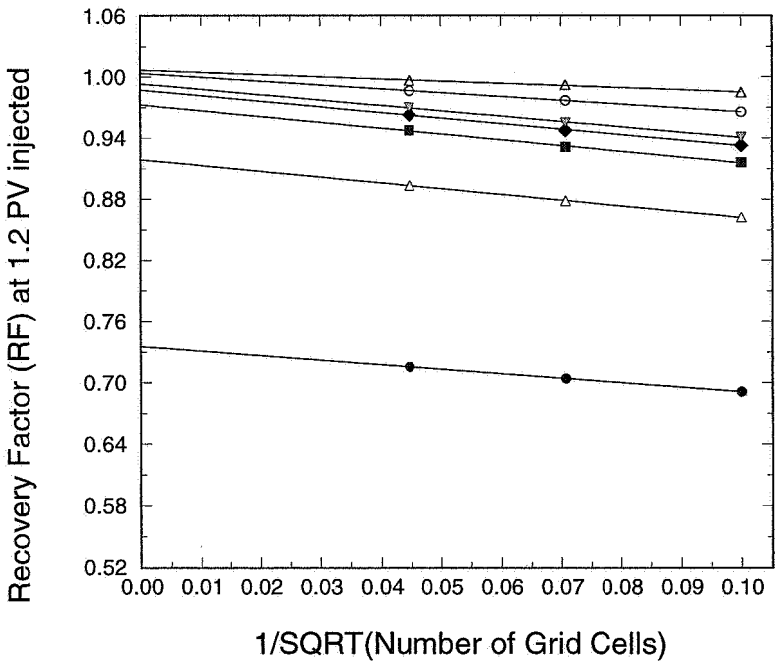

Fig. C.8 Elimination of numerical dispersion for the system in Fig. C.7.

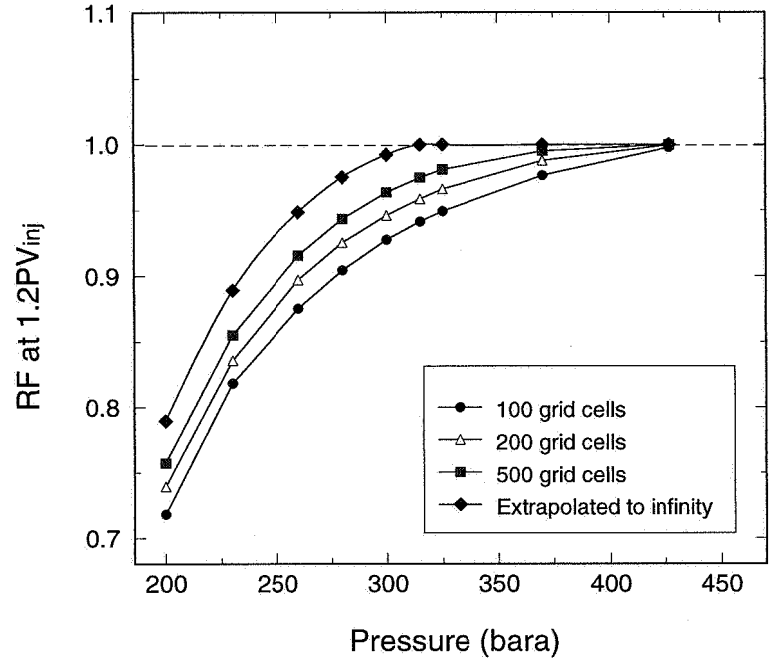

Fig. C.9 MMP determination for SVO system at ref. conditions. E=0.7.

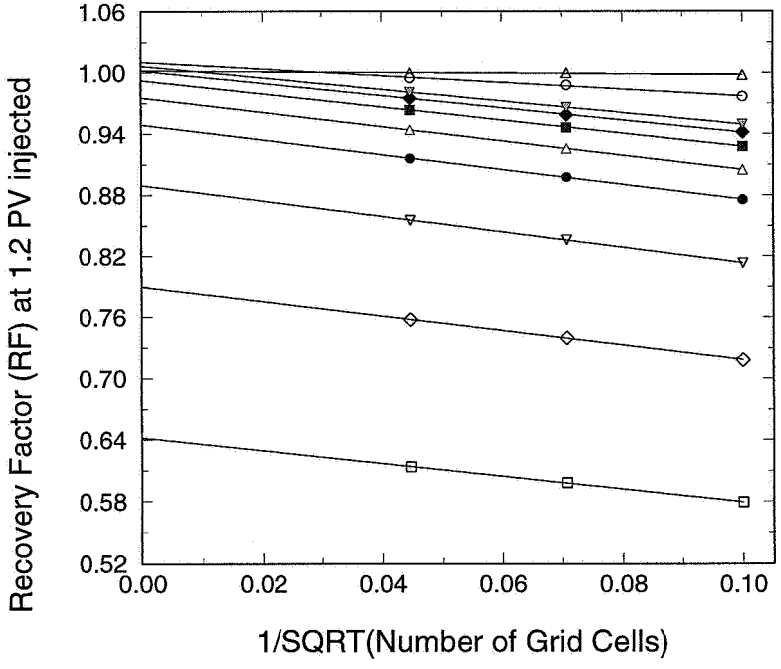

Fig. C.10 Elimination of numerical dispersion for the system in Fig. C.9.

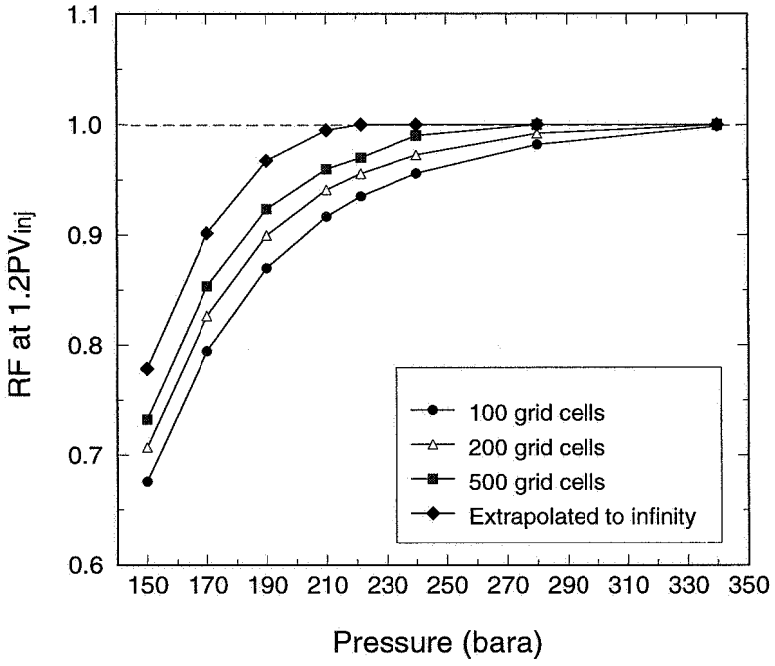

Fig. C.11 MMP determination for SVO system at ref. conditions. Injection gas B.

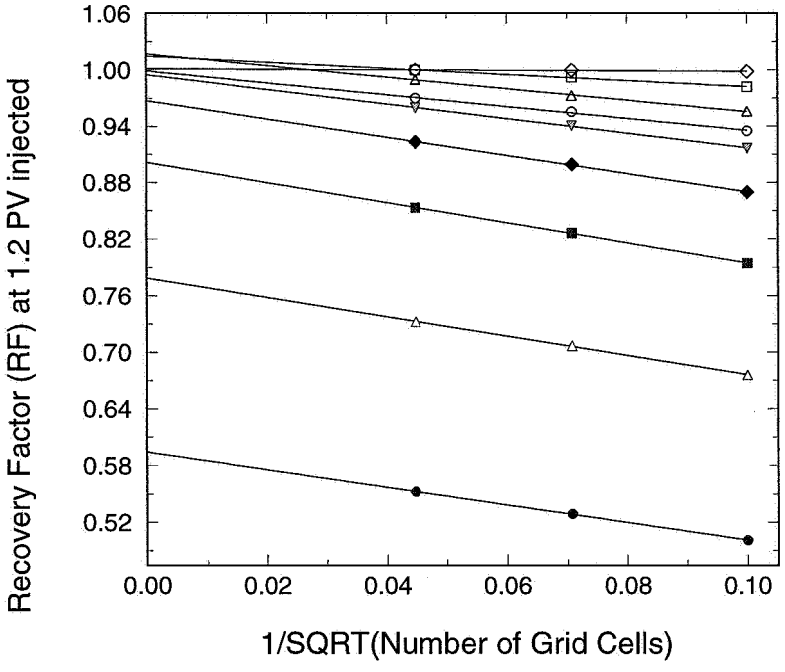

Fig. C.12 Elimination of numerical dispersion of the system in Fig. C.11.

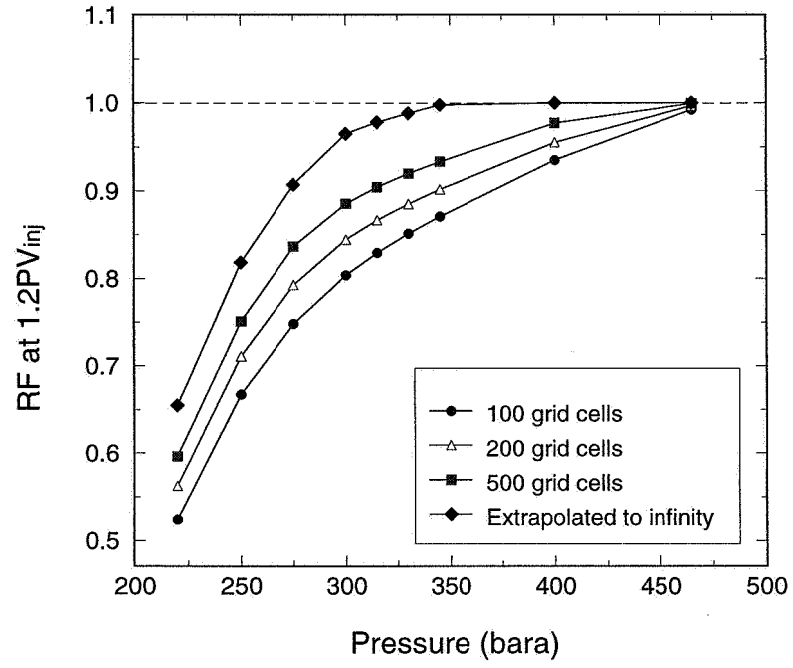

Fig. C.13 MMP determination for 7 component VOA system. Injection gas D.

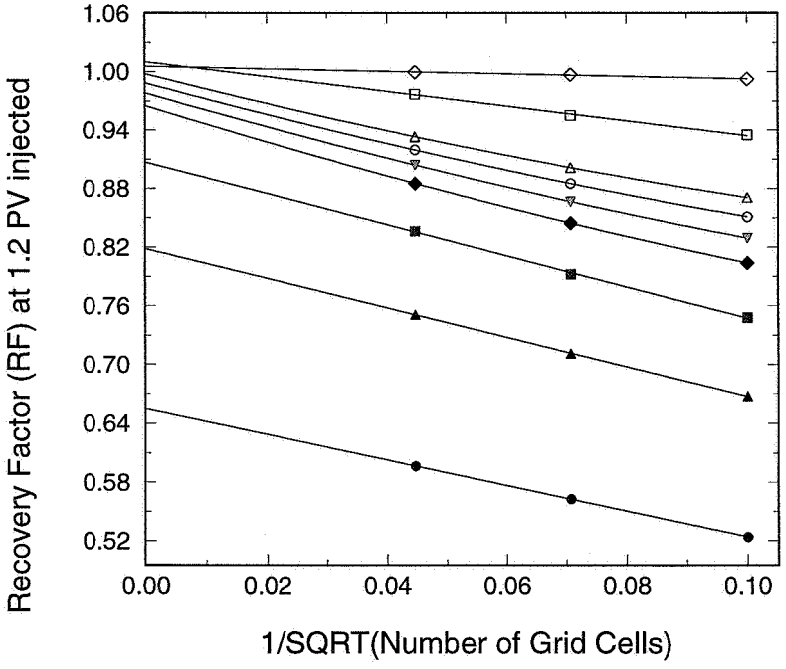

Fig. C.14 Elimination of numerical dispersion for the system in Fig. C.13.

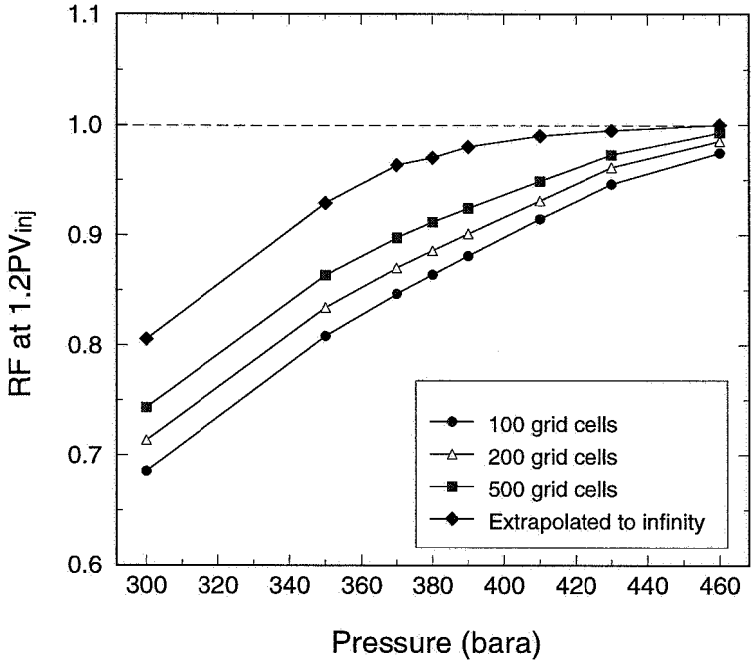

Fig. C.15 MMP determination for VOA system with initial gradient. E=0.47.

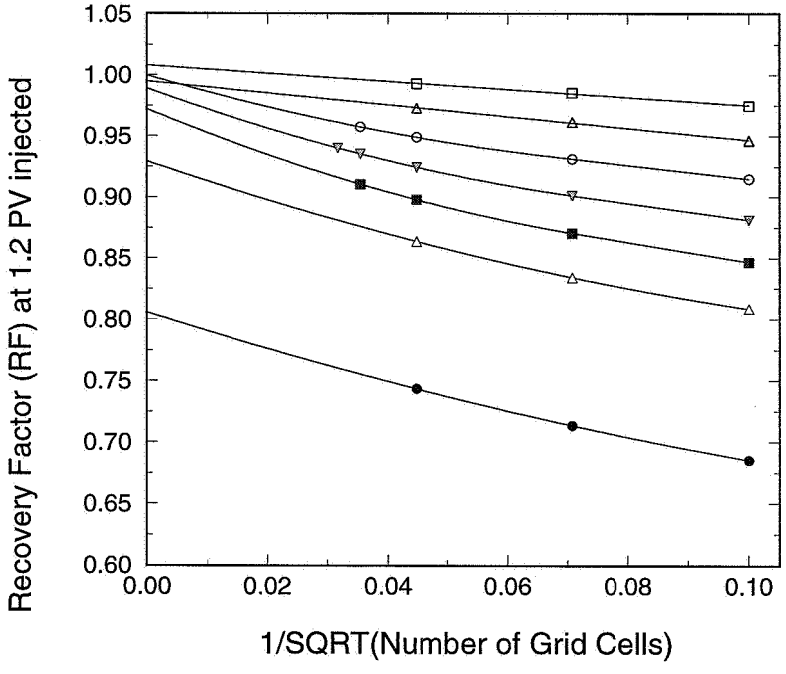

Fig. C.16 Elimination of numerical dispersion for the system in Fig. C.15.

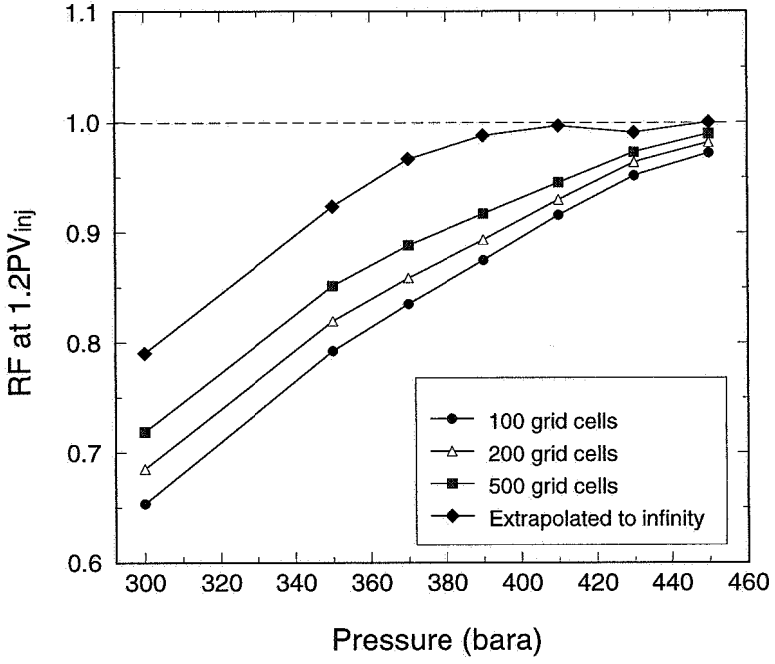

Fig. C.17 MMP determination for VOA system at -2895 mSSL. E=0.47.

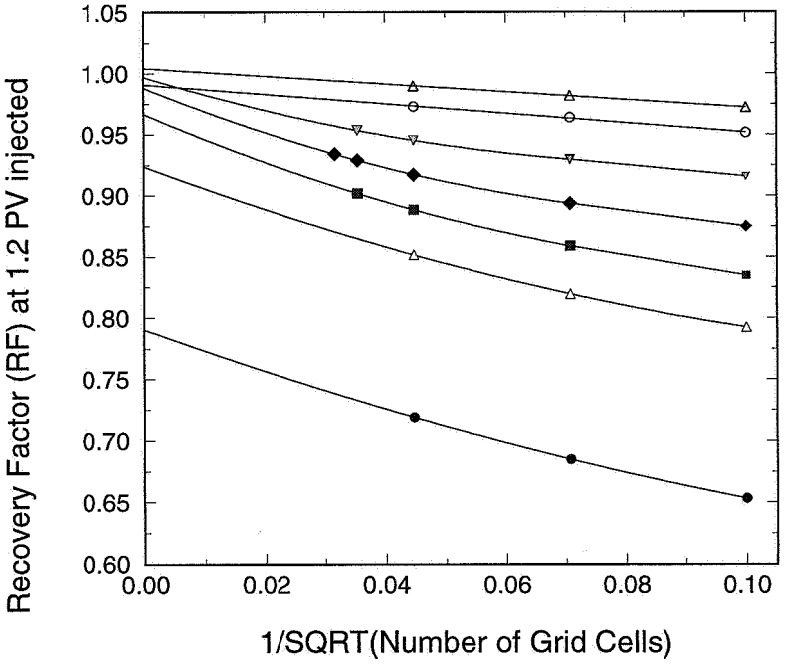

Fig. C.18 Elimination of numerical dispersion for the system given in Fig. C.17.

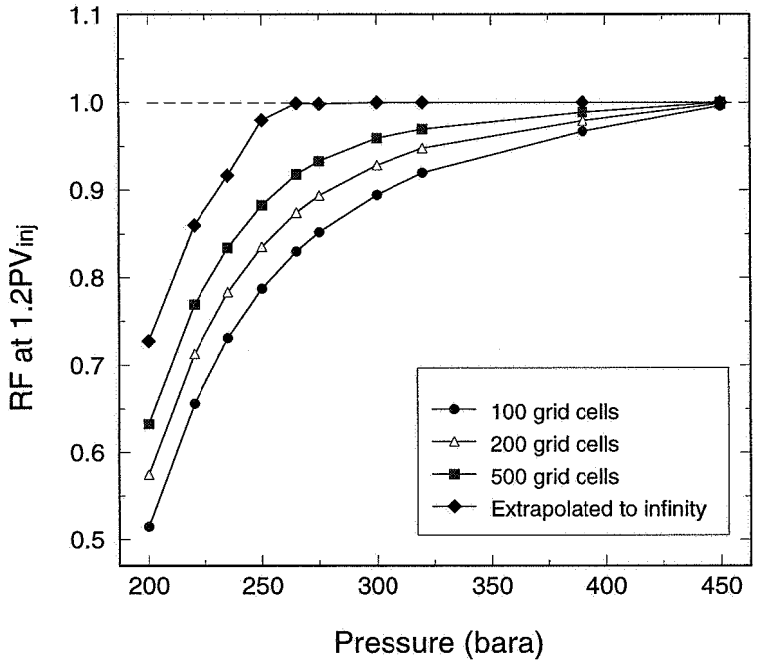

Fig. C.19 MMP determination for VOA system at -2895 mSSL. Injection gas C.

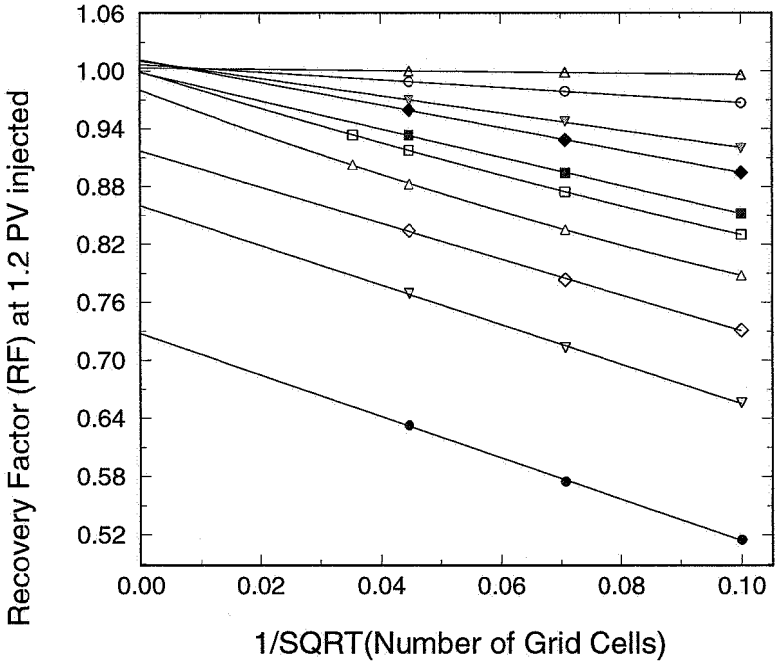

Fig. C.20 Elimination of numerical dispersion for the system in Fig. C.19.

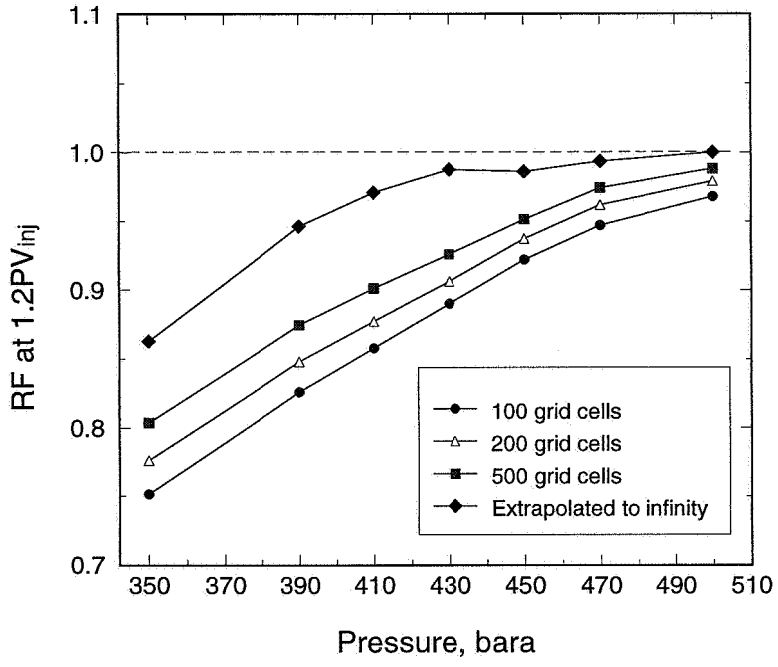

Fig. C.21 MMP determination for VOA system at -3159 mSSL. E=0.47

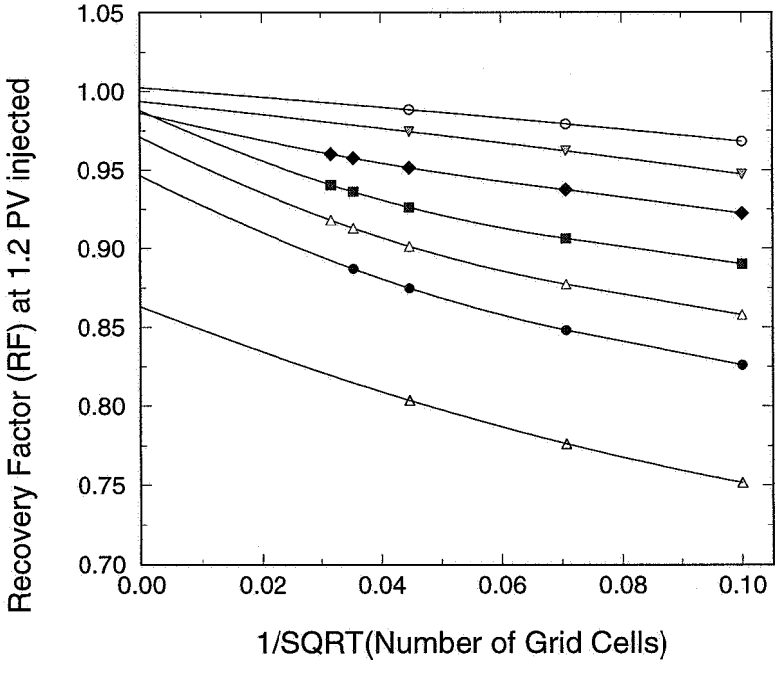

Fig. C.22 Elimination of numerical dispersion for the system in Fig. C.21.

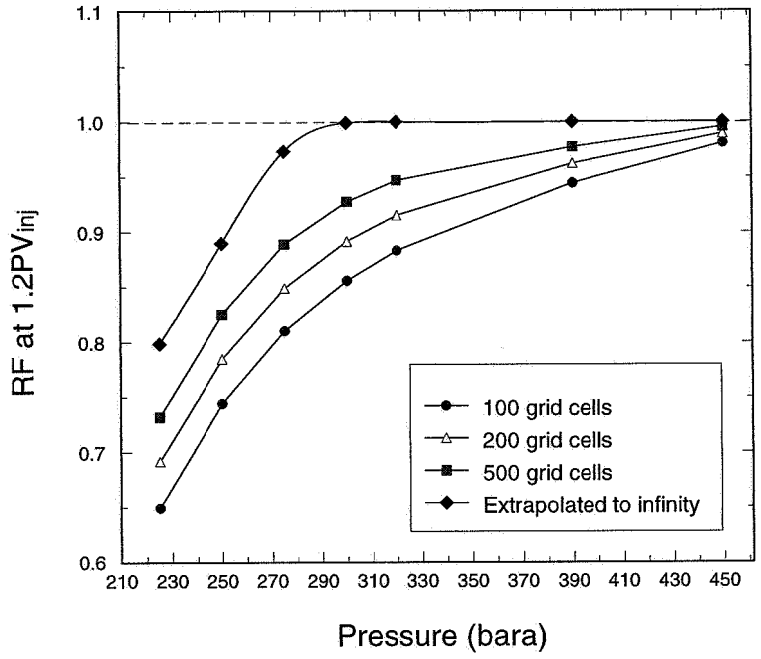

Fig. C.23 MMP determination for VOA system at -3159 mSSL. Injection gas C.

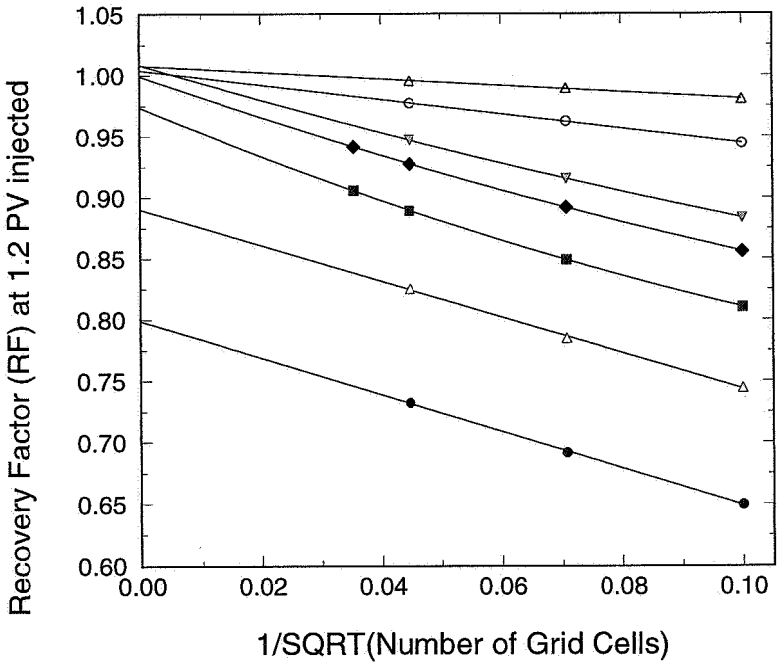

Fig. C.24 Elimination of numerical dispersion for the system in Fig. C.23.

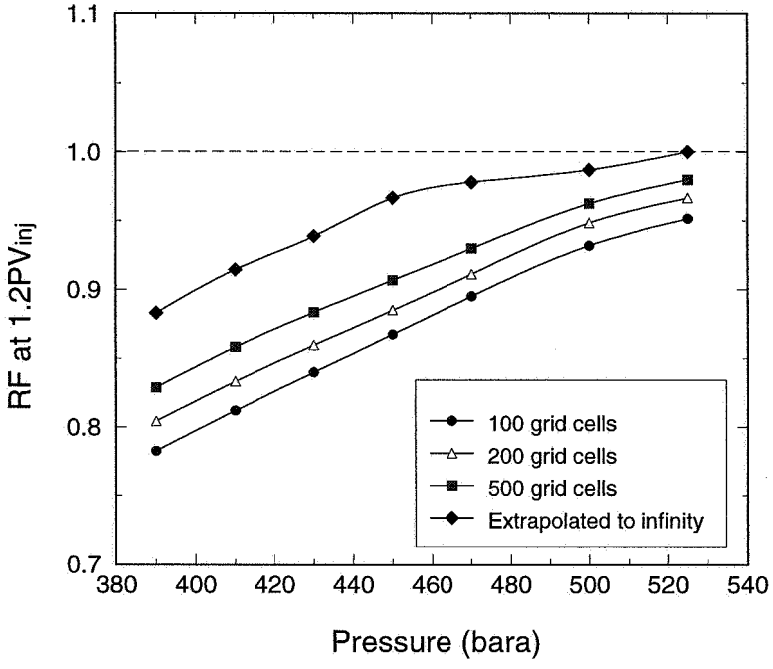

Fig. C.25 MMP determination for VOA system at -3505 mSSL. E=0.47

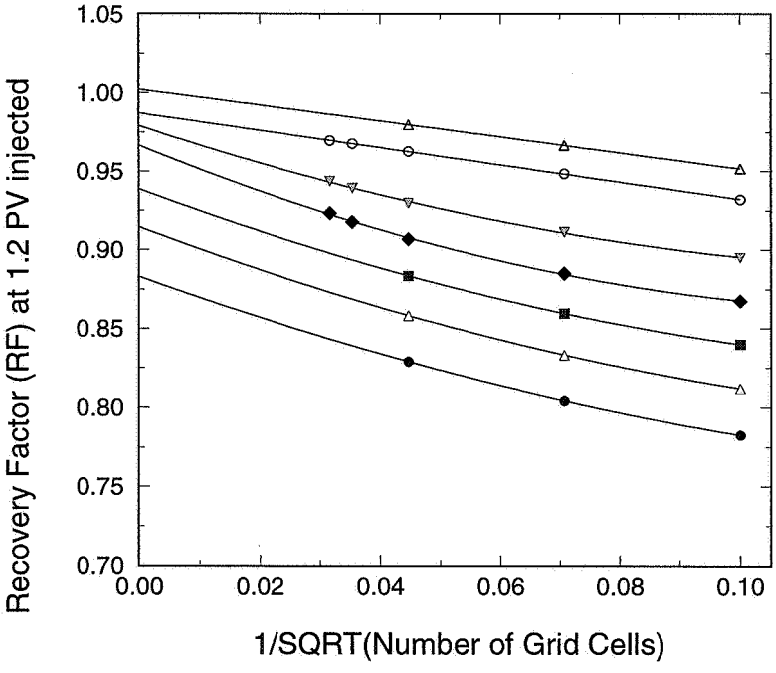

Fig. C.26 Elimination of numerical dispersion for the system in Fig. C.25.

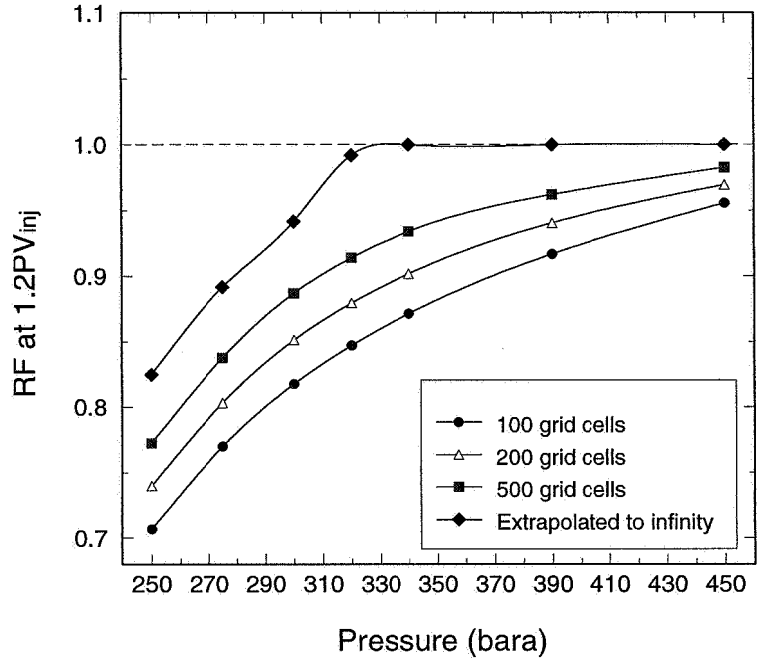

Fig. C.27 MMP determination for VOA system at -3505 mSSL. Injection gas C.

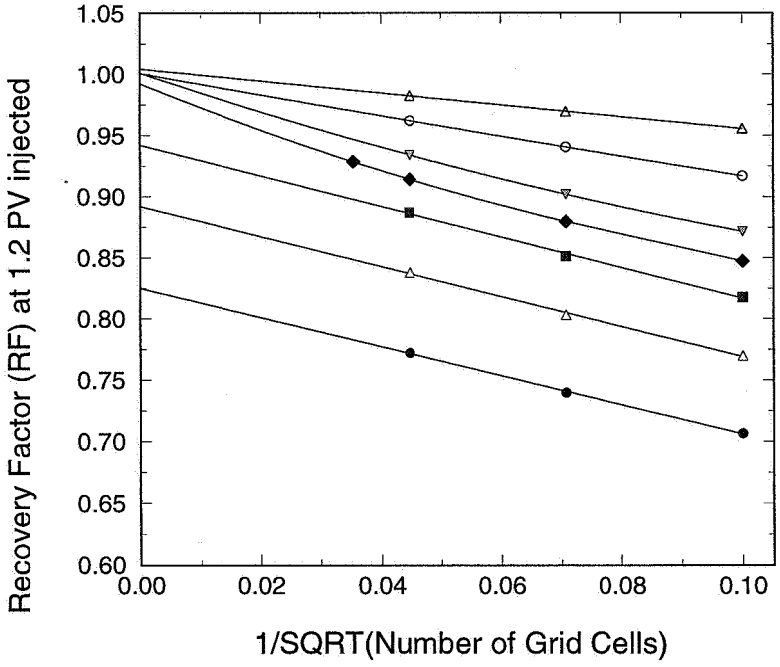

Fig. C.28 Elimination of numerical dispersion for the system in Fig. C.27.

Appendix D

Grid Effect in the Zick Multicell Algorithm

In this appendix we give additional investigations of grid effect in the Zick multicell algorithm. The algorithm was investigated and applied on several fluid systems in Chapter 3. Sensitivity plots of MMP as a function of grid numbers for different reservoir fluid-, and gas-systems are given.

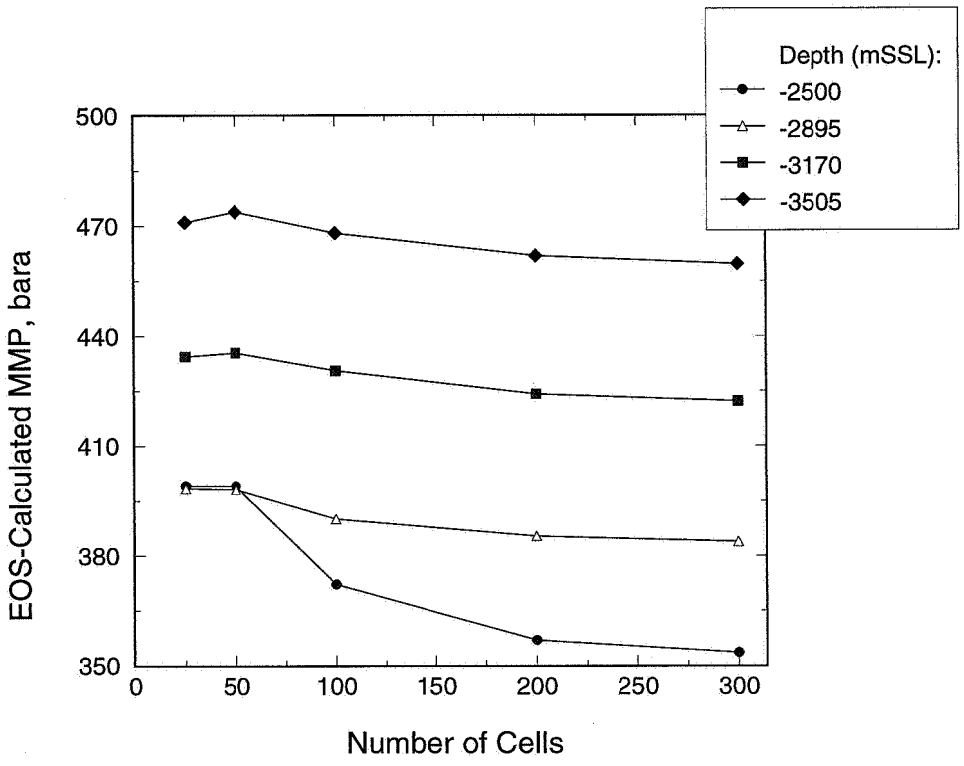

Fig. D.1 Sensitivity study of grid effect in the Zick multicell algorithm. 15 component VOA system at four depths. Oil compositions determined by the isothermal GCE algorithm. Injection gas: gas A enriched with gas B. E=0.47.

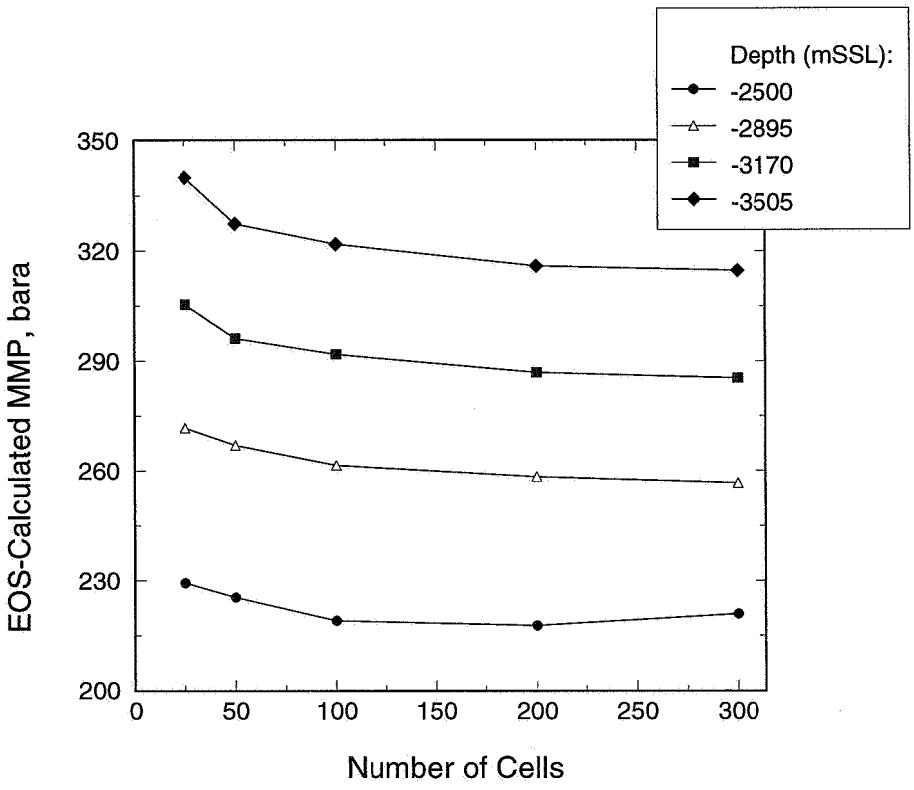

Fig. D.2 Sensitivity study of grid effect in the Zick multicell algorithm. 15 component VOA system at four depths. Oil compositions determined by the isothermal GCE algorithm. Injection gas C (Chapter 3).

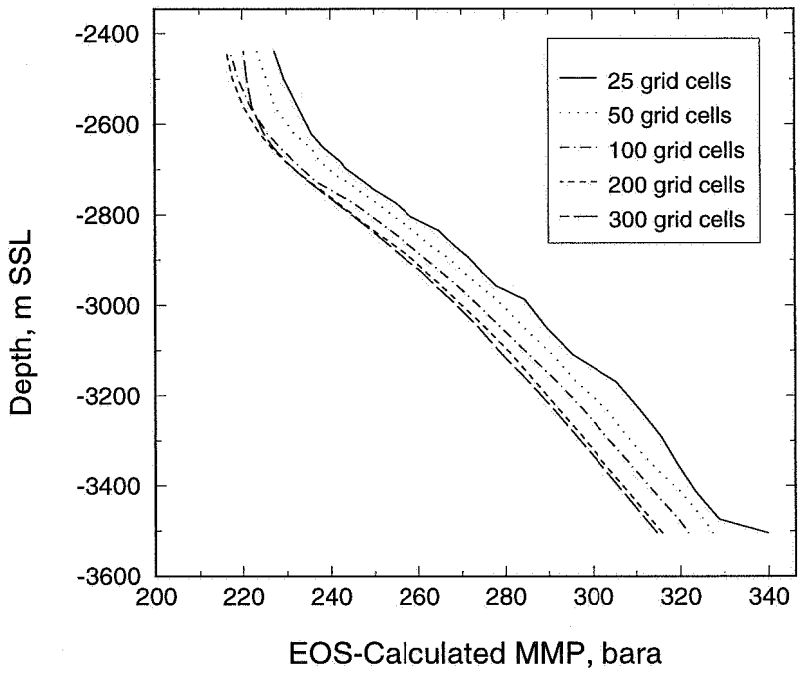

Fig. D.3 Sensitivity study of grid effect in the Zick multicell algorithm. 15 component VOA system. Oil compositions taken from isothermal GCE calculations at 28 different depths. Injection gas C.

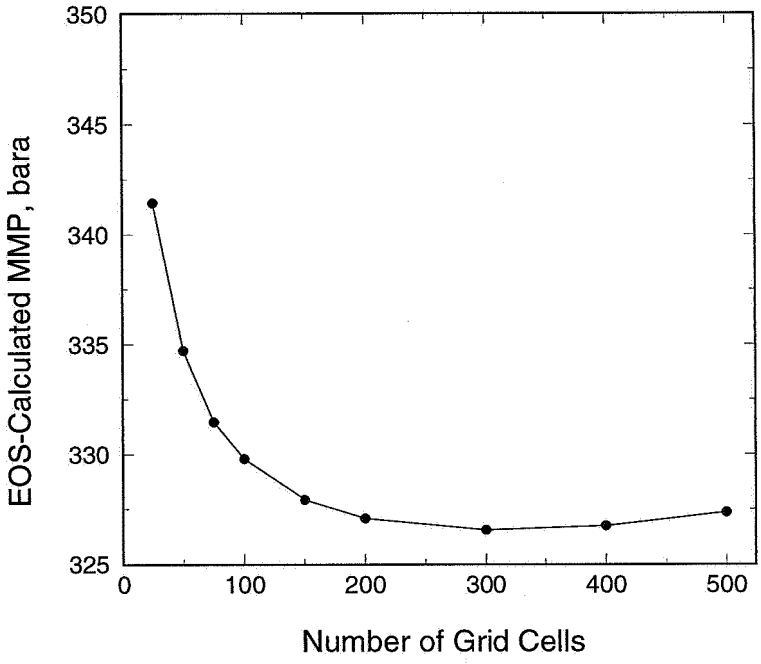

Fig. D.4 Sensitivity study of grid effect in the Zick multicell algorithm. 7 component VOA system (Chapter 3). Injection gas: pseudoized 7 component gas D (Chapter 2).